Technische Universität München
TUM School of Natural Sciences

Quantum and classical methods for lattice gauge theories in higher dimensions

Julian Bender

Vollständiger Abdruck der von der TUM School of Natural Sciences der Technischen Universität München zur Erlangung eines

Doktors der Naturwissenschaften (Dr. rer. nat.)

genehmigten Dissertation.

Vorsitz: Prof. Dr. Rudolf Gross

*Prüfer*innen der Dissertation:* Hon-Prof. Dr. Ignacio Cirac
Prof. Dr. Johannes Knolle

Die Dissertation wurde am 11.05.2023 bei der Technischen Universität München eingereicht und durch die TUM School of Natural Sciences am 06.06.2023 angenommen.

Abstract

Three of the four fundamental forces in nature are described by the Standard model of particle physics. While particles in some sectors only interact weakly and can be studied using perturbative expansions, other sectors, e.g. quantum chromodynamics, exhibit strong interactions. Lattice gauge theory, a discretized version of quantum field theories on the lattice, offers a computational framework for a non-perturbative treatment. The conventional approach to lattice gauge theories is based on Monte Carlo simulations of the Euclidean path-integral. However, studying real-time dynamics and theories with a finite chemical potential are challenging due to the sign-problem which prevents efficient Monte Carlo simulations.

Hamiltonian methods have provided new insights into sign-problem affected phenomena in lattice gauge theories, in particular in one dimension. This includes quantum simulation, where quantum systems are designed to mimic the behaviour of complex many-body systems, but also classical, variational methods such as tensor networks.

The central goal of this thesis is the development of Hamiltonian methods to study sign-problem affected regimes in higher-dimensional lattice gauge theories, using both classical and quantum simulation techniques. Lattice gauge theories in two and more spatial dimensions are qualitatively different from one dimension as it is possible in one dimension to integrate out the gauge field. Higher-dimensional lattice gauge theories, even without fermions, have non-trivial interactions and an infinite-dimensional gauge field Hilbert space that needs to be taken into account. Thus, one needs to find methods that avoid truncating the Hilbert space or at least allow to control this truncation.

The methods in this thesis are specifically designed for continuous gauge groups in order to avoid such truncations. They are demonstrated by studying the two prime examples for sign-problem affected phenomena, real-time dynamics and theories at finite chemical potential. Since the presented methods are based on the variational principle, they are thoroughly benchmarked against other methods, e.g. Euclidean Monte Carlo simulations in regimes where the sign-problem is absent. Moreover, reformulations of Hamiltonian lattice gauge theories are provided which eliminate gauge-redundancies and thus allow to save resources, relevant for both classical and quantum algorithms.

First, we present a gauge-invariant reformulation of lattice quantum electrodynamics with dynamical fermions. A unitary transformation of the Hamiltonian is performed which allows to decouple the fermionic degrees of freedom from the local gauge constraints. The remaining local redundancies, involving only gauge fields, can be incorporated in a gauge-invariant formulation by changing from a link-based description of the gauge field to a plaquette-based description.

Secondly, we present a variational method based on complex periodic Gaussian states which allows to study real-time dynamics in $(2+1)$-dimensional lattice quantum electrodynamics. The idea of the ansatz is to take into account the compact nature of the $U(1)$ gauge group by constructing a periodic Gaussian wavefunction in the gauge field plaquette variables. Periodicity is achieved by an infinite sum over Gaussian

wavefunctions where the sums can be shown to be evaluated efficiently numerically. The method is benchmarked against exact solutions known for the one-plaquette case, against a Euclidean Monte Carlo study and against exact diagonalization for a truncated $U(1)$ gauge field Hilbert space. The method is then demonstrated in a sign-problem affected regime by studying global quench dynamics for various types of quenches, e.g. the real-time evolution of a strongly confined flux tube between two static charges after a quench to weak coupling.

Finally, we present a variational Monte Carlo algorithm that enables the study of lattice gauge theories with continuous gauge groups at finite density, exemplary shown for $(2+1)$-dimensional lattice quantum eletrodynamics. The method is benchmarked against various limiting cases, including the pure gauge theory and a Euclidean Monte Carlo simulation for two fermion flavors at zero chemical potential where the sign-problem is absent. The method is then demonstrated in a sign-problem affected regime by studying density-induced phase transitions for two fermion flavors at varying flavor-dependent chemicial potentials.

Zusammenfassung

Drei der vier fundamentalen Wechselwirkungen der Natur werden durch das Standardmodell der Teilchenphysik beschrieben. Während die Teilchen in einigen Bereichen nur schwach wechselwirken und mit Hilfe von Störungstheorie untersucht werden können, weisen andere Bereiche, z. B. die Quantenchromodynamik, starke Wechselwirkungen auf. Gittereichtheorie, eine diskretisierte Version der Quantenfeldtheorien auf dem Gitter, bietet den Rahmen für eine computergestützte, nicht-perturbative Behandlung. Der herkömmliche Ansatz für Gittereichtheorien basiert auf Monte-Carlo Simulationen des euklidischen Pfadintegrals. Die Untersuchung von Echtzeitdynamik und Theorien mit einem endlichen chemischen Potenzial sind jedoch aufgrund des Vorzeichenproblems, das effiziente Monte-Carlo-Simulationen verhindert, eine Herausforderung.

Methoden basierend auf der Hamiltonschen Formulierung von Gittereichtheorien haben neue Einblicke in die vom Vorzeichenproblem betroffenen Phänomene ermöglicht, insbesondere in einer Dimension. Dazu gehören Quantensimulationen, bei denen Quantensysteme das Verhalten komplexer Vielteilchensysteme nachahmen sollen, aber auch klassische Variationsmethoden wie Tensornetzwerke.

Das zentrale Thema dieser Arbeit ist die Entwicklung von Hamiltonschen Methoden zur Untersuchung von Regimen mit Vorzeichenproblemen in höherdimensionalen Gittereichtheorien, basierend auf sowohl klassischen als auch Quantensimulationstechniken. Gittereichtheorien in zwei und mehr räumlichen Dimensionen unterscheiden sich qualitativ von eindimensionalen Theorien, da es in einer Dimension möglich ist, das Eichfeld zu eliminieren. Höherdimensionale Gittereichtheorien, auch ohne Fermionen, haben nicht-triviale Wechselwirkungen, und es muss ein unendlich dimensionaler Hilbert-Raum für das Eichfeld berücksichtigt werden. Daher muss man es entweder ganz vermeiden den Hilbert-Raum künstlich abzuschneiden oder dieses Abschneiden zumindest kontrollieren.

Die in dieser Arbeit vorgestellten Methoden sind speziell für kontinuierliche Eichgruppen entwickelt worden, um solche Abschneidungen zu vermeiden. Sie werden anhand von zwei Beispielen für vorzeichenbehaftete Phänomene demonstriert: Echtzeitdynamik und Theorien mit endlichem chemischem Potential. Da die vorgestellten Methoden auf dem Variationsprinzip beruhen, werden sie ausführlich mit anderen Methoden verglichen, z. B. mit euklidischen Monte-Carlo Simulationen in Regimen, in denen das Vorzeichenproblem nicht auftritt. Darüber hinaus werden Umformulierungen von Hamiltonschen Gittereichtheorien bereitgestellt, die Eichredundanzen eliminieren und somit Ressourcen einsparen, was sowohl für klassische als auch für Quantenalgorithmen von Bedeutung ist.

Zunächst stellen wir eine eichinvariante Reformulierung der Gitterquantenelektrodynamik mit dynamischen Fermionen vor. Es wird eine unitäre Transformation des Hamiltonians durchgeführt, die es erlaubt, die fermionischen Freiheitsgrade von den lokalen Eichtransformationen zu entkoppeln. Die verbleibenden lokalen Redundanzen, die nur Eichfelder betreffen, können in eine eichinvariante Formulierung gebracht werden, indem von einer link-basierten Beschreibung des Eichfeldes zu einer plaketten-

basierten Beschreibung gewechselt wird.

Zweitens stellen wir eine Variationsmethode vor, die auf komplexen periodischen Gaußschen Zuständen basiert und es ermöglicht, die Echtzeitdynamik in der $(2+1)$-dimensionalen Gitterquantenelektrodynamik zu untersuchen. Die Idee des Ansatzes besteht darin, die kompakte Natur der $U(1)$-Eichgruppe zu berücksichtigen, indem eine periodische Gaußsche Wellenfunktion in den Eichfeld-Plakettenvariablen konstruiert wird. Die Periodizität wird durch eine unendliche Summe über die Gaußschen Wellenfunktionen erreicht, wobei gezeigt werden kann, dass die Summen effizient numerisch ausgewertet werden können. Die Methode wird mit exakten Lösungen verglichen, die für den Ein-Plakette Fall bekannt sind, mit einer euklidischen Monte-Carlo Studie und mit exakter Diagonalisierung für einen abgeschnittenen $U(1)$-Eichfeld Hilbert-Raum. Die Methode wird dann in einem vom Vorzeichenproblem betroffenen Regime demonstriert, indem die globale Quench-Dynamik für verschiedene Arten von Quenches untersucht wird, z.B. die Echtzeitentwicklung eines stark eingesperrten Eichfelds zwischen zwei statischen Ladungen nach einem Quench zu schwacher Kopplung.

Schließlich stellen wir einen variationellen Monte-Carlo Algorithmus vor, der die Untersuchung von Gittereichtheorien mit kontinuierlichen Eichgruppen bei endlichem chemischen Potenzial ermöglicht, wie am Beispiel der $(2+1)$-dimensionalen Gitterquantenelektrodynamik gezeigt wird. Die Methode wird mit verschiedenen Grenzfällen verglichen, einschließlich der reinen Eichtheorie und einer euklidischen Monte-Carlo Simulation für zwei Fermionenflavors bei einem chemischen Potential von null, bei dem das Vorzeichenproblem nicht auftritt. Die Methode wird dann in einem vom Vorzeichenproblem betroffenen Regime demonstriert, indem dichteinduzierte Phasenübergänge für zwei Fermionenflavors bei unterschiedlichen flavorabhängigen chemischen Potenzialen untersucht werden.

List of Publications

Publications and Preprints related to this Thesis

[1] *A gauge redundancy-free formulation of compact QED with dynamical matter for quantum and classical computations*
J. Bender, and E. Zohar
Phys. Rev. D 102, 114517 (2020).
See chapter 3.

[2] *Real-time dynamics in 2 + 1D compact QED using complex periodic Gaussian states*
J. Bender, P. Emonts, E. Zohar, and J. I. Cirac
Phys. Rev. Research 2, 043145 (2020).
See chapter 4.

[3] *A variational Monte Carlo algorithm for lattice gauge theories with continuous gauge groups: a study of (2+1)-dimensional compact QED with dynamical fermions at finite density*
J. Bender, P. Emonts, and J. I. Cirac
arxiv: 2304.05916 [hep-lat] (under review).
See chapter 5.

Further publications

[4] *Digital quantum simulation of lattice gauge theories in three spatial dimensions*
J. Bender. E. Zohar, A. Farace, and J. I. Cirac
New J. Phys. 20, 093001 (2018).

Contents

1 Introduction

The quest to understand all phenomena in nature in terms of only a few fundamental principles has been a central goal of physicists throughout centuries. This idea dates back to Newton who introduced in 1687 his law of universal gravitation that described gravity as an attractive force between massive objects, providing a foundational understanding of the motion of such objects. Subsequently, physicists formulated theories for other fundamental forces and attempted to unify them into a single framework, one prominent example being Maxwell's formulation of electromagnetism which unified the description of electric and magnetic phenomena. This effort is continuing to this day, where to our current understanding there are four fundamental forces: gravity, electromagnetism, the weak nuclear force and the strong nuclear force. While the gravitational force is described by Einstein's general theory of relativity, the other three forces are explained within the Standard Model of particle physics [5]. Unifying these two theories is an active frontier in modern physics [6].

There is, however, another aspect of our understanding of these theories that arises from the recognition that while we may be able to explain the interactions of individual objects it does not necessarily guarantee that we fully understand the interplay between many of them, which is crucial for comprehending emergent phenomena such as magnetism or superconductivity. This challenge is particularly severe in quantum theories with strong interactions, as they cannot be easily treated using perturbative expansions unlike weakly coupled theories. Moreover, the quantum nature of these systems leads to an exponential scaling of computational resources with system size, making it impractical to compute emergent phenomena exactly. This is known as the many-body problem.

The Standard Model of particle physics falls into this category as it is a quantum field theory (QFT) that becomes strongly coupled in certain regimes, e.g. in the sector describing the strong force, quantum chromodynamics (QCD). Significant efforts have been dedicated to the development of numerical methods to approximate the behavior of non-perturbative quantum field theories. A computational framework is provided by lattice gauge theory (LGT), a discretized version of quantum field theory on the lattice [7, 8]. Besides its relevance for the Standard Model of particle physics, lattice gauge theories also emerge in condensed matter physics as low-energy effective theories of strongly correlated electron systems [9, 10]. Thus, developing methods for the study of lattice gauge theories is quintessential for our understanding of fundamental physical phenomena ranging from the confinement of quarks in particle physics to quantum spin liquids with fractionalized excitations in condensed matter physics.

The conventional approach to lattice gauge theories is based on the path integral formulation where the theory is defined by an action. Expectation values are computed by integrating over all possible paths, with each path being weighted by the exponential of the corresponding action. A Wick rotation is performed from real to imaginary time to render the path integral convergent. The exponential of the action in this Euclidean formulation can be interpreted as a probability distribution. This enables the

use of Monte Carlo techniques, where an integral is approximated by sampling from a probability distribution and taking an average over all sampled configurations. As a result, numerous intriguing aspects of non-perturbative quantum field theories have been revealed [11].

However, in certain regimes of quantum field theories the implementation of this approach becomes difficult. First, gaining insights into real-time dynamics, necessary to study phenomena out-of-equilibrium, can be challenging due to the formulation in Euclidean space-time. Secondly, for fermionic theories with a finite chemical potential the Euclidean action can become complex preventing an interpretation as a probability distribution and thus Monte Carlo sampling to evaluate the path integral. This problem is known as the sign-problem [12]. Hence, alternative approaches are necessary to investigate regimes where Euclidean Monte Carlo techniques are not applicable.

Over the last decades, new techniques have emerged to tackle this problem which are connected to the *second quantum revolution* [13]. The *first quantum revolution* is often referred to discoveries in the field of quantum mechanics during the early 20th century, where ideas by pioneers like Planck, Bohr, Heisenberg and Einstein fundamentally changed our understanding of the physical world, laying the foundations for modern quantum physics. The *second quantum revolution* is referred to more recent developments where quantum systems in laboratories have become controlled to such a degree that quantum phenomena can be utilized for different applications. This has resulted in the emergence of new research areas such as quantum computing, quantum cryptography, quantum sensing or quantum communication. One application, originally proposed by Feynman [14], is quantum simulation, where quantum systems are designed to mimic the behaviour of complex many-body systems, providing new insights into phenomena which are otherwise difficult to access due to the many-body problem. Since sign-problem affected regimes of lattice gauge theories can in principle be studied using quantum simulation, a lot of efforts have been made both theoretically and experimentally to use quantum technologies for problems in high-energy physics [15].

This requires a different formulation compared to the traditional action-based approach mentioned above since quantum devices are described by Hamiltonians. As a result, there has been a renewed interest in Hamiltonian formulations of lattice gauge theories which also stimulated the development of new Hamiltonian-based classical algorithms, such as tensor networks or variational Monte Carlo methods [15].

Hamiltonian simulation methods, both quantum and classical, have been applied to lattice gauge theories, with the main focus being one-dimensional models. The central theme of this thesis will be the development of Hamiltonian methods to study sign-problem affected regimes in higher-dimensional lattice gauge theories, using both classical and quantum simulation techniques.

Lattice gauge theories in two and more spatial dimensions are qualitatively different from one dimension as it is possible in one dimension to integrate out the gauge field degrees of freedom and to remain with a purely fermionic theory, whose degrees of freedom can be mapped to spins by a Jordan-Wigner transformation [16, 17]. On the other hand, higher-dimensional lattice gauge theories, even without fermions, have non-trivial interactions and exhibit interesting phenomena such as confinement [18]. This poses a different level of difficulty compared to one dimension as the gauge field degrees of freedom have to be taken into account which is complicated by the fact that the gauge field Hilbert space is infinite-dimensional. Thus, special care needs to

be paid in the development of higher-dimensional methods to the description of gauge fields in order to avoid truncating the Hilbert space or to at least control this truncation.

In this thesis, different numerical methods for the study of lattice gauge theories are presented, specifically suited for the study of higher-dimensional theories as the infinite-dimensional Hilbert space of continuous gauge groups is incorporated in these methods. The methods are demonstrated by computing sign-problem affected phenomena, such as real-time evolution and quantities at finite chemical potential. Moreover, reformulations of Hamiltonian lattice gauge theories are provided which eliminate gauge-redundancies and thus allow to save resources, relevant for both classical and quantum algorithms.

1.1 Outline

The central goal of this thesis is to provide new techniques to study higher-dimensional lattice gauge theories in regimes which are difficult to access with conventional Euclidean Monte Carlo simulations due to the sign-problem, with a particular focus on lattice gauge theories with continuous gauge groups so as not to be required to truncate the gauge field Hilbert space or to be restricted to finite gauge groups.

The two prime examples for phenomena in lattice gauge theories affected by the sign-problem are real-time evolution and finite chemical potential. A natural candidate for a physically relevant lattice gauge theory in higher dimensions is $(2+1)$-dimensional lattice quantum electrodynamics, characterized by the gauge group $U(1)$. We thus demonstrate the methods presented in this theses by studying real-time dynamics and ground state properties at finite chemical potential for $(2+1)$-dimensional lattice QED. Since the presented methods are based on the variational principle, they are thoroughly benchmarked against other methods, e.g. Euclidean Monte Carlo simulations in regimes where the sign-problem is absent.

In addition to the numerical methods we present reformulations of lattice QED with dynamical fermions in terms of gauge-invariant degrees of freedom, allowing for a wider range of possible variational ansatz states and a reduction in computational resources.

The thesis is structured as follows. In chapter 2, we motivate the work presented in this thesis by reviewing various methods to study strongly coupled quantum field theories and their limitations. First, we give a short review on quantum field theories, explain the concept of running coupling which explains why non-perturbative methods are required in certain regimes. We then show how lattice gauge theories serve as non-perturbative regularizations of quantum field theories. We discuss the conventional approach to lattice gauge theories, employing Euclidean Monte Carlo techniques, and explain how the sign-problem arises for real-time evolution and finite densities. Additionally, we present the Hamiltonian formulation of lattice gauge theory, which is used throughout this thesis. Finally, we discuss Hamiltonian methods for lattice gauge theories and their limitations.

In chapter 3, we present a gauge-invariant reformulation of lattice quantum electrodynamics with dynamical fermions. A unitary transformation of the Hamiltonian is performed which allows to decouple the fermionic degrees of freedom from the local Gauss' law constraints. The remaining local redundancies, involving only gauge degrees of freedom, can be incorporated in a gauge-invariant formulation by changing

from a link-based description of the gauge field to a plaquette-based description.

In chapter 4, we present a variational method based on complex periodic Gaussian states which allows to study real-time dynamics in $(2+1)$-dimensional lattice QED. The idea of the ansatz is to take into account the compact nature of the $U(1)$ gauge group by constructing a periodic Gaussian wavefunction in the gauge field plaquette variables. Periodicity is achieved by an infinite sum over Gaussian wavefunctions where the sums can be shown to be evaluated efficiently numerically. The method is benchmarked against exact solutions known for the one-plaquette case, against a Euclidean Monte Carlo study and against exact diagonalization for a truncated $U(1)$ gauge field Hilbert space. The method is then demonstrated by studying global quench dynamics for various types of quenches, e.g. the real-time evolution of a strongly confined flux tube between two static charges after a quench to weak coupling.

In chapter 5, we present a variational Monte Carlo algorithm that enables the study of lattice gauge theories with continuous gauge groups at finite density, exemplary shown for $(2+1)$-dimensional lattice QED. The method is benchmarked against various limiting cases, including the pure gauge theory, and a Euclidean Monte Carlo simulation for two fermion flavors at zero chemical potential where the sign-problem is absent. The method is then demonstrated in a sign-problem affected regime by studying density-induced phase transitions for two fermion flavors at varying flavor-dependent chemicial potentials.

2 Preliminaries

In this chapter, we present a comprehensive overview of the models and methods employed throughout the thesis. The guiding principle is to explain why, starting from the Standard model of particle physics and recognizing limitations of existing methods, new approaches are desirable for investigating higher-dimensional lattice gauge theories with continuous gauge groups in regimes affected by the sign-problem.

We first explain in the context of the Standard model of particle physics why non-perturbative methods are needed in quantum field theories and how this naturally leads to lattice gauge theories. Subsequently, we describe the conventional approach in lattice gauge theories based on the action formulation and Euclidean Monte Carlo simulations. We discuss its limitations by explaining in more detail what the sign-problem is and how it arises in certain regimes. In the next step, we present the Hamiltonian formulation of lattice gauge theory which forms the basis of alternative approaches. Two significant approaches, namely quantum simulation and variational methods, are discussed in detail. For both approaches conceptual challenges are emphasized when going from one to two dimensions, mainly related to the infinite-dimensional gauge field Hilbert space, and why this poses a challenge to currently available Hamiltonian methods.

2.1 Perturbative quantum field theories and running coupling

To our current understanding, three of the four fundamental forces in nature can be described within the Standard model of particle physics: the electromagnetic, weak and strong force, excluding gravity. It is a widely accepted theory that has been extensively tested and validated through experiments at particle accelerators [5]. Usually, one is not interested in the full Standard model but in a certain sector of it depending on the physical phenomena that one wants to study. If the strength of the interactions of that particular sector is small enough one can treat the theory in a perturbative series.

In the following we want to explain the running coupling, i.e. the dependence of the coupling strength on the energy scale, and show why in certain regimes a peturbative treatment is not possible. An example for a perturbative sector of the Standard model is quantum electrodynamics with the Lagrangian

$$\mathcal{L}_{\text{QED}} = \underbrace{\bar{\psi}_0(i\gamma^\mu\partial_\mu - m_0)\psi_0 - \frac{1}{4}F_{\mu\nu,0}F_0^{\mu\nu}}_{=\mathcal{L}_{\text{free}}} \underbrace{- e_0\bar{\psi}_0\gamma^\mu\psi_0 A_{\mu,0}}_{=\mathcal{L}_{\text{int}}} \tag{2.1}$$

with the field strength tensor $F_{\mu\nu,0} = \partial_\mu A_{\nu,0} - \partial_\nu A_{\mu,0}$. $A_{\mu,0}$ denotes the $U(1)$ gauge field, the photon field, and ψ_0 a Dirac spinor field, describing a fermion with spin $1/2$. γ^μ are the usual gamma matrices. One can separate the Lagrangian in a free part $\mathcal{L}_{\text{free}}$ and an interacting part $\mathcal{L}_{\text{int}}$. The interaction strength is characterized by

the bare coupling parameter e_0. However, the bare quantities denoted by a subscript 0 do not actually correspond to physical quantities measured in experiments. This is because if one naively tries to compute quantum corrections in perturbation theory due to virtual-particle loops one typically obtains loop integrals that are divergent. To address these divergences, the theory needs to be regulated and renormalized.

Regularization can be thought of as introducing an ultraviolet (UV) cutoff Λ to render the divergent loop integrals finite. Renormalization amounts then to redefining the bare parameters in the Lagrangian in such a way that the infinities arising in the limit of removing the regulator ($\Lambda \to \infty$) are absorbed, resulting in finite predictions for physical observables O. The redefinition of the bare parameters can also be viewed as introducing counterterms in the Lagrangian to cancel out the divergencies. A crucial feature of renormalizable quantum field theories is that the predictions will be independent of the choice of regularization scheme.

To make this procedure a bit more explicit, we schematically show it for the QED Lagrangian above. We focus in our discussion mainly on the coupling constant (which for QED is the electric charge) as it quantifies the strength of the interactions and indicates whether a perturbative treatment is possible. As mentioned above, with a finite bare electric charge e_0 expressions for physical observables become infinite due to UV divergences. To approach that problem, one first regulates the theory, i.e. a UV cutoff Λ is introduced. The bare coupling constant is then modified as a function of the cutoff, denoted as $e_0(\Lambda)$. This process is called renormalization. This modification is performed in such a way that as the cutoff is removed ($\Lambda \to \infty$), the resulting predictions for physical observables become finite and meaningful.

In the limit of removing the cutoff the bare coupling will become infinite, which is, however, not a problem since the bare coupling e_0 has no physical meaning. In modern understanding of quantum field theories due to Wilson [19], this is related to the concept of viewing quantum field theories as effective field theories. The central idea of this concept is that such theories have an intrinsic cutoff, beyond which their descriptions are no longer valid, and a more fundamental theory is required to explain the phenomena at higher energy scales.

For the renormalization procedure, one splits the behavior of the bare coupling into a singular part absorbing the divergences, the renormalization factor $Z_e(\Lambda, \mu)$, and a regular part, the effective coupling $e(\mu)$:

$$e_0(\Lambda) = Z_e(\Lambda, \mu) e(\mu). \tag{2.2}$$

Note that renormalization introduces a new scale, the renormalization scale μ, which is in principle arbitrary and does not influence physical observables. In practice, however, one chooses the renormalization scale to be close to the energy Q of the physical process that one is interested in. In that case, the calculations for physical observables simplify and the coupling $e(Q)$ gives a good estimate for the effective coupling strength and whether perturbation theory is valid.

Eq. (2.2) defines a renormalization scheme. Note that there are many different choices for such schemes as the renormalization factor Z_e is only required to absorb the divergencies but the finite part of Z_e can be chosen arbitrarily. However, all renormalization schemes are supposed to give the same predictions for physical observables O_j in the limit of $\Lambda \to \infty$:

$$O_j^\infty \equiv \lim_{\Lambda \to \infty} O_j(e(\mu), Z_e(\Lambda, \mu), ...). \tag{2.3}$$

The dots denote that there are typically several renormalization factors Z_i involved in a renormalization scheme. For QED one needs to define in addition to the electric charge also similar renormalization relations for the mass, the photon field and the fermion field. A theory is said to be renormalizable if O_j^∞ is finite for all physical observables even though only a finite number of Z_i are adjusted. Note that there are infinitely many observables O_j making the above a non-trivial statement.

Since also every choice of renormalization scale μ should lead to the same predictions for physical observables, one can derive equations that relate the effective couplings at different renormalization scales. These equations are called *renormalization group equations* [5]. An essential part of them are the so called *beta-functions* that are defined for every effective coupling $\alpha(\mu)$ and quantify the change in coupling strength with energy scale μ:

$$\beta(\alpha(\mu)) \equiv \frac{d\alpha(\mu)}{d\ln\mu}. \tag{2.4}$$

For QED one obtains for the beta function in first-order perturbation theory [5]:

$$\beta(e(\mu)) = \frac{e^3(\mu)}{12\pi^2}. \tag{2.5}$$

What enters the expressions for physical observables is actually not the electric charge but the fine-structure constant, which are related in natural units $\hbar = c = 1$ as $\alpha_{\text{QED}}(\mu) = \frac{e^2(\mu)}{4\pi}$. The beta-function written in terms of α_{QED} takes the form:

$$\beta(\alpha_{\text{QED}}(\mu)) = \frac{2\alpha_{\text{QED}}^2(\mu)}{3\pi^2}. \tag{2.6}$$

By solving the differential equation given by the beta-function one can relate effective couplings at two energy scales μ_1 and μ_2:

$$\alpha_{\text{QED}}(\mu_2) = \frac{\alpha_{\text{QED}}(\mu_1)}{1 - \frac{1}{3\pi}\alpha_{\text{QED}}(\mu_1)\ln\frac{\mu_2^2}{\mu_1^2}}. \tag{2.7}$$

In order to get absolute values for the coupling, one needs to perform an experiment at some energy scale which allows to fix the coupling at this scale. For QED one typically fixes the coupling in the low-energy limit where α_{QED} is the well-known fine-structure constant at zero momentum transfer, given by $\alpha \approx \frac{1}{137}$. This results in the expression:

$$\alpha_{\text{QED}}(\mu) = \frac{\alpha}{1 - \frac{1}{3\pi}\alpha\ln\frac{\mu^2}{m^2}}. \tag{2.8}$$

where m is the mass of the electron which also needs to be determined experimentally. One can then compute the fine-structure constant at higher energy scales, e.g. at the mass of the Z boson, $m_Z \approx 91.188\,\text{GeV}$, and obtains a slightly higher value $\alpha_{\text{QED}}(m_Z) \approx \frac{1}{127}$.

An intuitive explanation why the interaction strength depends on the energy scale is given by charge screening: at low energies, i.e. long distances far away from an electron, the electron can attract virtual positively charged particles from the vacuum, which effectively screen the electric charge. This screening reduces the coupling strength. This behavior is also reflected in the positive value of the beta-function. However, for all energy scales where it is known that quantum electrodynamics is a valid

description, the increase in coupling strength is only moderate so that perturbation theory can still be applied.

The situation is drastically different in quantum chromodynamics which is based on the gauge group $SU(3)$ instead of $U(1)$ as in quantum electrodynamics. The Lagrangian has the form

$$\mathcal{L}_{\text{QCD}} = -\frac{1}{4} G^a_{\mu\nu,0} G^{\mu\nu}_{a,0} + \bar{\psi}_{i,0}(i\gamma^\mu \partial_\mu - m_0)\psi_{i,0} - g_0 \bar{\psi}_{i,0}\gamma^\mu (T_a)_{ij} A^a_{\mu,0}\psi_{j,0} \tag{2.9}$$

with $G^a_{\mu\nu,0} = \partial_\mu A^a_{\nu,0} - \partial_\nu A^a_{\mu,0} + g_0 f^{abc} A^b_{\mu,0} A^c_{\nu,0}$. The subscript 0 denotes again bare quantities which need to be renormalized to get finite predicition for physical obersvables. $\psi_{i,0}$ ($i = 1, 2, 3$) are the three quark fields, T_a are the $SU(3)$ generators in the fundamental representation. $G^a_{\mu\nu,0}$ denotes the gluon field strength tensor, constructed out of the gluon fields $A^a_{\mu,0}$ with f^{abc} being the structure constants of $SU(3)$.

In analogy to the QED case, one can carry out the regularization and renormalization procedure and compute the beta-function for the effective coupling $\alpha_s(\mu) = \frac{g^2(\mu)}{4\pi}$ to first order in perturbation theory:

$$\beta(\alpha_s(\mu)) = \left(\frac{2n_f}{3} - 11\right)\frac{\alpha_s^2(\mu)}{2\pi} \equiv -\beta_0 \frac{\alpha_s^2(\mu)}{2\pi} \tag{2.10}$$

with n_f the number of flavors. Hence, the beta-function is negative for $n_f < 17$ which includes the case of the standard model with six quark flavors. Since the beta-function is negative, the strength of the coupling in QCD increases for lower energies, leading to the confinement of quarks and gluons within hadrons. On the other hand, the coupling strength becomes small at large energy scales. This phenomenon is known as *asymptotic freedom*.

As in QED, one can compute the running of the effective coupling by solving the corresponding differential equation given by the beta-function. In QCD, however, it is not possible to fix the coupling at low energy as the theory becomes strongly coupled. Instead, one chooses a different scale, typically the scale of the Z boson ($m_Z \approx 91.188\text{GeV}$) where the strong coupling strength is experimentally determined as $\alpha_s(m_Z) = 0.1179(10)$ [20]. One can then compute the running of the strong coupling as

$$\alpha_s(\mu) = \frac{\alpha_s(m_Z)}{1 + \alpha_s(m_Z)\frac{\beta_0}{4\pi}\ln\frac{\mu^2}{m_Z^2}}. \tag{2.11}$$

By computing the point at which the denominator in the above relation blows up, one can estimate the scale Λ_{QCD} at which perturbation theory breaks down in QCD [21]:

$$\Lambda_{QCD} = m_Z \exp\left(-\frac{2\pi}{\beta_0 \alpha_s(m_Z)}\right) \approx 0.2\text{GeV} \tag{2.12}$$

Below that energy scale QCD becomes strongly coupled, requiring new approaches beyond perturbation theory. This naturally gives rise to the formulation of lattice gauge theory, a non-perturbative regularization of quantum field theories.

2.2 Path-integral formulation of lattice gauge theory

Finding a gauge-invariant, non-perturbative regularization of quantum field theories, in particular for QCD, led to the invention of lattice gauge theories. The theory is placed on a lattice, thus naturally introducing a UV cutoff at a scale $1/a$ where a is the lattice spacing. Moreover, by using a finite lattice the theory can also be regulated in the infrared. One remains with a finite number of degrees of freedom, making lattice gauge theories amendable to numerical simulations.

To simplify the discussion, we will initially focus on the pure gauge sector of quantum electrodynamics. Subsequently, we discuss the incorporation of fermions and the extension to non-abelian gauge groups. The action of pure gauge quantum electrodynamics is given by

$$S_{\text{QED}}[A_\mu] = -\frac{1}{4}\int d^4x F_{\mu\nu}(x)F^{\mu\nu}(x) \tag{2.13}$$

with the usual definition of the field strength tensor, $F_{\mu\nu}(x) = \partial_\mu A_\nu(x) - \partial_\nu A_\mu(x)$.

To find a lattice discretization one needs to define a lattice analogue of the gauge field $A_\mu(x)$, a vector field. A natural candidate is a lattice gauge field $U_\mu(x)$ residing on the links of the lattice, where x denotes a lattice site and μ the direction in which the link emanates. The connection between the continuum and the lattice is made by the concept of a *parallel transporter* [22], given for neighboring lattice sites as

$$U_\mu(x) = e^{ig\int_0^a dt A_\mu(x+e_\mu t)} \tag{2.14}$$

where e_μ denotes the unit vector in direction μ and g the coupling constant. In contrast to the continuum, where the gauge field A_μ takes values in the Lie algebra, U_μ is described by elements of the compact gauge group. For the $U(1)$ gauge group of QED this means that the lattice gauge field U_μ takes values in $U(1)$ whereas the gauge field A_μ takes values in $\mathbb{R}$.

The analogue of the field strength tensor $F_{\mu\nu}(x)$ is a plaquette variable $U_{\mu\nu}(x)$, constructed as the clockwise multiplication of the four link variables around the plaquette:

$$U_{\mu\nu}(x) = U_\mu(x)U_\nu(x+e_\mu)U_\mu^\dagger(x+e_\nu)U_\nu^\dagger(x) \tag{2.15}$$

In the following we will often denote the plaquette variables as $U_{\mathbf{p}}$. Out of these plaquette variables one can construct a lattice action that recovers the continuum action in the limit of vanishing lattice spacing $a \to 0$:

$$S_{\text{cQED}}[U_\mu] = \frac{1}{g^2}\sum_{\mathbf{p}} \text{Re}\left(1 - U_{\mathbf{p}}\right) = \frac{1}{g^2}\sum_{\mathbf{p}}\left(1 - \cos(\theta_{\mathbf{p}})\right) \tag{2.16}$$

where $\theta_{\mathbf{p}} \in [0, 2\pi)$ is the angle that describes $U_{\mathbf{p}} = e^{i\theta_{\mathbf{p}}}$. The model defined by the lattice action S_{cQED} is known as compact QED, due to the compact nature of the gauge link variables $U_\mu(x)$.

In analogy to the discussion for QED, one can define a lattice action for the pure gauge sector of quantum chromodynamics by assigning to the link variables $U_\mu(x)$ elements of the gauge group $SU(3)$. One arrives at an action of a similar form

$$S_{\text{QCD}}[U_\mu] = \frac{1}{g^2}\sum_{\mathbf{p}} \text{Re}\,\text{Tr}\left(1 - U_{\mathbf{p}}\right). \tag{2.17}$$

where the trace is required to make the plaquette variable gauge-invariant. This action is also known as the *Wilson action* [7].

Corrections to the continuum action come in at order $\mathcal{O}(a^2)$. Note that the choice of lattice action is not unique, one can construct more complicated actions to improve the convergence towards the continuum limit.

Given a lattice action $S[U_\mu]$, one can compute observables with the path-integral formalism. Since the gauge field on the lattice takes values in a compact Lie Group (here either $U(1)$ or $SU(3)$) there is a well-defined measure given by the Haar measure, $DU = \prod_{x,\mu} dU_\mu(x)$. Expectation values are of the form

$$\langle O[U_\mu] \rangle = \frac{\int DU O[U_\mu] e^{iS[U_\mu]}}{\int DU e^{iS[U_\mu]}}. \tag{2.18}$$

Since the oscillatory behavior of the action complicates the numerical evaluation, one performs a Wick-rotation to imaginary time in order to get a convergent behavior:

$$\begin{aligned} t &\to -i\tau \\ iS[U_\mu] &\to -S_E[U_\mu]. \end{aligned} \tag{2.19}$$

With the Euclidean action $S_E[U_\mu]$, the path-integral can be interpreted in terms of a well-defined probability distribution $p[U_\mu]$:

$$\langle O[U_\mu] \rangle = \frac{\int DU O[U_\mu] e^{-S_E[U_\mu]}}{\int DU e^{-S_E[U_\mu]}} \equiv \int DU O[U_\mu] p[U_\mu] \tag{2.20}$$

with

$$p[U_\mu] = \frac{e^{-S_E[U_\mu]}}{\int DU e^{-S_E[U_\mu]}}. \tag{2.21}$$

This form of the path-integral is well-suited for Monte Carlo simulations [23, 24]. The interpretation in terms of a probability distribution allows to generate a certain number of samples U_i ($i = 1, .., N$) from $p(U)$ and approximate the expectation values as

$$\langle O \rangle = \int O(U) p(U) \approx \frac{1}{N} \sum_{i=1}^{N} O(U_i). \tag{2.22}$$

Over the last decades, advanced Monte Carlo algorithms have been developed to sample the probability distributions corresponding to path-integrals in lattice gauge theories. Their effectiveness in computing static properties in high-energy physics is unmatched, as evidenced by the remarkable agreement between experimentally measured hadronic particle masses and their numerically computed values [11]. However, the use of the action formalism comes with a limitation: because the action is defined in Euclidean spacetime, simulating real-time evolution becomes extremely difficult. For the study of dynamic phenomena, such as string-breaking in a confining theory, other methods must be employed.

Moreover, additional problems arise upon the inclusion of fermions. We first discuss free lattice fermions and then their coupling to a gauge field. To include fermions in the path-integral, one uses the so-called Grassmann algebra which involves anticommuting variables η_i ($i = 1, .., N$) characterized by the anticommutation relations

$$\{\eta_i, \eta_j\} = \eta_i \eta_j + \eta_j \eta_i = 0. \tag{2.23}$$

Importantly, one can formally define integration as

$$\int d\eta_i = 0, \quad \int d\eta_i \eta_i = 1, \quad \int d\eta_i d\eta_j \eta_i \eta_j = -1. \tag{2.24}$$

Fermion fields can then be defined by assigning to every spacetime point x two independent Grassmann variables Ψ_x and $\bar{\Psi}_x$. An instructive integral to perform is

$$\int d\bar{\Psi}_x d\Psi_x \exp\left(-m\bar{\Psi}_x\Psi_x\right) = \int d\bar{\Psi}_x d\Psi_x \left(1 - m\bar{\Psi}_x\Psi_x\right) = m \tag{2.25}$$

where we used the fact that the exponential terminates after the first order as $\Psi_x^2 = \bar{\Psi}_x^2 = 0$. Generalizing this integral to the whole spacetime lattice, results in expressions of the form

$$\int D\bar{\Psi} D\Psi \exp\left(-\bar{\Psi} M \Psi\right) \equiv \prod_x \int d\bar{\Psi}_x d\Psi_x \exp\left(-\bar{\Psi}_x M_{xy} \Psi_y\right) = \det M. \tag{2.26}$$

These types of Grassmann integrals can be used to construct discretized fermion actions.

One would like to approximate the Euclidean action of free Dirac fermions, whose action is given by

$$S_{\text{Dirac}}[\bar{\psi}, \psi] = \int d^4x\, \bar{\psi}(x) \left(\gamma^\mu \partial_\mu + m\right) \psi(x). \tag{2.27}$$

A straightforward, naive lattice discretization where the derivative is replaced by a finite difference is

$$S_{\text{naive}}[\bar{\Psi}, \Psi] = a^4 \sum_{x,\mu} \frac{1}{2a} \left(\bar{\Psi}_x \gamma_\mu \Psi_{x+e_\mu} - \bar{\Psi}_{x+e_\mu} \gamma_\mu \Psi_x\right) + \sum_x m\bar{\Psi}_x\Psi_x \tag{2.28}$$

where the Grassmann variables Ψ_x and $\bar{\Psi}_x$ implicitly have an additional spinor index in analogy to the continuum Dirac spinor which has four components in four spacetime dimensions. If one computes the lattice propagator for a fermion with momentum p^μ one obtains

$$\left\langle \bar{\Psi}_{-p} \Psi_p \right\rangle = \frac{1}{\frac{i}{a}\sum_\mu \gamma_\mu \sin\left(p^\mu a\right) + m}. \tag{2.29}$$

In the continuum limit one recovers the expected pole at $p^\mu = (m, 0, 0, 0)$. However, there are additional poles located at the corners of the Brillouin zone where the components of the momentum vector can take the value π/a such that $\sin(p^\mu a) = 0$. Therefore, there are extra states in the spectrum that are not present in the continuum theory and do not vanish in the continuum limit. This means that the naive lattice fermion action does not result in the accurate continuum theory. The appearance of these extra states in the lattice dispersion relation gives rise to $2^d - 1$ additional physical particles called fermion doublers, so in four spacetime dimensions there are 15 additional fermion flavors.

When regularizing a continuum theory on the lattice one tries to preserve as many symmetries of the continuum theory as possible. One of the strengths of lattice gauge theory is its ability to preserve gauge invariance. Moreover, although space-time symmetries are explicitly broken down to discrete translations and rotations on the lattice,

this is not a major issue as the full Poincaré symmetry of the continuum is recovered in the continuum limit $a \to 0$. Additionally, discrete symmetries such as parity and charge conjugation can be easily maintained on the lattice. The problem of fermion doubling as described above is related to preserving chiral symmetry on the lattice. The core of the problem is the Nielsen-Ninomiya theorem [25] which states that a chirally symmetric free fermion lattice action, which is local, translation invariant and real necessarily has fermion doubling. Hence, there are different formulations for fermions in lattice gauge theory corresponding to different violations of the conditions of the theorem. One can either prevent fermion doubling by explicitly breaking chiral symmetry. The most prominent formulation in this regard are Wilson fermions [7]. On the other hand, on can preserve chiral symmetry but partially break translational symmetry and reduce the number of additional fermion flavors emerging in the continuum but not remove them entirely. This description is known as staggered fermions [8]. Other fermion formulations include Ginsparg-Wilson fermions [26] or domain wall fermions [27].

To give an explicit example of how fermion doubling can be prevented, we present the formulation of Wilson fermions. The action is similar to the naive fermion action but includes an additional term to cure the fermion doubling:

$$\begin{aligned} S_W[\bar{\Psi}, \Psi] = a^4 \sum_{x,\mu} \frac{1}{2a} \left(\bar{\Psi}_x \gamma_\mu \Psi_{x+e_\mu} - \bar{\Psi}_{x+e_\mu} \gamma_\mu \Psi_x \right) + \sum_x m \bar{\Psi}_x \Psi_x \\ + a^4 \sum_{x,\mu} \frac{1}{2a} \left(2\bar{\Psi}_x \Psi_x - \bar{\Psi}_x \Psi_{x+e_\mu} - \bar{\Psi}_{x+e_\mu} \Psi_x \right). \end{aligned} \tag{2.30}$$

The fermion propagator corresponding to that action is slightly modified compared to the naive action:

$$\left\langle \bar{\Psi}_{-p} \Psi_p \right\rangle = \frac{1}{\frac{i}{a} \sum_\mu \gamma_\mu \sin\left(p^\mu a\right) + m + \sum_\mu \frac{2}{a} \sin^2\left(\frac{p^\mu a}{2}\right)}. \tag{2.31}$$

The additional term in the action, the Wilson term, has the effect of a momentum-dependent mass term. For small momenta the Wilson term is negligible, and thus does not significantly impact the dispersion of the physical fermion, particularly in the continuum limit. However, for the fermion doublers, which possess higher momenta, the Wilson term becomes non-negligible and assigns a mass to them of the same order as the lattice cutoff, 1/a. As a result, in the continuum limit, the fermion doublers are effectively removed from the theory's spectrum.

So far we have only considered free fermions. The same minimal coupling procedure in the continuum to create gauge-invariant interactions between gauge fields and fermions can also be applied on the lattice. The finite difference, approximating the derivative in the fermion action, corresponds on the lattice to fermion hopping to a neighboring site. The coupling procedure includes now the gauge field on the link in that hopping process. To give an explicit example for this coupling procedure we give the minimally coupled gauge-matter action for Wilson fermions which now involves a gauge field U_μ:

$$\begin{aligned} S_W[\bar{\Psi}, \Psi, U] = a^4 \sum_{x,\mu} \frac{1}{2a} \left(\bar{\Psi}_x \gamma_\mu U_{x,\mu} \Psi_{x+e_\mu} - \bar{\Psi}_{x+e_\mu} \gamma_\mu U^\dagger_{x,\mu} \Psi_x \right) + \sum_x m \bar{\Psi}_x \Psi_x \\ + a^4 \sum_{x,\mu} \frac{1}{2a} \left(2\bar{\Psi}_x \Psi_x - \bar{\Psi}_x U_{x,\mu} \Psi_{x+e_\mu} - \bar{\Psi}_{x+e_\mu} U^\dagger_{x,\mu} \Psi_x \right). \end{aligned} \tag{2.32}$$

The minimally coupled action above can be written in the very general form

$$S_W[\bar{\Psi}, \Psi, U] = \bar{\Psi}_x M_W[U]_{xy} \Psi_y. \tag{2.33}$$

We will use this general form of the gauge-matter action, which also includes other fermion formulations if the matrix $M[U]$ is adapted, to discuss the path-integral for the full lattice gauge theory which will also include a pure gauge contribution $S_{\text{pg}}[U]$ as discussed above.

In order to evaluate an observable $O[U]$ which only depends on the gauge field U_μ, one needs to evaluate the path integral

$$\begin{aligned} \langle O[U] \rangle &= \frac{\int D\bar{\Psi} D\Psi DU O[U] e^{-S_{\text{pg}}[U] - S[\bar{\Psi}, \Psi, U]}}{\int D\bar{\Psi} D\Psi DU e^{-S_{\text{pg}}[U] - S[\bar{\Psi}, \Psi, U]}} \\ &= \frac{\int DU O[U] \det M[U] e^{-S_{\text{pg}}[U]}}{\int DU \det M[U] e^{-S_{\text{pg}}[U]}} \end{aligned} \tag{2.34}$$

where we used in the second row the rules for Grassmann integrations from eq. (2.26). We can in principle still interpret the path-integral in terms of a probability distribution $p(U)$:

$$p(U) = \frac{\det M[U] e^{-S_{\text{pg}}[U]}}{\int DU \det M[U] e^{-S_{\text{pg}}[U]}}. \tag{2.35}$$

However, this is only possible if the determinant of M is real-valued. When one modifies the action to include a finite chemical potential for the fermions, this determinant becomes complex, $M[U] \in \mathbb{C}$. This results in the well-known sign-problem [12], and the Monte Carlo approximation fails to converge. Instead of converging to the true mean in $\mathcal{O}(1/\sqrt{N})$, the convergence becomes exponentially slow. This prevents the study of many interesting non-perturbative pheonomena in quantum field theories, in particular in quantum chromodynamics where it obstructs the understanding of parts of the phase diagram related to high baryon density.

It is thus natural to look for frameworks beyond the path-integral formalism to study lattice gauge theories. This leads us to the Hamiltonian formulation of lattice gauge theory.

2.3 Hamiltonian formulation of lattice gauge theory

At first sight, a Hamiltonian formulation of lattice gauge theory might not seem suitable as Lorentz symmetry is explicitly broken. However, it is eventually restored as the system approaches the continuum limit. Moreover, the Hamiltonian formalism can be directly connected to the path-integral formalism by the transfer matrix [28] which provides a natural way to define a Hamiltonian from a Lagrangian or an action.

Before we demonstrate this procedure for lattice gauge theory, we provide some intuition for the transfer matrix technique through its application to the simple example of a harmonic oscillator. The Lagrangian for a harmonic oscillator is given by

$$\mathcal{L}[x, \dot{x}] = \frac{1}{2}\dot{x}^2 - \frac{1}{2}\omega x^2 \tag{2.36}$$

We discretize the time direction and perform a Wick rotation (as presented in the previous section for convergence in the path-integral) to obtain a Euclidean action:

$$S_E[x,\dot{x}] = a\sum_i \left(\frac{1}{2}\left(\frac{x_{i+1}-x_i}{a}\right)^2 + \frac{\omega^2}{2}x_i^2\right) \tag{2.37}$$

where x_i denotes the coordinate of the harmonic oscillator on the i-th imaginary time slice. The path integral has the form

$$Z = \int \prod_i dx_i e^{-S_E[x,\dot{x}]}. \tag{2.38}$$

Since the action is local in (imaginary) time the exponential factor only connects neighboring time slices and can be written in the factorized way:

$$Z = \int \prod_i dx_i T_{x_{i+1}x_i}. \tag{2.39}$$

The matrix T is called the transfer matrix.

To connect to the Hamiltonian framework, one now constructs a Hilbert space. The basis of the Hilbert space can be naturally chosen as the one corresponding to the variables in which the path integral is formulated, here the position basis:

$$\hat{x}\,|x\rangle = x\,|x\rangle\,. \tag{2.40}$$

By considering the operator that generates translations in that basis, here the momentum operator $\hat{p}$,

$$e^{-i\hat{p}x_0}\,|x\rangle = |x+x_0\rangle\,, \tag{2.41}$$

one obtains a pair of canonical variables, $[\hat{x},\hat{p}] = i$. In this Hilbert space one can define the transfer operator $\hat{T}$ via the matrix elements $T_{x_{i+1}x_i}$ as

$$T_{x_{i+1}x_i} = \langle x_{i+1}|\hat{T}|x_i\rangle \tag{2.42}$$

For a lattice that is finite in the time direction with N time slices and periodic boundary conditions one can therefore describe the path-integral with the transfer operator as

$$Z = \mathrm{Tr}\big(\hat{T}^N\big) \tag{2.43}$$

The path-integral formulation is recovered from the equation above by inserting N times the identity represented in the position basis. If we take the continuum limit in the imaginary time direction, $a \to 0$, the path-integral can be related to a Hamiltonian by

$$Z = \mathrm{Tr}(e^{-\beta H}). \tag{2.44}$$

This allows to identify the linear term in a when taking the logarithm of the transfer operator as the Hamiltonian:

$$\hat{T} = \exp\left(-aH + \mathcal{O}(a^2)\right). \tag{2.45}$$

The transfer matrix for the harmonic oscillator is easily constructed by rewriting the kinetic term in the action as

$$\begin{aligned}\hat{T} &= \int dx_0\, e^{-\frac{1}{2a}x_0^2} e^{-i\hat{p}x_0} e^{-a\omega^2\hat{x}^2/2} \\ &= \sqrt{2\pi a}\, e^{-a\hat{p}^2/2} e^{-a\omega^2\hat{x}^2/2} \\ &= \sqrt{2\pi a}\, e^{-aH+\mathcal{O}(a^2)}\end{aligned} \tag{2.46}$$

with $H = \frac{1}{2}\left(\hat{p}^2 + \omega^2 \hat{x}^2\right)$ the standard Hamiltonian for the harmonic oscillator.

We now turn to lattice gauge theory. For simplicity, we restrict ourselves to the pure gauge sector of compact QED. First, it is necessary to partially fix the gauge. In the path-integral formalism this was not required since all integrals over the gauge fields are over a compact domain as the gauge group is compact. Hence, no infinites arise from integrating over all gauges. In a Hamiltonian framework, due to the need to quantize, we need to fix the gauge. The appropriate choice, as will become clear in a moment, is the temporal gauge $A_0 = 0$, respectively $U_0 = 1$. Thus, from now on we will label the unfixed gauge fields along the spatial directions as U_i ($i = 1, 2, 3$). We also explicitly separate the (imaginary) time dependence τ from the spatial dependence $\vec{x}$, denoting gauge links as $U_i(\tau, \vec{x})$. Moreover, we will use the description of $U(1)$ elements in terms of the compact angles $\theta_i(\tau, \vec{x}) \in [0, 2\pi)$,

$$U_i(\tau, \vec{x}) = e^{i\theta_i(\tau, \vec{x})}. \tag{2.47}$$

If we write the Euclidean action for compact QED, as given in eq. (2.16), in the temporal gauge, we obtain

$$S_{\text{cQED}}[\theta_i] = \frac{a_0}{ag^2} \sum_{\mathbf{p},\text{spacelike}} \left(1 - \cos(\theta_{\mathbf{p}})\right) + \frac{a}{a_0 g^2} \sum_{\tau,\vec{x},i} \left(1 - \cos\left(\theta_i(\tau, \vec{x}) - \theta_i(\tau + a_0, \vec{x})\right)\right) \tag{2.48}$$

where a_0 is the lattice spacing in time direction and a in space directions. We choose them anisotropically as we want to take the limit $a_0 \to 0$ at the end. This splits the action into two parts. The first part involves spacelike plaquettes which only contain gauge fields on spatial links and has the same form as the original action in eq. (2.16) without gauge fixing. The second part involves timelike plaquettes that contain two spatial links and two links in the time direction. Since the links in time direction are fixed to the identity due to the temporal gauge, only two unfixed spatial gauge fields remain.

We now want to identify the transfer operator $\hat{T}_{\text{cQED}}$ in analogy to the harmonic oscillator example above:

$$Z = \int D\theta \, e^{-S_{\text{cQED}}[\theta_i]} = \text{Tr}\left(\hat{T}_{\text{cQED}}^N\right). \tag{2.49}$$

For that we first construct the Hilbert space, considering for the moment only the Hilbert space of a single link. We choose, in analogy to the position basis, the group element basis $\{|U\rangle\}$ with $U \in U(1)$, respectively $\{|\theta\rangle\}$ with $\theta \in [0, 2\pi)$, such that:

$$\begin{aligned} \hat{\theta}\,|\theta\rangle &= \theta\,|\theta\rangle \\ \hat{U}\,|U\rangle &= U\,|U\rangle\,. \end{aligned} \tag{2.50}$$

Similarly to the momentum operator, one can define an operator $\hat{E}$ that generates shifts in θ such that

$$\begin{aligned} e^{-i\hat{E}a}\,|\theta\rangle &= |\theta + a\rangle \pmod{2\pi} \\ e^{-i\hat{E}a}\left|U = e^{i\theta}\right\rangle &= \left|U' = e^{i(\theta+a)}\right\rangle. \end{aligned} \tag{2.51}$$

$\hat{\theta}$ and $\hat{E}$ fulfill the canonical commutation relations $\left[\hat{\theta}, \hat{E}\right] = i$. To extend the above discussion from a single link Hilbert space $\mathcal{H}_{\mathbf{x},i}$ to the gauge field Hilbert space $\mathcal{H}_g$ for the whole lattice, we construct a tensor product of all spatial links,

$$\mathcal{H}_g = \bigotimes_{\mathbf{x},i} \mathcal{H}_{\mathbf{x},i}. \tag{2.52}$$

Note that the tensor product only involves spatial links $\mathbf{x}, i$ with $i = 1, 2, 3$ as the temporal links were eliminated by gauge fixing. We can write down the more general commutation relations for gauge field operators on the whole lattice:

$$\begin{aligned}[\hat{\theta}_{\mathbf{x},i}, \hat{E}_{\mathbf{y},j}] &= i\delta_{\mathbf{xy}}\delta_{ij} \\ [\hat{U}_{\mathbf{x},i}, \hat{E}_{\mathbf{y},j}] &= -\hat{U}_{\mathbf{x},i}\delta_{\mathbf{xy}}\delta_{ij}.\end{aligned} \tag{2.53}$$

From now on we will sometimes use the shorthand notation $|\theta\rangle \equiv \otimes_{\mathbf{x},\mathbf{i}} |\theta_{\mathbf{x},i}\rangle$ to denote the state of the gauge field on the whole lattice in the group element basis.

The transfer matrix can be written as

$$\begin{aligned}\langle\theta'|\hat{T}_{\text{cQED}}|\theta\rangle = \exp&\left(-\frac{a_0}{ag^2}\sum_{\mathbf{p},\text{spacelike}}\left(1-\cos\left(\theta_{\mathbf{p}}\right)\right)\right)\times \\ &\exp\left(-\frac{a}{a_0 g^2}\sum_{\vec{x},i}\left(1-\cos\left(\theta_i(\vec{x})-\theta'_i(\vec{x})\right)\right)\right)\end{aligned} \tag{2.54}$$

We can now, in analogy to the harmonic oscillator example, use the momentum operator, here the electric field operator, to express the transfer operator as

$$\begin{aligned}\hat{T}_{\text{cQED}} = \exp&\left(-\frac{a_0}{ag^2}\sum_{\mathbf{p},\text{spacelike}}\left(1-\cos\left(\hat{\theta}_{\mathbf{p}}\right)\right)\right)\times \\ &\prod_{\mathbf{x},i}\int da_{\mathbf{x},i}\,\exp\left(-i\hat{E}_{\mathbf{x},i}a_{\mathbf{x},i}\right)\exp\left(-\frac{a}{a_0 g^2}\sum_{\mathbf{x},i}\left(1-\cos\left(a_{\mathbf{x},i}\right)\right)\right)\end{aligned} \tag{2.55}$$

If $a_0 \to 0$ the integrals over $a_{\mathbf{x},i}$ are dominated by $a_{\mathbf{x},i}$ near the maximum at $a_{\mathbf{x},i} = 0$, thus allowing to Taylor expand,

$$\cos\left(a_{\mathbf{x},i}\right) = 1 - \frac{1}{2}(a_{\mathbf{x},i})^2 + \mathcal{O}\left((a_{\mathbf{x},i})^4\right), \tag{2.56}$$

and approximate the integrals as

$$\begin{aligned}&\prod_{\mathbf{x},i}\int da_{\mathbf{x},i}\exp\left(-i\hat{E}_{\mathbf{x},i}a_{\mathbf{x},i}\right)\exp\left(-\frac{a}{a_0 g^2}\sum_{\mathbf{x},i}\left(1-\cos\left(a_{\mathbf{x},i}\right)\right)\right) \\ \underset{a_0\to 0}{\to}&\prod_{\mathbf{x},i}\int da_{\mathbf{x},i}\exp\left(-i\hat{E}_{\mathbf{x},i}a_{\mathbf{x},i}\right)\exp\left(-\frac{a}{2a_0 g^2}\sum_{\mathbf{x},i}a^2_{\mathbf{x},i}\right) \sim e^{-a_0\frac{g^2}{2a}\sum_{\mathbf{x},i}E^2_{\mathbf{x},i}}\end{aligned} \tag{2.57}$$

Reading off the Hamiltonian as the first order in a_0 in the logarithm of $\hat{T}_{\text{cQED}}$, results in the well-known Kogut-Susskind Hamiltonian [8]:

$$H_{\text{cQED}} = \frac{g^2}{2a}\sum_{\mathbf{x},i}\hat{E}^2_{\mathbf{x},i} + \frac{1}{g^2 a}\sum_{\mathbf{p}}\left(1-\cos\left(\hat{\theta}_{\mathbf{p}}\right)\right) \tag{2.58}$$

The transfer matrix method shows that the Euclidean path integral formulation and the Hamiltonian formalism are intimately related. At first sight this was not necessarily obvious as the Hamiltonian is not Lorentz invariant. Therefore, computations can be performed equivalently in each framework.

A few comments are in order regarding gauge transformations. In the beginning, we fixed the temporal gauge $A_0 = 0$ which eliminated time-dependent gauge transformations. However, there is a residual gauge freedom corresponding to space-dependent gauge transformations. Intuitively, one can think about it with the analogy of the photon, which is described by a vector field A_μ having four components. However, there are only two physical degrees of freedom, the two transverse polarizations. After having eliminated the timelike component by $A_0 = 0$, there is still an unphysical part present in form of the longitudinal component of the photon. The lattice gauge theory analogue that restricts our theory to the physical, transverse subspace is the *Gauss law* which needs to be fulfilled for states to be physical. For the pure gauge sector, it is defined by the Gauss law operators $G_{\mathbf{x}}$:

$$\hat{G}_{\mathbf{x}} = \sum_{i=1}^{3} \left(\hat{E}_{\mathbf{x},i} - \hat{E}_{\mathbf{x}-\mathbf{e}_i,i} \right). \tag{2.59}$$

Physical states $|\text{phys}\rangle$ must be eigenstates of all Gauss law operators

$$\hat{G}_{\mathbf{x}} |\text{phys}\rangle = q_{\mathbf{x}} |\text{phys}\rangle \quad \forall \mathbf{x} \tag{2.60}$$

where eigenvalues $q_{\mathbf{x}}$ correspond to different static charge configurations.

The transfer matrix method can be performed in an analogous way for the Wilson action of lattice QCD, $S_{\text{QCD}}[U_\mu]$, given in eq. (2.17). The Hilbert space is constructed in a similar way with the $U(1)$ gauge group replaced by $SU(3)$. The shifts, or rather roations on $SU(3)$, are generated by the generators T^a of $SU(3)$ which allows to define conjugate momentum operators analogous to the electric operator $\hat{E}$ for the $U(1)$ case. The resulting Hamiltonian formulation for the pure gauge sector of lattice QCD is

$$H_{\text{QCD}} = \frac{g^2}{2a} \sum_{\mathbf{x},i} L^2_{\mathbf{x},i} - \frac{1}{g^2 a} \sum_{\mathbf{p}} \text{Tr} \left(\hat{U}_{\mathbf{p}} + \hat{U}^\dagger_{\mathbf{p}} \right) \tag{2.61}$$

where L^2 corresponds to the quadratic Casimir operator for $SU(3)$.

The transfer matrix method can also be used to connect the path-integral and the Hamiltonian formulation in the presence of dynamical fermions. The discussion of fermions on the lattice in the previous section applies in the same way to the Hamiltonian framework with the slight difference that the severity of the fermion doubling problem is reduced as the dimensionality is reduced from $D = d + 1$ to d.

In the following, we will focus on one specific formulation of lattice fermions, namely staggered fermions as that formulation will be used quite extensively throughout the thesis. In the staggered fermion discretization, each lattice point is associated with a single fermionic degree of freedom, as opposed to the four degrees of freedom associated with a Dirac spinor. The staggered fermions have a reduced symmetry compared to the continuum Dirac basis, but still retain a residual chiral symmetry, which allows to study interesting observables such as chiral condensates. By using a staggered structure, such that the model is only invariant under shifts by two lattice sites, the fermion doubling problem can be reduced. In one dimensions it can even be resolved completely.

We consider staggered fermions in the context of compact QED, whose Hamiltonian for the pure gauge sector is given in eq. (2.58). Upon coupling to several flavors ψ_α of

staggered fermions, the Hamiltonian takes the form:

$$\begin{aligned} H =& \frac{g^2}{2a} \sum_{\mathbf{x},i} \hat{E}^2_{\mathbf{x},i} + \frac{1}{ag^2} \sum_{\mathbf{p}} \left(1 - \cos\left(\hat{\theta}_{\mathbf{p}}\right)\right) \\ & - t \sum_{\mathbf{x},i,\alpha} \psi^\dagger_{\mathbf{x},\alpha} e^{i\hat{\theta}_{\mathbf{x},i}} \psi_{\mathbf{x}+\mathbf{e}_i,\alpha} + h.c. \\ & + \sum_{\mathbf{x},\alpha} \left(m(-1)^{\mathbf{x}} + \mu_\alpha\right) \psi^\dagger_{\mathbf{x},\alpha} \psi_{\mathbf{x},\alpha} \end{aligned} \tag{2.62}$$

It includes a staggered mass term with mass m and chemical potentials μ_α for the different fermion flavors ψ_α. Due to the appearance of dynamical charges, the Gauss law operator for pure gauge in eq. (2.59) is modified as

$$\hat{G}_{\mathbf{x}} = \sum_i \left(\hat{E}_{\mathbf{x},i} - \hat{E}_{\mathbf{x}-\mathbf{e}_i,i}\right) - \hat{Q}_{\text{stag},\mathbf{x}} \tag{2.63}$$

with the staggered charge $\hat{Q}_{\text{stag},\mathbf{x}}$ defined as

$$\hat{Q}_{\text{stag},\mathbf{x}} = \sum_{\alpha=1}^{N_f} \left(\psi^\dagger_{\mathbf{x},\alpha} \psi_{\mathbf{x},\alpha} - \frac{1}{2}(1 + (-1)^{\mathbf{x}})\right). \tag{2.64}$$

This Hamiltonian provides the possibility due to the finite chemical potentials to study regimes which are in a Euclidean Monte Carlo simulation affected by the sign-problem. Thus, this formulations provides in principle the possibility to use Hamiltonian many-body methods to overcome the sign-problem, as will be discussed in the next section.

2.4 Existing methods and limitations

Having discussed the Hamiltonian framework, we proceed to examine different techniques that have been employed within it and the difficulties that emerge when working in higher dimensions, which is the primary focus of this thesis. Two types of Hamiltonian methods are distinguished: quantum simulation methods which are based on recent developments in building powerful quantum devices, and classical methods based on the variational principle that involve constructing efficient ansatz states to capture the relevant physical behavior of the model.

2.4.1 Quantum simulation

We begin with an exploration of quantum simulation methods, discussing the basic idea and various schemes that can be employed to simulate lattice gauge theories. The objective of quantum simulation is to achieve a better understanding of intricate physical quantum systems that are computationally challenging or unfeasible to solve on classical computers. In the 1980's, Richard Feynman laid the foundation for this interdisciplinary field, where he predicted the enormous potential of precisely controllable quantum systems to solve complex quantum physics problems. Quantum simulation has diversified into various fields, including quantum optics, condensed matter physics and high-energy physics, which will be our focus here. Researchers are investigating

and utilizing different systems for quantum simulation, such as ion chains, superconducting circuits or ultracold atoms in optical lattices [29].

Quantum simulations can be divided based on their simulation scheme into analog and digital quantum simulations. An analog quantum simulator is a physical system that can mimic the behavior of the quantum system that one wants to study by engineering the interactions between its constituent particles. In other words, an analog quantum simulator does not implement a specific quantum algorithm but rather replicates the behavior given by the full Hamiltonian one is interested in.

On the other hand, digital simulation schemes simulate the Hamiltonian in a sequential order which is based on the Trotter formula [30]. For a Hamiltonian consisting of two parts, $H = H_1 + H_2$, the unitary evolution can be rewritten as

$$e^{-i(H_1+H_2)t} = \lim_{N\to\infty} \left(e^{-iH_1 t/N} e^{-iH_2 t/N}\right)^N . \tag{2.65}$$

Quantum devices that can implement H_1 and H_2 separately, can in this way also approximate the behavior of the full Hamiltonian H. A quantum device that can implement a universal set of Hamiltonians, more specifically that can perform an arbitrary quantum operation on a set of qubits, is called a quantum computer [31]. Quantum computers require, due to the sensitivity of quantum devices to noise and decoherence, an error correction procedure, called quantum error correction, crucial for building large-scale, fault-tolerant quantum computers [32]. However, the current capabilities of quantum devices are often summarized in the term NISQ, standing for noisy, intermediate-scale quantum era [33]. They contain on the order of 100 qubits and are not yet advanced enough for fault-tolerance.

Current experiments aiming for quantum simulations of lattice gauge theories are thus mainly based on analog quantum simulation schemes. The implementation of quantum simulators has been demonstrated in one dimension using trapped ions and ultracold atoms [34–38].

The problems in higher dimensions are related to the magnetic interaction term in the Hamiltonian, given for compact QED as (see eq. (2.58)):

$$H_B = \frac{1}{g^2 a} \sum_{\mathbf{p}} \mathrm{Re}\left(1 - U_{\mathbf{p}}\right) \tag{2.66}$$

where the plaquette interactions $U_{\mathbf{p}} = U_1 U_2 U_3^\dagger U_4^\dagger$ involves all four gauge fields around the plaquette. Such four-body interactions are difficult to implement in quantum simulators or quantum computers as typically two-body interactions or two-qubit gates are available. One can thus obtain the four-body interactions effectively in perturbation theory but this allows typically only to reach low coupling strength [39, 40]. An alternative is to introduce auxiliary degrees of freedom which allows to mediate the four-body interactions at higher coupling strength but this requires more experimental effort [4, 41, 42].

Another problem for quantum simulation techniques is that quantum platforms, in particular the ones aiming to build quantum computers, are based on a local Hilbert space of dimension two, representing a qubit. This is suitable for studying many models in condensed matter systems, as the degrees of freedom are often spins. However, in high-energy physics the local Hilbert space of the gauge field is infinite-dimensional, posing a significant challenge for quantum simulators. One can aim at building quantum devices that have a larger local Hilbert space, but ultimately some kind of truncation is required. This can either mean to truncate the Hilbert space in the Hamiltonian

formulation presented in the previous section, or define a new Hamiltonian formulation of lattice gauge theories that is from the beginning based on finite-dimensional Hilbert spaces, such as quantum link models [43–46]. Both approaches will require an extrapolation procedure to a limit with an infinite-dimensional Hilbert space. Classical, variational methods, where the infinite-dimensional gauge field Hilbert space can in principle be captured, can provide valuable assistance in this regard, allowing to benchmark different truncation methods for quantum simulators directly in the Hamiltonian framework.

2.4.2 Variational methods

Another way to overcome the issue of exponential scaling in computational methods is through variational approaches. Rather than examining the entire Hilbert space, these methods consider a parameterized subset of the space, with the aim of finding the closest approximation to the ground state (variational states can also be used to study real-time dynamics and other phenomena). Ansatz states, which are parameterized by a set of parameters γ, are optimized to minimize the energy expectation value, i.e.

$$\min_{\gamma} E_{\gamma} = \min_{\gamma} \frac{\langle \Psi_{\gamma} | H | \Psi_{\gamma} \rangle}{\langle \Psi_{\gamma} | \Psi_{\gamma} \rangle}. \tag{2.67}$$

The variational principle ensures that the approximated energy can never be lower than the actual ground state. The quality of the approximation of the minimized variational ground state energy to the exact ground state is heavily reliant on the choice of ansatz states. Hence, it is crucially important, to heavily benchmark a variational method in regimes where the ground state is known (e.g. for very small system sizes or regimes where other methods give reliable results).

In the following, we will discuss one common type of variational ansatz, namely tensor networks, which have been successfully applied in many areas of many-body physics. In the context of lattice gauge theory, they have shown great results in particular in the study of one-dimensional lattice gauge theories, even in regimes which are otherwise affected by the sign-problem.

We will therefore focus on their one-dimensional version, matrix product states (MPS). Similarly as quantum simulators, they are constructed for theories with a local Hilbert space with finite dimension d. We will therefore denote it by a spin variable s_i. A general state in that basis can be defined as

$$|\Psi\rangle = \sum_{s_1,..,s_N} c_{s_1..s_N} |s_1..s_N\rangle \,. \tag{2.68}$$

The resources to describe such a state exactly scale exponentially with system size. An MPS approximates the coefficients $c_{s_1..s_N}$ as

$$|\Psi_{MPS}\rangle = \sum_{s_1,..,s_N} \sum_{a_1,..,a_N} A^{s_1}_{a_1 a_2} A^{s_2}_{a_2 a_3} .. A^{s_{N-1}}_{a_{N-1} a_N} A^{s_N}_{a_N a_1} |s_1..s_N\rangle \tag{2.69}$$

where the matrices $A^{s_i}_{a_i a_{i+1}}$ define the MPS, hence the name matrix product states. We assumed periodic boundary conditions for the matrices A. The upper index s_i corresponds to the physical index, having d entries. The virtual indices a_i have D entries and are only used to construct the MPS as they are summed over, often referred to as

contraction of the MPS. The parameter D is called the bond dimension, quantifying the extent of variational parameters that one wants to include, which can in turn be related to the entanglement properties of the state $|\Psi_{MPS}\rangle$. The scaling of the number of parameters with system size is $\mathcal{O}(NdD^2)$ instead of a scaling of $\mathcal{O}(d^N)$ for the number of coefficients $c_{s_1..s_N}$. This demonstrates the general concept in variational methods of trying to describe the exponentially many parameters of a state in terms of a set of physically relevant parameters, that only scale polynomially with system system size. Further details on matrix product states and tensor networks can be found in [47].

The way in which matrix product states were used for one-dimensional lattice gauge theories was by first reformulating the lattice gauge theory in terms of gauge-invariant variables. The local Gauss' law constraints for the physical subspace of the Hilbert space allow in one dimension to completely fix the gauge field in terms of the charge configuration. One remains with a purely fermionic theory that exhibits long-range interactions. Using a Jordan-Wigner transformation, one can map the fermions to spins, resulting in a formulation very suitable for matrix product states [17].

In higher dimensions such a reformulation will only be able to reduce the number of gauge fields but not eliminate them completely, as will be shown in chapter 3. This reestablishes the requirement to deal with the infinite-dimensional gauge field Hilbert space in two and more spatial dimensions, making higher-dimensional lattice gauge theories qualitatively different to one dimensional theories.

Hence, for higher-dimensional lattice gauge theories new variational methods are desirable that do not require any kind of truncation, which will be one of the central goals of this thesis.

3 Gauge-redundancy free formulations of compact QED with dynamical fermions in higher dimensions

3.1 Motivation

Gauge theories form a fundamental aspect of modern physics, serving as the mechanism for mediating interactions in the standard model of particle physics [5, 48]. Despite their crucial role in physics, they pose a significant challenge due to their strongly coupled nature that necessitates the use of non-perturbative techniques. Lattice gauge theories [7, 8] have been a useful tool for studying gauge theories for decades by discretizing them on a lattice, thus providing a non-perturbative framework for numerical simulations using quantum Monte Carlo. The numerical computations are performed in a Wick-rotated, Euclidean spacetime. There are two significant restrictions related to this approach. One such limitation is the inability to observe real-time dynamics directly in Euclidean spacetime. The other limitation is the sign-problem [12] that obstructs the study of various crucial physical phases in gauge theories such as quantum chromodynamics with a finite chemical potential [49, 50].

As discussed in section 2, lattice gauge theories can be formulated either on a discretized spacetime or a discretized space [7, 8]. The former is suitable for the path integral, action formalism, which is widely used for Monte-Carlo computations [11]. The latter is better suited for a Hamiltonian approach.

Over the past decade, there has been increased interest in Hamiltonian formulations of lattice gauge theories, partly due to the development of new techniques in quantum many-body physics that may help overcome the limitations of the action formalism. One such technique involves quantum simulation [14, 29], which maps lattice gauge theories into controllable quantum devices, such as cold atoms, trapped ions, or superconducting qubits, enabling laboratory experiments that could potentially overcome the difficulties posed by strongly coupled nature and the sign-problem [15, 35–38, 51–53]. Classical computation with variational ansatz states, such as tensor networks, is another approach that aims to find efficiently computable classes of states that capture the relevant features of the theory [15, 53, 54].

Gauge theories impose local constraints, known as Gauss' laws, on physical states. These constraints have important implications for both quantum simulations and classical computations with variational states. In quantum simulations, experimental errors must be carefully controlled to prevent violations of gauge invariance [55, 56]. In classical computations, the local constraints must be incorporated into the variational ansatz, which can make it more challenging to find suitable ansatz states. While these constraints can be helpful in some cases for constructing variational states, they

generally make the process more difficult.

One way to avoid issues related to local constraints in gauge theories is to formulate them directly in terms of gauge-invariant variables. This approach would ensure that gauge invariance is robust against experimental errors in quantum simulations and would provide a wider class of ansatz states for variational computations. In addition, the required computational resources related to the full Hilbert space are reduced to the physical subspace. It would be advantageous to find gauge-invariant formulations that preserve the original symmetries as much as possible. Previous works in this area have primarily focused on $(1+1)$-dimensional lattice gauge theories with dynamical matter and pure gauge theories in $2+1$ dimensions [57–61]. The local gauge constraints have also been used to eliminate the matter degrees of freedom from the theory, including in the Abelian Higgs model [62, 63], where unitary gauge fixing is used, as well as in recent extensions to fermionic scenarios [64, 65].

The work presented in this chapter aims at extending these gauge-redundancy-free descriptions to higher dimensions including dynamical matter for compact quantum electrodynamics while preserving most of the symmetries of the original theory, in particular translational invariance. We demonstrate a method of expressing compact QED in two and three space dimensions using dual plaquette variables, which helps to reduce the number of local constraints. This method allows for the removal of all local constraints in two space dimensions, and for the constraints to not involve matter in three dimensions. It utilizes a decomposition of lattice vector fields into longitudinal and transverse parts, enabling the decoupling of matter from the constraints by a unitary transformation. The gauge-invariant matter degrees of freedom after the unitary transformation interact according to a lattice analogue of Coulomb's law.

The content of this chapter is based on Ref. [1].

3.2 Executive summary

Hamiltonian methods, both classical and quantum simulations, for lattice gauge theory, face the problem of dealing with the local gauge constraints, the Gauss' law constraints. Gauge-invariant formulations can help on the classical side by enlarging the set of possible classes of variational states and on the quantum simulation side by removing the need for making sure that gauge invariance is not broken experimentally.

We extend the range of gauge-invariant formulations to higher-dimensional theories with dynamical matter, whereas previous gauge-invariant descriptions were formulated either in one dimension or, when considering higher dimensions, were focused on the pure gauge theory without dynamical fermions. The presented method can eliminate gauge-redundancies in compact quantum electrodynamics coupled to dynamical matter in two and three spatial dimensions, while preserving translational invariance.

In a first step, the Hamiltonian undergoes a unitary transformation to a rotating frame, in which the matter degrees of freedom become decoupled from the gauge constraints. The intuition behind this unitary transformation lies in the structure of the Gauss law, which involves charges on lattice sites and gauge fields on adjacent links. By examining this relation, it becomes apparent that the longitudinal part of the gauge field is completely determined by the charge configuration. The longitudinal component on the lattice can be defined in similar way to the continuum version where it is given by the Helmholtz decomposition. The separation of a vector field on the lattice, i.e. a field defined on the links of a lattice, into a longitudinal (curl-free) part and a transverse (divergence-free) component will be a key ingredient of the gauge-invariant formulation.

Even though the longitudinal part of the gauge field is not dynamical, it still appears in several places in the Hamiltonian. Note that in contrast to static charges, incorporating dynamical matter poses an additional challenge due to the presence of gauge-matter interactions that involve the longitudinal component of the gauge field, whereas only the transverse component contributes to the magnetic Hamiltonian. The frame the unitary transformation rotates to is therefore one in which the longitudinal part of the gauge field vanishes in the Hamiltonian, i.e. we rotate to a frame where Coulomb gauge holds in the physical subspace. Such a transformation is not required in pure gauge theories.

After the transformation the Hamiltonian only depends on the transverse part of the gauge field. This alone, however, is not useful for a gauge-invariant description as the definition of transverse degrees of freedom is non-local in terms of the original degrees of freedom.

Therefore, in a second step, it is shown how the transverse degrees of freedom can be represented by dual variables residing on the plaquettes. We present two versions of such a dual formulation. The intuition is again similar to the continuum where transverse components of a vector field can be represented as curls of the vector potential. The lattice analogue is a plaquette field, for which one can define a lattice curl, such that the tranverse component on a link can be expressed by the difference between the plaquette field corresponding to the two neighboring plaquettes of that link. One can show that these plaquette variables have similar properties as the link variables w.r.t. the Hilbert space and commutation relations. Formulating the Hamiltonian in terms of these new plaquette variables leads to a gauge-invariant description in two dimensions. In three dimensions, these plaquette variables still have to fulfill some

constraints related to all plaquettes of the same cube. The matter degrees of freedom, however, are completely gauge-invariant.

The rest of the chapter is structured as follows: in section 3.3, we provide some lattice vector calculus that is required for our procedure, in particular how the lattice analogue of the Helmholtz decomposition is constructed. In section 3.4, we explain in more detail the unitary transformation that enables the separation of the longitudinal and transverse components of the gauge field, eliminating the matter from the constraints. In section 3.5, we demonstrate in two dimensions how to express the transformed model using dual variables and describe the interactions between the dual, gauge-invariant variables. In section 3.6, we discuss the extension of the model to three spatial dimensions and compare it to the two-dimensional case, highlighting the differences between them.

3.3 Lattice vector calculus for compact QED

We focus for the moment on $(2+1)$-dimensional compact QED with dynamical matter, i.e. a compact $U(1)$ gauge field coupled to some dynamical fermions, such as in Kogut and Susskind's formulation [8] as presented in section 2.3. The discussion is applicable to both periodic and open boundary conditions. In the following, we will use an $N \times N$ lattice sites with periodic boundary conditions. Any differences that arise with open boundary conditions, where the lattice is made up of $(N+1) \times (N+1)$ sites, corresponding to $N \times N$ plaquettes, will be mentioned throughout the chapter.

3.3.1 The Lattice

The matter degrees of freedom reside on the sites of the lattice, labeled for periodic boundary conditions by integers $\mathbf{x} = (x_1, x_2) \in \{0, .., N-1\}^2$ (for open boundary conditions $(x_1, x_2) \in \{0, .., N\}^2$), while the gauge fields - on the links, labeled by the site $\mathbf{x}$ from which they emanate and a direction $i = 1, 2$ to which they extend. The link labeled by $\mathbf{x}, i$ connects the site $\mathbf{x}$ with the site $\mathbf{x} + \hat{\mathbf{e}}_i$, where $\hat{\mathbf{e}}_i$ is a unit vector pointing in the positive i direction.

We consider three different kinds of lattice fields: Fields $f(\mathbf{x})$, residing on the lattice sites $\mathbf{x}$ (such as matter fields or scalar fields), vector fields $\mathbf{F}(\mathbf{x})$, whose components $F_i(\mathbf{x})$ reside on the links of the lattice (such as vector potentials and electric fields) and pseudovector fields $B(\mathbf{x})$ (such as the magnetic field), residing on the plaquettes (denoted by the site $\mathbf{x}$ at the bottom left corner).

We define difference operators - forward

$$\Delta_i^{(+)} f(\mathbf{x}) = f(\mathbf{x} + \hat{\mathbf{e}}_i) - f(\mathbf{x}) \tag{3.1}$$

and backward

$$\Delta_i^{(-)} f(\mathbf{x}) = f(\mathbf{x}) - f(\mathbf{x} - \hat{\mathbf{e}}_i) \tag{3.2}$$

(acting similarly on vector and pseudovector fields). Out of those, we can construct the lattice versions of the central differential operators in vector calculus:

1. The *gradient* of a scalar field on the lattice sites is a vector field on the links, involving the field's value on the links ends:

$$(\nabla f(\mathbf{x}))_i = \Delta_i^{(+)} f(\mathbf{x}) = f(\mathbf{x} + \hat{\mathbf{e}}_i) - f(\mathbf{x}) \tag{3.3}$$

2. The *divergence* of a vector field on the links is a scalar field on the lattice sites. Its value on a site involves the values of the vector components of all the links surrounding it:

$$\nabla \cdot \mathbf{F}(\mathbf{x}) = \Delta_i^{(-)} F_i(\mathbf{x}) = \sum_i \left(F_i(\mathbf{x}) - F_i(\mathbf{x} - \hat{\mathbf{e}}_i)\right) \tag{3.4}$$

3. The *Laplacian* of a scalar field or a component of another field is given by combining the gradient and the divergence (see Fig. 3.1):

$$\nabla^2 f(\mathbf{x}) = \Delta_i^{(-)} \Delta_i^{(+)} f(\mathbf{x}) = \sum_i \left(f(\mathbf{x} + \hat{\mathbf{e}}_i) + f(\mathbf{x} - \hat{\mathbf{e}}_i)\right) - 4f(\mathbf{x}) \tag{3.5}$$

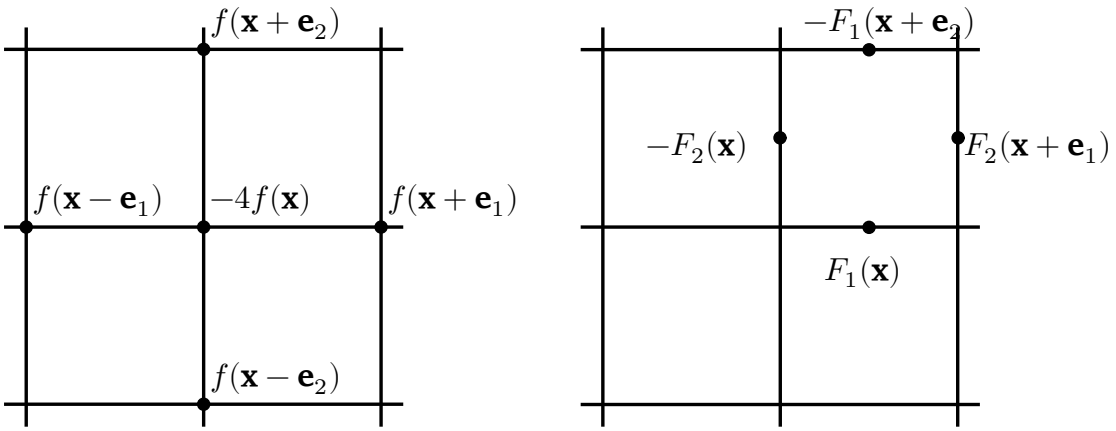

Figure 3.1: Illustration of the lattice Laplacian $\nabla^2 f(\mathbf{x})$ of a scalar field $f(\mathbf{x})$ (left) and the lattice curl $\nabla\times\mathbf{F}(\mathbf{x})$ of a vector field $F_i(\mathbf{x})$ (right). The lattice Laplacian at a site $\mathbf{x}$ involves all adjacent sites. The resulting field resides again on the sites. The lattice curl transforms a vector field, a field on the links, into a field on the plaquettes, where the plaquette is labeled by the site at its bottom left corner.

4. The *curl* of a vector field gives rise to a pseudovector residing on the plaquettes (dual lattice sites) as illustrated in Fig. 3.1,

$$\nabla \times \mathbf{F}(\mathbf{x}) = \epsilon_{ij}\Delta_i^{(+)} F_j(\mathbf{x}) \tag{3.6}$$

5. The *curl* of a pseudovector field on the plaquettes gives rise to a vector field on the links,

$$(\nabla \times L(\mathbf{x}))_i = \epsilon_{ij}\Delta_j^{(-)} L(\mathbf{x}) \tag{3.7}$$

where ϵ_{ij} is completely antisymmetric.

As in the continuum, each vector field $\mathbf{F}(\mathbf{x})$ may be decomposed into the sum of *longitudinal* and *transverse* parts, $\mathbf{F}^L(\mathbf{x})$ and $\mathbf{F}^T(\mathbf{x})$ respectively,

$$\mathbf{F}(\mathbf{x}) = \mathbf{F}^L(\mathbf{x}) + \mathbf{F}^T(\mathbf{x}) \tag{3.8}$$

The longitudinal part is the gradient of some scalar function $f(\mathbf{x})$, and therefore, using the definitions above and similar to the continuous case, it is curl-free:

$$\mathbf{F}^L(\mathbf{x}) = -\nabla f(\mathbf{x}) \iff \nabla \times \mathbf{F}^L(\mathbf{x}) = 0 \tag{3.9}$$

Similarly, the transverse part is the curl of some pseudovector, and its divergence vanishes:

$$\mathbf{F}^T(\mathbf{x}) = \nabla \times L(\mathbf{x}) \iff \nabla \cdot \mathbf{F}^T(\mathbf{x}) = 0 \tag{3.10}$$

The decomposition into transverse and longitudinal parts (illustrated in Fig. 3.2), normally referred to as the *Helmholtz decomposition*, is proven similarly to its continuum version, as discussed in Appendix 3.B. This decomposition will be crucial in separating the dynamical (transverse) from the gauge-constrained (longitudinal) degrees of freedom.

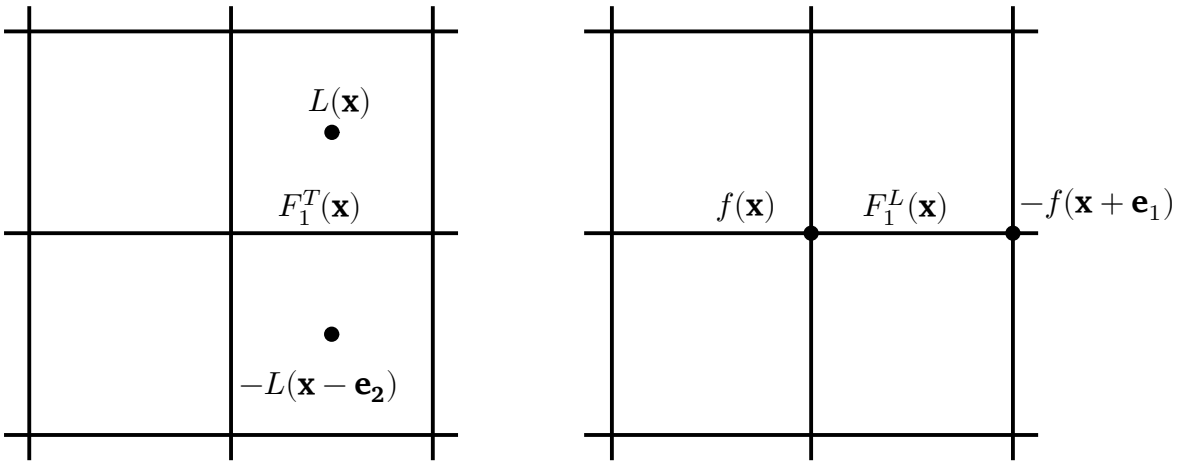

Figure 3.2: Illustration of the Helmholtz decomposition on the lattice. Analogous to the continuum, a vector field can be split into a transverse component (left) and a longitudinal component (right). The transverse component can be expressed as the lattice curl of a field L on the plaquettes (the analog of a vector potential), whereas the longitudinal component is generated as the (negative) gradient of a scalar field f on the sites. For details on this decomposition see Appendix 3.B.

3.3.2 The Matter

Matter particles reside on the lattice sites $\mathbf{x}$. At each site we define an operator $Q(\mathbf{x})$ which measures the local charge. The charge operators commute with one another,

$$[Q(\mathbf{x}), Q(\mathbf{y})] = 0 \tag{3.11}$$

We define, on each site, matter field operators $\Psi(\mathbf{x})$ which lower the local charge, and their hermitian conjugate which raise it:

$$\begin{aligned} [Q(\mathbf{x}), \Psi(\mathbf{y})] &= -\delta(\mathbf{x},\mathbf{y})\,\Psi(\mathbf{x}) \\ [Q(\mathbf{x}), \Psi^\dagger(\mathbf{y})] &= \delta(\mathbf{x},\mathbf{y})\,\Psi^\dagger(\mathbf{x}) \end{aligned} \tag{3.12}$$

where $\delta(\mathbf{x},\mathbf{y})$ is the Kronecker delta function for the lattice discrete coordinates (sites).

There are various options to achieve these fairly general commutation relations. In the most common choice, the matter will be fermionic, and each site may host a single species, that is,

$$\{\Psi(\mathbf{x}), \Psi^\dagger(\mathbf{y})\} = \delta(\mathbf{x},\mathbf{y}); \qquad \{\Psi(\mathbf{x}), \Psi(\mathbf{y})\} = 0 \tag{3.13}$$

Then, following Susskind [66], we can define staggered charges, which split the lattice into two sublattices (even and odd) of particles and anti-particles,

$$Q(\mathbf{x}) = \begin{cases} \Psi^\dagger(\mathbf{x})\,\Psi(\mathbf{x}), & \mathbf{x} \text{ is even} \\ \Psi^\dagger(\mathbf{x})\,\Psi(\mathbf{x}) - 1, & \mathbf{x} \text{ is odd} \end{cases} \tag{3.14}$$

On even sites, the charges can be 0 or 1 while on odd ones they are -1 or 0, depending on whether a fermion is absent or present. Otherwise, one can use naive or Wilson fermions [67], in which several spin components (two or four) are introduced at each site, and charges are defined with some choice of Dirac matrices implementing the Dirac-Clifford algebra. In all these fermionic options, the desired commutation relations (3.11) and (3.12) are satisfied.

Typical Hamiltonian terms that involve only the matter will commute with the charge operators. For example, in the case of staggered fermions, one typically uses the mass Hamiltonian [66],

$$H_m = m\sum_{\mathbf{x}} (-1)^{x_1+x_2}\, \Psi^\dagger(\mathbf{x})\, \Psi(\mathbf{x}). \tag{3.15}$$

3.3.3 The Gauge Field

As already explained in section 2.3, on each link of the lattice we introduce the Hilbert space of a particle on a ring, where the canonical pair of an angular, compact coordinate $\theta_i(\mathbf{x})$ and its conjugate $U(1)$ angular momentum operator $E_i(\mathbf{x})$, which takes an integer, non-bounded spectrum, is defined, satisfying the canonical relation

$$\left[\theta_i(\mathbf{x}), E_j(\mathbf{y})\right] = i\delta_{ij}\delta(\mathbf{x},\mathbf{y}). \tag{3.16}$$

θ plays the role of the (compact) vector potential while E is the electric field. The pure-gauge parts of the Hamiltonian [8, 68] are the electric energy term

$$H_E = \frac{g^2}{2}\sum_{\mathbf{x},i} E_i^2(\mathbf{x}) = \frac{g^2}{2}\sum_{\mathbf{x}} E_i(\mathbf{x})\, E_i(\mathbf{x}) \tag{3.17}$$

(with g^2 the coupling constant) and the magnetic energy,

$$H_B = -\frac{1}{g^2}\sum_{\mathbf{x}} \cos\left(\theta_1(\mathbf{x}) + \theta_2(\mathbf{x}+\mathbf{e}_1) - \theta_1(\mathbf{x}+\mathbf{e}_2) - \theta_2(\mathbf{x})\right) \tag{3.18}$$

involving plaquette interactions. The argument of the cosine is nothing but the curl of the vector potential, which is the magnetic field - a pseudovector residing at the center of plaquettes (dual lattice sites):

$$B(\mathbf{x}) = \nabla \times \theta(\mathbf{x}) = \epsilon_{ij}\Delta_i^{(+)}\theta_j(\mathbf{x}) \tag{3.19}$$

where ϵ_{ij} is the completely antisymmetric symbol. Therefore,

$$H_B = -\frac{1}{g^2}\sum_{\mathbf{x}} \cos\left(B(\mathbf{x})\right) \tag{3.20}$$

The remaining piece of the Hamiltonian couples the matter to the gauge fields. Conventional interaction terms (the result of standard minimal coupling procedures) involve charge hopping to the nearest neighbor site, combined with the increase or decrease of the electric field on the connecting link,

$$H_{int} = \sum_{\mathbf{x},i} t_{\mathbf{x},i}\Psi^\dagger(\mathbf{x})\, e^{i\theta_i(\mathbf{x})}\Psi(\mathbf{x}+\hat{\mathbf{e}}_i) + h.c. \tag{3.21}$$

with $t_{\mathbf{x},i}$ the tunneling amplitude (which might be position and/or direction dependent). In the case of naive/Wilson fermions, spin components are included, requiring to add some Dirac matrix coupling between them. In all these interactions, the gauge field on the links mediates the movement of the charge to maintain gauge invariance, as shall be discussed now.

3.3.4 Gauge Invariance and the Gauss Law

The full Hamiltonian of a lattice gauge theory as the one discussed above is

$$H = H_E + H_B + H_{int} + H_m \tag{3.22}$$

It has a local gauge symmetry; that is, there exist local operators $\mathcal{G}(\mathbf{x})$, which all commute with the Hamiltonian

$$[\mathcal{G}(\mathbf{x}), H] = 0 \quad \forall \mathbf{x} \tag{3.23}$$

These local symmetry generators are nothing but the *Gauss law operators*, defined by the difference between the electric field divergence on a site and the local charge,

$$\begin{aligned} \mathcal{G}(\mathbf{x}) &= \nabla \cdot \mathbf{E}(\mathbf{x}) - Q(\mathbf{x}) = \Delta_i^{(-)} E_i(\mathbf{x}) - Q(\mathbf{x}) \\ &= \sum_i \left(E_i(\mathbf{x}) - E_i(\mathbf{x} - \hat{\mathbf{e}}_i) \right) - Q(\mathbf{x}) \end{aligned} \tag{3.24}$$

The commutation of all the local constants of motion $\mathcal{G}(\mathbf{x})$ with the Hamiltonian splits the Hilbert space to different sectors, disconnected by the Hamiltonian dynamics, classified by the eigenstates of these operators $q(\mathbf{x})$ which are nothing but static charge configurations, and thus these sectors are simply a formulation of a *charge superselection rule*; so-called *physical states* satisfy

$$\mathcal{G}(\mathbf{x}) |\text{phys}\rangle = q(\mathbf{x}) |\text{phys}\rangle \quad \forall \mathbf{x} \tag{3.25}$$

or

$$\Delta_i^{(-)} E_i(\mathbf{x})(\mathbf{x}) |\text{phys}\rangle = (Q(\mathbf{x}) + q(\mathbf{x})) |\text{phys}\rangle \quad \forall \mathbf{x} \tag{3.26}$$

Below, we will always assume that the static charges $q(\mathbf{x})$ are fixed, which we can do due to the superselection rule.

3.4 Decoupling the dynamical matter

In order to arrive at a redundancy-free formulation, it is necessary to identify the degrees of freedom which are constrained by the Gauss law. Examining eq. (3.26), it is evident that in the physical Hilbert space the longitudinal part of the electric field is completely determined by the charge configuration. The transverse part of the electric field is unaffected by these constraints.

In contrast to previous works that only dealt with static charges, constructing a Hamiltonian in terms of transverse gauge field degrees of freedom in the presence of dynamical matter is more challenging. This is because gauge-matter interactions H_{int} appear that involve the longitudinal component of the gauge field, whereas only the transverse component contributes to the magnetic Hamiltonian H_B.

Hence, a central part of the gauge-invariant formulation is to find a unitary transformation to a frame in which the longitudinal part of the gauge field disappears from the Hamiltonian (one can intuitively think about it as rotating to a frame such that Coulomb gauge holds in the physical subspace, $\Delta_i^{(-)} \theta_i(\mathbf{x}) = 0$). A unitary transformation $\mathcal{U}$, which accomplishes that, can be defined as

$$\mathcal{U} = \exp\left(-i \sum_{\mathbf{x}} \theta_i(\mathbf{x}) \beta_i(\mathbf{x}) \right) \tag{3.27}$$

with

$$\beta_i(\mathbf{x}) = -\sum_{\mathbf{y}} \Delta^{(+)}_{i,\mathbf{x}} G(\mathbf{x},\mathbf{y}) \left(Q(\mathbf{y}) + q(\mathbf{y})\right) \tag{3.28}$$

where $G(\mathbf{x},\mathbf{y})$ is the Green's function of the (negative) lattice Laplacian (see Appendix 3.A). $\Delta^{(+)}_{i,\mathbf{x}}$ denotes the lattice forward derivative in direction $\hat{\mathbf{e}}_i$ with respect to the variable $\mathbf{x}$. $\beta_i(\mathbf{x})$ is nothing but the longitudinal electric field in the physical Hilbert space before the transformation, $\beta_i(\mathbf{x})\,|\text{phys}\rangle = E^L_i(\mathbf{x})\,|\text{phys}\rangle$ (see Appendix 3.B for details).

We start by studying the effect of this transformation on the Gauss law in eq. (3.26). It is clear that the charge operator $Q(\mathbf{x})$ commutes with the transformation:

$$\mathcal{U} Q(\mathbf{x}) \mathcal{U}^\dagger = Q(\mathbf{x}). \tag{3.29}$$

The electric field gets shifted by β:

$$\mathcal{U} E_i(\mathbf{x}) \mathcal{U}^\dagger = E_i(\mathbf{x}) + \beta_i(\mathbf{x}) \tag{3.30}$$

Thus, the divergence of the electric field gives

$$\begin{aligned} \mathcal{U} \Delta^{(-)}_i E_i(\mathbf{x}) \mathcal{U}^\dagger &= \Delta^{(-)}_i E_i(\mathbf{x}) - \sum_{\mathbf{y}} \Delta^{(-)}_{i,\mathbf{x}} \Delta^{(+)}_{i,\mathbf{x}} G(\mathbf{x},\mathbf{y}) \left(Q(\mathbf{y}) + q(\mathbf{y})\right) \\ &= \Delta^{(-)}_i E_i(\mathbf{x}) + Q(\mathbf{x}) + q(\mathbf{x}) \end{aligned} \tag{3.31}$$

Hence, the physical states in the rotated frame, $\left|\widetilde{\text{phys}}\right\rangle \equiv \mathcal{U}\,|\text{phys}\rangle$, obey the transformed matter-free Gauss law,

$$\Delta^{(-)}_i E_i(\mathbf{x}) \left|\widetilde{\text{phys}}\right\rangle = 0 \quad \forall \mathbf{x} \tag{3.32}$$

or, in other words, the electric field in the physical subspace is transverse (divergence-free) after the unitary transformation $\mathcal{U}$. This was to be expected since we removed the longitudinal part of the electric field (in the physical subspace).

It is worth noting that the spectrum of $E_i(\mathbf{x})$ changes in the rotated physical subspace, with the integer spectrum becoming fractional. As demonstrated in [2, 57], each charge configuration results in a constant shift in the original integer spectrum of the electric field in the physical Hilbert space. However, in the presence of dynamical matter, the various static charge sectors are mixed due to gauge-matter interactions, resulting in a shifted integer spectrum where the shift is not constant but varies with the charge configuration.

In the next step, we consider the transformation of the electric part of the Hamiltonian. Using (3.30) and (3.28), we obtain that the transformed electric Hamiltonian has three parts,

$$\begin{aligned} \tilde{H}_E = \mathcal{U} H_E \mathcal{U}^\dagger &= \frac{g^2}{2} \sum_{\mathbf{x},i} \left(E_i(\mathbf{x}) - \sum_{\mathbf{y}} \Delta^{(+)}_{i,\mathbf{x}} G(\mathbf{x},\mathbf{y}) \left(Q(\mathbf{y}) + q(\mathbf{y})\right) \right)^2 \\ &\equiv \tilde{H}^T_E + \tilde{H}^L_E + \tilde{H}^{TL}_E \end{aligned} \tag{3.33}$$

The first term will have the same mathematical form as the pre-transformed Hamiltonian, but now, in the physical Hilbert space, it will only correspond to the transverse parts of the field (which no longer possess an integer spectrum),

$$\tilde{H}^T_E = \frac{g^2}{2} \sum_{\mathbf{x},i} E^2_i(\mathbf{x}) = \frac{g^2}{2} \sum_{\mathbf{x}} E_i(\mathbf{x}) E_i(\mathbf{x}) \tag{3.34}$$

The second part is the purely longitudinal one, taking the form

$$\begin{aligned}\tilde{H}_E^L &= -\frac{g^2}{2}\sum_{\mathbf{x},\mathbf{y},\mathbf{y}',i}\Delta_{i,\mathbf{x}}^{(-)}\Delta_{i,\mathbf{x}}^{(+)}G\left(\mathbf{x},\mathbf{y}\right)\left(Q\left(\mathbf{y}\right)+q\left(\mathbf{y}\right)\right)\times \\ &\qquad \times G\left(\mathbf{x},\mathbf{y}'\right)\left(Q\left(\mathbf{y}'\right)+q\left(\mathbf{y}'\right)\right) \\ &= \frac{g^2}{2}\sum_{\mathbf{x},\mathbf{y}}\left(Q\left(\mathbf{x}\right)+q\left(\mathbf{x}\right)\right)G\left(\mathbf{x},\mathbf{y}\right)\left(Q\left(\mathbf{y}\right)+q\left(\mathbf{y}\right)\right)\end{aligned} \tag{3.35}$$

where in the first row we used a lattice analogue of integrating by parts (which is valid for both periodic and open boundary conditions) and in the second row the definition of the Green's function. The resulting interaction between the charges (both dynamical and static) is of Coulomb-type, since the Green's function $G(\mathbf{x},\mathbf{y})$ is nothing but the lattice Coulomb potential generated by a unit charge at $\mathbf{y}$ experienced by another unit charge at $\mathbf{x}$.

The third part involves the cross terms. If we write it as

$$\begin{aligned}\tilde{H}_E^{TL} &= -g^2\sum_{\mathbf{x},\mathbf{y},i}E_i(\mathbf{x})\Delta_{i,\mathbf{x}}^{(+)}G\left(\mathbf{x},\mathbf{y}\right)\left(Q\left(\mathbf{y}\right)+q\left(\mathbf{y}\right)\right) \\ &= g^2\sum_{\mathbf{x},\mathbf{y},i}\Delta_{i,\mathbf{x}}^{(-)}E_i(\mathbf{x})G\left(\mathbf{x},\mathbf{y}\right)\left(Q\left(\mathbf{y}\right)+q\left(\mathbf{y}\right)\right)\end{aligned} \tag{3.36}$$

it becomes clear that it vanishes in the physical Hilbert space using the transformed Gauss law in eq. (3.32). Intuitively, it can be understood since it corresponds to the scalar product of the longitudinal and transverse component of the electric field. We are only interested in the physical subspace and will therefore neglect this term in the following.

To study the transformation of the matter degrees of freedom it is useful to rewrite the transformation $\mathcal{U}$ in the following way:

$$\begin{aligned}\mathcal{U} &= \exp\left(i\sum_{\mathbf{x},\mathbf{y}}\theta_i\left(\mathbf{x}\right)\Delta_{i,\mathbf{x}}^{(+)}G\left(\mathbf{x},\mathbf{y}\right)\left(Q\left(\mathbf{y}\right)+q\left(\mathbf{y}\right)\right)\right) \\ &= \exp\left(-i\sum_{\mathbf{x},\mathbf{y}}\left(Q\left(\mathbf{x}\right)+q\left(\mathbf{x}\right)\right)G\left(\mathbf{x},\mathbf{y}\right)\Delta_{i,\mathbf{y}}^{(-)}\theta_i\left(\mathbf{y}\right)\right)\end{aligned} \tag{3.37}$$

(where we used again the lattice analog of integrating by parts). Using (3.11) and (3.12), we obtain the transformation rule of the charge raising operator,

$$\mathcal{U}\Psi^\dagger\left(\mathbf{x}\right)\mathcal{U}^\dagger = \Psi^\dagger\left(\mathbf{x}\right)\exp\left(-i\sum_{\mathbf{y}}G\left(\mathbf{x},\mathbf{y}\right)\Delta_{i,\mathbf{y}}^{(-)}\theta_i\left(\mathbf{y}\right)\right) \tag{3.38}$$

and thus the gauge-matter interactions in the transformed picture are

$$\begin{aligned}\tilde{H}_{int} &= \mathcal{U}H_{int}\mathcal{U}^\dagger \\ &= \sum_{\mathbf{x},i}t_{\mathbf{x},i}\Psi^\dagger\left(\mathbf{x}\right)\exp\left[i\left(\theta_i\left(\mathbf{x}\right)+\sum_{\mathbf{y}}\Delta_{i,\mathbf{x}}^{(+)}G\left(\mathbf{x},\mathbf{y}\right)\Delta_{i,\mathbf{y}}^{(-)}\theta_i\left(\mathbf{y}\right)\right)\right]\Psi\left(\mathbf{x}+\hat{\mathbf{e}}_i\right)+h.c.\end{aligned} \tag{3.39}$$

Using the Helmholtz decomposition (see Appendix 3.B for details), one obtains that the longitudinal part of $\theta_i(\mathbf{x})$ is given by

$$\theta_i^L(\mathbf{x}) = -\Delta_{i,\mathbf{x}}^{(+)} \sum_{\mathbf{y}} G(\mathbf{x},\mathbf{y}) \Delta_{i,\mathbf{y}}^{(-)} \theta_i(\mathbf{y}) \tag{3.40}$$

and hence we remain only with the transverse, divergence free field in the transformed interaction Hamiltonian,

$$\tilde{H}_{int} = \sum_{\mathbf{x},i} t_{\mathbf{x},i} \left(\Psi^\dagger(\mathbf{x}) e^{i\theta_i^T(\mathbf{x})} \Psi(\mathbf{x}+\hat{\mathbf{e}}_i) + h.c. \right) \tag{3.41}$$

This can also easily be checked by taking the lattice divergence of the argument in the exponential in eq. (3.39).

H_B does not change under the transformation, because it commutes with $\mathcal{U}$, i.e. $\tilde{H}_B = H_B$. It depends on the *curl* of the vector potential θ so that only the transverse part of θ contributes (since the longitudinal one is curl-free). Therefore, $\tilde{H}_B$ can be formulated with the transverse field only,

$$\tilde{H}_B = -\frac{1}{g^2} \sum_{\mathbf{x}} \cos\left(\epsilon_{ij} \Delta_i^{(+)} \theta_j^T(\mathbf{x}) \right) \tag{3.42}$$

H_m commutes with $\mathcal{U}$ as well, and thus $\tilde{H}_m = H_m$.

Hence, after the transformation, the Hamiltonian depends only on the transverse component of the vector potential, θ^T, so that we indeed transformed to a frame where the lattice version of Coulomb gauge holds. We can therefore proceed to formulate the remaining transverse degrees of freedom in terms of dual variables. For that, we will restrict ourselves from now on to the physical Hilbert space.

3.5 Dual formulation

In the transformed picture, the Gauss law (3.26) becomes decoupled from the matter degrees of freedom, leaving the electric field transverse (3.32). Therefore it makes sense to change from the gauge field variables on the links to another set of variables that will respect this transverse nature of the electric field. This will allow us to directly incorporate the Gauss law constraint (3.32), making the formulation manifestly gauge-invariant.

Since the electric field in the physical Hilbert space of the transformed frame is transverse, we may express it as the curl of a pseudovector field $L(\mathbf{x})$ defined on the plaquettes (dual lattice sites), $\nabla \times L(\mathbf{x})$. If we apply the lattice curl again, this gives rise to a Poisson equation for $L(\mathbf{x})$ in terms of $E_i(\mathbf{x})$, whose solution is

$$L(\mathbf{x}) = \sum_{\mathbf{y}} G(\mathbf{x},\mathbf{y}) \epsilon_{ij} \Delta_{i,\mathbf{y}}^{(+)} E_j(\mathbf{y}) \tag{3.43}$$

Using that, one can show that $L(\mathbf{x})$ is canonically conjugate to the magnetic field (see Appendix 3.C for details),

$$[B(\mathbf{x}), L(\mathbf{y})] = i\delta(\mathbf{x},\mathbf{y}) \tag{3.44}$$

The idea behind these variables is that all transverse configurations of the electric field are made out of loops and the local B/L-variables are a good basis to construct

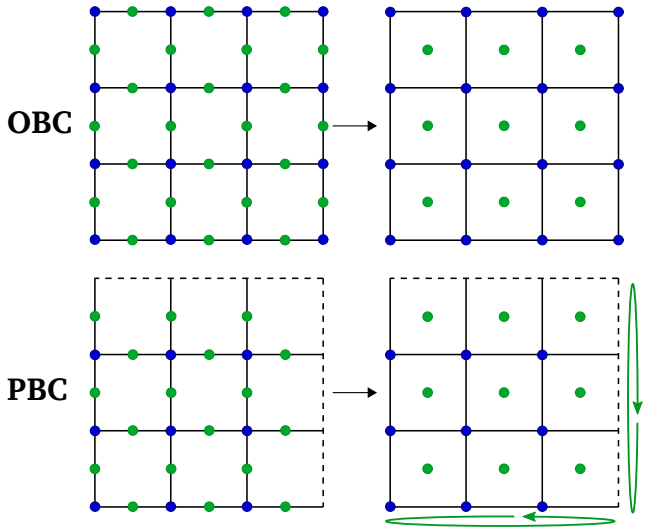

Figure 3.3: Illustration of the dual formulation in the transformed frame for a 3×3 lattice with both open boundary conditions (upper row) and periodic boundary conditions (lower row). In the left column, the original formulation is shown in terms of the matter degrees of freedom on the sites (blue) and the gauge degrees of freedom on the links (green). In the right column, the degrees of freedom of the dual formulation are shown: the matter still resides on the lattice sites, but the gauge degrees of freedom are described in terms of plaquette variables. While in the original formulation there were gauge constraints for every site, there are no local gauge constraints left in the dual formulation. For open boundary conditions, there are no gauge constraints in the dual formulation and for periodic boundary conditions there is a global constraint left involving all plaquette variables. Since periodic boundary conditions allow closed loops around the lattice, there are two global gauge variables, one for each spatial direction (green circles in the figure).

these loops. This geometric picture is also the basis for the dual formulation in [60]. However, with periodic boundary conditions there are two global loops (up to modifications by plaquette operators, similar to the toric code) that can not be created out of the B/L-variables (they do not appear in the case of open boundary conditions). These are independent variables, denoted as B_1, L_1 and B_2, L_2. We choose the B_1/L_1-variable to wind around the torus along the $\hat{\mathbf{e}}_1$-axis whereas the B_2/L_2-variable is chosen to wind around the torus along the $\hat{\mathbf{e}}_2$-axis. The sets of degrees of freedom in the dual formulation for both periodic and open boundary conditions are illustrated in Fig. 3.3, exemplary for a 3×3 lattice. Therefore, to express the electric field in terms of L-variables for periodic boundary conditions, we need in addition to the curl of L the contributions of the global loops, i.e.

$$E_i(\mathbf{x}) = \epsilon_{ij}\Delta_j^{(-)} L(\mathbf{x}) + \delta_{x_j,0} L_i \tag{3.45}$$

with $i \neq j$. The second term is only present on the two axes and vanishes completely for open boundary conditions. By formulating the theory in terms of dual variables, there are no local constraints left. However, there is a global constraint left (in case of periodic boundary conditions, this is not the case for open boundary conditions) which can be seen by summing eq. (3.19) over the whole lattice:

$$\sum_{\mathbf{x}} B(\mathbf{x}) \, |\text{phys}\rangle = 0 \tag{3.46}$$

This is intuitively clear since raising the electric flux around every plaquette should give the same state (on a lattice with periodic boundary conditions). To convince us that the number of physical degrees of freedom in the dual formulation matches the number in the original formulation we can do a short counting of degrees of freedom. We can neglect the matter degrees of freedom in this calculation since it is the same in both cases.

Starting with periodic boundary conditions, there are in the original formulation $2N^2$ links and N^2-1 Gauss laws (the constraint at one lattice site is redundant). The number of physical degrees of freedom is thus N^2+1. In the dual formulation, we have N^2 plaquette variables, two global loop variables and one global constraint, which amounts also to N^2+1 physical degrees of freedom.

With open boundary conditions, there are originally $2N(N+1)$ links and $(N+1)^2-1$ Gauss law constraints, i.e. N^2 physical degrees of freedom. In the dual formulation, there are N^2 plaquette variables which are not subject to any constraints, thus giving the same number of physical degrees of freedom.

We can now rewrite the transformed Hamiltonian in terms of the dual variables. This does not change $\tilde{H}_m$ and $\tilde{H}_E^L$; the magnetic part will now be non-interacting,

$$\tilde{H}_B = -\frac{1}{g^2}\sum_{\mathbf{x}} \cos\left(B\left(\mathbf{x}\right)\right). \tag{3.47}$$

Following eq. (3.45), the transverse electric part will involve some local interactions,

$$\tilde{H}_E^T = \frac{g^2}{2}\sum_{\mathbf{x},i}\left(\epsilon_{ij}\left(L\left(\mathbf{x}\right)-L\left(\mathbf{x}-\hat{\mathbf{e}}_j\right)\right)+\delta_{x_j,0}L_i\right)^2 \tag{3.48}$$

where the last term denotes the contribution of the two global loops which is only present on the axes ($x_1=0$ or $x_2=0$). This term drops out in the case of open boundary conditions.

To rewrite the gauge-matter interactions in terms of dual variables, we express the transverse part of the gauge field in terms of the magnetic field $B(\mathbf{x})$ (the calculation of the shifts $s_{\mathbf{x},i}(\mathbf{y})$ is presented in Appendix 3.B)

$$\phi_i^T(\mathbf{x}) = \sum_{\mathbf{y}} s_{\mathbf{x},i}(\mathbf{y})B(\mathbf{y}) \tag{3.49}$$

(note that the sum over $\mathbf{y}$ also contains the two global loops B_1 and B_2). The gauge-matter interactions then take the form

$$\tilde{H}_{int} = \sum_{\mathbf{x},i} t_{\mathbf{x},i}\Psi^\dagger\left(\mathbf{x}\right)e^{i\sum_{\mathbf{y}} s_{\mathbf{x},i}(\mathbf{y})B(\mathbf{y})}\Psi\left(\mathbf{x}+\hat{\mathbf{e}}_i\right)+h.c. \tag{3.50}$$

The hopping of a matter degree of freedom from some site $\mathbf{x}$ to an adjacent site $\mathbf{x}+\hat{\mathbf{e}}_i$ introduces shifts $s_{\mathbf{x},i}(\mathbf{y})$ ($-1/2 < s_{\mathbf{x},i}(\mathbf{y}) \leq 1/2$) in the $L(\mathbf{y})$ operators since B is canonically conjugate to L. This can be understood in the following way: the hopping changes the electric field configuration (by raising/lowering the electric field on that link) and the change in the transverse part of the electric field is characterized by the s-shifts. Although the size of these shifts decays with distance to the link where hopping occurs, the interaction involves many degrees of freedom which might be difficult to

deal with, in particular for a quantum simulation. Summing up, the whole transformed Hamiltonian in the dual formulation with B/L-variables takes the form

$$\begin{aligned}\tilde{H} =& H_m + \frac{g^2}{2}\sum_{\mathbf{x},i}\left(\epsilon_{ij}\left(L\left(\mathbf{x}\right) - L\left(\mathbf{x}-\hat{\mathbf{e}}_j\right)\right) + \delta_{x_j,0}L_i\right)^2 \\ &+ \frac{g^2}{2}\sum_{\mathbf{x},\mathbf{y}}\left(Q\left(\mathbf{x}\right)+q\left(\mathbf{x}\right)\right)G\left(\mathbf{x},\mathbf{y}\right)\left(Q\left(\mathbf{y}\right)+q\left(\mathbf{y}\right)\right) \\ &- \frac{1}{g^2}\sum_{\mathbf{x}}\cos\left(B\left(\mathbf{x}\right)\right) + \sum_{\mathbf{x},i} t_{\mathbf{x},i}\Psi^\dagger\left(\mathbf{x}\right)e^{i\sum_{\mathbf{y}} s_{\mathbf{x},i}(\mathbf{y})B(\mathbf{y})}\Psi\left(\mathbf{x}+\hat{\mathbf{e}}_i\right) + h.c.\end{aligned} \tag{3.51}$$

with $i \neq j$. In the case of open boundary conditions, the global loop contributions in $\tilde{H}_E^T$ and $\tilde{H}_{int}$ vanish.

We proceed to define another canonical pair of operators which makes the gauge-matter interactions local again. The idea is to carry out the same procedure as before but now with the transverse component of the gauge field $\theta_i^T(\mathbf{x})$ as a starting point, instead of the electric field.

In complete analogy to eq. (3.45), we can express $\theta_i^T(\mathbf{x})$ by a compact field on the plaquettes $\phi\left(\mathbf{x}\right)$ (and for periodic boundary conditions two additional global loops ϕ_1 and ϕ_2), such that

$$\theta_i^T\left(\mathbf{x}\right) = \epsilon_{ij}\Delta_j^{(-)}\phi\left(\mathbf{x}\right) + \delta_{x_j,0}\phi_i \tag{3.52}$$

with $i \neq j$. As before, the global loop contribution vanishes for open boundary conditions. The expression for ϕ in terms of θ has the same form as the expression for L in terms of E in eq. (3.43):

$$\phi\left(\mathbf{x}\right) = \sum_{\mathbf{y}} G\left(\mathbf{x},\mathbf{y}\right)\epsilon_{ij}\Delta_{i,\mathbf{y}}^{(+)}\theta_j\left(\mathbf{y}\right) \tag{3.53}$$

The canonically conjugate variable to ϕ is the curl of the electric field,

$$M\left(\mathbf{x}\right) = \epsilon_{ij}\Delta_i^{(+)}E_j\left(\mathbf{x}\right) \tag{3.54}$$

Since $E_i(\mathbf{x})$ is integer-valued, $M(\mathbf{x})$, as the sum of integer-valued operators, will also have an integer spectrum. Using the expression for ϕ in terms of θ from eq. (3.53), the definition of M in terms of E in eq. (3.54), one can show that also ϕ and M fulfill the canonical commutation relations,

$$\left[\phi\left(\mathbf{x}\right), M\left(\mathbf{y}\right)\right] = i\delta(\mathbf{x},\mathbf{y}). \tag{3.55}$$

Analogous to the B/L-variables, there are two global non-contractible loops denoted as ϕ_1/M_1 and ϕ_2/M_2 winding along the respective axis (again, this is only the case for periodic boundary conditions, not for open ones). Since both dual formulations share the same locations on the lattice, the counting of degrees of freedom can be done in the same way as for the B/L-variables. The relation between the two sets of dual variables is illustrated in Fig. 3.4.

If we express the gauge-matter interactions in terms of the newly introduced field $\phi\left(\mathbf{x}\right)$, we arrive at

$$\tilde{H}_{int} = \sum_{\mathbf{x},i} t_{\mathbf{x},i}\Psi^\dagger\left(\mathbf{x}\right)e^{i\left(\epsilon_{ij}\Delta_j^{(-)}\phi(\mathbf{x})+\delta_{x_j,0}\phi_i\right)}\Psi\left(\mathbf{x}+\hat{\mathbf{e}}_i\right) + h.c. \tag{3.56}$$

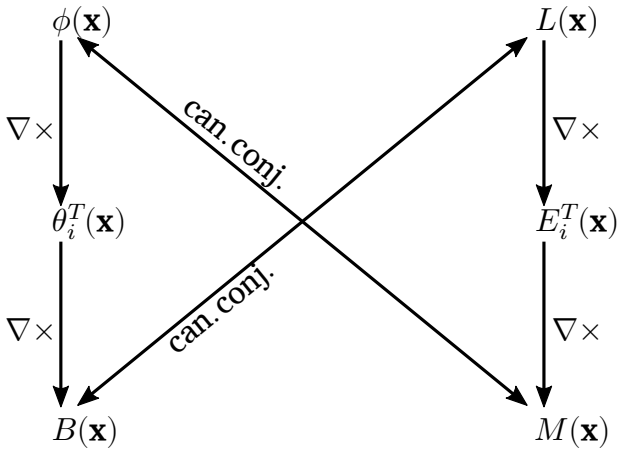

Figure 3.4: Illustration of the two dual formulations in terms of B/L-variables and ϕ/M-variables. Both formulations are based on expressing the transverse part of either the gauge field $\theta_i(\mathbf{x})$ or the electric field $E_i(\mathbf{x})$. While the transverse component of the electric field, $E_i^T(\mathbf{x})$, can be obtained as the lattice curl $\nabla\times$ of the plaquette field L, the lattice curl of the plaquette field ϕ gives rise to $\theta_i^T(\mathbf{x})$. It can then be shown that the curl of θ, which is the magnetic field B, is canonically conjugate to L. In the same way, it can be shown that the curl of E is canonically conjugate to ϕ. Thus, the two dual formulations are based on the same principle and complement each other.

with $i \neq j$, a local interaction again (up to the contribution of the global loops ϕ_i which is only present on the two axes and vanishes in the case of open boundary conditions). It has the following interpretation: when a matter charge hops from site $\mathbf{x}$ to a neighboring site, say $\mathbf{x}+\hat{\mathbf{e}}_1$, the curl of the electric field on the plaquette above the link gets raised by one and the curl of the electric field on the plaquette below the link gets lowered by one.

To express the transverse part of the electric energy in terms of the M-variables, we need to find a relation between the M- and L-variables which can then be inserted in the formula for $\tilde{H}_E^T$ in terms of L, eq. (3.48). Such a relation can be obtained by plugging the electric field in terms of L, eq. (3.45), into the definition of M, eq. (3.54):

$$M(\mathbf{x}) = -\nabla^2 L(\mathbf{x}) + \epsilon_{ij}\Delta_i^{(+)}\delta_{x_i,0}L_j \tag{3.57}$$

The second term is a boundary term coming from the global loops (only present for periodic boundary conditions). For open boundary conditions, the relation contains only the first term, leading to a Poisson equation on the plaquettes. Thus, for open boundary conditions, L can be expressed in terms of M by the Green's function. Inserting this in eq. (3.48) and using the lattice analog of integrating by parts, gives a Coulomb interaction between the M-variables. For periodic boundary conditions, this interaction potential is slightly modified by boundary effects due to the second term in eq. (3.57), i.e.

$$\tilde{H}_E^T = \frac{g^2}{2}\sum_{\mathbf{x},\mathbf{y}} M(\mathbf{x})\,\widetilde{G}(\mathbf{x},\mathbf{y})\,M(\mathbf{y}) \tag{3.58}$$

where $\widetilde{G}(\mathbf{x},\mathbf{y})$ denotes the modified interaction potential. Note that it also includes interactions with the two global variables, i.e. the sum above contains also M_1 and M_2 (for its exact form see Appendix 3.D). For open boundary conditions, $\widetilde{G}(\mathbf{x},\mathbf{y})$ reduces to

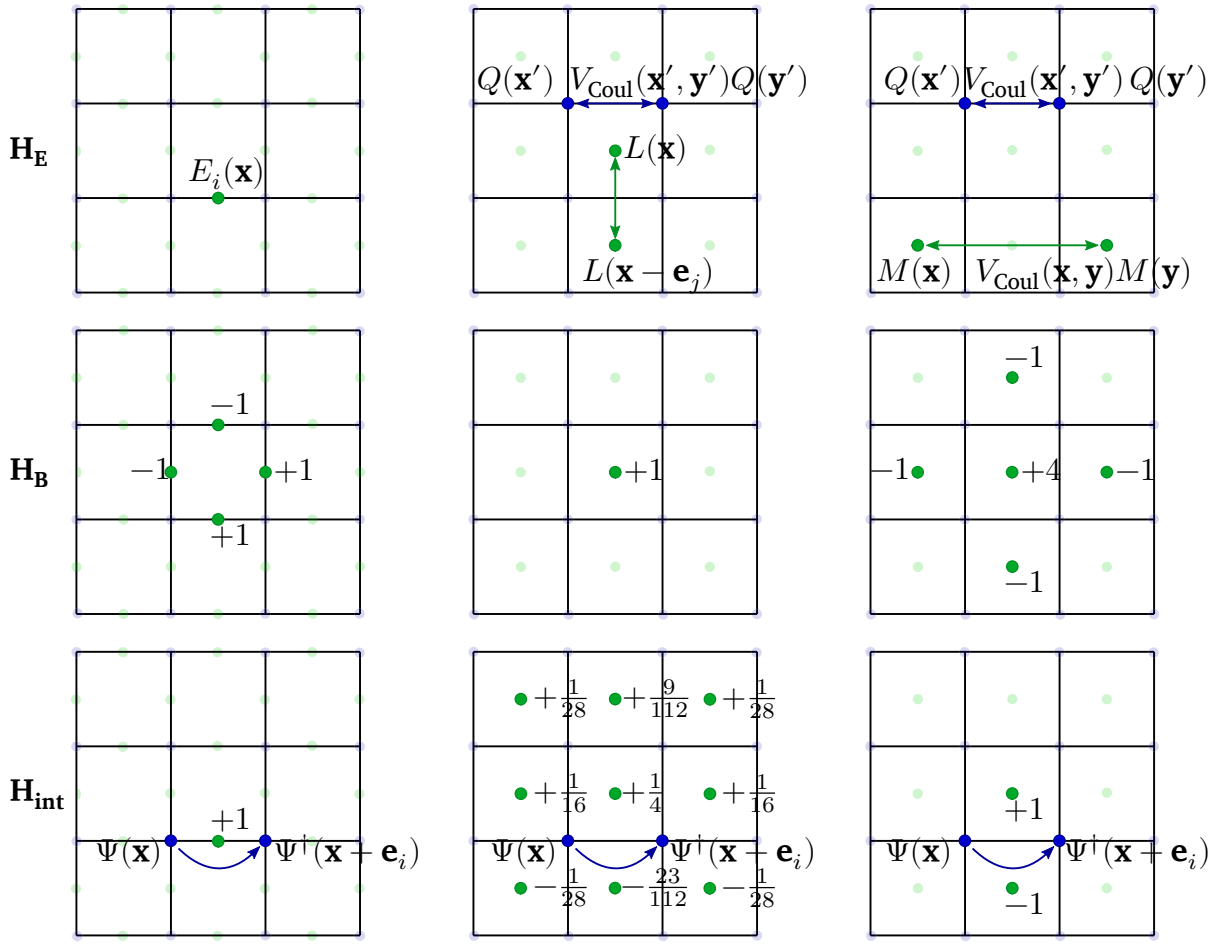

Figure 3.5: Illustration of the interactions in the Hamiltonian for a 3×3 lattice with open boundary conditions in the original formulation (left column), the dual formulation in terms of B/L-variables (middle column) and the dual formulation in terms of ϕ/M-variables (right column). We consider the electric Hamiltonian (upper row), the magnetic Hamiltonian (middle row) and the gauge-matter interactions (lower row). While the electric Hamiltonian in the original formulation is the sum over the square of the electric field on every link, in the dual picture it is split into a longitudinal part and a transverse part. The longitudinal part of the electric field gives rise to Coulomb interactions $V_{\text{Coul}}(\mathbf{x},\mathbf{y})$ between charges $Q(\mathbf{x})$ and $Q(\mathbf{y})$. The transverse part depends on the dual formulation: For the B/L-variables the transverse electric field is just the lattice curl of L so that the electric Hamiltonian on a link involves only the two neighboring plaquettes. For the ϕ/M-variables one can show that the transverse electric Hamiltonian leads to Coulomb interactions among the M-variables, thus generating very similar interactions as between the charges. The magnetic Hamiltonian in the original formulation is a four-body interaction among the links: it is the sum of a raising and a lowering operator of the electric field around the plaquette (in the figure we show the effect of the raising operator in the electric basis). In terms of the B/L-variables, since B is the lattice curl of the gauge field around a plaquette, it is a one-body term, raising the L-variable by one. In terms of the ϕ/M-variables, it is a five-body interaction, corresponding to the (negative) Laplacian of ϕ, which raises the M-variable in the center by four and lowers it on the neighboring plaquettes by one. The gauge-matter interactions in the original formulation raise the electric field along the link by one. In the rotated frame, only changes in the transverse part of the electric field need to be taken into account. In terms of the B/L-variables, this change can be expressed by shifting the L-variables by $s_{\mathbf{x},i}(\mathbf{y})$ as shown in the figure. They decay away from the link where hopping occurs, which can already be seen on the 3×3 lattice. In terms of the ϕ/M-variables, since the curl of the electric field is only affected on the two neighboring plaquettes, the gauge-matter interactions become local.

$G(\mathbf{x},\mathbf{y})$. Thus, the interactions between the curls of the electric field on the plaquettes are of Coulomb type; it shows some strong similarity with the longitudinal part $\tilde{H}_E^L$ in eq. (3.35) where exactly the same interaction appears between the matter degrees of freedom. The last remaining part is the magnetic Hamiltonian. If we express B in terms of ϕ in the same way as we did for M in terms of L in eq. (3.57), we can write down $\tilde{H}_B$ in terms of ϕ, following eq. (3.47):

$$\begin{aligned}\tilde{H}_B =& -\frac{1}{g^2}\sum_{\mathbf{x}}\cos\left(-\nabla^2\phi(\mathbf{x})+\epsilon_{ij}\Delta_i^{(+)}\delta_{x_i,0}\phi_j\right) \\ =& -\frac{1}{g^2}\sum_{\mathbf{x}}\cos\Big(4\phi(\mathbf{x})-\phi(\mathbf{x}+\hat{\mathbf{e}}_1)-\phi(\mathbf{x}+\hat{\mathbf{e}}_2) \\ & -\phi(\mathbf{x}-\hat{\mathbf{e}}_1)-\phi(\mathbf{x}-\hat{\mathbf{e}}_2) \\ & +\left(\delta_{x_2,0}-\delta_{x_2,-1}\right)\phi_1-\left(\delta_{x_1,0}-\delta_{x_1,-1}\right)\phi_2\Big)\end{aligned} \tag{3.59}$$

where the contributions of the global variables ϕ_1 and ϕ_2 are only present on plaquettes sharing a link with the $\hat{\mathbf{e}}_1$- or $\hat{\mathbf{e}}_2$-axis. They vanish completely for open boundary conditions and the magnetic Hamiltonian becomes a local interaction - a five-body one, involving a plaquette and its neighbors. The action of $\tilde{H}_B$ in the electric basis is illustrated in Fig. 3.5, for both the original and the dual formulations.

Analogous to the dual formulation with B and L, there is also a global constraint for the formulation in terms of ϕ and M. This constraint on physical states can be obtained if we sum eq. (3.54) over the whole lattice (again, this only holds true for periodic boundary conditions, it is not the case for open boundary conditions),

$$\sum_{\mathbf{x}} M(\mathbf{x})\,|\text{phys}\rangle = 0 \tag{3.60}$$

Overall, the original formulation of the lattice gauge theory has been replaced in this dual formulation of the transformed picture by (assuming periodic boundary conditions)

$$\begin{aligned}\tilde{H} =& H_m+\frac{g^2}{2}\sum_{\mathbf{x},\mathbf{y}}\left[(Q(\mathbf{x})+q(\mathbf{x}))\,G(\mathbf{x},\mathbf{y})\,(Q(\mathbf{y})+q(\mathbf{y}))+M(\mathbf{x})\,\widetilde{G}(\mathbf{x},\mathbf{y})\,M(\mathbf{y})\right] \\ & -\frac{1}{g^2}\sum_{\mathbf{x}}\cos\left(-\nabla^2\phi(\mathbf{x})+\epsilon_{ij}\Delta_i^{(+)}\delta_{x_i,0}\phi_j\right) \\ & +\sum_{\mathbf{x},i}t_{\mathbf{x},i}\,\Psi^\dagger(\mathbf{x})\,e^{i\left(\epsilon_{ij}\Delta_j^{(-)}\phi(\mathbf{x})+\delta_{x_j,0}\phi_i\right)}\Psi(\mathbf{x}+\hat{\mathbf{e}}_i)+h.c.\end{aligned} \tag{3.61}$$

with $i\neq j$. The link variables, the angle $\theta_i(\mathbf{x})$ and the integer-valued $E_i(\mathbf{x})$, and the multiple local constraints imposed by the Gauss law (3.26) are replaced by the dual plaquette variables, the angle $\phi(\mathbf{x})$ and the integer-valued $M(\mathbf{x})$, and the single global constraint (3.60). For open boundary conditions, the formulation simplifies since the modified interaction potential $\widetilde{G}(\mathbf{x},\mathbf{y})$ reduces to $G(\mathbf{x},\mathbf{y})$ and the global loop contributions corresponding to ϕ_1 and ϕ_2 drop out of the gauge-matter interactions and the magnetic interactions, rendering them completely local. Moreover, there is no global constraint left, making the formulation manifestly gauge-invariant. The reason why periodic boundary conditions are more difficult to deal with in the presence of

dynamical matter as compared to static matter is that the two global loops around the torus become dynamical due to the appearance of gauge-matter interactions. Thus, the choice of open boundary conditions should be preferred, in particular for quantum simulations as open boundary conditions are much more natural from an experimental point of view. To summarize, the required interactions for open boundary conditions in the original approach, the formulation in terms of B/L-variables and in terms of ϕ/M-variables are illustrated in Fig. 3.5, exemplary for a 3×3 lattice.

3.6 Three space dimensions

In this section we consider the generalization of the previous discussion to $3+1d$, i.e. three space dimensions. Difference operators are defined exactly in the same manner as in the two dimensional settings of section 3.3.1, as well as the gradient and the divergence. The Laplacian's definition changes by a numerical factor, to

$$\nabla^2 f(\mathbf{x}) = \Delta_i^{(-)} \Delta_i^{(+)} f(\mathbf{x}) = \sum_{i=1,2,3} \left(f(\mathbf{x} + \hat{\mathbf{e}}_i) - f(\mathbf{x} - \hat{\mathbf{e}}_i) \right) - 6 f(\mathbf{x}) \tag{3.62}$$

We need to generalize the definitions of the curl. The curl of a vector field on the links will be a pseudovector field residing at the centers of plaquettes,

$$\left(\nabla \times \mathbf{F}(\mathbf{x}) \right)_i = \epsilon_{ijk} \Delta_j^{(+)} F_k(\mathbf{x}) \tag{3.63}$$

while the curl of a pseudovector will be a regular vector field on the links,

$$\left(\nabla \times \mathbf{L}(\mathbf{x}) \right)_i = \epsilon_{ijk} \Delta_j^{(-)} L_k(\mathbf{x}) \tag{3.64}$$

If we fix $i = 3$, we recover the expressions for two space dimensions.

The original Hamiltonian H in eq. (3.22) is straightforwardly generalized: H_m still runs over all lattice sites, H_E and H_{int} run over all links (each vector now contains three components) and H_B now includes three differently oriented plaquette interactions (not a single one as for two space dimensions), taking the form

$$H_B = -\frac{1}{g^2} \sum_{\mathbf{x},i} \cos\left(\epsilon_{ijk} \Delta_j^{(+)} \theta_k(\mathbf{x}) \right) \tag{3.65}$$

which we will express in terms of the magnetic field variables

$$B_i(\mathbf{x}) = \epsilon_{ijk} \Delta_j^{(+)} \theta_k(\mathbf{x}) \tag{3.66}$$

The Gauss law takes the same form (3.26), this time with the three-dimensional divergence.

Decoupling the matter can be done with the same transformation $\mathcal{U}$ used in section 3.4, now in a three dimensional space and with the $d = 3$ Green's function (see Appendix 3.A) instead of the two dimensional one used above. Most of the transformed parts of the Hamiltonian ($\tilde{H}_E^T$, $\tilde{H}_E^L$ and $\tilde{H}_{int}$) will have an identical form as in the $d = 2$ case with the straightforward dimensional generalization, see eqs. (3.34), (3.35) and (3.41). Also the Gauss law transforms in the same manner, i.e. it gets decoupled from the matter degrees of freedom as in eq. (3.32). H_m and H_B still commute with the transformation $\mathcal{U}$.

The crucial difference in three space dimensions appears when formulating the transformed Hamiltonian in terms of dual variables. We start with the dual formulation in terms of the B- and L-variables in section 3.5. From eq. (3.66) it is clear that the divergence of B is zero, i.e. $\Delta_i^{(+)} B_i(\mathbf{x}) = 0 \, \forall \mathbf{x}$ holds on the operator level. Since this is an operator identity it is satisfied by any state; however, when building a classical or quantum simulation it cannot be assumed to be satisfied a priori and thus physical states need to fulfill a constraint for every cube:

$$\Delta_i^{(+)} B_i(\mathbf{x}) \, |\text{phys}\rangle = 0 \quad \forall \mathbf{x} \tag{3.67}$$

One can intuitively think about it in the electric basis, as raising the electric flux on all faces of a cube should leave the state invariant. Therefore, in three dimensions there are local constraints left. However, they do not involve the matter degrees of freedom. Note that for periodic boundary conditions these local constraints are not independent, since the sum over all local constraint gives zero, i.e. there are $N^3 - 1$ independent constraints. This is not the case for open boundary conditions. In addition there are three global constraints, which are a generalization of the single global constraint in two dimensions (again, only for periodic boundary conditions):

$$\sum_{\substack{x_i = 0 \\ x_j, x_k}} B_i(\mathbf{x}) \, |\text{phys}\rangle = 0 \quad \text{for} \quad i = 1, 2, 3 \tag{3.68}$$

with $i \neq j \neq k$ and $\mathbf{x} = (x_1, x_2, x_3)$. These global constraints correspond to slices through the lattice. There are only three independent ones since all other slices can be obtained by deforming them with the plaquette constraints from eq. (3.67).

We express the (transverse) electric field $E_i(\mathbf{x})$ after the transformation as the curl of a pseudovector $L_k(\mathbf{x})$. Thus, the definition of eq. (3.45) is replaced by

$$E_i(\mathbf{x}) = \epsilon_{ijk} \Delta_j^{(-)} L_k(\mathbf{x}) + \delta_{x_j,0} \delta_{x_k,0} L_i. \tag{3.69}$$

with $i \neq j \neq k$. The B_1/L_1-, B_2/L_2- and B_3/L_3-variables correspond to the three global loops winding around the lattice along a specific axis (only present for periodic boundary conditions). A discussion of the arising topological phenomena due to these global loops can be found in [62].

One can show that, similar to the two-dimensional case, the B- and L-variables fulfill canonical commutation relations,

$$\left[B_i(\mathbf{x}), L_j(\mathbf{y})\right] = i \delta_{ij} \delta(\mathbf{x}, \mathbf{y}). \tag{3.70}$$

Similar to the two dimensional case, we can perform a counting of degrees of freedom. For that we can neglect the matter degrees of freedom since their number is the same in both formulations. In the case of periodic boundary conditions, we have in the original link formulation $3N^3$ links and N^3 sites, thus $N^3 - 1$ independent Gauss laws, leading to $2N^3 + 1$ physical gauge degrees of freedom. In the dual formulation, there are $3N^3$ plaquettes, three global loop variables winding around the lattice, $N^3 - 1$ independent cube constraints as in eq. (3.67) and three global constraints, giving also a total of $2N^3 + 1$ physical gauge degrees of freedom.

In the case of open boundary conditions, we have in the original formulation $3N(N+1)^2$ links and $(N+1)^3$ sites, i.e $(N+1)^3 - 1$ Gauss law constraints and thus $2N^3 + 3N^2$ physical gauge degrees of freedom. In the dual formulation, we have $3N^2(N+1)$

plaquettes and N^3 cube constraints, resulting also in $2N^3+3N^2$ physical gauge degrees of freedom.

The (transverse) electric Hamiltonian written in terms of the L-variables takes a similar form as in the two-dimensional case,

$$\tilde{H}_E^T = \frac{g^2}{2}\sum_{\mathbf{x},i}\left(\epsilon_{ijk}\Delta_j^{(-)}L_k(\mathbf{x}) + \delta_{x_j,0}\delta_{x_k,0}L_i\right)^2 \tag{3.71}$$

with $i \neq j \neq k$ (the second term vanishes for open boundary conditions). The difference in three dimensions is that L-variables on four plaquettes (the ones containing the link) are required to express the transverse part of the electric field. The magnetic Hamiltonian is still a one-body term, as in two dimensions, which can be seen from eq. (3.65) and (3.66). The gauge-matter interactions have the same form as in (3.50) with the difference that the shifts $s_{\mathbf{x},i}(\mathbf{y})$ in the $L(\mathbf{y})$ variables in (3.49) are computed with the three-dimensional Green's function (see Appendix 3.A). Although this interaction involves many degrees of freedom, the shifts decay away from the link $(\mathbf{x}, i)$ (and even faster in three dimensions) which might allow one to neglect contributions above some certain distance.

The dual formulation in terms of the ϕ- and M-variables can be generalized in a similar fashion. We first define a pseudovector field on the plaquettes, $\phi_k(\mathbf{x})$, whose curl generates the transverse part of the gauge field (in addition to the global loop variables ϕ_i):

$$\theta_i^T(\mathbf{x}) = \epsilon_{ijk}\Delta_j^{(-)}\phi_k(\mathbf{x}) + \delta_{x_j,0}\delta_{x_k,0}\phi_i. \tag{3.72}$$

with $i \neq j \neq k$ (the second term vanishes for open boundary conditions). We also define M-variables as the curl of the electric field

$$M_i(\mathbf{x}) = \epsilon_{ijk}\Delta_j^{(+)}E_k(\mathbf{x}) \tag{3.73}$$

With the same reasoning as for the B-variables, we obtain similar local constraints as in eq. (3.67) for the M-variables

$$\Delta_i^{(+)}M_i(\mathbf{x})\,|\text{phys}\rangle = 0 \quad \forall\mathbf{x} \tag{3.74}$$

and the commutation relations

$$\left[\phi_i(\mathbf{x}), M_j(\mathbf{y})\right] = i\delta_{ij}\delta(\mathbf{x},\mathbf{y}). \tag{3.75}$$

As in the two dimensional case, the operators $M_i(\mathbf{x})$ have an integer spectrum. For periodic boundary conditions, the physical states need to fulfill the global constraints in eq. (3.68), with B replaced by M. The counting of degrees of freedom can be performed in the same way as for the B/L-variables.

The gauge-matter interactions written in terms of the ϕ-variables result again in local interactions (up to contributions from the global loop variables ϕ_i which are only present for periodic boundary conditions and then only on the axes),

$$\tilde{H}_{int} = \sum_{\mathbf{x},i} t_{\mathbf{x},i}\Psi^\dagger(\mathbf{x})\, e^{i\left(\epsilon_{ijk}\Delta_j^{(-)}\phi_k(\mathbf{x}) + \delta_{x_j,0}\delta_{x_k,0}\phi_i\right)}\Psi(\mathbf{x}+\hat{\mathbf{e}}_i) + h.c. \tag{3.76}$$

with $i \neq j \neq k$. In three dimensions four plaquettes are contributing compared to two in the two-dimensional case. If we express the magnetic interactions in terms of the ϕ-variables, we obtain

$$H_B = -\frac{1}{g^2}\sum_{\mathbf{x},i}\cos\left(\epsilon_{ijk}\epsilon_{klm}\Delta_j^{(+)}\Delta_l^{(-)}\phi_m(\mathbf{x})\right). \tag{3.77}$$

The magnetic interaction on a plaquette involves all ϕ-variables which share a link with the respective plaquette.

To conclude, in three space dimensions, the matter degrees of freedom can be decoupled from the gauge constraints, so that only the gauge field variables on the plaquettes are subject to constraints. However, compared to two dimensions, the remaining constraints are local, i.e. every cube on the lattice defines such a constraint. It involves six plaquette variables, compared to six link variables and the charge on the site in the original Gauss law. On the other hand, due to the additional dimension more degrees of freedom participate in the interactions, making the dual formulation in three dimensions more difficult to study compared to the two-dimensional version.

3.7 Conclusion

In this chapter, we have demonstrated a method for unitarily transforming compact QED with dynamical matter into a frame that allows for the expression of physical states through dual, gauge-invariant variables while preserving translational invariance. The transformation relies on the Helmholtz decomposition of lattice vector fields into transverse and longitudinal components. In the original formulation, the gauge constraints (known as Gauss laws) for physical states constrain the longitudinal component of the electric field based on the given charge configuration, while leaving the transverse component unaffected. However, since the gauge-matter interactions involve the longitudinal part of the gauge field, we rotate to a new frame where Coulomb gauge holds, and only the transverse component of the gauge field appears in the Hamiltonian. In this transformed formulation, the matter degrees of freedom become decoupled from the Gauss laws, and the physical (transverse) part of the gauge field and electric field can be expressed using a new set of canonical variables on the plaquettes, thus making the formulation manifestly gauge-invariant.

The transformation can be applied in both two and three spatial dimensions. Although the unitary transformation for two and three dimensions is quite similar, the formulation in terms of dual variables differs significantly. In two dimensions, the dual plaquette variables are entirely free of any local constraints. In contrast, in three dimensions, a local constraint exists for every cube on the lattice, involving all plaquette variables on that cube. This is due to the fact that every closed surface imposes a constraint on these dual variables because the integral of a transverse field (a curl field) over a closed surface must be zero. However, these local constraints solely involve the gauge field and do not affect the matter degrees of freedom.

The transformation is also applicable to systems with both periodic and open boundary conditions. The primary difference between the two is that in the case of periodic boundary conditions, there are global loop variables around the lattice for each spatial direction that do not exist in open boundary conditions. The introduction of *dynamical* charges and gauge-matter interactions makes these variables dynamic, which is a significant contrast to the case of static matter where these variables would only fix a topological sector [59]. Furthermore, periodic boundary conditions lead to an additional closed surfaces, as the lattice becomes a torus in $2+1d$, which generates a global

constraint on the dual plaquette variables.

After performing the unitary transformation, there are two sets of dual variables that can be used to represent the transverse part of the gauge field and electric field. The dual variables have the same locations for their degrees of freedom, but they differ in the complexity of the different terms in the Hamiltonian. The terms not involving the (transverse) gauge field, such as the mass term for the matter and the (longitudinal) electric Hamiltonian, are the same for both sets of dual variables. The mass term is not altered at all and the electric Hamiltonian containing the longitudinal electric field mediates Coulomb interactions between charges.

However, the gauge-matter interactions differ significantly: they become more complex in the dual formulation using B/L-variables, as the hopping of a matter degree of freedom affects numerous plaquette variables on the lattice. In contrast, the dual formulation in terms of ϕ/M-variables makes the gauge-matter interactions local, involving only the plaquette variables containing the link where the hopping occurs. It is the other way around for the magnetic term: in two dimensions, the magnetic interaction using ϕ/M-variables is a five-body interaction among a plaquette and its four neighbors while, using B/L-variables, the magnetic term is only a one-body term. The last term, the transverse electric Hamiltonian is a Coulomb interaction among the plaquette variables for the ϕ/M-variables and a local two-body interaction between neighboring plaquettes for the B/L-variables.

Both dual formulations could be advantageous for classical variational studies and quantum simulation/computation of lattice gauge theories. They provide descriptions with reduced or no gauge redundancies, thereby minimizing the resources required and avoiding possible violations of gauge-invariance. The absence of constraints in these dual formulations also permits one to examine a wider range of potential ansatz states, making them useful for variational studies.

The B/L-formulation could be used to extend variational ansatz states for compact QED with static fermions (as presented in chapter 4 to study real-time dynamics, based on ref. [2]) to dynamical fermions to design ansatz states similar to the one presented in chapter 5 (based on ref. [3]), allowing the study of lattice gauge theories at finite density.

The ϕ/M-formulation may be useful in designing a quantum simulation, as the challenging terms in its implementation are the Coulomb interactions and the five-body interaction of the magnetic Hamiltonian. However, the latter is merely the ordinary four-body (plaquette) interaction in the Kogut-Susskind Hamiltonian, with an additional degree of freedom in the center of the relevant plaquette. In recent years, there has been significant effort to implement this interaction in a quantum simulation, e.g. with the use of optical lattices [4, 41, 69]. These efforts can serve as a starting point for implementing the interaction above. The more challenging aspect is generating a Coulomb potential using quantum devices. This challenge is also present in the quantum simulation of quantum chemistry, where a Coulomb potential is a crucial building block. In the last years, there have been proposals to implement such a potential using ultracold atoms [70], which may also be useful in lattice gauge theory. To further reduce the necessary resources for a quantum simulation, one could combine our approach with a truncation scheme for the gauge field Hilbert space of the dual variables, e.g. according to ref. [61]. Note that this approach is much more efficient compared to truncating already in the original, gauge-constrained theory.

The method can be straightforwardly extended to $\mathbb{Z}_N$ groups, which are subgroups of

$U(1)$. However, for non-Abelian groups, decomposing the gauge field and electric field in a similar manner to the Abelian case into a longitudinal and transverse part, results in non-linear equations, preventing the construction of a unitary transformation similar to the Abelian case. Other methods for separating the constrained and unconstrained parts of the gauge field exist, such as the maximal tree approach [71], but do not preserve translational invariance.

APPENDIX

3.A THE LATTICE POISSON EQUATION

In this section, we discuss the calculation of the lattice Green's function $G(\mathbf{x},\mathbf{y})$ for both periodic and open boundary conditions, defined by the equation

$$-\nabla^2 G\left(\mathbf{x},\mathbf{y}\right) = \delta\left(\mathbf{x},\mathbf{y}\right). \tag{3.78}$$

The solutions to Poisson's equation

$$-\nabla^2 f\left(\mathbf{x}\right) = Q\left(\mathbf{x}\right) \tag{3.79}$$

can be constructed out of it as a superposition,

$$f(\mathbf{x}) = \sum_{\mathbf{y}} G(\mathbf{x},\mathbf{y}) Q(\mathbf{y}). \tag{3.80}$$

Starting with periodic boundary conditions in d space dimensions, the (negative) Laplacian takes the form

$$-\nabla^2 f\left(\mathbf{x}\right) = 2d f\left(\mathbf{x}\right) - \sum_{i=1}^{d} \left(f\left(\mathbf{x}+\hat{\mathbf{e}}_i\right) + f\left(\mathbf{x}-\hat{\mathbf{e}}_i\right)\right). \tag{3.81}$$

We define the Fourier transformation on the lattice as

$$\mathcal{F}\left[f\left(\mathbf{x}\right)\right] = \tilde{f}\left(\mathbf{k}\right) = \frac{1}{N^{d/2}} \sum_{\mathbf{x}} e^{i\frac{2\pi}{N}\mathbf{k}\cdot\mathbf{x}} f\left(\mathbf{x}\right). \tag{3.82}$$

We can now obtain the lattice Green's function by Fourier transformation of eq. (3.78),

$$G(\mathbf{x},\mathbf{y}) = G(\mathbf{x}-\mathbf{y}) = \sum_{\mathbf{k}\neq 0} \frac{e^{i\frac{2\pi}{N}(\mathbf{x}-\mathbf{y})\mathbf{k}}}{2\left(d - \sum_i \cos\left(\frac{2\pi}{N}k_i\right)\right)} \tag{3.83}$$

with $\mathbf{x} = (x_1,..,x_d)$, $\mathbf{k} = (k_1,..,k_d)$ and $x_i, k_i \in \{0,..,N-1\}$. The $\mathbf{k} = \mathbf{0}$ mode can be neglected, since the total charge on the lattice is always zero due to gauge invariance. The Green's function in two and three dimensions differs only by an additional term in the denominator in eq. (3.83) due to the additional dimension.

For open boundary conditions, one cannot obtain such an explicit formula due to boundary effects. The lattice sites on the corners only have half the number of neighboring sites compared to the bulk so that the Laplace operator looks different (3.81) (say e.g. the bottom left corner, $\mathbf{x} = \mathbf{0}$):

$$-\nabla^2 f(\mathbf{0}) = d f(\mathbf{0}) - \sum_{i=1}^{d} f(\mathbf{0}+\hat{\mathbf{e}}_i) \tag{3.84}$$

The Laplace operator on the edges is modified in an analogous way. Therefore, the operator cannot be diagonalized by a discrete Fourier transform but needs to be inverted numerically. Since the Laplace matrix is singular one needs to fix a condition, e.g. $\sum_{\mathbf{x}} G(\mathbf{x},\mathbf{y}) = 0$. By fixing $\mathbf{y}$ for different lattice positions and inverting the Laplace matrix, one can then obtain the Green's function $G(\mathbf{x},\mathbf{y})$.

3.B The lattice Helmholtz decomposition

With the Green's function from the previous section, we can write down the (Helmholtz) decomposition of a lattice vector field into transverse and longitudinal components, as written in eq. (3.8). For that, we will need the double curl identity

$$\begin{aligned}\left[\nabla\times\left(\nabla\times\mathbf{F}\right)\right]_i(\mathbf{x}) &= \epsilon_{ijk}\Delta_j^{(-)}\epsilon_{klm}\Delta_l^{(+)}F_m(\mathbf{x})\\ &= (\delta_{il}\delta_{jm}-\delta_{im}\delta_{jl})\Delta_j^{(-)}\Delta_l^{(+)}F_m(\mathbf{x})\\ &= \Delta_i^{(+)}\Delta_j^{(-)}F_j(\mathbf{x})-\Delta_j^{(-)}\Delta_j^{(+)}F_i(\mathbf{x})\\ &= \nabla_i\left(\nabla\cdot\mathbf{F}(\mathbf{x})\right)-\nabla^2F_i(\mathbf{x}).\end{aligned} \tag{3.85}$$

One should note that for periodic boundary conditions there is an additional contribution in the double curl coming from global loops around the lattice which need to be taken into account.

3.B.1 Periodic boundary conditions

We can now derive the Helmholtz decomposition in an analogous way to the continuum version (for periodic boundary conditions):

$$F_i(\mathbf{x}) = \sum_{\mathbf{y}}\delta(\mathbf{x},\mathbf{y})F_i(\mathbf{y}) = -\nabla^2_{\mathbf{x}}\sum_{\mathbf{y}}G(\mathbf{x},\mathbf{y})F_i(\mathbf{y}) \tag{3.86}$$

Inserting the double curl identity (3.85), we get the separation into a longitudinal and a transverse component. The longitudinal component has the form

$$F_i^L(\mathbf{x}) = -\Delta_i^{(+)}\phi(\mathbf{x}) \tag{3.87}$$

with the scalar field ϕ on the sites

$$\begin{aligned}\phi(\mathbf{x}) &= \sum_{\mathbf{y}}\Delta_{j,\mathbf{x}}^{(-)}G(\mathbf{x},\mathbf{y})F_j(\mathbf{y})\\ &= \sum_{\mathbf{y}}G(\mathbf{x},\mathbf{y})\Delta_{j,\mathbf{y}}^{(-)}F_j(\mathbf{y})\end{aligned} \tag{3.88}$$

The transverse component is a little more complicated since we also need to take into account the contributions from the global loops L_i around the lattice. Without the global part, we obtain for the transverse component

$$F^T_{\text{plaq},i}(\mathbf{x}) = \epsilon_{ijk}\Delta_j^{(-)}L_{\text{plaq},k}(\mathbf{x}) \tag{3.89}$$

with the pseudovector field L on the plaquettes

$$\begin{aligned}L_{\text{plaq},k}(\mathbf{x}) &= \sum_{\mathbf{y}}\epsilon_{klm}\Delta_{l,\mathbf{x}}^{(+)}G(\mathbf{x},\mathbf{y})F_m(\mathbf{y})\\ &= \sum_{\mathbf{y}}G(\mathbf{x},\mathbf{y})\epsilon_{klm}\Delta_{l,\mathbf{y}}^{(+)}F_m(\mathbf{y}).\end{aligned} \tag{3.90}$$

If we look at the field generated by the scalar field ϕ and the pseudovector field L_{plaq} in Fourier space, it is clear that all momentum modes of F can be obtained apart from

the $\mathbf{k} = 0$ mode, i.e. a constant field. For that, the global loop L_i is required, which needs to be fixed to

$$L_i = \frac{1}{N} \sum_{\mathbf{x}} F_i(\mathbf{x}). \tag{3.91}$$

This gives the correct $\mathbf{k} = 0$ mode but in order to get a constant field this contribution needs to be equally distributed over the lattice. Thus, we define an additional L_{const}-field on the plaquettes, on top of L_{plaq} (exemplary for L_1, the other spatial directions follow analogously):

$$\begin{aligned} L_{\text{const},3}(\mathbf{x}) &= \frac{\sum_{\mathbf{y}} F_1(\mathbf{y})}{N^2} x_2 \quad \text{if} \quad x_3 = 0 \\ L_{\text{const},2}(\mathbf{x}) &= -\frac{\sum_{\mathbf{y}} F_1(\mathbf{y})}{N^3} x_3. \end{aligned} \tag{3.92}$$

$L_{\text{const},3}$ distributes the field of the global loop L_1 in the $\hat{\mathbf{e}}_2$-direction and $L_{\text{const},2}$ from the $\hat{\mathbf{e}}_1, \hat{\mathbf{e}}_2$-plane in the $\hat{\mathbf{e}}_3$-direction over the whole lattice, giving us a constant field in the $\hat{\mathbf{e}}_1$-direction. The total plaquette field of the L-variables is then $L \equiv L_{\text{plaq}} + L_{\text{const}}$ and the total transverse component $F_i^T(\mathbf{x}) \equiv F_{\text{plaq},i}^T(\mathbf{x}) + \frac{\sum_{\mathbf{y}} F_i(\mathbf{y})}{N^3}$. The Helmholtz decomposition of F can thus be written as

$$\begin{aligned} F_i(\mathbf{x}) &= -\Delta_i^{(+)} \phi(\mathbf{x}) + \epsilon_{ijk} \Delta_j^{(-)} (L_{\text{plaq}} + L_{\text{const}})_k(\mathbf{x}) + \delta_{x_j,0} \delta_{x_k,0} L_i. \\ &= -\Delta_i^{(+)} \phi(\mathbf{x}) + \epsilon_{ijk} \Delta_j^{(-)} L_k(\mathbf{x}) + \delta_{x_j,0} \delta_{x_k,0} L_i. \\ &= F_i^L(\mathbf{x}) + F_{\text{plaq},i}^T(\mathbf{x}) + \frac{\sum_{\mathbf{y}} F_i(\mathbf{y})}{N^3} \\ &= F_i^L(\mathbf{x}) + F_i^T(\mathbf{x}) \end{aligned} \tag{3.93}$$

with $i \neq j \neq k$.

3.B.2 Open boundary conditions

For open boundary conditions, one can perform a similar decomposition, with the major difference that there is no global loop participating. It can be written as

$$F_i(\mathbf{x}) = -\Delta_i^{(+)} \phi(\mathbf{x}) + \epsilon_{ijk} \Delta_j^{(-)} L_k(\mathbf{x}) \tag{3.94}$$

where the scalar field ϕ has the same form as in eq. (3.88), with the Green's function replaced by the one for open boundary condition. The plaquette field L also has the same form as in eq. (3.90), but the sum goes only over all plaquettes (not all lattice sites) and the Green's function $G_{\text{plaq}}(\mathbf{x}, \mathbf{y})$ is determined by a modified Laplace operator ∇^2_{plaq} on the plaquettes:

$$-\nabla^2_{\text{plaq}} f(\mathbf{x}) = 2d f(\mathbf{x}) - \sum_{i=1}^{d} (f(\mathbf{x} + \hat{\mathbf{e}}_i) + f(\mathbf{x} - \hat{\mathbf{e}}_i)) \tag{3.95}$$

where the difference is the constant factor of $2d$, also at the boundaries, e.g. at $\mathbf{x} = 0$:

$$-\tilde{\nabla}^2 f(\mathbf{0}) = 2d f(\mathbf{0}) - \sum_{i=1}^{d} f(\mathbf{0} + \hat{\mathbf{e}}_i) \tag{3.96}$$

All the above discussion applies immediately to the $d = 2$ case, by embedding it in $d = 3$.

3.B.3 The shifts $s_{\mathbf{x},i}(\mathbf{y})$

As a result of the Helmholtz decomposition, we obtain the shifts $s_{\mathbf{x},i}(\mathbf{y})$ discussed in section 3.5, which describe the shifts in the electric plaquette variables $L(\mathbf{x})$ when a matter degree of freedom hops to an adjacent site. We just need to replace the general field $F_i(\mathbf{x})$ with a field which is zero everywhere and one on the link where hopping occurs. The resulting values for L computed by eq. (3.90), (3.91) and (3.92) adapted to two dimensions give exactly the shifts $s_{\mathbf{x},i}(\mathbf{y})$ (analogously for open boundary conditions), e.g. for a shift in $\hat{\mathbf{e}}_1$-direction:

$$\begin{aligned} s_{\text{plaq},\mathbf{x},1}(\mathbf{y}) &= G(\mathbf{y},\mathbf{x}) - G(\mathbf{y},\mathbf{x}-\hat{\mathbf{e}}_2) \\ s_{\text{const},\mathbf{x},1}(\mathbf{y}) &= \frac{1}{N^2} y_2 \\ s_{\mathbf{x},1}(1) &= \frac{1}{N} \end{aligned} \tag{3.97}$$

so that $s_{\mathbf{x},1}(\mathbf{y}) = s_{\text{plaq},\mathbf{x},1}(\mathbf{y}) + s_{\text{const},\mathbf{x},1}(\mathbf{y})$ and with $s_{\mathbf{x},1}(1)$ the shift in the global loop variable L_1.

3.C Canonical commutation relations

In this section we show that the dual B/L-variables fulfill canonical commutation relations as stated in eq. (3.44). Using the expression of $L(\mathbf{y})$ in terms of the original electric field $E_i(\mathbf{y})$ on the links (see eq. (3.43)), the expression of $B(\mathbf{x})$ as the lattice curl of the gauge field $\theta_j(\mathbf{x})$ (see eq. (3.19)) and the original canonical commutation relations in eq. (3.16), we obtain

$$\begin{aligned} [B(\mathbf{x}), L(\mathbf{y})] &= \epsilon_{ij}\epsilon_{kl} \sum_{\mathbf{y}'} \Delta^{(+)}_{k,\mathbf{y}} G(\mathbf{y},\mathbf{y}') \left[\Delta^{(+)}_{i,\mathbf{x}} \theta_j(\mathbf{x}), E_l(\mathbf{y}')\right] \\ &= \epsilon_{ij}\epsilon_{kl} \sum_{\mathbf{y}'} \Delta^{(+)}_{k,\mathbf{y}} G(\mathbf{y},\mathbf{y}') i\delta_{jl} \left(\delta_{\mathbf{x}+\hat{\mathbf{e}}_i,\mathbf{y}'} - \delta_{\mathbf{x},\mathbf{y}'}\right) \\ &= \epsilon_{ij}\epsilon_{kj} i \Delta^{(+)}_{k,\mathbf{y}} \Delta^{(+)}_{i,\mathbf{x}} G(\mathbf{y},\mathbf{x}) \\ &= -i\Delta^{(-)}_{i,\mathbf{x}} \Delta^{(+)}_{i,\mathbf{x}} G(\mathbf{y},\mathbf{x}) \\ &= i\delta_{\mathbf{x},\mathbf{y}} \end{aligned} \tag{3.98}$$

canonical commutation relations also for B and L. In a completely analogous way one can derive the canonical commutation relations for ϕ and M.

3.D The modified Coulomb potential between the dual M-variables for periodic boundary conditions

If we consider periodic boundary conditions in the dual formulation in terms of the ϕ/M-variables, the electric Hamiltonian gives rise to Coulomb-type interactions between the M-variables. The interaction potential $\widetilde{G}(\mathbf{x},\mathbf{y})$ is slightly modified compared to the potential for the matter degrees of freedom due to the global loops as discussed

in section 3.5 in eq. (3.58). They change the Laplace operator (here in two dimensions) on the plaquettes to, see eq. (3.57):

$$\begin{aligned} M(\mathbf{x}) = &- \nabla^2 L(\mathbf{x}) + \epsilon_{ij}\Delta_i^{(+)}\delta_{x_i,0}L_j \\ &- \nabla^2 L(\mathbf{x}) + \left(\delta_{x_2,0} - \delta_{x_2,-1}\right) L_1 - \left(\delta_{x_1,0} - \delta_{x_1,-1}\right) L_2 \end{aligned} \tag{3.99}$$

The plaquettes where the Laplace operator is altered are the ones sharing a link with one of the two axes. The relation between the global M-variables M_1 and M_2 and L is

$$\begin{aligned} M_1 &= NL_1 + \sum_{\substack{x_2=0 \\ x_1}} \left(L(\mathbf{x}) - L(\mathbf{x} - \hat{\mathbf{e}}_2)\right) \\ M_2 &= NL_2 - \sum_{\substack{x_1=0 \\ x_2}} \left(L(\mathbf{x}) - L(\mathbf{x} - \hat{\mathbf{e}}_1)\right) \end{aligned} \tag{3.100}$$

If one defines an M-vector out of the plaquette variables $M(\mathbf{x})$ and the global variables M_1 and M_2, $M \equiv (M(\mathbf{x}), M_1, M_2)$, and analogously for L, one can construct a system of linear equations for M and L out of eq. (3.99) and eq. (3.100), denoted by D, i.e $DL \equiv M$, which can be inverted (after fixing some condition), resulting in

$$L(\mathbf{x}) = \sum_{\mathbf{y}} D^{-1}(\mathbf{x}, \mathbf{y})\, M(\mathbf{y}). \tag{3.101}$$

Note that the sum over $\mathbf{y}$ also contains 1 and 2, corresponding to the global loop variables M_1 and M_2. Inserting this relation in the electric Hamiltonian in terms of L in eq. (3.48), gives eq. (3.58)

$$H_E^T = \frac{g^2}{2} \sum_{\mathbf{x},\mathbf{y}} M(\mathbf{x}) \widetilde{G}(\mathbf{x}, \mathbf{y})\, M(\mathbf{y}) \tag{3.102}$$

with

$$\begin{aligned} \widetilde{G}(\mathbf{x}, \mathbf{y}) = \sum_{\mathbf{x}', i} &\left(\epsilon_{ij}\Delta_{i,\mathbf{x}'}^{(-)} D^{-1}(\mathbf{x}', \mathbf{x}) + \delta_{x_j,0} D^{-1}(i, \mathbf{x})\right) \\ &\times \left(\epsilon_{ik}\Delta_{i,\mathbf{x}'}^{(-)} D^{-1}(\mathbf{x}', \mathbf{y}) + \delta_{x_k,0} D^{-1}(i, \mathbf{y})\right) \end{aligned} \tag{3.103}$$

with $i \neq j$ and $i \neq k$. Since $\mathbf{x}$ and $\mathbf{y}$ also include the global variables M_1 and M_2 (denoted by 1 and 2, as for example in $D^{-1}(i, \mathbf{x})$), there are non-trivial interactions between the global variables and the plaquette variables. For open boundary conditions, the above equation expression for $\widetilde{G}(\mathbf{x}, \mathbf{y})$ reduces to $G(\mathbf{x}, \mathbf{y})$.

4 Real-time dynamics in 2+1D compact QED using complex periodic Gaussian states

4.1 Motivation

Gauge theories play a crucial role in fundamental physics, with the standard model of particle physics being a prominent example that describes electromagnetic, weak, and strong interactions. While perturbative expansions can be used to treat interactions in some regimes, the coupling in quantum field theories varies with scale, which means that non-perturbative methods are necessary in certain cases, such as in low-energy QCD [5, 72].

Lattice gauge theory is a method of discretizing either spacetime or space, which allows for the investigation of non-perturbative quantum field theories while maintaining gauge invariance [7, 8]. Monte-Carlo simulations have been instrumental in uncovering many interesting features of these theories [73]. However, there are certain challenges associated with this approach. For instance, fermionic theories with finite chemical potentials may be affected by the sign problem [12], and accessing time dynamics can be challenging since Monte-Carlo simulations require a formulation in Euclidean spacetime.

To address the challenges faced in action-based formulations of lattice gauge theories, other approaches have been proposed based on the Hamiltonian formulation. Kogut and Susskind were the first to propose this approach [8], which has inspired also other Hamiltonian formulations like the quantum link model [43–46] or the prepotential approach [74]. Recent advances have shown that these Hamiltonians can be simulated on quantum devices like ultracold atoms, trapped ions, and superconducting qubits [15]. Additionally, variational ansatz states can be designed to efficiently capture the most relevant features of the theory.

Both quantum simulation and classical numerical methods have been successfully applied to one-dimensional lattice gauge theories. The feasibility of quantum simulation has been demonstrated with trapped ions and ultracold atoms [34–38]. On the numerical side, matrix product state (MPS) methods have been applied to $(1+1)$-dimensional Abelian and non-Abelian lattice gauge theories [75–82]. These MPS methods enable the study of finite chemical potential scenarios and out-of-equilibrium dynamics, which are difficult to access with Monte-Carlo simulations of Euclidean lattice gauge theory.

In higher spatial dimensions, the presence of magnetic interactions leads to the appearance of four-body plaquette interactions on the lattice, making the situation more challenging. For quantum simulators solutions to this problem have been proposed, based on digital or analog simulation schemes, but they are currently beyond experimental capabilities. In two spatial dimensions, tensor network methods have been successfully applied to ground state problems in pure gauge theories with a finite-

dimensional gauge field Hilbert space, which can be achieved either by truncating the $U(1)$ gauge group to $\mathbb{Z}_3$ [83] or using a $U(1)$ quantum link formulation [84, 85].

This chapter focuses on $(2+1)$-dimensional compact quantum electrodynamics, which has an infinite-dimensional gauge field Hilbert space and shares some characteristics with $(3+1)$-dimensional quantum chromodynamics. It is a suitable starting point for the investigation of higher-dimensional lattice gauge theories since it is in a confined phase for all values of the coupling constant [18]. To explore physics that is challenging to simulate using Monte-Carlo simulations of Euclidean lattice gauge theories, we investigate not only ground state properties but also real-time dynamics after a quantum quench.

As system sizes increases, exact diagonalization methods become more and more impractical. However, due to the infinite-dimensional local Hilbert space of the gauge field, they are already impractical for the study of compact QED on a single plaquette. Therefore, one needs to resort to variational techniques. In one spatial dimension, the infinite dimension can be circumvented by integrating out the gauge field [16, 17, 86], which becomes impossible in two and more spatial dimensions.

In this chapter, a new class of variational ansatz states is presented that is suitable to capture the infinite-dimensional Hilbert space of compact QED. These states are complex periodic Gaussian states, which are a generalization of the periodic Gaussian states introduced in a previous study [57]. It is a Gaussian state in the gauge field plaquette variables, which is made periodic by an infinite summation over integer-valued variables. The periodicity is crucial to capture the compactness of the $U(1)$ gauge field. A numerical approximation scheme is developed to evaluate these infinite sums so that the states can be efficiently evaluated for all variational parameters. By extending the variational manifold to include complex periodic Gaussian states, it is possible to study real-time dynamics and thus the non-equilibrium dynamics after a global quench. Since these states do not require any truncation in Hilbert space, it also allows to investigate truncation effects and determine in which coupling regimes such truncations are justified.

The content of this chapter is based on Ref. [2].

4.2 Executive summary

As opposed to lattice gauge theories in one dimension, it is not possible to integrate out the gauge field in two and more spatial dimensions. Therefore, one needs to find a way how to deal with the infinite-dimensional Hilbert space of the gauge field.

One way is to use a truncated formulation which requires to justify the truncation for every scenario that one considers (a truncation might work for ground state problems but might fail for out-of-equilibrium dynamics). Another approach is to find variational methods that do not need such a truncation which will be pursued in this chapter. This also allows to guide other methods which only work for finite-dimensional Hilbert spaces to guide the search for possible truncation schemes.

Such variational states, so called complex periodic Gaussian states, will be presented for the study of $(2+1)$-dimensional comapct QED, i.e. a lattice gauge theory based on the compact $U(1)$ gauge group. The gauge field on every link can be characterized either by a compact angular variable $\theta \in [0, 2\pi)$ or an integer-valued electric field variable. The compact nature of the gauge field is crucial to observe certain non-perturbative effects on the lattice such as confinement. It is known that in the continuum limit compact QED becomes a free theory and the ground state of the gauge field can be described by a Gaussian.

The intuition behind the construction of the variational ansatz is to take a Gaussian state in the gauge field and make it periodic to account for the compactness of the $U(1)$ gauge group. Periodicity can be achieved by infinite sums over integer-valued variables. A numerical scheme is presented that can evaluate these infinite sums efficiently. A major reason for its efficiency is that a periodic Gaussian state is self-similar in the sense that the infinite sum over a very slowly decaying Gaussian state can be rewritten as the sum over a very strongly decaying Gaussian state. This allows to find a form of the variational state that where it is possible to truncate the infinite sums after a rather small finite order. Hence, the ansatz can be efficiently evaluated for all variational parameters.

The variational method is used to study ground state properties and real-time dynamics. First, for the one plaquette case, where an exact solution of the ground state is known, the variational ground state energy is compared to the exact result, showing very good agreement over the whole coupling region, with a maximal relative error of 0.005. Secondly, ground state properties are studied, in particular confinement. The string tension, is computed with two methods, via the area law of Wilson loops and the potential between two static charges, showing that confinement persists throughout the whole coupling region, in agreement with theory [18]. Moreover truncation effects in the gauge field hilbert space are investigated, showing that a common truncation in the electric basis is justified for the ground state at strong coupling but fails for the ground state in the weak-coupling region.

For the study of real-time dynamics the ansatz is first benchmark against exact diagonalizaton in the strong coupling region where a truncation can be justified, thus enabling exact diagonalization methods. We observe relatively good agreement. We then study out-of-equilibrium dynamics by considering various quantum quenches. First, the variational ground state at a certain coupling is prepared and then the coupling constant is changed to a different regime. We can observe rather long, stable time dynamics where the variational energy stays constant to very high accuracy. All quenches show equilibrating behavior. One interesting such quench is the real-time

evolution of a strongly confined flux tube after a quench to weak-coupling where we see equilibration to a state where no remnant of confinement is present, indicating possible thermalization at a temperature above the confinement-deconfinement transition [87].

The following sections are structured as follows: section 4.3 presents the variational ansatz, along with a numerical scheme for its evaluation. The first part of section 4.4 examines the ground state energy density and string tension across the entire coupling range. In the second part, truncation effects are explored by comparing the variational ground state energy with exact diagonalization results obtained by truncating the local Hilbert space in the electric basis. Section 4.5 focuses on real-time dynamics following a quantum quench, using the time-dependent variational principle.

4.3 The variational method: complex periodic Gaussian states

4.3.1 (2+1)-dimensional compact QED

We briefly review (2+1)-dimensional compact QED on a square lattice of extent $L \times L$ with periodic boundary conditions. The gauge fields reside on the links; $U_{\mathbf{x},i}$ denotes the gauge field operator on the link emanating from site $\mathbf{x}$ in direction $\mathbf{e}_i$. The Hamiltonian in lattice units takes the following form, originally proposed by Kogut and Susskind [8]:

$$H_{KS} = \frac{g^2}{2} \sum_{\mathbf{x},i} E_{\mathbf{x},i}^2 + \frac{1}{2g^2} \sum_{\mathbf{p}} 2 - (U_{\mathbf{p}} + U_{\mathbf{p}}^\dagger) \tag{4.1}$$

with g^2 being the coupling constant and $U_{\mathbf{p}} = U_{\mathbf{x},1} U_{\mathbf{x}+\mathbf{e}_1,2} U_{\mathbf{x}+\mathbf{e}_2,1}^\dagger U_{\mathbf{x},2}^\dagger$ where $\mathbf{x}$ is the bottom left corner of plaquette $\mathbf{p}$. $U_{\mathbf{x},i}$ is in the fundamental representation of $U(1)$, it can also be written in terms of an angle $\theta_{\mathbf{x},i}$, $U_{\mathbf{x},i} = e^{i\theta_{\mathbf{x},i}}$ with $-\pi < \theta_{\mathbf{x},i} \leq \pi$. The restriction of the gauge field to this compact interval is the reason why the model is called compact QED and why it exhibits interesting features such as confinement in contrast to the non-compact theory [88]. $E_{\mathbf{x},i}$ is the electric field operator fulfilling the following commutation relations:

$$\begin{aligned} [E_{\mathbf{x},i}, U_{\mathbf{y},j}] &= \delta_{\mathbf{x},\mathbf{y}} \delta_{i,j} U_{\mathbf{x},i} \\ [\theta_{\mathbf{x},i}, E_{\mathbf{y},j}] &= i \delta_{\mathbf{x},\mathbf{y}} \delta_{i,j} \end{aligned} \tag{4.2}$$

Since we work in the temporal gauge, there is a residual spatial gauge symmetry defined by the Gauss law operators $G_{\mathbf{x}}$. All physical states need to be eigenstates of them:

$$G_{\mathbf{x}} |\text{phys}\rangle = \sum_{i=1}^{2} \left(E_{\mathbf{x},i} - E_{\mathbf{x}-\mathbf{e}_i,i} \right) |\text{phys}\rangle = Q_{\mathbf{x}} |\text{phys}\rangle \quad \forall \mathbf{x} \tag{4.3}$$

where the eigenvalue $Q_{\mathbf{x}}$ gives the static charge configuration at $\mathbf{x}$.

These local constraints put quite severe restrictions on the choice of variational states. Thus, we change to a gauge-invariant description of compact QED as presented in chapter 3, but restricted to the case of static charges as opposed to the general discussion of chapter 3 involving dynamical fermions. This allows, without performing a unitary transformation, to change to variables where gauge invariance is already incorporated (at least up to a global constraint) using the splitting of the electric field $E_{\mathbf{x},i}$ into a transvere part $E_{\mathbf{x},i}^T$, which is dynamical, and a longitudinal part $E_{\mathbf{x},i}^L$ which is fixed by the static charge configuration. Since the transverse part of the electric field can be expressed by a plaquette field $L_{\mathbf{p}}$ (the lattice analogue of a solenoidal vector field), the remaining dynamical degrees of freedom $\{L_{\mathbf{p}}, U_{\mathbf{p}} = e^{i\theta_{\mathbf{p}}}\}$ reside on plaquettes, having the same Hilbert space structure and fulfilling the same commutation relations as the link variables:

$$\begin{aligned} [L_{\mathbf{p}}, U_{\mathbf{p}'}] &= \delta_{\mathbf{p},\mathbf{p}'} U_{\mathbf{p}'} \\ [\theta_{\mathbf{p}}, L_{\mathbf{p}'}] &= i \delta_{\mathbf{p},\mathbf{p}'} . \end{aligned} \tag{4.4}$$

The operator $U_{\mathbf{p}}$ creates an electric flux excitation around plaquette $\mathbf{p}$. However, to construct all possible gauge-invariant flux configurations two global non-contractible

flux loops around the torus (one for each spatial direction) are required, their operators are denoted as $\{\theta_1, L_1\}$ and $\{\theta_2, L_2\}$ specifying the topological sector of the flux configuration. L_1 and L_2 commute with the Hamiltonian and we will restrict ourselves to the topological sector with $L_1 = L_2 = 0$ which corresponds to no electric flux loops winding around the torus. This is in stark contrast to compact QED with dynamical fermions as the appearance of gauge-matter interactions makes the global loop variables dynamical. For more details see Appendix 4.A or chapter 3. Writing the Hamiltonian in terms of these new variables, reads

$$\begin{aligned} H_{KS} =& E_C + \frac{1}{g^2}\sum_{\mathbf{p}}(1-\cos\theta_{\mathbf{p}}) \\ &+\frac{g^2}{2}\sum_{\mathbf{p}}\sum_{i=1}^{2}\left(L_{\mathbf{p}} - L_{\mathbf{p}-\mathbf{e}_i} + \epsilon_{\mathbf{p}} - \epsilon_{\mathbf{p}-\mathbf{e}_i}\right)^2 \end{aligned} \tag{4.5}$$

where E_C is an energy offset given by the lattice Coulomb energy (note that upon the inclusion of dynamical fermions this term will involve interactions between dynamical charges as discussed in chapter 3) and $\epsilon_{\mathbf{p}}$ accounts for the transversal part of the electric field caused by the static charges only, i.e $\epsilon_{\mathbf{p}} = 0$ in case of no static charges. Even in this formulation there is one remaining global constraint left which is intuitively clear since raising the electric flux around all plaquettes should return the same state due to the periodic boundary conditions. Thus,

$$\prod_{\mathbf{p}} U_{\mathbf{p}} \left|\text{phys}\right\rangle = \left|\text{phys}\right\rangle . \tag{4.6}$$

An explicit formula for the calculation of $\epsilon_{\mathbf{p}}$ and E_C depending on the static charge configuration can be found in Appendix 4.A.

4.3.2 The variational ansatz

We formulate our variational ansatz states in terms of the $\theta_{\mathbf{p}}$-variables defined above such that it only needs to fulfill the global constraint (4.6). Starting from periodic Gaussian states introduced in [57], we extend the variational wavefunction to have an imaginary part in order to account for real-time dynamics. The ansatz is based on a complex Gaussian state:

$$\Psi_{CG}(\{x_{\mathbf{p}}\}) \equiv e^{-\frac{1}{2}\sum_{\mathbf{p},\mathbf{p}'} x_{\mathbf{p}} A_{\mathbf{p}\mathbf{p}'} x_{\mathbf{p}'} - i\sum_{\mathbf{p}} \epsilon_{\mathbf{p}} x_{\mathbf{p}}} \tag{4.7}$$

with $x_{\mathbf{p}} \in \mathbb{R}$ and $\mathbf{p} = (p_1, p_2)$, $p_1, p_2 \in [0, .., L-1]$. The linear part in the exponent, i.e. $\epsilon_{\mathbf{p}}$, is fixed by the static charge configuration (see section 4.3.1 and Appendix 4.A) and

$$A_{\mathbf{p}\mathbf{p}'} \equiv \frac{1}{\pi L^2}\sum_{k_1,k_2=0}^{L-1} e^{2\pi i \frac{(p_1-p_1')k_1 + (p_2-p_2')k_2}{L}} \left(\gamma_{\mathbf{k}}^R + i\gamma_{\mathbf{k}}^I\right) \tag{4.8}$$

is defined by the variational parameters $\{\gamma_{\mathbf{k}}^R\}$ and $\{\gamma_{\mathbf{k}}^I\}$. In the following, we will use the shorthand notation $\mathbf{pk} \equiv 2\pi\frac{p_1k_1 + p_2k_2}{L}$. Since the disorder introduced by static charges is incorporated in $\epsilon_{\mathbf{p}}$, the quadratic part A is assumed to be translationally invariant. The factor of $1/\pi$ is chosen for later convenience. Written in terms of

Fourier components $x_{\mathbf{k}} = \frac{1}{L}\sum_{\mathbf{p}} e^{i\mathbf{pk}} x_{\mathbf{p}}$, the quadratic part in the exponential becomes $\sum_{\mathbf{p},\mathbf{p}'} x_{\mathbf{p}} A_{\mathbf{p}\mathbf{p}'} x_{\mathbf{p}'} = \frac{1}{\pi}\sum_{\mathbf{k}} |x_{\mathbf{k}}|^2 \left(\gamma_{\mathbf{k}}^R + i\gamma_{\mathbf{k}}^I\right)$. Thus, to guarantee convergence of Ψ_{CG} we need to require $\gamma_{\mathbf{k}}^R > 0\,\forall\mathbf{k}$. Since $|x_{\mathbf{k}}|^2 = |x_{-\mathbf{k}}|^2$, the variational parameters $\gamma_{\mathbf{k}}^{R/I}$ and $\gamma_{-\mathbf{k}}^{R/I}$ are redundant. We define the equivalence relation

$$\begin{aligned} \mathbf{k} \sim_k \mathbf{k}' \quad \text{if} \quad & k_1 = -k_1' \pmod L \\ \text{and} \quad & k_2 = -k_2' \pmod L \end{aligned} \tag{4.9}$$

With the quotient set $\mathcal{K} \equiv \left\{[0,..,L-1]^2 \;\; (0,0)\right\}/\sim_k$ we can define a set of independent variational parameters, $\left\{\gamma_{\mathbf{k}}^{R/I}\right\}_{\mathbf{k}\in\mathcal{K}}$. Choosing a set of independent parameters will be important later on for applying the time dependent variational principle (see section 4.5.1).

To construct a suitable ansatz state for compact $U(1)$ gauge fields ($\theta_{\mathbf{p}} \in [-\pi,\pi]$) we sum over complex Gaussian states, thus ensuring periodicity:

$$\Psi_{CPG}\left(\{\theta_{\mathbf{p}}\}\right) \equiv \prod_{\mathbf{p}} \left(\sum_{N_{\mathbf{p}}=-\infty}^{+\infty}\right) \Psi_{CG}\left(\{\theta_{\mathbf{p}} - 2\pi N_{\mathbf{p}}\}\right) \delta\left(\sum_{\mathbf{p}} \theta_{\mathbf{p}} - 2\pi N_{\mathbf{p}}\right). \tag{4.10}$$

The delta function needs to be included in order to satisfy condition (4.6) for physical states. To shorten notation, we will denote the product over infinite sums $\prod_{\mathbf{p}} \sum_{N_{\mathbf{p}}=-\infty}^{+\infty}$ by $\sum_{\{N_{\mathbf{p}}\}}$ and the product over integrals $\prod_{\mathbf{p}} \int_{-\pi}^{\pi} d\theta_{\mathbf{p}}$ by $\int_{-\pi}^{\pi} D\theta$. The Gaussian nature of the wavefunction is exploited when evaluating expectation values of observables O by combining the integral over 2π with one of the two infinite sums to an integration over the real axis

$$\langle\Psi_{CPG}|O|\Psi_{CPG}\rangle = \sum_{\{N_{\mathbf{p}}\}} \delta\left(\sum_{\mathbf{p}} N_{\mathbf{p}}\right) f_O(\{N_{\mathbf{p}}\}) \tag{4.11}$$

with

$$f_O(\{N_{\mathbf{p}}\}) \equiv \int_{-\infty}^{+\infty} D\theta \overline{\Psi_{CG}}\left(\theta_{\mathbf{p}} - 2\pi N_{\mathbf{p}}\right) O\left(\theta_{\mathbf{p}}\right) \Psi_{CG}\left(\theta_{\mathbf{p}}\right) \delta\left(\sum_{\mathbf{p}} \theta_{\mathbf{p}}\right). \tag{4.12}$$

The integral $f_O(\{N_{\mathbf{p}}\})$ can be carried out analytically and the remaining infinite sum needs to be evaluated numerically.

Exemplary, we show this procedure for the norm of the variational state, $\langle\Psi_{CPG}|\Psi_{CPG}\rangle$. The computation of observables follows analagously; details on their exact form can be found in Appendix 4.C. After carrying out the integrals, the remaining function $f_1\left(\{N_{\mathbf{p}}\}\right)$ is

$$f_1(\{N_{\mathbf{p}}\}) = \prod_{\mathbf{k}\neq 0} \sqrt{\frac{\pi}{\gamma_{\mathbf{k}}^R}} e^{2\pi i \sum_{\mathbf{p}} \epsilon_{\mathbf{p}} N_{\mathbf{p}}} e^{-\pi \sum_{\mathbf{k}} |N_{\mathbf{k}}|^2 \gamma_{\mathbf{k}}} \tag{4.13}$$

with $N_{\mathbf{k}} \equiv \frac{1}{L}\sum_{\mathbf{p}} e^{i\mathbf{pk}} N_{\mathbf{p}}$ the discrete Fourier transform of $N_{\mathbf{p}}$ and $\gamma_{\mathbf{k}} \equiv \gamma_{\mathbf{k}}^R + (\gamma_{\mathbf{k}}^I)^2 (\gamma_{\mathbf{k}}^R)^{-1}$. The $\gamma_{\mathbf{k}}$ parameters determine how fast contributions to the sum in eq. (4.11) decrease exponentially with increasing $|N_{\mathbf{k}}|^2$.

We group the configurations $N_{\mathbf{p}}$ of this sum in different orders such that within one order the configurations only change up to permutations. Since all relevant configurations will contain mostly zeros, we will denote orders by its non-zero elements, e.g.

$\{N\}_1$ is the set of all permutations of the configuration N' defined by $N'_{\mathbf{p}=0} = 1$ and $N'_{\mathbf{p}\neq 0} = 0$, i.e. $\{N\}_1 \equiv S_{N'}$. If the parameters $\gamma_{\mathbf{k}}$ are large enough, the sum can be approximated by orders having small Euclidean norm, $||N_{\mathbf{p}}||_2^2 = \sum_{\mathbf{p}} |N_{\mathbf{p}}|^2 = ||N_{\mathbf{k}}||_2^2$. The higher number of permutations in orders with larger norm cannot compensate for the exponential suppression (this would not be the case if the $\gamma_{\mathbf{k}}$ were arbitrarily small). Using this scheme, the constraint $\delta\left(\sum_{\mathbf{p}} N_{\mathbf{p}}\right)$ is useful since it excludes many orders, e.g. $\{N\}_1$ or $\{N\}_{-1}$. The order with the lowest non-zero norm is therefore $\{N\}_{1,-1}$. In fact, the sum in eq. (4.11) can be expanded in orders containing only pairs of $1, -1$:

$$\begin{aligned}\langle \Psi_{CPG}|\Psi_{CPG}\rangle =& \prod_{\mathbf{k}\neq 0}\sqrt{\frac{\pi}{\gamma_{\mathbf{k}}^R}} \sum_{\{N_{\mathbf{k}=\mathbf{0}}=0\}} e^{2\pi i \sum_{\mathbf{p}} \epsilon_{\mathbf{p}} N_{\mathbf{p}}} e^{-\pi \sum_{\mathbf{k}} |N_{\mathbf{k}}|^2 \gamma_{\mathbf{k}}} \\ =& \prod_{\mathbf{k}\neq 0}\sqrt{\frac{\pi}{\gamma_{\mathbf{k}}^R}} \left(1 + \sum_{\{N\}_{1,-1}} e^{2\pi i \sum_{\mathbf{p}} \epsilon_{\mathbf{p}} N_{\mathbf{p}}} e^{-\pi \sum_{\mathbf{k}} |N_{\mathbf{k}}|^2 \gamma_{\mathbf{k}}} \right. \\ & \left. + \sum_{\{N\}_{1,1,-1,-1}} e^{2\pi i \sum_{\mathbf{p}} \epsilon_{\mathbf{p}} N_{\mathbf{p}}} e^{-\pi \sum_{\mathbf{k}} |N_{\mathbf{k}}|^2 \gamma_{\mathbf{k}}} + .. \right). \end{aligned} \tag{4.14}$$

$\sum_{\{N_{\mathbf{k}=\mathbf{0}}=0\}}$ denotes the sum over the set of all $N_{\mathbf{p}}$ configurations with $N_{\mathbf{k}=\mathbf{0}} = 0$, i.e. fulfilling the global constraint. For sufficiently large $\gamma_{\mathbf{k}}$ higher orders of the type $\{N\}_{2,-2}$ or $\{N\}_{-2,1,1}$ are exponentially suppressed as well as orders with a large number of $1, -1$ pairs. Thus, the above expansion can be truncated after the first few terms. Each of the remaining orders is evaluated numerically. The fact that configurations only change up to permutations within one order can be used to highly parallelize the computation. On an 8×8 lattice we are able to compute the first three orders exactly. This procedure is sufficient for most configurations of variational parameters with $\gamma_{\mathbf{k}} \gtrsim 1$. However, in the intermediate regime $\gamma_{\mathbf{k}} \approx 1$ more orders are required to obtain good convergence. In these cases, higher orders are computed using uniform sampling. Since for all our purposes the different $\gamma_{\mathbf{k}}$ parameters were of the same order of magnitude and the $N_{\mathbf{p}}$ configurations only change up to a permutation within an order, a uniform probability distribution is a suitable ansatz for the exponential in eq. (4.13). This is only the case for sampling within one order; it would fail if one tried to sample the whole sum. This combined approach of exact evaluation and uniform sampling has the advantage that it introduces almost no error for most of the variational manifold (up to truncated orders which are exponentially suppressed) and even for regions where uniform sampling is required the error is still suppressed since it only occurs in higher orders. For a detailed error analysis due to truncating orders and uniform sampling see Appendix 4.B.

When the $\gamma_{\mathbf{k}}$ become small, the above approximation fails. In that case, one can exploit the fact that $\langle \Psi_{CPG}|\Psi_{CPG}\rangle$ can be written as a multidimensional Riemann theta function [89] which is defined as

$$\theta(z|\Omega) = \sum_{N\in\mathbb{Z}^g} e^{2\pi i (z\cdot N + \frac{1}{2} N\cdot\Omega\cdot N)} \tag{4.15}$$

where $z \in \mathbb{C}^g$, $\Omega \in \mathbb{C}^{g\times g}$, such that $\Omega = \Omega^T$ and $\mathrm{Im}(\Omega)$ is strictly positive definite. To bring $\langle \Psi_{CPG}|\Psi_{CPG}\rangle$ into this form one can rewrite the delta function as the limit of a Gaussian and exchange the limit with the infinite sum due to uniform convergence. One can now exploit invariance of the Riemann theta function under modular

transformations, in particular the following relation holds (for details see [89]):

$$\theta\left(z|\Omega\right)=\frac{1}{\sqrt{\det(-i\Omega)}}e^{-i\pi z\cdot\Omega\cdot z}\theta\left(\Omega^{-1}z|-\Omega^{-1}\right) \tag{4.16}$$

If we insert this relation and take the limit, we obtain:

$$\begin{aligned}\langle\Psi_{CPG}|\Psi_{CPG}\rangle&=\prod_{\mathbf{k}\neq 0}\sqrt{\frac{\pi}{\gamma_{\mathbf{k}}^{R}\gamma_{\mathbf{k}}}}\sum_{\{N_{\mathbf{p}}\}}e^{-\pi\sum_{\mathbf{k}}|N_{\mathbf{k}}-\epsilon_{\mathbf{k}}|^{2}\gamma_{\mathbf{k}}^{-1}}\\&\equiv\sum_{\{N_{\mathbf{p}}\}}f_{\text{inv},1}\left(\{N_{\mathbf{k}\neq 0}\}\right).\end{aligned} \tag{4.17}$$

with $\gamma_{\mathbf{0}}^{-1}=0$. The exponential weight depends now on $\gamma_{\mathbf{k}}^{-1}$ which allows in principle to approximate the sum with only a very limited number of orders for sufficiently small $\gamma_{\mathbf{k}}$. However, the sum is not well defined since all constant configurations $N_{\mathbf{p}}=c(1,1,...,1)$ have weight one for $c\in\mathbb{Z}$. Fortunately, since all $f_{\text{inv},O}(\{N_{\mathbf{k}\neq 0}\})$ are independent of $N_{\mathbf{k}=\mathbf{0}}$ (as a result of the global constraint on physical states), all these configurations can be factored out such that they cancel when calculating expectation values. This can be formulated rigorously by defining an equivalence relation for $N_{\mathbf{p}}$ configurations:

$$N_{\mathbf{p}}\sim_{1}N'_{\mathbf{p}}\quad\text{if }\exists\quad c\in\mathbb{Z}\quad\text{s.t. }N_{\mathbf{p}}-N'_{\mathbf{p}}=c(1,1,...,1) \tag{4.18}$$

When calculating expectation values of observables only a sum over representatives of this equivalence relation is required:

$$\frac{\langle\Psi_{CPG}|O|\Psi_{CPG}\rangle}{\langle\Psi_{CPG}|\Psi_{CPG}\rangle}=\frac{\sum_{\{N_{\mathbf{p}}\}/\sim_{1}}f_{\text{inv},O}(\{N_{\mathbf{k}\neq 0}\})}{\sum_{\{N_{\mathbf{p}}\}/\sim_{1}}f_{\text{inv},1}(\{N_{\mathbf{k}\neq 0}\})} \tag{4.19}$$

If we choose the representative to be the one closest in norm to the $N_{\mathbf{p}}=\mathbf{0}$ configuration, we can expand the sum again in orders having mostly 0's. In this case we have no constraint so that all orders must be taken into account. For more details see Appendix 4.B.

A nice way to check the validity of both numerical approximation schemes presented above is to see whether they agree in the parameter region $\gamma_{\mathbf{k}}\approx 1$. This check has been carried out throughout this work since it also indicates that the whole variational manifold can be accessed which is required in order to study the whole coupling region.

To illustrate that both approximation schemes complement each other, we give the variational energy of Ψ_{CPG} with respect to the Kogut-Susskind Hamiltonian given in eq. (4.5), written both in the infinite sum representation for high and for low $\gamma_{\mathbf{k}}$:

$$\begin{aligned}&\frac{\langle\Psi_{CPG}|H_{KS}|\Psi_{CPG}\rangle}{\langle\Psi_{CPG}|\Psi_{CPG}\rangle}\\=&E_{C}+\frac{g^{2}}{4\pi}\sum_{\mathbf{k}}\gamma_{\mathbf{k}}\left(4-2\cos\left(\frac{2\pi k_{1}}{L}\right)-2\cos\left(\frac{2\pi k_{2}}{L}\right)\right)\\&-\frac{g^{2}}{2}\sum_{\mathbf{k}}\gamma_{\mathbf{k}}^{2}\left(4-2\cos\left(\frac{2\pi k_{1}}{L}\right)-2\cos\left(\frac{2\pi k_{2}}{L}\right)\right)\langle|N_{\mathbf{k}}|^{2}\rangle\\&+\frac{1}{g^{2}}\sum_{\mathbf{p}}\left(1-e^{-\frac{\pi}{4L^{2}}\sum_{\mathbf{k}\neq\mathbf{0}}\left(\gamma_{\mathbf{k}}^{R}\right)^{-1}}\left\langle(-1)^{N_{\mathbf{p}}}\cosh\left(\pi\sum_{\mathbf{k}}\text{Re}\left(N_{\mathbf{k}}b_{\mathbf{k}}^{\mathbf{p}}\right)\right)\right\rangle\right)\end{aligned} \tag{4.20}$$

with $b_{\mathbf{k}}^{\mathbf{p}} = \frac{1}{L}\gamma_{\mathbf{k}}^{I}\left(\gamma_{\mathbf{k}}^{R}\right)^{-1} e^{-i\mathbf{pk}}$. The brackets denote an infinite sum for the electric energy

$$\begin{aligned}\left\langle |N_{\mathbf{k}}|^2 \right\rangle \equiv & \frac{\sum_{\{N_{\mathbf{k}=\mathbf{0}}=0\}} e^{2\pi i \sum_{\mathbf{p}} \epsilon_{\mathbf{p}} N_{\mathbf{p}}} e^{-\pi \sum_{\mathbf{k}'} |N_{\mathbf{k}'}|^2 \gamma_{\mathbf{k}'}} |N_{\mathbf{k}}|^2}{\sum_{\{N_{\mathbf{k}=\mathbf{0}}=0\}} e^{2\pi i \sum_{\mathbf{p}} \epsilon_{\mathbf{p}} N_{\mathbf{p}}} e^{-\pi \sum_{\mathbf{k}'} |N_{\mathbf{k}'}|^2 \gamma_{\mathbf{k}'}}} \\ = & \frac{1}{2\pi}\gamma_{\mathbf{k}}^{-1}\left(4 - 2\cos\left(\frac{2\pi k_1}{L}\right) - 2\cos\left(\frac{2\pi k_2}{L}\right)\right) \\ & - \gamma_{\mathbf{k}}^{-2} \frac{\sum_{\{N_{\mathbf{p}}\}/\sim_1} e^{-\pi \sum_{\mathbf{k}'} |N_{\mathbf{k}'} - \epsilon_{\mathbf{k}'}|^2 \gamma_{\mathbf{k}'}^{-1}} |N_{\mathbf{k}} - \epsilon_{\mathbf{k}}|^2}{\sum_{\{N_{\mathbf{p}}\}/\sim_1} e^{-\pi \sum_{\mathbf{k}'} |N_{\mathbf{k}'} - \epsilon_{\mathbf{k}'}|^2 \gamma_{\mathbf{k}'}^{-1}}}\end{aligned}$$

and the following infinte sum for the magnetic energy

$$\begin{aligned}& \left\langle (-1)^{N_{\mathbf{p}}} \cosh\left(\pi \sum_{\mathbf{k}} \mathrm{Re}\left(N_{\mathbf{k}} b_{\mathbf{k}}^{\mathbf{p}}\right)\right)\right\rangle \\ = & \frac{\sum_{\{N_{\mathbf{k}=\mathbf{0}}=0\}} (-1)^{N_{\mathbf{p}}} \cosh\left(\pi \sum_{\mathbf{k}} \mathrm{Re}\left(N_{\mathbf{k}} b_{\mathbf{k}}^{\mathbf{p}}\right)\right) e^{2\pi i \sum_{\mathbf{p}} \epsilon_{\mathbf{p}} N_{\mathbf{p}}} e^{-\pi \sum_{\mathbf{k}} |N_{\mathbf{k}}|^2 \gamma_{\mathbf{k}}}}{\sum_{\{N_{\mathbf{k}=\mathbf{0}}=0\}} e^{2\pi i \sum_{\mathbf{p}} \epsilon_{\mathbf{p}} N_{\mathbf{p}}} e^{-\pi \sum_{\mathbf{k}} |N_{\mathbf{k}}|^2 \gamma_{\mathbf{k}}}} \\ = & \frac{\sum_{\{N_{\mathbf{p}}\}/\sim_1} e^{-\pi \sum_{\mathbf{k}} \left(|N_{\mathbf{k}} - \epsilon_{\mathbf{k}} - \frac{1}{2}\frac{\mathbf{p}}{\mathbf{k}}|^2 - \frac{1}{4}|b_{\mathbf{k}}^{\mathbf{p}}|^2\right)\gamma_{\mathbf{k}}^{-1}} \cos\left(\pi \sum_{\mathbf{k}} \gamma_{\mathbf{k}}^{-1} \mathrm{Re}\left[(N_{\mathbf{k}} - \epsilon_{\mathbf{k}} - \frac{1}{2}\frac{\mathbf{p}}{\mathbf{k}}) b_{\mathbf{k}}^{\mathbf{p}}\right]\right)}{\sum_{\{N_{\mathbf{p}}\}/\sim_1} e^{-\pi \sum_{\mathbf{k}} |N_{\mathbf{k}} - \epsilon_{\mathbf{k}}|^2 \gamma_{\mathbf{k}}^{-1}}}\end{aligned}$$

with $\frac{1}{2}\frac{\mathbf{p}}{\mathbf{k}} = \frac{1}{2L} e^{-i\mathbf{pk}}$. If we set $\gamma_{\mathbf{k}}^{I} = 0\ \forall \mathbf{k}$ the expressions for high $\gamma_{\mathbf{k}}^{R}$, i.e. with the sums $\sum_{\{N_{\mathbf{k}=\mathbf{0}}=0\}}$, agree with the results given in [57] up to redefinitions. It is important to emphasize that the convergence of infinite sums is determined by $\gamma_{\mathbf{k}} = \gamma_{\mathbf{k}}^{R} + \left(\gamma_{\mathbf{k}}^{I}\right)^2 \left(\gamma_{\mathbf{k}}^{R}\right)^{-1}$ or $\gamma_{\mathbf{k}}^{-1}$, respectively. For real-time evolutions, e.g. a quantum quench, $\left(\gamma_{\mathbf{k}}^{I}\right)^2$ will typically become large and so will $\gamma_{\mathbf{k}}$, irrespective of the real part $\gamma_{\mathbf{k}}^{R}$. This allows to truncate the expansion in eq. (4.14) already after the first term such that everything can be evaluated without resorting to sampling. This property makes the ansatz well suited for real-time evolution compared with other methods where sampling at all times often makes it difficult to reach long times.

4.4 Ground state properties

In this section, we study the variational ground state of $2+1$d compact QED over the whole coupling region. To minimize the energy we applied a gradient descent algorithm (the formula for the gradient can be found in Appendix 4.C). We used different initial seeds to prevent the possibility of getting stuck in local minima. To make sure that our variational state can approximate the ground state, we compare it first to known exact results. One should note that exact diagonalization methods cannot be applied to the full theory since the local Hilbert space is infinite. However, for the case of a single plaquette exact analytical solutions are known, namely the Mathieu functions.

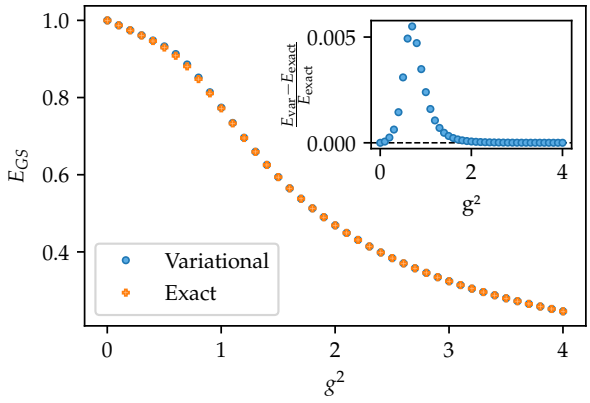

Figure 4.4.1: Benchmark of the variational ground state energy for one plaquette against the value of the exact ground state, given by the Mathieu function with the lowest characteristic value. The inset shows the relative error of the variational ground state energy with respect to the exact goundstate energy.

4.4.1 Benchmark for one plaquette

For benchmarking our variational ansatz, we will restrict ourselves to the sector without static charges. The Hamiltonian given in the formulation of the previous chapter, written in the basis of θ, reads:

$$H_{\text{1plaq}} = -2g^2 \frac{\partial^2}{\partial\theta^2} + \frac{1}{g^2}(1-\cos\theta). \tag{4.21}$$

The corresponding Schroedinger equation for $\xi(\theta)$ can be written as a Mathieu equation:

$$\left(\frac{\partial^2}{\partial z^2} + a - 2q\cos(2z)\right)\tilde{\xi}(z) = 0 \tag{4.22}$$

with $q \equiv -\frac{1}{g^4}$, $a \equiv \frac{2}{g^2}\left(E - \frac{1}{g^2}\right)$ and $\tilde{\xi}(z) \equiv \xi(\theta/2)$. $\tilde{\xi}$ is therefore not 2π-periodic but π-periodic. The π-periodic solutions are usually separated into even $ce_{2r}(z,q)\,(r \geq 0)$ and odd $se_{2r}(z,q)\,(r \geq 1)$ solutions. The lowest energy, i.e. the lowest characteristic value a, corresponds to the solution $ce_0(z,q)$. In Fig. 4.4.1, this exact ground state energy is plotted against the minimized variational energy. They agree very well over the whole coupling region, even in the regime where the difference is maximal ($g^2 \sim 0.7$) the relative error is still around 0.5%.

4.4.2 Confinement and string tension

In this section, we study the properties of the varational ground state for an extended lattice and investigate its finite size effects. We start by studying the ground state energy density $e_0(L)$ for lattice sizes up to 8×8 plaquettes without static charges. We see that for couplings $g^2 \gtrsim 1.0$ this size is already enough to get a linear scaling with $\frac{1}{L^2}$. The thermodynamic limit $e_0(L=\infty)$ is then extracted with the following fit

$$e_0(L) = e_0(L=\infty) + \frac{a}{L^2}. \tag{4.23}$$

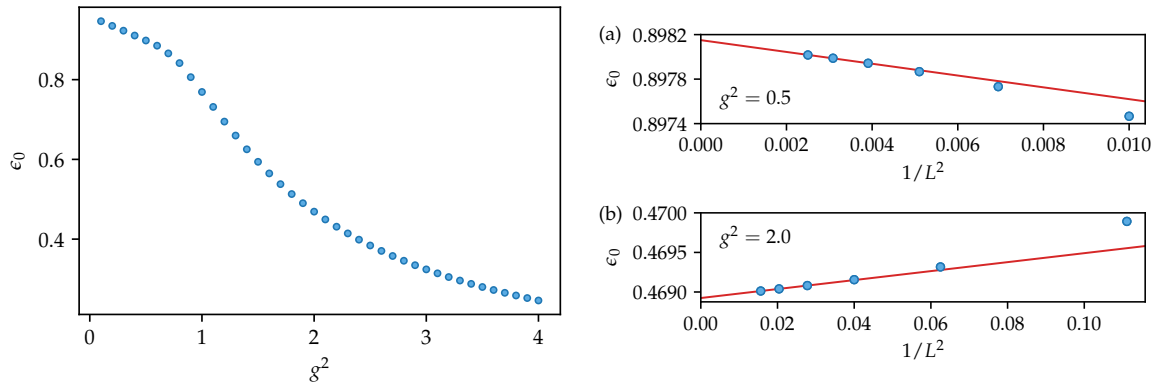

Figure 4.4.2: (Left): Groundstate energy density extrapolated to the thermodynamic limit. The available lattice sizes are 8×8 for couplings $g^2 \geq 1.0$, 14×14 for $g^2 = 0.8, 0.9$ and 20×20 for $g^2 \leq 0.7$. (Right): Finite size scaling for the ground state energy density at $g^2 = 0.5$ (a) and $g^2 = 2.0$ (b). For $g^2 = 2.0$, the ground state energy density for $L = 8, 7, 6$ is fitted according to eq. (4.23). The remaining data points correspond to $L = 5, 4, 3$. For $g^2 = 0.5$, lattice sizes of $L = 20, 18, 16$ are used for the fit, the remaining data points correspond to $L = 14, 12, 10$.

For large couplings the thermodynamic limit can be reached with even smaller lattice sizes. The region which limits the evaluation of our variational state to 8×8 is around $g^2 \sim 1.1$ since the variational parameters are of order one ($\gamma_{\mathbf{k}}^R \sim 1$, $\gamma_{\mathbf{k}}^I = 0$) and thus both approximation schemes agree (see Appendix 4.B). Hence, for couplings below this transition region we can simulate larger lattices, namely 14×14 for $g^2 = 0.8, 0.9$ and 20×20 for $0.1 \leq g^2 \leq 0.7$. For such lattice sizes, the finite size effects become again small enough to extrapolate to the thermodynamic limit. The result for the ground state energy density in the thermodynamic limit over the whole coupling region is shown in Fig. 4.4.2, including the extrapolation to the thermodynamic limit for $g^2 = 0.5$ and $g^2 = 2.0$.

In the next step, we study the string tension over the whole coupling region. We can measure it in two ways: First, we place static charges and analyze the scaling of the ground state energy depending on the distance between static charges. We will fit the potential with the following function:

$$V(d) = \sigma d + b V_{Coul}(d) \tag{4.24}$$

where σ is the string tension and V_{Coul} is the lattice Coulomb potential in two dimensions which becomes a logarithmic potential in the continuum limit. The values for $V(d)$ are computed as the difference between the ground state energy with static charges separated by a distance d and the ground state energy without static charges.

In the second approach we use the scaling of spatial Wilson loops to extract the string tension. This works at zero temperature since on the Euclidean lattice spatial and temporal Wilson loops are related by $O(4)$ symmetry. At finite temperature this symmetry is broken due to a compactified temporal dimension [90]. The formula to calculate Wilson loops of arbitrary size with complex periodic Gaussian states in both the low and high $\gamma_{\mathbf{k}}$ approximation can be found in Appendix 4.C. On 8×8 lattices, we consider all rectangular loops $R_1 \times R_2$ with $R_1, R_2 \leq 4$ (four is the maximal physical length due to the periodic boundary conditions). Furthermore, we require $|R_1 - R_2| \leq 1$ to avoid additional finite size effects coming from an asymmetry in the edges. For weak couplings, where larger lattices are accessible, we extend the allowed maximal edge

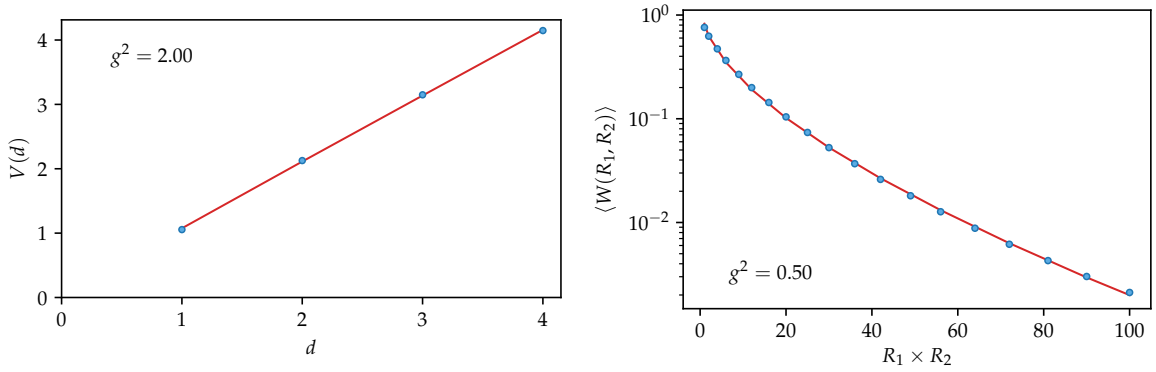

Figure 4.4.3: (Left): the static potential $V(d)$ of two charges separated by a distance d at $g^2 = 2.0$. The data points are computed on an 8×8 lattice as the difference between the ground state energy with the respective static charge configuration and the ground state energy without static charges. The red line is a fit to the potential according to eq. (4.24) with $\sigma = 1.001$ and $b = 0.146$. (Right): the data points show different spatial Wilson loops $\langle W(R_1, R_2) \rangle$ in the ground state at $g^2 = 0.5$, computed on a 20×20 lattice, as a function of the area $R_1 \times R_2$. The maximally used edge length of a Wilson loops is 10 ($R_1, R_2 \leq 10$), with a maximum difference between the edges of one ($|R_2 - R_1| \leq 1$). The red line is a fit to the exponential decay of Wilson loops according to eq. (4.25) with $\sigma = 0.013$, $a = 0.132$ and $c = 0.349$.

length to 7 and 10 (for 14×14, resp. 20×20). We fit the Wilson loop scaling according to the following formula:

$$W(R_1, R_2) = e^{-\sigma R_1 R_2 - 2a(R_1 + R_2) + c} \tag{4.25}$$

The first term corresponds to area law scaling with string tension σ and the second term to perimeter law scaling. Both procedures to extract the string tension are illustrated in Fig. 4.4.3, the extraction via the static potential at $g^2 = 2.0$ and the extraction via Wilson loops at $g^2 = 0.5$. We also tried to extract the string tension via Creutz ratios [91] but the results were less reliable than the Wilson loop fits.

The result for both approaches over the whole coupling region is shown in Fig. 4.4.4. For large values of the coupling constant, the fit for the static potential works well and agrees with the strong-coupling prediction $\frac{g^2}{2}$. Since a large coupling implies a significant distance from the continuum limit, moderate lattice sizes are sufficient to observe the onset of the linear part of the potential. The scaling of Wilson loops is prone to errors in that regime as expectation values of large Wilson loops become close to machine precision. However, for small couplings the Wilson loop scaling is the better method since expectation values of Wilson loops do not decay as fast due to the small string tension. Since both methods complement each other we chose to make the string tension data for the static potential transparent for couplings $g^2 \leq 1.5$ and the ones extracted by Wilson loops scaling for $g^2 > 1.5$. The remaining full data points in Fig. 4.4.4 are the most reliable estimates for the string tension.

For small couplings an exponential decay of the string tension is expected according to the formula [92]:

$$\sigma = c\sqrt{\frac{g^2}{\pi^2}} e^{-\frac{\pi^2}{g^2}\nu_0}. \tag{4.26}$$

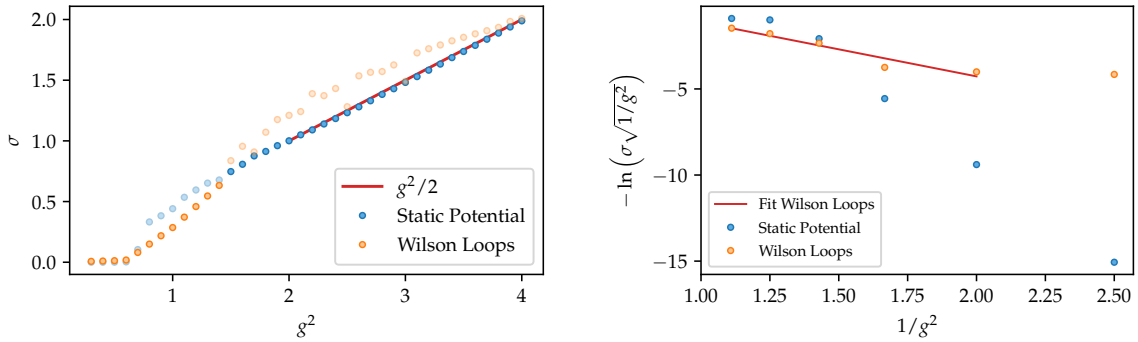

Figure 4.4.4: (Left): String tension fitted via the static potential (blue) and via the decay of spatial Wilson loops (orange). For larger couplings ($g^2 \geq 1.5$) the static potential fit performs better than the fit of Wilson loops and agrees with the strong-coupling prediction $g^2/2$. For small couplings ($g^2 \leq 1.4$) Wilson loop fits are more suitable. The more reliable method is shown with full data points while data points of the other method are made transparent. (Right): String tension in the weak-coupling regime. While the Wilson loop fits show exponential decay of the string tension close to the theoretical value ($\nu_0 = 0.318$ compared to $\nu_{0,\text{theo}} = 0.321$), the static potential fits become unreliable for couplings $g^2 \leq 0.6$.

If we fit this formula to the string tension data of the Wilson loop fits between $0.5 \leq g^2 \leq 0.9$ (see Fig. 4.4.4) we obtain $c = 23.53$ and $\nu_0 = 0.318$ which is close to the theoretical prediction ($\nu_{0,\text{theo}} = 0.321$) [93].

4.4.3 Truncation effects

Since our wave function does not require a truncation, we can study truncation effects of other methods. Here, we will focus on a truncation in the electric basis. To see these effects we will study the variance of the electric field operator. For simplicity, we will look at this effect without static charges, since they only introduce ϵ-shifts ($-1/2 < \epsilon < 1/2$) in the electric field. Since the expectation value of the electric field vanishes in the absence of static charges, we can write the variance in terms of the electric energy

$$\text{Var}(E_{\mathbf{x},i}) = \left\langle E_{\mathbf{x},i}^2 \right\rangle - \left\langle E_{\mathbf{x},i} \right\rangle^2 = \frac{1}{L^2 g^2} \left\langle H_E \right\rangle . \tag{4.27}$$

The variance is plotted in the inset of Fig. 4.4.5 for the ground state which was computed in the last section. To quantitatively show the difference, we compare our variational state to an exact diagonalization calculation of a $\mathbb{Z}_3$ lattice gauge theory. To reduce the required Hilbert space dimension, we formulate it in terms of plaquette variables, in the same style as we did for the $U(1)$ theory. The Hilbert space is truncated in the eigenbasis of $L_{\mathbf{p}}$ to three states (corresponding to the eigenvalues $m = 0, 1, -1$). To make this a consistent theory we define the gauge field operators cyclically:

$$U_p^\dagger \left| m \right\rangle = \left| m' \right\rangle \quad \text{with } m' = m + 1 \pmod 3. \tag{4.28}$$

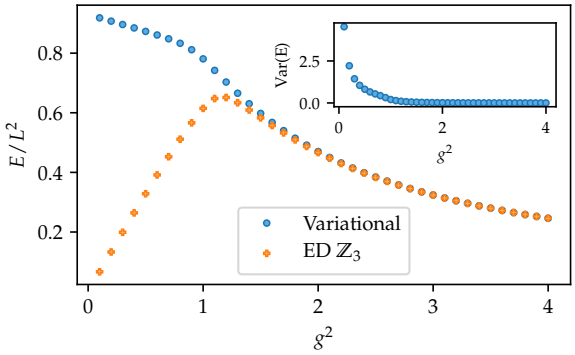

Figure 4.4.5: Comparison of the ground state energy density on a 3×3 lattice without static charges, computed for a $\mathbb{Z}_3$ lattice gauge theory by exact diagonalization (orange) and for the full $U(1)$ theory by minimizing the variational energy (blue). The inset shows the variance of the electric field on a link in the variational ground states.

This is equivalent to a $\mathbb{Z}_3$ lattice gauge theory formulated in link variables:

$$H_{Z3} = \frac{g^2}{6} \sum_{\mathbf{x},i} (2 - P_{\mathbf{x},i} - P^\dagger_{\mathbf{x},i}) + \frac{1}{2g^2} \sum_{\mathbf{p}} (2 - Q_{\mathbf{p}} - Q^\dagger_{\mathbf{p}}) \tag{4.29}$$

with $Q_{\mathbf{p}} \equiv Q_{\mathbf{x},1} Q_{\mathbf{x}+\mathbf{e}_1,2} Q^\dagger_{\mathbf{x}+\mathbf{e}_2,1} Q^\dagger_{\mathbf{x},2}$ where $\mathbf{x}$ is the vertex at the bottom left corner of plaquette $\mathbf{p}$ and $Q_{\mathbf{x},i}$ the cyclic raising operator of the electric field on link $(\mathbf{x}, i)$, such that (see [94] for details)

$$\begin{aligned} &P^N_{\mathbf{x},i} = Q^N_{\mathbf{x},i} = 1 && P^\dagger_{\mathbf{x},i} P_{\mathbf{x},i} = Q^\dagger_{\mathbf{x},i} Q_{\mathbf{x},i} = 1 \\ &P^\dagger_{\mathbf{x},i} Q_{\mathbf{x},i} P_{\mathbf{x},i} = e^{i\frac{2\pi}{3} Q_{\mathbf{x},i}}. \end{aligned} \tag{4.30}$$

The maximal lattice size we can achieve in our ED calculation for a reasonable amount of time is 3×3 plaquettes. We calculate the ground state energy density for this lattice size with ED and our variational ansatz. The result is shown in Fig. 4.4.5. The two approaches exhibit good agreement in the strong coupling regime. For intermediate couplings differences becomes more pronounced leading to qualitatively different results in the weak-coupling limit $g \to 0$.

Since the electric Hamiltonian becomes bounded in the truncated theory, it does not contribute in the weak coupling limit. In the $U(1)$ theory, however, the electric Hamiltonian is unbounded and the growth in electric energy leads to a finite result for the ground state energy in the continuum limit.

4.5 Real-time dynamics

In this section, we study out-of-equilibrium dynamics by applying the following quench protocol: We prepare the ground state for the compact QED Hamiltonian at some coupling g^2, quench to a Hamiltonian with a different coupling constant g^2_{quench} and observe the subsequent time evolution. The observables we track during the evolution are Wilson loops and the electric field (their expectation values in terms of the variational parameters can be found in Appendix 4.C). In addition we check whether the energy is conserved throughout the whole time evolution.

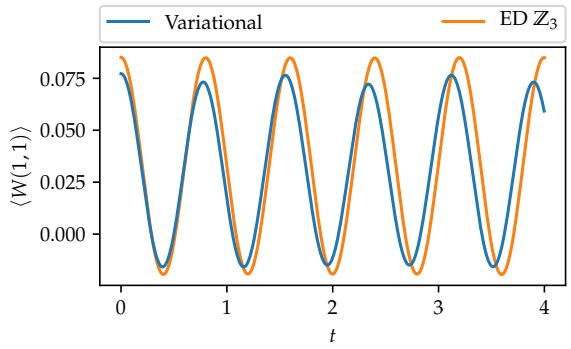

Figure 4.5.1: Benchmark of the variational time evolution of the 1×1 Wilson loop after a quench from $g^2 = 2.5$ to $g^2 = 4.0$ on a 3×3 lattice. It is compared with the time evolution of $\mathbb{Z}_3$ lattice gauge theory computed by exact diagonalization (the truncation from $U(1)$ to $\mathbb{Z}_3$ should only play a minor role in the strong-coupling regime).

4.5.1 Time-dependent variational principle

To study dynamical phenomena, we employ the time-dependent variational principle. The equations of motion are projected onto the tangent plane of our variational manifold. For every variational parameter $\gamma_{\mathbf{k}}^{R/I}$ we define a corresponding tangent vector $\left|\Psi_{\mathbf{k}}^{R/I}\right\rangle \equiv \mathbb{P}_\Psi \left(\frac{\partial}{\partial \gamma_{\mathbf{k}}^{R/I}} |\Psi_{CPG}\rangle \right)$ where $\mathbb{P}_\Psi$ ensures orthogonality to $|\Psi_{CPG}\rangle$:

$$\mathbb{P}_\Psi(|\psi\rangle) \equiv |\psi\rangle - \langle \Psi_{CPG}|\psi\rangle \, |\Psi_{CPG}\rangle \tag{4.31}$$

If we restrict the momenta $\mathbf{k}$ of the variational parameters to the set $\mathcal{K}$ defined in eq. (4.9), all tangent vectors become linearly independent. This allows to invert the Gram matrix $G_{\mathbf{k}'\mathbf{k}} \equiv \langle \Psi_{\mathbf{k}'}^R | \Psi_{\mathbf{k}}^R \rangle$ with $\mathbf{k}, \mathbf{k}' \in \mathcal{K}$. Since our variational manifold is Kähler, we can express the time evolution of the variational parameters $\gamma_{\mathbf{k}}^{R/I}$ ($\mathbf{k} \in \mathcal{K}$) in the following way [95]:

$$i \left(\dot{\gamma}_{\mathbf{k}}^R + i \dot{\gamma}_{\mathbf{k}}^I \right) = \frac{1}{2} \sum_{\mathbf{k}' \in \mathcal{K}} (G^{-1})_{\mathbf{k}\mathbf{k}'} \left(\frac{\partial E}{\partial \gamma_{\mathbf{k}'}^R} + i \frac{\partial E}{\partial \gamma_{\mathbf{k}'}^I} \right) \tag{4.32}$$

with $E \equiv \frac{\langle \Psi_{CPG}|H_{KS}|\Psi_{CPG}\rangle}{\langle \Psi_{CPG}|\Psi_{CPG}\rangle}$ the variational energy in eq. (4.20) and $\dot{\gamma} \equiv \frac{\partial \gamma}{\partial t}$. The formula for the calculation of the Gram matrix and the gradient of the variational energy can be found in Appendix 4.C.

4.5.2 Benchmark of variational ansatz

Since we are dealing with a variational ansatz, one should try to test it against exact results. For a comparison, we use the exact diagonalization results of the $\mathbb{Z}_3$ theory. Since the truncation in the electric basis led to significant differences in the ground state energy already for intermediate coupling and time-dynamics increase the variance in the electric field, we can only expect reasonable agreement for a quench within the strong coupling region. We choose to quench the Hamiltonian from $g^2 = 2.5$ to $g^2 = 4.0$. The result is shown in Fig. 4.5.1. Even though truncation effects might still play a minor role in that quench, the comparison shows that the variational state can approximate amplitude and frequency of the oscillation.

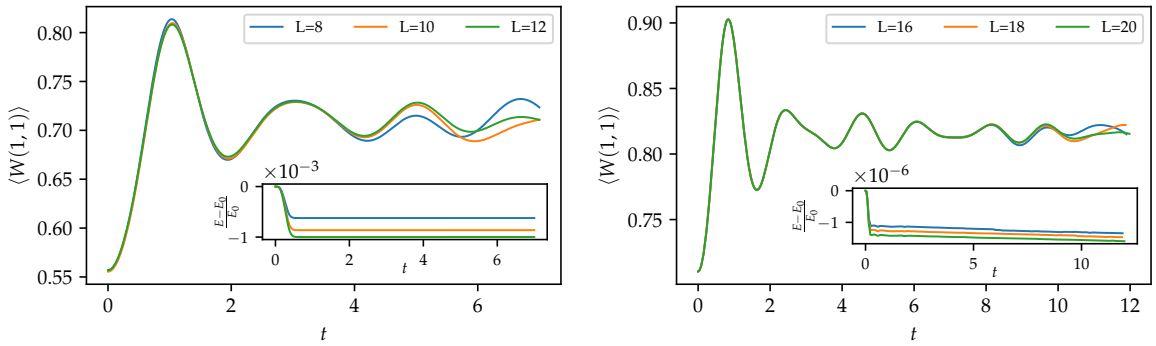

Figure 4.5.2: (Left): Variational time evolution after a quench from $g^2 = 0.8$ to $g^2 = 0.5$ for lattice sizes of 8×8, 10×10 and 12×12. The inset shows the relative error in energy E with respect to the initial energy E_0 after the quench. (Right): Variational time evolution after a quench from $g^2 = 0.6$ to $g^2 = 0.3$ for lattice sizes of 16×16, 18×18 and 20×20. The inset shows the relative error in energy E with respect to the initial energy E_0 after the quench.

4.5.3 Quench dynamics

We start with quenches in the weak-coupling regime where finite-size effects are most pronounced. We are interested in the maximal time up to which we can extract physics in the thermodynamic limit before boundary effects due to our finite lattice start to play a role. To compute that point in time, we perform the same quench on different lattice sizes and check where they start to deviate from each other. In order to easily compare observables for different lattice sizes, we restrict ourselves to the sector without static charges. We will focus on tracking the 1×1 Wilson loop during time evolution. We probed two different quenches, one from $g^2 = 0.8$ to $g^2 = 0.5$ for an 8×8, 10×10 and 12×12 lattice and another one from $g^2 = 0.6$ to $g^2 = 0.3$ for lattice sizes of 16×16, 18×18 and 20×20 (shown in Fig. 4.5.2).

In the first quench, the time evolution on the 8×8 lattice agrees with the 12×12 lattice up to $t_{\text{max},8} \sim 3.8$, the 10×10 lattice up to $t_{\text{max},10} \sim 4.8$. The energy is conserved for all lattice sizes up to a relative error of the order 10^{-3}. During the time spans where we can reliably extract the time evolution, the Wilson loops indicate equilibrating behavior.

This statement is supported by the second quench, where the smaller coupling constants allow us to reach larger lattices. The 16×16 and 18×18 lattice agree with the 20×20 lattice up to $t_{\text{max},16} \sim 8.5$ and $t_{\text{max},18} \sim 9.5$. The energy is conserved up to a relative error of 10^{-6}. We can only make a statement about the equilibration of Wilson loops since we do not have access to thermal expectation values. An interesting direction for future research would be to check whether the Wilson loops thermalize. For the calculation of thermal expectation values one could use Monte-Carlo simulations which have been proven successful in computing thermal properties in lattice gauge theory [96, 97].

In the next step, we look at a quench from weak to strong coupling ($g^2 = 0.5$ to $g^2 = 4.0$) for an 8×8 lattice without static charges. We track the time evolution of quadratic Wilson loops with edge sizes ranging from one to four. The result is shown in Fig. 4.5.3. All Wilson loops equilibrate at zero on short time scales (between $t_{\text{eq},4} \sim 0.2$ for the 4×4 Wilson loop and $t_{\text{eq},1} \sim 0.5$ for the 1×1 Wilson loop). We carried out the same evolution on a 7×7 lattice and found the same behavior. The coupling constant at $g^2 = 4.0$ is large enough to approximate the spectrum by the strong-coupling limit $g^2 \to$

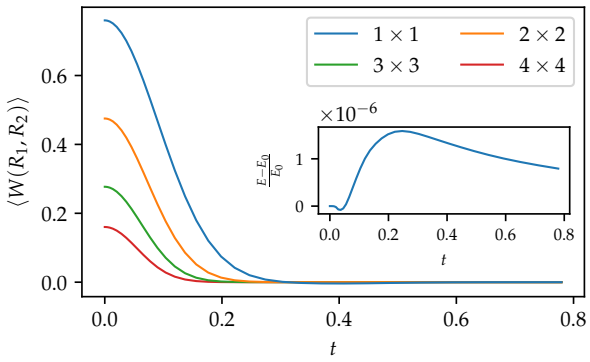

Figure 4.5.3: Variational time evolution of the 1×1, 2×2, 3×3 and 4×4 Wilson loop after a quench from $g^2 = 0.5$ to $g^2 = 4.0$ on an 8×8 lattice. The inset shows the relative error in energy E with respect to the initial energy E_0 after the quench.

∞, where the eigenstates $|n\rangle$ become diagonal in the electric basis (this can be seen e.g. in the spectrum of the $\mathbb{Z}_3$ theory which is available due to exact diagonalization). In this limit the thermal expectation value of Wilson loops vanishes trivially:

$$\langle W(C)\rangle_{\text{th}} = \frac{1}{Z}\sum_n e^{-\beta E_n}\left\langle n\left|\prod_{\mathbf{p}\in C}\frac{1}{2}(U_{\mathbf{p}} + U_{\mathbf{p}}^\dagger)\right|n\right\rangle = 0. \tag{4.33}$$

For this special quench, we can thus verify that the Wilson loops equilibrate at their thermal expectation value.

The next quench we will study is from strong to weak coupling. We quench on an 8×8 lattice from $g^2 = 4.0$ to $g^2 = 0.5$ with static charges horizontally separated by four links. Besides the 1×1 Wilson loop at the origin, we observe how the electric field of the ground state at $g^2 = 4.0$, a strongly confined fluxtube, evolves after the quench, in particular the electric field $E_1(x_1 = 2, x_2 = 4)$ (one of the links inside the fluxtube, see Fig. 4.5.4). It starts close to one, the strong-coupling value of the electric field, and decreases rapidly to $E_1^C(2, 4) = 0.322$, the value of the Coulomb electric field on that link (shown in the red dashed line). The Wilson loop seems to equilibrate on longer time scales. The energy is conserved up to a relative error of 10^{-2}. The larger error compared to previous quenches can be explained by the fact that around $t \sim 0.25$ the approximation method of the infinite sums appearing in the evaluation of expectation values changes from the low $\gamma_{\mathbf{k}}$ to the high $\gamma_{\mathbf{k}}$ approximation (see section 4.3.2). In that transition region higher orders need to be calculated using uniform sampling (see Appendix 4.B) which introduces additional errors. However, the relative error is still small and observables have no visible jump in this region, indicating that the two approximation schemes work. After the transition region the energy is well conserved due to the fact that the variational parameters $\gamma_{\mathbf{k}}^I$ increase, making the approximation of the infinite sums involved in the calculation of expectation values very easy (see section 4.3.2).

The spreading of the electric field from inside the flux tube between the two charges towards the Coulomb configuration of the electric field is illustrated in Fig. 4.5.4. An interesting question is whether the state becomes deconfined at long times. We cannot use the scaling of spatial Wilson, this only serves as an indicator for confinement in the ground state [90]. Since in our formulation the value of the longitudinal (Coulomb) part of the electric field is fixed and only the transversal part is dynamical (see Ap-

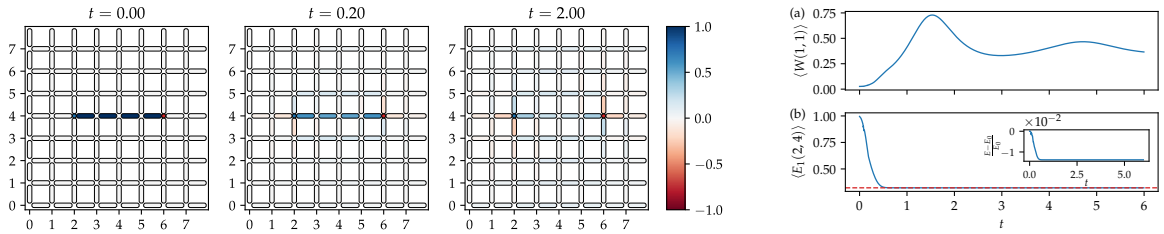

Figure 4.5.4: Variational time evolution on an 8×8 lattice after a quench from $g^2 = 4.0$ to $g^2 = 0.5$ with a positive charge placed at $(x_1 = 2, x_2 = 4)$ (blue dot) and a negative charge at $(x_1 = 6, x_2 = 4)$ (red dot). (Left): the expectation value of the electric field is shown at $t = 0.0$, $t = 0.2$ and $t = 2.0$. At $t = 0.0$, the state is in the variational ground state for $g^2 = 4.0$ where the electric flux is confined between the two charges. After the quench, the electric field starts to spread over the lattice ($t = 0.2$) and equilibrates at the Coulomb value for this charge configuration ($t = 2.0$). (Right): (a) the 1×1 Wilson loop at the origin $W(1,1)$ and (b) the electric field on a link between the two charges $E_1(2,4)$ is shown. The red dashed line represents the Coulomb value of the electric field. The inset shows the relative error in energy E with respect to the initial energy E_0 after the quench.

pendix 4.A), we can measure precisely how much an electric field configuration differs from the Coulomb configuration. At $t = 2.0$, in the last of the three pictures in Fig. 4.5.4, the difference to the Coulomb configuration is of order 10^{-12} for the whole lattice, with no remnant of an electric flux tube between the two charges. This is a strong indication that the state becomes deconfined, corresponding possibly to a thermal state with a temperature above the confinement-deconfinement transiton [87, 98].

4.6 Conclusion

In this chapter, we presented a novel class of variational states called complex periodic Gaussian states, which can be used to investigate ground state properties and real-time dynamics in $(2+1)$-dimensional $U(1)$ lattice gauge theory. The evaluation of expectation values is performed in a first step analytically, such that it remains to numerically compute an infinite sum. We propose an approach to approximate these sums for all variational parameters on an 8×8 lattice and up to 20×20 in the weak-coupling regime. This enables us to study the variational ground state over the entire coupling range and extract the thermodynamic limit. Our ansatz is validated against the exact ground state for the one-plaquette case. We compute the string tension using two methods: firstly, by fitting the static potential between two charges with a two-dimensional Coulomb potential and a linear potential, and secondly, by fitting the exponential decay of Wilson loops with an area and a perimeter law. The two approaches are complementary, as Wilson loops become challenging to fit in the strong-coupling regime due to the small value of large Wilson loops. Conversely, the static potential approach works well as energy differences become larger. In the weak-coupling regime, the string tension is too small to extract the linear part of the potential on the given lattice sizes, but Wilson loops decay modestly, enabling reliable fits. We confirm the expected exponential decay of the string tension in the weak-coupling regime.

As complex periodic Gaussian states do not require truncation in the local Hilbert

space, we compare our $U(1)$ ground state data to exact diagonalization results for a $\mathbb{Z}_3$ theory to investigate truncation effects in the electric basis. The comparison shows agreement for strong couplings but significant differences for intermediate couplings. While the ground state energy of the truncated theory approaches zero in the continuum limit $g^2 \to 0$ (due to the bounded electric energy), the variational ground state energy tends towards a finite value because of the unbounded growth of the electric field's variance.

Based on the time-dependent variational principle, we explored the out-of-equilibrium dynamics after a global quench, i.e. a sudden change in the coupling constant. We first benchmarked the variational time evolution in the strong-coupling regime with exact diagonalization results of the $\mathbb{Z}_3$ theory. Seeing reasonable agreement, we proceeded to investigate quenches in the weak-coupling regime, where we anticipate finite size effects to be significant. To assess at what time scales smaller lattices begin to deviate from the thermodynamic limit, we compared the time evolution of a Wilson loop after the same quench for various lattice sizes. The temporal intervals we attained are extensive enough to indicate the equilibration of Wilson loops.

We also investigated the time evolution after a quench from weak ($g^2 = 0.5$) to strong coupling ($g^2 = 4.0$), for which we monitored Wilson loops of different size. We found that all Wilson loops equilibrate at zero, which is the thermal expectation value in the strong-coupling limit ($g^2 \to \infty$). This suggests that the Wilson loops equilibrate at their thermal expectation values since the spectrum at $g^2 = 4.0$ is close to the strong-coupling limit.

Additionally, we explore a quench from strong to weak coupling with two static charges, one positively charged, the other negatively charged. In the strong-coupling ground state the electric field is perfectly confined between the two charges. We observe that after the quench the electric field now spreads over the entire lattice and equilibrates at the Coulomb value for the electric field with high accuracy, a deconfined state.

Throughout all the studied quenches, we observe equilibration of observables up until the point where boundary effects become significant. Comparing the equilibrated expectation values with thermal expectation values, which can be calculated through Monte Carlo simulations [96, 97], would be an interesting future direction. Monte Carlo methods could also be used to numerically evaluate the variational ansatz by approximating the infinite sums, enabling simulations of larger system sizes. These simulations must be highly accurate to carry out evolution over reasonable time scales and ensure energy conservation.

The ansatz can in principle be extended to three dimensions, even though additional constraints arise in three dimensions compared to two dimensions as discussed in chapter 3. One would need to find more advanced numerical schemes for the evaluation of the sums appearing in that case.

Another possible extension of this work is the inclusion of dynamical matter, which requires finding a gauge-invariant formulation of the theory that admits the same gauge-invariant variables used in this study for static matter. A formulation for this theory was proposed in chapter 3, based on Ref. [1]. Combining a periodic Gaussian state for the gauge field with a fermionic ansatz state describing dynamical matter could be achieved using this formulation.

What we will see in chapter 5 is that there is also another application: knowing that periodic Gaussian states are well suited for compact QED with static charges, we

constructed a variational ansatz, which can be shown to be related by the Villain approximation [99], that is more amendable to Monte Carlo sampling, thus allowing an efficient variational Monte Carlo algorithm. More generally, complex periodic Gaussian states provide a useful benchmark for the static charge sector of compact QED with the full, untruncated $U(1)$ gauge field Hilbert space. This will be used in chapter 5 and has also been used recently to benchmark certain neural-network ansatz states for lattice gauge theories [100].

Extending the ansatz to non-Abelian gauge theories is more challenging since they do not permit a translationally invariant formulation in terms of gauge-invariant plaquette variables. However, constructing similar ansatz states using other gauge-invariant variables is in principle possible [71].

APPENDIX

4.A FORMULATION IN TERMS OF PLAQUETTE VARIABLES

In this section, we want to give a short review on the separation of gauge fields into (almost) gauge invariant plaquette variables and a static part corresponding to the longitudinal Coulomb field. For simplicity and since this is the charge configuration used throughout the chapter, we will focus on a situation with two static charges placed vertically at $x_2 = d_2$ separated horizontally by a distance d. Other charge configurations follow analogously. We want to split the electric flux line between the two charges into a transversal component, generated by the lattice curl of a field ϵ on the plaquettes and into a longitudinal component, generated by the lattice gradient of a scalar field ϕ on the vertices. All other electric flux configurations can be created on top of it by exciting an electric flux loop around a plaquette or around the whole lattice.

The longitudinal part is by definition of the form

$$E_i^L(\mathbf{x}) = -\nabla^{(+)}\phi(\mathbf{x}) \equiv -(\phi(\mathbf{x}+e_i) - \phi(\mathbf{x})) \tag{4.34}$$

where $\nabla^{(+)}$ is the lattice forward derivative. Using Gauss law,

$$\sum_i \nabla_i^{(-)} E_i^L(\mathbf{x}) = \sum_i E_i^L(\mathbf{x}) - E_i^L(\mathbf{x}-\mathbf{e}_i) = Q(\mathbf{x}) \tag{4.35}$$

with $\nabla^{(-)}$ the lattice backward derivative, we arrive at a lattice version of Poisson's equation:

$$-\nabla^{(-)}\nabla^{(+)}\phi(\mathbf{x}) = Q(\mathbf{x}) \tag{4.36}$$

The solution for ϕ is

$$\phi(\mathbf{x}) = \frac{1}{L}\sum_{\mathbf{y}} Q(\mathbf{y}) \sum_{\mathbf{k}\neq\mathbf{0}} \frac{e^{2\pi i \frac{k_1(x_1-y_1)+k_2(x_2-y_2)}{L}}}{4 - 2\cos\left(\frac{2\pi k_1}{L}\right) - 2\cos\left(\frac{2\pi k_2}{L}\right)} \tag{4.37}$$

with $\mathbf{x} = (x_1, x_2)$ and x_1, x_2 ranging from 0 to $L-1$. The same applies to $\mathbf{y}$ and $\mathbf{k}$. There is no $\mathbf{k} = \mathbf{0}$ contribution since the total charge on a periodic lattice needs to be zero because of gauge invariance. $E_i^L(\mathbf{x})$ then follows straightforwardly from (4.34).

We write the transversal part as the curl of an ϵ-field on the plaquettes,

$$E_i^T(\mathbf{x}) = \nabla^{(-)} \times \epsilon \equiv \epsilon_{ij}\nabla_j^{(-)}\epsilon(\mathbf{x}) \tag{4.38}$$

where the plaquette corresponding to $\mathbf{x}$ is the one having $\mathbf{x}$ as its the bottom left corner. We take the curl of the above expression and use a lattice analog of the vector identity $\nabla \times \nabla \times A = \nabla(\nabla \cdot A) - \Delta A$, here in two dimensions, to obtain a Poisson equation for the ϵ-field:

$$-\nabla^{(+)}\nabla^{(-)}\epsilon(\mathbf{x}) = \epsilon_{ij}\nabla_i^{(+)}E_j(\mathbf{x}) \tag{4.39}$$

where we sum over repeated indices. This equation is solved by

$$\epsilon(\mathbf{x}) = \frac{1}{L}\sum_{\mathbf{y}} \epsilon_{ij}\nabla_i^{(+)}E_j(\mathbf{y}) \sum_{\mathbf{k}\neq\mathbf{0}} \frac{e^{2\pi i \frac{k_1(x_1-y_1)+k_2(x_2-y_2)}{L}}}{4 - 2\cos\left(\frac{2\pi k_1}{L}\right) - 2\cos\left(\frac{2\pi k_2}{L}\right)} \tag{4.40}$$

In our case, $\epsilon_{ij}\nabla_i^{(+)}E_j(\mathbf{x})$ is 1 on the plaquettes above the electric string connecting the charges and -1 below the string. However, since the sum over this expression will always be zero, we cannot generate a constant electric field with the ϵ-field which is required since $\tilde{E}_1(\mathbf{k}=\mathbf{0}) = \frac{d}{L}$. It is important to also consider the Polyakov loop winding horizontally around the lattice. We choose it to wind around the lattice at $x_2 = d_2$ and the electric field along it to be $\epsilon_{\text{poly},1} = \frac{d}{L}$. We define an additional ϵ-field ϵ_{const} on the plaquettes, on top of ϵ:

$$\epsilon_{\text{const}}(\mathbf{x}) = \begin{cases} \frac{d}{L^2}(x_2 - d_2) & x_2 \geq d_2 \\ \frac{d}{L} - (d_2 - x_2)\frac{d}{L^2} & x_2 < d_2 \end{cases} \tag{4.41}$$

It is defined in such a way that

$$E_{\text{const},1}(\mathbf{x}) = \nabla^{(-)} \times \epsilon_{\text{const}} + \epsilon_{\text{poly},1}\delta_{x_2,d_2} = \frac{d}{L^2} \tag{4.42}$$

giving us the $\mathbf{k} = 0$ component of the electric field. We can now rewrite the electric field operator as:

$$\begin{aligned}\hat{E}_i(\mathbf{x}) =& E_i^L(\mathbf{x}) + \left(\nabla^{(-)} \times (\hat{L}(\mathbf{x}) + \epsilon(\mathbf{x}) + \epsilon_{\text{const}}(\mathbf{x}))\right)_i \\ &+ \delta_{i,1}\delta_{x_2,d_2}(\hat{L}_{\text{poly},1} + \epsilon_{\text{poly},1}) + \delta_{i,2}\delta_{x_1,d_1}\hat{L}_{\text{poly},2}.\end{aligned} \tag{4.43}$$

d_1 is the x_1-position where the Polyakov loop winds vertically around the lattice. The operators $\hat{L}(\mathbf{x})$ and $\hat{L}_{\text{poly}}$ measure the electric flux around a plaquette, resp. around the lattice, on top of the contributions given by the charge configuration. Their eigenvalues are integer-valued. If we insert the restriction to the topological sector with $L_{\text{poly},1} = L_{\text{poly},2} = 0$ and define $E_i^C(\mathbf{x}) = E_i^L(\mathbf{x}) + \delta_{i,1}\frac{d}{L^2}$ as the Coulomb electric field, we obtain the electric Hamiltonian given in eq. (4.5):

$$\begin{aligned}H_E &= \frac{g^2}{2}\sum_{\mathbf{x},i}\left(E_i^C(\mathbf{x}) + \epsilon_{ij}(L(\mathbf{x}) - L(\mathbf{x}-\mathbf{e}_j) + \epsilon(\mathbf{x}) - \epsilon(\mathbf{x}-\mathbf{e}_j))\right)^2 \\ &= E_C + \frac{g^2}{2}\sum_{\mathbf{x},i}(L(\mathbf{x}) - L(\mathbf{x}-\mathbf{e}_i) + \epsilon(\mathbf{x}) - \epsilon(\mathbf{x}-\mathbf{e}_i))^2\end{aligned} \tag{4.44}$$

with the Coulomb energy $E_C = \frac{g^2}{2}\left(\frac{d^2}{L^2} + \sum_{\mathbf{x},i} E_i^L(\mathbf{x})\right)$. Besides orthogonality between longitudinal and transversal component of the electric field, we also used Plancherel's theorem which ensures orthogonality between the constant part and the other two since their $\mathbf{k} = 0$ component is zero.

k_x \ k_y	0	1	2	3	4	5	6	7
0		1.289	1.108	0.978	0.937	0.978	1.108	1.289
1	1.288	1.206	1.050	0.937	0.897	0.936	1.051	1.207
2	1.109	1.050	0.937	0.849	0.819	0.849	0.936	1.050
3	0.979	0.935	0.849	0.781	0.756	0.781	0.849	0.937
4	0.935	0.897	0.819	0.756	0.732	0.756	0.819	0.897
5	0.979	0.937	0.849	0.781	0.756	0.781	0.849	0.935
6	1.109	1.050	0.936	0.849	0.819	0.849	0.937	1.050
7	1.288	1.207	1.051	0.936	0.897	0.937	1.050	1.206

k_x \ k_y	0	1	2	3	4	5	6	7
0		1.140	1.002	0.889	0.852	0.889	1.002	1.140
1	1.137	1.078	0.944	0.855	0.826	0.855	0.949	1.075
2	0.999	0.956	0.858	0.779	0.753	0.783	0.859	0.946
3	0.893	0.853	0.783	0.721	0.699	0.721	0.785	0.857
4	0.862	0.823	0.752	0.695	0.676	0.695	0.752	0.823
5	0.893	0.857	0.785	0.721	0.699	0.721	0.783	0.853
6	0.999	0.946	0.859	0.783	0.753	0.779	0.858	0.956
7	1.137	1.075	0.949	0.855	0.826	0.855	0.944	1.078

Figure 4.B.1: Variational parameters $\gamma_{\mathbf{k}}^R$ for the variational ground state at $g^2 = 1.1$ (left) and $g^2 = 1.2$ (right).

4.B Numerical evaluation of complex periodic Gaussian states

In this section, we review the numerical evaluation of complex periodic Gaussian states in more detail. We saw in section 4.3.2 that the region with $\gamma_{\mathbf{k}} = \gamma_{\mathbf{k}}^R + (\gamma_{\mathbf{k}}^I)^2 (\gamma_{\mathbf{k}}^R)^{-1} \approx 1$ is the most difficult to evaluate. Since the variational ground state (for which $\gamma_{\mathbf{k}}^I = 0$) varies from high $\gamma_{\mathbf{k}}^R$ for low couplings to low $\gamma_{\mathbf{k}}^R$ for large couplings, there is a transition region at $g^2 \sim 1.1$ where $\gamma_{\mathbf{k}}$ approaches one. We therefore want to study the approximations to all infinite sums involved in the computation of the variational energy in eq. (4.20) on an 8×8 lattice without static charges for the ground state at $g^2 = 1.1$ which is the highest coupling where the high $\gamma_{\mathbf{k}}$ approximation is used and $g^2 = 1.2$ which is the lowest coupling for which the low $\gamma_{\mathbf{k}}$ approximation is used. For all other couplings the contributions to infinite sums decay faster with higher orders compared to one of the two examples discussed below. The variational parameters $\gamma_{\mathbf{k}}^R$ for these states (rounded to three digits) are shown in Fig. 4.B.1. The values are displayed not only for the independent $\gamma_{\mathbf{k}}^R$ ($\mathbf{k} \in \mathcal{K}$), but are split between the dependent parameters $\gamma_{\mathbf{k}}^R$ and $\gamma_{-\mathbf{k}}^R$, to illustrate that they lie in the transition region $\gamma_{\mathbf{k}} \approx 1$ between the two approximation methods.

Using $\gamma_{\mathbf{k}}^I = 0$ and $\epsilon_{\mathbf{p}} = 0$, the expressions we need to compute for the variational ground state at $g^2 = 1.1$ simplify significantly:

$$I_{el} \equiv \sum_{\{N_{\mathbf{k}=\mathbf{0}}=0\}} e^{-\pi \sum_{\mathbf{k}} |N_{\mathbf{k}}|^2 \gamma_{\mathbf{k}}^R} \sum_{\mathbf{k}} (\gamma_{\mathbf{k}}^R)^2 |N_{\mathbf{k}}|^2 \left(4 - 2\cos\left(\frac{2\pi k_1}{L}\right) - 2\cos\left(\frac{2\pi k_2}{L}\right)\right) \tag{4.45}$$

for the electric energy,

$$I_{mag} \equiv \sum_{\{N_{\mathbf{k}=\mathbf{0}}=0\}} e^{-\pi \sum_{\mathbf{k}} |N_{\mathbf{k}}|^2 \gamma_{\mathbf{k}}^R} \sum_{\mathbf{p}} (-1)^{N_{\mathbf{p}}} \tag{4.46}$$

for the magnetic energy and the normalization

$$I_0 = \sum_{\{N_{\mathbf{k}=\mathbf{0}}=0\}} e^{-\pi \sum_{\mathbf{k}} |N_{\mathbf{k}}|^2 \gamma_{\mathbf{k}}^R}. \tag{4.47}$$

We include orders with $N_{\mathbf{p}}$ configurations of up to 8 pairs of $\{1, -1\}$ and the rest zeros. The first three are computed exactly and the remaining five by uniform sampling. Additionally, we compute exactly the orders $\{N\}_{2,-1,-1}$ and $\{N\}_{-2,1,1}$ to show they have negligible contributions. Orders like these, whose $N_{\mathbf{p}}$ configurations differ only by a minus sign can be evaluated together by evaluating for every permutation not

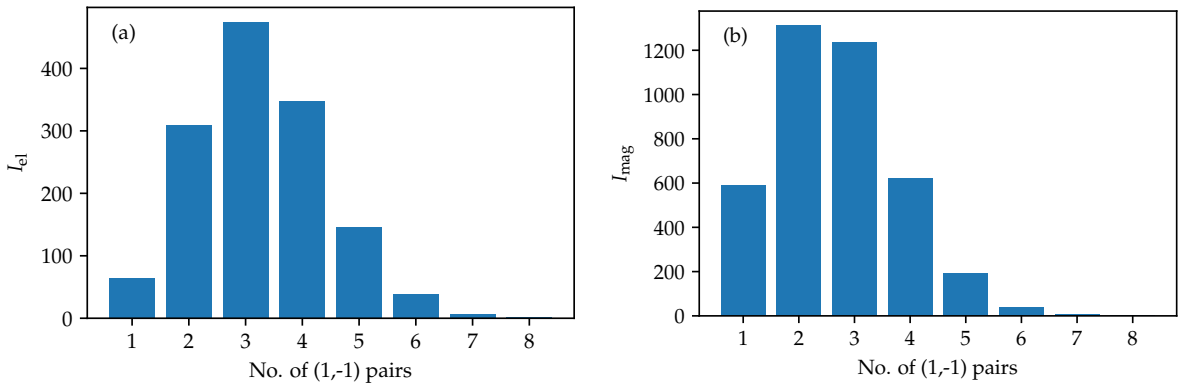

Figure 4.B.2: Contributions of different orders of $N_{\mathbf{p}}$ configurations to the infinite sums I_{el} (a) and I_{mag} (b) appearing in the high $\gamma_{\mathbf{k}}$ approximation of the variational energy. Due to the constraint $N_{\mathbf{k}=0} = 0$, the sum over all elements of $N_{\mathbf{p}}$ needs to be zero. Every bar represents the summed contributions of all $N_{\mathbf{p}}$ configurations containing a certain number of (1,-1) pairs and the remaining entries zero. Orders which are not of this type have a negligible contribution, e.g. $\{N\}_{-2,1,1}$ has a summed contribution to I_{el} of 0.076 and a summed contribution to I_{mag} of 0.23.

only the contribution of $N_{\mathbf{p}}$ but also of $-N_{\mathbf{p}}$. Therefore, from now on orders which are not closed under reflection will also include all their permutations multiplied by minus one. This will be heavily used in the low $\gamma_{\mathbf{k}}$ approximation.

The exact evaluation of orders is based on an algorithm which generates all permutations of a multiset in $O(1)$ time [101], i.e. the time to generate a new permutation is independent of the permutation size. It is much smaller than the time needed to do computations with a permutation which allows to highly parallelize the process and reach higher orders. The evaluation of an observable with respect to a set of permutations $\{N\}$ with uniform sampling is based on the approximation:

$$\sum_{N_{\mathbf{p}}\in\{N\}} O(N_{\mathbf{p}}) \approx \frac{p}{s} \sum_{N_{\mathbf{p}}\in S} O(N_{\mathbf{p}}) \tag{4.48}$$

where S is a set of s randomly drawn $N_{\mathbf{p}}$ configurations from $\{N\}$ and p the number of permutations within this order. For all orders which are computed with uniform sampling we use $s = 10^8$ in the high $\gamma_{\mathbf{k}}$ approximation and $s = 10^7$ in the low $\gamma_{\mathbf{k}}$ approximation. The contributions to I_{el} and I_{mag} for the high $\gamma_{\mathbf{k}}$ approximation are displayed in Fig. 4.B.2. We do not show this analysis for the normalization since its contributions decay faster than the ones for I_{el} and I_{mag}. The errors due to uniform sampling are too small to be shown in the plot, the biggest error occurs in the order with four pairs of $\{1,-1\}$ which has a contribution of $347.54(15)$ to I_{el} and of $622.70(24)$ to I_{mag}.

For the variational ground state at $g^2 = 1.2$, the infinite sums in eq. (4.20) reduce to

$$J_{el} = \sum_{\{N_{\mathbf{p}}\}/\sim_1} e^{-\pi \sum_{\mathbf{k}} |N_{\mathbf{k}}|^2 (\gamma_{\mathbf{k}}^R)^{-1}} \sum_{\mathbf{k}} \left(4 - 2\cos\left(\frac{2\pi k_1}{L}\right) - 2\cos\left(\frac{2\pi k_2}{L}\right)\right) |N_{\mathbf{k}}|^2 \tag{4.49}$$

for the computation of the electric energy,

$$J_{mag} = \sum_{\{N_{\mathbf{p}}\}/\sim_1} \sum_{\mathbf{p}} e^{-\pi \sum_{\mathbf{k}} |N_{\mathbf{k}} - \frac{1}{2}\mathbf{p}_{\mathbf{k}}|^2 (\gamma_{\mathbf{k}}^R)^{-1}} \tag{4.50}$$

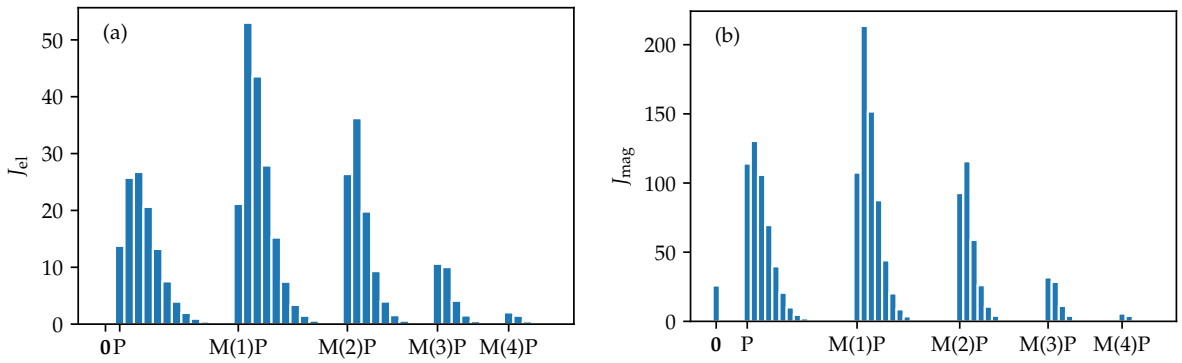

Figure 4.B.3: Contributions of different orders of $N_{\mathbf{p}}$ configurations to the infinite sums J_{el} (a) and J_{mag} (b) appearing in the low $\gamma_{\mathbf{k}}$ approximation of the variational energy. Due to absence of a constraint, all $N_{\mathbf{p}}$ configurations need to be considered. The orders are organized in groups. P denotes orders which contain a growing number of 1's. Since $N_{\mathbf{p}}$ and $-N_{\mathbf{p}}$ are evaluated together, P also represents orders with a growing number of -1's. $M(1)P$ contains orders whose non-zero elements are a single -1 and a growing number of 1's. The first order in $M(1)P$ contains a pair of (1,-1) as non-zero elements. $M(2)P$ is structured in the same way as $M(1)P$ but with two -1's. Analogously for the other groups. The $N_{\mathbf{p}} = \mathbf{0}$ configuration (denoted as $\mathbf{0}$) has vanishing contribution to J_{el} but a non-zero contribution to J_{mag}.

with $\frac{1}{2}^{\mathbf{p}}_{\mathbf{k}} = \frac{1}{2L} e^{-i\mathbf{pk}}$ for the computation of the magnetic energy and

$$J_0 = \sum_{\{N_{\mathbf{p}}\}/\sim_1} e^{-\pi \sum_{\mathbf{k}} |N_{\mathbf{k}}|^2 (\gamma^R_{\mathbf{k}})^{-1}} \tag{4.51}$$

for the normalization. Since we do not have a global constraint in the low $\gamma_{\mathbf{k}}$ approximation, more orders contribute to the infinite sums. The contributions to J_{el} and J_{mag} of different orders are given in Fig. 4.B.3. The errors are again too small to be displayed, the biggest one occurs in the order $\{N\}_{-1,1,1,1,1,1}$ with contributions of $15.22(1)$ to J_{el} and of $44.07(4)$ to J_{mag}.

Both approximation schemes decay reasonably well with higher orders and the truncation of even higher orders can be justified. Moreover, the errors introduced due to uniform sampling are small, in particular since the lowest orders were still calculated exactly. The algorithm we applied during computations to decide with which approximation method an expectation value should be evaluated was to select higher orders and compute them by uniform sampling with a low sample size of $s = 10^5$. This allowed us to choose the scheme which had a better decay with higher orders.

4.C Observables

In this section, we provide formulas for important quantities which are too lengthy to fit into the main body of the chapter. This includes formulas for expectation values of observables, namely Wilson loops and electric field, and a formula for the gradient of the energy with respect to the variational parameters which is essential to minimize the variational energy and carry out the time-dependent varational principle. For the

latter, we present additionally a formula for the Gram matrix. For every infinite sum appearing in the expressions, we provide both the high and low $\gamma_{\mathbf{k}}$ approximation.

We start with the expectation value of a Wilson loop along a contour C, where $\mathbf{p} \in C$ denotes all plaquettes within this contour:

$$\begin{aligned}&\frac{\langle\Psi_{CPG}|W(C)|\Psi_{CPG}\rangle}{\langle\Psi_{CPG}|\Psi_{CPG}\rangle}\\ =&e^{-\frac{\pi}{4L^2}\sum_{\mathbf{k}\neq\mathbf{0}}(\gamma_{\mathbf{k}}^R)^{-1}\sum_{\mathbf{p},\mathbf{p}'}\cos(\mathbf{k}(\mathbf{p}-\mathbf{p}'))}\left\langle\prod_{\mathbf{p}\in C}(-1)^{N_{\mathbf{p}}}\cosh\left(\pi\sum_{\mathbf{k}}\mathrm{Re}\left(N_{\mathbf{k}}b_{\mathbf{k}}^C\right)\right)\right\rangle\end{aligned} \tag{4.52}$$

with $b_{\mathbf{k}}^C = \frac{1}{L}\gamma_{\mathbf{k}}^I\left(\gamma_{\mathbf{k}}^R\right)^{-1}\sum_{\mathbf{p}\in C}e^{-i\mathbf{pk}}$ and

$$\begin{aligned}&\left\langle\prod_{\mathbf{p}\in C}(-1)^{N_{\mathbf{p}}}\cosh\left(\pi\sum_{\mathbf{k}}\mathrm{Re}(N_{\mathbf{k}}b_{\mathbf{k}}^C)\right)\right\rangle\\ =&\frac{\sum_{\{N_{\mathbf{k}=\mathbf{0}}=0\}}\prod_{\mathbf{p}\in C}(-1)^{N_{\mathbf{p}}}\cosh\left(\pi\sum_{\mathbf{k}}\mathrm{Re}(N_{\mathbf{k}}b_{\mathbf{k}}^C)\right)e^{2\pi i\sum_{\mathbf{p}}\epsilon_{\mathbf{p}}N_{\mathbf{p}}}e^{-\pi\sum_{\mathbf{k}}|N_{\mathbf{k}}|^2\gamma_{\mathbf{k}}}}{\sum_{\{N_{\mathbf{k}=\mathbf{0}}=0\}}e^{2\pi i\sum_{\mathbf{p}}\epsilon_{\mathbf{p}}N_{\mathbf{p}}}e^{-\pi\sum_{\mathbf{k}}|N_{\mathbf{k}}|^2\gamma_{\mathbf{k}}}}\\ =&\frac{\sum_{\{N_{\mathbf{p}}\}/\sim_1}e^{-\pi\sum_{\mathbf{k}}\left(|N_{\mathbf{k}}-\epsilon_{\mathbf{k}}-\frac{1}{2}{}_{\mathbf{k}}^C|^2-\frac{1}{4}|b_{\mathbf{k}}^C|^2\right)\gamma_{\mathbf{k}}^{-1}}\cos\left(\pi\sum_{\mathbf{k}}\gamma_{\mathbf{k}}^{-1}\mathrm{Re}[(N_{\mathbf{k}}-\epsilon_{\mathbf{k}}-\frac{1}{2}{}_{\mathbf{k}}^C)b_{\mathbf{k}}^C]\right)}{\sum_{\{N_{\mathbf{p}}\}/\sim_1}e^{-\pi\sum_{\mathbf{k}}|N_{\mathbf{k}}-\epsilon_{\mathbf{k}}|^2\gamma_{\mathbf{k}}^{-1}}}\end{aligned} \tag{4.53}$$

with $\frac{1}{2}{}_{\mathbf{k}}^C = \frac{1}{2L}\sum_{\mathbf{p}\in C}e^{-i\mathbf{pk}}$ and $\gamma_{\mathbf{k}} = \gamma_{\mathbf{k}}^R + \left(\gamma_{\mathbf{k}}^I\right)^2\left(\gamma_{\mathbf{k}}^R\right)^{-1}$. Another observable which is used in the main part of this chapter is the electric field. We present for simplicity the expectation value of a horizontal link emanating from vertex $\mathbf{x}$, $\langle E_{\mathbf{x},1}\rangle$. The plaquette above the link is denoted as $\tilde{\mathbf{p}}$.

$$\frac{\langle\Psi_{CPG}|E_{\mathbf{x},1}|\Psi_{CPG}\rangle}{\langle\Psi_{CPG}|\Psi_{CPG}\rangle} \tag{4.54}$$

$$\begin{aligned}=&\frac{\sum_{\{N_{\mathbf{k}=\mathbf{0}}=0\}}\sin\left(2\pi\sum_{\mathbf{p}}\epsilon_{\mathbf{p}}N_{\mathbf{p}}\right)e^{-\pi\sum_{\mathbf{k}}|N_{\mathbf{k}}|^2\gamma_{\mathbf{k}}}\frac{1}{L}\sum_{\mathbf{k}}\gamma_{\mathbf{k}}\mathrm{Re}\left(N_{\mathbf{k}}\left(e^{-i\mathbf{k}\tilde{\mathbf{p}}}-e^{-i\mathbf{k}(\tilde{\mathbf{p}}-\mathbf{e_2})}\right)\right)}{\sum_{\{N_{\mathbf{k}=\mathbf{0}}=0\}}e^{2\pi i\sum_{\mathbf{p}}\epsilon_{\mathbf{p}}N_{\mathbf{p}}}e^{-\pi\sum_{\mathbf{k}}|N_{\mathbf{k}}|^2\gamma_{\mathbf{k}}}}\\ =&\epsilon_{\tilde{\mathbf{p}}}-\epsilon_{\tilde{\mathbf{p}}-\mathbf{e_2}}+\frac{\sum_{\{N_{\mathbf{p}}\}/\sim_1}e^{-\pi\sum_{\mathbf{k}}|N_{\mathbf{k}}-\epsilon_{\mathbf{k}}|^2\gamma_{\mathbf{k}}^{-1}}(N_{\tilde{\mathbf{p}}-\mathbf{e_2}}-N_{\tilde{\mathbf{p}}})}{\sum_{\{N_{\mathbf{p}}\}/\sim_1}e^{-\pi\sum_{\mathbf{k}}|N_{\mathbf{k}}-\epsilon_{\mathbf{k}}|^2\gamma_{\mathbf{k}}^{-1}}}\end{aligned} \tag{4.55}$$

The expectation value for a vertical link follows analogously. The next quantity we present is the gradient of the variational energy with respect to the independent parameters $\gamma_{\mathbf{k}}^R$ and $\gamma_{\mathbf{k}}^I$ ($\mathbf{k} \in \mathcal{K}$). We split the energy into an electric and a magnetic part to make the expressions less cumbersome. We start with the derivatives of the electric energy with respect to $\gamma_{\mathbf{k}}^R$ and $\gamma_{\mathbf{k}}^I$ ($\mathbf{k} \in \mathcal{K}$):

$$
\begin{aligned}
&\frac{\partial}{\partial\gamma_{\mathbf{k}}^{R}}\frac{\langle\Psi_{CPG}|H_E|\Psi_{CPG}\rangle}{\langle\Psi_{CPG}|\Psi_{CPG}\rangle}\\
=&\frac{g^2}{4\pi}m_{\mathbf{k}}\left(1-\frac{\left(\gamma_{\mathbf{k}}^{I}\right)^2}{\left(\gamma_{\mathbf{k}}^{R}\right)^2}\right)\left(4-2\cos\left(\frac{2\pi k_1}{L}\right)-2\cos\left(\frac{2\pi k_2}{L}\right)\right)\\
&-g^2m_{\mathbf{k}}\left(\gamma_{\mathbf{k}}^{R}-\frac{\left(\gamma_{\mathbf{k}}^{I}\right)^4}{\left(\gamma_{\mathbf{k}}^{R}\right)^3}\right)\left(4-2\cos\left(\frac{2\pi k_1}{L}\right)-2\cos\left(\frac{2\pi k_2}{L}\right)\right)\left\langle|N_{\mathbf{k}}|^2\right\rangle\\
&+\frac{g^2\pi}{2}m_{\mathbf{k}}\left(1-\frac{\left(\gamma_{\mathbf{k}}^{I}\right)^2}{\left(\gamma_{\mathbf{k}}^{R}\right)^2}\right)\sum_{\mathbf{k}'}\gamma_{\mathbf{k}'}^{2}\left(4-2\cos\left(\frac{2\pi k_1'}{L}\right)-2\cos\left(\frac{2\pi k_2'}{L}\right)\right)\times\\
&\qquad\times\left(\left\langle|N_{\mathbf{k}'}|^2|N_{\mathbf{k}}|^2\right\rangle-\left\langle|N_{\mathbf{k}'}|^2\right\rangle\left\langle|N_{\mathbf{k}}|^2\right\rangle\right)
\end{aligned}
\tag{4.56}
$$

$$
\begin{aligned}
&\frac{\partial}{\partial\gamma_{\mathbf{k}}^{I}}\frac{\langle\Psi_{CPG}|H_E|\Psi_{CPG}\rangle}{\langle\Psi_{CPG}|\Psi_{CPG}\rangle}\\
=&\frac{g^2}{2\pi}m_{\mathbf{k}}\frac{\gamma_{\mathbf{k}}^{I}}{\gamma_{\mathbf{k}}^{R}}\left(4-2\cos\left(\frac{2\pi k_1}{L}\right)-2\cos\left(\frac{2\pi k_2}{L}\right)\right)\\
&-2g^2m_{\mathbf{k}}\left(\gamma_{\mathbf{k}}^{I}+\frac{\left(\gamma_{\mathbf{k}}^{I}\right)^3}{\left(\gamma_{\mathbf{k}}^{R}\right)^2}\right)\left(4-2\cos\left(\frac{2\pi k_1}{L}\right)-2\cos\left(\frac{2\pi k_2}{L}\right)\right)\left\langle|N_{\mathbf{k}}|^2\right\rangle\\
&+g^2\pi m_{\mathbf{k}}\frac{\gamma_{\mathbf{k}}^{I}}{\gamma_{\mathbf{k}}^{R}}\sum_{\mathbf{k}'}\gamma_{\mathbf{k}'}^{2}\left(4-2\cos\left(\frac{2\pi k_1'}{L}\right)-2\cos\left(\frac{2\pi k_2'}{L}\right)\right)\times\\
&\qquad\times\left(\left\langle|N_{\mathbf{k}'}|^2|N_{\mathbf{k}}|^2\right\rangle-\left\langle|N_{\mathbf{k}'}|^2\right\rangle\left\langle|N_{\mathbf{k}}|^2\right\rangle\right)
\end{aligned}
\tag{4.57}
$$

with

$$
\begin{aligned}
\left\langle|N_{\mathbf{k}'}|^2|N_{\mathbf{k}}|^2\right\rangle&=\frac{\sum_{\{N_{\mathbf{k}=\mathbf{0}}=0\}}e^{2\pi i\sum_{\mathbf{p}}\epsilon_{\mathbf{p}}N_{\mathbf{p}}}e^{-\pi\sum_{\mathbf{k}}|N_{\mathbf{k}}|^2\gamma_{\mathbf{k}}}|N_{\mathbf{k}}|^2|N_{\mathbf{k}'}|^2}{\sum_{\{N_{\mathbf{k}=\mathbf{0}}=0\}}e^{2\pi i\sum_{\mathbf{p}}\epsilon_{\mathbf{p}}N_{\mathbf{p}}}e^{-\pi\sum_{\mathbf{k}}|N_{\mathbf{k}}|^2\gamma_{\mathbf{k}}}}\\
&=\frac{1}{4\pi^2}\gamma_{\mathbf{k}}^{-1}\gamma_{\mathbf{k}'}^{-1}+\gamma_{\mathbf{k}}^{-2}\gamma_{\mathbf{k}'}^{-2}\frac{\sum_{\{N_{\mathbf{p}}\}/\sim_1}e^{-\pi\sum_{\mathbf{k}}|N_{\mathbf{k}}-\epsilon_{\mathbf{k}}|^2\gamma_{\mathbf{k}}^{-1}}|N_{\mathbf{k}}-\epsilon_{\mathbf{k}}|^2|N_{\mathbf{k}'}-\epsilon_{\mathbf{k}'}|^2}{\sum_{\{N_{\mathbf{p}}\}/\sim_1}e^{-\pi\sum_{\mathbf{k}}|N_{\mathbf{k}}-\epsilon_{\mathbf{k}}|^2\gamma_{\mathbf{k}}^{-1}}}\\
&\quad-\frac{1}{2\pi}\gamma_{\mathbf{k}'}^{-2}\gamma_{\mathbf{k}}^{-1}\frac{\sum_{\{N_{\mathbf{p}}\}/\sim_1}e^{-\pi\sum_{\mathbf{k}}|N_{\mathbf{k}}-\epsilon_{\mathbf{k}}|^2\gamma_{\mathbf{k}}^{-1}}|N_{\mathbf{k}'}-\epsilon_{\mathbf{k}'}|^2}{\sum_{\{N_{\mathbf{p}}\}/\sim_1}e^{-\pi\sum_{\mathbf{k}}|N_{\mathbf{k}}-\epsilon_{\mathbf{k}}|^2\gamma_{\mathbf{k}}^{-1}}}\\
&\quad-\frac{1}{2\pi}\gamma_{\mathbf{k}}^{-2}\gamma_{\mathbf{k}'}^{-1}\frac{\sum_{\{N_{\mathbf{p}}\}/\sim_1}e^{-\pi\sum_{\mathbf{k}}|N_{\mathbf{k}}-\epsilon_{\mathbf{k}}|^2\gamma_{\mathbf{k}}^{-1}}|N_{\mathbf{k}}-\epsilon_{\mathbf{k}}|^2}{\sum_{\{N_{\mathbf{p}}\}/\sim_1}e^{-\pi\sum_{\mathbf{k}}|N_{\mathbf{k}}-\epsilon_{\mathbf{k}}|^2\gamma_{\mathbf{k}}^{-1}}}\\
&\quad+\delta_{\mathbf{k},\mathbf{k}'}\frac{1}{m_{\mathbf{k}}}\left(\frac{1}{2\pi^2}\gamma_{\mathbf{k}}^{-2}-\frac{2}{\pi}\gamma_{\mathbf{k}}^{-3}\frac{\sum_{\{N_{\mathbf{p}}\}/\sim_1}e^{-\pi\sum_{\mathbf{k}}|N_{\mathbf{k}}-\epsilon_{\mathbf{k}}|^2\gamma_{\mathbf{k}}^{-1}}|N_{\mathbf{k}}-\epsilon_{\mathbf{k}}|^2}{\sum_{\{N_{\mathbf{p}}\}/\sim_1}e^{-\pi\sum_{\mathbf{k}}|N_{\mathbf{k}}-\epsilon_{\mathbf{k}}|^2\gamma_{\mathbf{k}}^{-1}}}\right)
\end{aligned}
\tag{4.58}
$$

We denote by $m_{\mathbf{k}}$ the number of elements in the equivalence class $\mathbf{k} \in K$ which is two if $\mathbf{k} \neq -\mathbf{k}$ and one if $\mathbf{k} = -\mathbf{k}$. The expression for $\langle |N_{\mathbf{k}}|^2 \rangle$ for both high and low $\gamma_{\mathbf{k}}$ approximation can be found in eq. (4.21). The gradient of the magnetic energy with respect to $\gamma_{\mathbf{k}}^R$ and $\gamma_{\mathbf{k}}^I$ takes the form:

$$\begin{aligned}
&\frac{\partial}{\partial \gamma_{\mathbf{k}}^R} \frac{\langle \Psi_{CPG}|H_B|\Psi_{CPG}\rangle}{\langle \Psi_{CPG}|\Psi_{CPG}\rangle} \\
=&\frac{\pi}{g^2} m_{\mathbf{k}} e^{-\frac{\pi}{4L^2}\sum_{\mathbf{k}\neq\mathbf{0}}(\gamma_{\mathbf{k}}^R)^{-1}} \sum_{\mathbf{p}} \left[-\frac{1}{4L^2} \left(\gamma_{\mathbf{k}}^R\right)^{-2} \left\langle (-1)^{N_{\mathbf{p}}} \cosh\left(\pi \sum_{\mathbf{k}'} \mathrm{Re}(N_{\mathbf{k}'} b_{\mathbf{k}'}^{\mathbf{p}})\right)\right\rangle \right. \\
&+\frac{1}{L}\frac{\gamma_{\mathbf{k}}^I}{\left(\gamma_{\mathbf{k}}^R\right)^2} \left\langle (-1)^{N_{\mathbf{p}}} \mathrm{Re}(N_{\mathbf{k}} e^{-i\mathbf{k}\mathbf{p}}) \sinh\left(\pi \sum_{\mathbf{k}'} \mathrm{Re}(N_{\mathbf{k}'} b_{\mathbf{k}'}^{\mathbf{p}})\right)\right\rangle \\
&+\left(1 - \frac{\left(\gamma_{\mathbf{k}}^I\right)^2}{\left(\gamma_{\mathbf{k}}^R\right)^2}\right) \left(\left\langle (-1)^{N_{\mathbf{p}}} |N_{\mathbf{k}}|^2 \cosh\left(\pi \sum_{\mathbf{k}'} \mathrm{Re}(N_{\mathbf{k}'} b_{\mathbf{k}'}^{\mathbf{p}})\right)\right\rangle \right. \\
&\qquad \left. \left. - \left\langle (-1)^{N_{\mathbf{p}}} \cosh\left(\pi \sum_{\mathbf{k}'} \mathrm{Re}(N_{\mathbf{k}'} b_{\mathbf{k}'})\right)\right\rangle \langle |N_{\mathbf{k}}|^2 \rangle \right) \right]
\end{aligned} \tag{4.59}$$

$$\begin{aligned}
&\frac{\partial}{\partial \gamma_{\mathbf{k}}^I} \frac{\langle \Psi_{CPG}|H_B|\Psi_{CPG}\rangle}{\langle \Psi_{CPG}|\Psi_{CPG}\rangle} \\
=&\frac{\pi}{g^2} m_{\mathbf{k}} e^{-\frac{\pi}{4L^2}\sum_{\mathbf{k}\neq\mathbf{0}}(\gamma_{\mathbf{k}}^R)^{-1}} \sum_{\mathbf{p}} \left[-\frac{1}{\gamma_{\mathbf{k}}^R L} \left\langle (-1)^{N_{\mathbf{p}}} \mathrm{Re}(N_{\mathbf{k}} e^{-i\mathbf{k}\mathbf{p}}) \sinh\left(\pi \sum_{\mathbf{k}'} \mathrm{Re}(N_{\mathbf{k}'} b_{\mathbf{k}'}^{\mathbf{p}})\right)\right\rangle \right. \\
&+2\frac{\gamma_{\mathbf{k}}^I}{\gamma_{\mathbf{k}}^R} \left(\left\langle (-1)^{N_{\mathbf{p}}} |N_{\mathbf{k}}|^2 \cosh\left(\pi \sum_{\mathbf{k}'} \mathrm{Re}(N_{\mathbf{k}'} b_{\mathbf{k}'}^{\mathbf{p}})\right)\right\rangle \right. \\
&\qquad \left. \left. - \left\langle (-1)^{N_{\mathbf{p}}} \cosh\left(\pi \sum_{\mathbf{k}'} \mathrm{Re}(N_{\mathbf{k}'} b_{\mathbf{k}'}^{\mathbf{p}})\right)\right\rangle \langle |N_{\mathbf{k}}|^2 \rangle \right) \right]
\end{aligned} \tag{4.60}$$

with the usual definition of $b_{\mathbf{k}}^{\mathbf{p}}$ and $\frac{1}{2}_{\mathbf{k}}^{\mathbf{p}}$ from eq. (4.20) and the infinite sums

$$\begin{aligned}
&\left\langle (-1)^{N_{\mathbf{p}}} |N_{\mathbf{k}}|^2 \cosh\left(\pi \sum_{\mathbf{k}'} \mathrm{Re}(N_{\mathbf{k}'} b_{\mathbf{k}'}^{\mathbf{p}})\right)\right\rangle \\
=&\frac{\sum_{\{N_{\mathbf{k}=\mathbf{0}}=0\}} (-1)^{N_{\mathbf{p}}} |N_{\mathbf{k}}|^2 \cosh\left(\pi \sum_{\mathbf{k}'} \mathrm{Re}\left(N_{\mathbf{k}'} b_{\mathbf{k}'}^{\mathbf{p}}\right)\right) e^{2\pi i \sum_{\mathbf{p}} \epsilon_{\mathbf{p}} N_{\mathbf{p}}} e^{-\pi \sum_{\mathbf{k}} |N_{\mathbf{k}}|^2 \gamma_{\mathbf{k}}}}{\sum_{\{N_{\mathbf{k}=\mathbf{0}}=0\}} e^{2\pi i \sum_{\mathbf{p}} \epsilon_{\mathbf{p}} N_{\mathbf{p}}} e^{-\pi \sum_{\mathbf{k}} |N_{\mathbf{k}}|^2 \gamma_{\mathbf{k}}}} \\
=&-\frac{\sum_{\{N_{\mathbf{p}}\}/\sim_1} e^{-\pi \sum_{\mathbf{k}} \left(|\tilde{N}_{\mathbf{k}} - \frac{1}{2}_{\mathbf{k}}^{\mathbf{p}}|^2 - \frac{1}{4}|b_{\mathbf{k}}^{\mathbf{p}}|^2\right)\gamma_{\mathbf{k}}^{-1}} \sin\left(\sum_{\mathbf{k}'} \frac{\pi}{\gamma_{\mathbf{k}'}} \mathrm{Re}\left[(\tilde{N}_{\mathbf{k}'} - \frac{1}{2}_{\mathbf{k}'}^{\mathbf{p}}) b_{\mathbf{k}'}^{\mathbf{p}}\right]\right) \mathrm{Re}\left[(\tilde{N}_{\mathbf{k}} - \frac{1}{2}_{\mathbf{k}}^{\mathbf{p}}) b_{\mathbf{k}}^{\mathbf{p}}\right]}{\gamma_{\mathbf{k}}^2 \sum_{\{N_{\mathbf{p}}\}/\sim_1} e^{-\pi \sum_{\mathbf{k}} |\tilde{N}_{\mathbf{k}}|^2 \gamma_{\mathbf{k}}^{-1}}} \\
&-\frac{\sum_{\{N_{\mathbf{p}}\}/\sim_1} e^{-\pi \sum_{\mathbf{k}} \left(|\tilde{N}_{\mathbf{k}} - \frac{1}{2}_{\mathbf{k}}^{\mathbf{p}}|^2 - \frac{1}{4}|b_{\mathbf{k}}^{\mathbf{p}}|^2\right)\gamma_{\mathbf{k}}^{-1}} \cos\left(\sum_{\mathbf{k}'} \frac{\pi}{\gamma_{\mathbf{k}'}} \mathrm{Re}\left[(\tilde{N}_{\mathbf{k}'} - \frac{1}{2}_{\mathbf{k}'}^{\mathbf{p}}) b_{\mathbf{k}'}^{\mathbf{p}}\right]\right) \left(|\tilde{N}_{\mathbf{k}} - \frac{1}{2}_{\mathbf{k}}^{\mathbf{p}}|^2 - \frac{1}{4}|b_{\mathbf{k}}^{\mathbf{p}}|^2\right)}{\gamma_{\mathbf{k}}^2 \sum_{\{N_{\mathbf{p}}\}/\sim_1} e^{-\pi \sum_{\mathbf{k}} |\tilde{N}_{\mathbf{k}}|^2 \gamma_{\mathbf{k}}^{-1}}}
\end{aligned} \tag{4.61}$$

$$
\begin{aligned}
&\left\langle (-1)^{N_{\mathbf{p}}} \mathrm{Re}(N_{\mathbf{k}} e^{-i\mathbf{kp}}) \sinh\left(\pi \sum_{\mathbf{k}'} \mathrm{Re}(N_{\mathbf{k}'} b^{\mathbf{p}}_{\mathbf{k}'})\right)\right\rangle \\
=&\frac{\sum_{\{N_{\mathbf{k}=\mathbf{0}}=0\}} (-1)^{N_{\mathbf{p}}} \mathrm{Re}(N_{\mathbf{k}} e^{-i\mathbf{kp}}) \sinh\left(\pi \sum_{\mathbf{k}'} \mathrm{Re}(N_{\mathbf{k}'} b^{\mathbf{p}}_{\mathbf{k}'})\right) e^{2\pi i \sum_{\mathbf{p}} \epsilon_{\mathbf{p}} N_{\mathbf{p}}} e^{-\pi \sum_{\mathbf{k}} |N_{\mathbf{k}}|^2 \gamma_{\mathbf{k}}}}{\sum_{\{N_{\mathbf{k}=\mathbf{0}}=0\}} e^{2\pi i \sum_{\mathbf{p}} \epsilon_{\mathbf{p}} N_{\mathbf{p}}} e^{-\pi \sum_{\mathbf{k}} |N_{\mathbf{k}}|^2 \gamma_{\mathbf{k}}}} \\
=&\frac{1}{2L} \frac{\gamma^I_{\mathbf{k}}}{\left(\gamma^R_{\mathbf{k}}\right)^2 + \left(\gamma^I_{\mathbf{k}}\right)^2} \left\langle (-1)^{N_{\mathbf{p}}} \cosh\left(\pi \sum_{\mathbf{k}'} \mathrm{Re}(N_{\mathbf{k}'} b^{\mathbf{p}}_{\mathbf{k}'})\right)\right\rangle \qquad (4.62) \\
-&\frac{\sum_{\{N_{\mathbf{p}}\}/\sim_1} e^{-\pi \sum_{\mathbf{k}} \left(|\tilde{N}_{\mathbf{k}} - \frac{1}{2}\mathbf{p}_{\mathbf{k}}|^2 - \frac{1}{4}|b^{\mathbf{p}}_{\mathbf{k}}|^2\right)\gamma^{-1}_{\mathbf{k}}} \sin\left(\pi \sum_{\mathbf{k}'} \gamma^{-1}_{\mathbf{k}'} \mathrm{Re}\left[(\tilde{N}_{\mathbf{k}'} - \frac{1}{2}\mathbf{p}_{\mathbf{k}'}) b^{\mathbf{p}}_{\mathbf{k}'}\right]\right) \mathrm{Re}\left[(\tilde{N}_{\mathbf{k}} - \frac{1}{2}\mathbf{p}_{\mathbf{k}}) e^{-i\mathbf{kp}}\right]}{\gamma_{\mathbf{k}} \sum_{\{N_{\mathbf{p}}\}/\sim_1} e^{-\pi \sum_{\mathbf{k}} |\tilde{N}_{\mathbf{k}}|^2 \gamma^{-1}_{\mathbf{k}}}} \qquad (4.63)
\end{aligned}
$$

with $\tilde{N}_{\mathbf{k}} = N_{\mathbf{k}} - \epsilon_{\mathbf{k}}$ and the expression for $\left\langle (-1)^{N_{\mathbf{p}}} \cosh\left(\pi \sum_{\mathbf{k}'} \mathrm{Re}(N_{\mathbf{k}'} b^{\mathbf{p}}_{\mathbf{k}'})\right)\right\rangle$ can be found in eq. (4.21). A crucial quantity for the time-dependent variational principle is the Gram matrix. It is defined as the overlap between two tangent vectors on the variational manifold. Therefore, it is not only the overlap between the derivatives of the ansatz with respect to the variational parameters but it also needs to be projected onto the variational manifold (see eq. (4.31)):

$$
\begin{aligned}
G_{\mathbf{k}\mathbf{k}'} =& \frac{\pi^2}{4} m_{\mathbf{k}} m_{\mathbf{k}'} \left(\left\langle |N_{\mathbf{k}}|^2 |N_{\mathbf{k}'}|^2 \right\rangle - \left\langle |N_{\mathbf{k}}|^2 \right\rangle \left\langle |N_{\mathbf{k}'}|^2 \right\rangle\right) \\
&\left[\left(1 - \frac{\left(\gamma^I_{\mathbf{k}}\right)^2}{\left(\gamma^R_{\mathbf{k}}\right)^2}\right)\left(1 - \frac{\left(\gamma^I_{\mathbf{k}'}\right)^2}{\left(\gamma^R_{\mathbf{k}'}\right)^2}\right) - 4\frac{\gamma^I_{\mathbf{k}}}{\gamma^R_{\mathbf{k}}}\frac{\gamma^I_{\mathbf{k}'}}{\gamma^R_{\mathbf{k}'}} + 2i\frac{\gamma^I_{\mathbf{k}}}{\gamma^R_{\mathbf{k}}}\left(1 - \frac{\left(\gamma^I_{\mathbf{k}'}\right)^2}{\left(\gamma^R_{\mathbf{k}'}\right)^2}\right)\right. \\
&\left. -2i\left(1 - \frac{\left(\gamma^I_{\mathbf{k}}\right)^2}{\left(\gamma^R_{\mathbf{k}}\right)^2}\right)\frac{\gamma^I_{\mathbf{k}'}}{\gamma^R_{\mathbf{k}'}}\right] + \delta_{\mathbf{k},\mathbf{k}'} m_{\mathbf{k}} \left(\frac{1}{8\left(\gamma^R_{\mathbf{k}}\right)^2} - \frac{\pi}{2}\left\langle |N_{\mathbf{k}}|^2 \right\rangle \left(\frac{1}{\gamma^R_{\mathbf{k}}} + \frac{\left(\gamma^I_{\mathbf{k}}\right)^2}{\left(\gamma^R_{\mathbf{k}}\right)^3}\right)\right)
\end{aligned} \qquad (4.64)
$$

5 Variational Monte Carlo algorithm for lattice gauge theories with continuous gauge groups: A study of compact QED at finite density

5.1 Motivation

Gauge theories are essential in various fields of physics. The standard model of particle physics, a gauge theory, describes three of the four fundamental forces in nature. While perturbative methods can be applied to interactions at high energy scales, non-perturbative techniques are required for lower energy regimes [5, 72]. This necessity naturally leads to lattice gauge theories as they provide a non-perturbative and gauge-invariant regularization of quantum field theories [7, 8]. Additionally, lattice gauge theories can arise as effective theories for strongly correlated electron systems in condensed matter, such as quantum spin liquids or high-temperature superconductors [9, 10].

Lattice gauge theories have been extensively studied using Euclidean Monte Carlo simulations, resulting in significant progress in both high-energy physics and condensed matter research [11]. However, there are still challenges in accessing certain regimes within this framework. For example, fermionic theories with finite density or an odd number of fermion flavors may be affected by the sign problem [12], and computing real-time dynamics is challenging because Monte Carlo algorithms are typically formulated in Euclidean spacetime.

To tackle the difficulty of simulating lattice gauge theories in certain regimes, various approaches have been explored in recent years. One of the prominent ones is quantum simulation, which utilizes quantum devices such as ultracold atoms, trapped ions, or superconducting qubits to implement lattice gauge theory Hamiltonians. In one dimension, successful implementations have been demonstrated using trapped ions and ultracold atoms [34–38]. However, in higher dimensions, the appearance of magnetic interactions, resulting in four-body plaquette terms on the lattice, poses a challenge. Several proposals have been made to overcome this problem in quantum simulators, including digital [4, 41, 42, 102–104] and analog [39, 40] simulation schemes. Nonetheless, experimental realization of these proposals is still pending.

Another significant strategy to tackle the problem of simulating lattice gauge theories is the use of variational ansatz states which can efficiently capture the relevant physics of the theory. In the case of lattice gauge theories, these states must either satisfy the local gauge symmetries or require a reformulation of the theory in terms of gauge-invariant variables, at the cost of more complex interactions [1, 61, 105]. One

type of ansatz states are tensor networks that have been successfully applied to $(1+1)$-dimensional Abelian and non-Abelian lattice gauge theories [17, 75, 76, 78–82, 106–108]. These methods enable the study of out-of-equilibrium dynamics and finite chemical potential scenarios, which are not accessible using Monte Carlo simulations of Euclidean lattice gauge theory. In higher dimensions, tensor network methods have been applied to lattice gauge theories with a finite-dimensional gauge field Hilbert space. Other types of ansatz states can be formulated in the infinite-dimensional Hilbert space of continuous gauge groups, including periodic Gaussian states [2] or neural network-based ansatz states [100, 109].

In the realm of both high-energy and condensed matter physics, $(2+1)$-dimensional compact QED with dynamical charges is a particularly intriguing model. It is significant in high-energy physics because it is the simplest theory that can be used to explore confinement and chiral symmetry breaking, which are fundamental to our understanding of quantum chromodynamics. Even without dynamical fermions, the theory exhibits non-trivial interactions owing to the presence of four-body magnetic terms and is known to be confining for all couplings [18]. However, when dynamical fermions are introduced, the confinement phenomenon becomes less apparent as the fermionic matter may lead to deconfinement. These phenomena also have relevance in condensed matter physics since many low-energy effective theories of two-dimensional strongly coupled electron systems can be described by massless dynamical fermions coupled to a compact $U(1)$ gauge field. Although sign-problem-free Monte Carlo simulations were demonstrated for an even number of fermion flavors in $\mathbb{Z}_2$ lattice gauge theories, even at non-zero density [110], for the $U(1)$-theory, the sign-problem is only resolved for an even number of fermion flavors at half-filling [111].

In this chapter, a variational approach is presented that allows to investigate the sign-problem affected regimes of compact QED with dynamical charges, while keeping the full $U(1)$ gauge field Hilbert space. The ansatz consists of a pure gauge part, which captures the self-interactions of the gauge field, and a fermionic part that describes the dynamics of the matter degrees of freedom coupled to the gauge field. The pure gauge part is a Jastrow wave function that is constructed using gauge-invariant plaquette variables, which is similar in form to certain neural network quantum states [112]. This choice is motivated by the variational method presented in chapter 4 that successfully approximated the ground states and real-time dynamics in compact QED with static charges. The fermionic part is an infinite superposition of gauge-field dependent fermionic Gaussian states, which are parametrized in a way that guarantees the resulting state is gauge-invariant. Importantly, this parametrization ensures that the number of parameters scales only polynomially with system size. Monte Carlo sampling is used to compute expectation values and stochastic reconfiguration [113] to optimize our variational states.

The variational method is extensively benchmarked. It is shown that in limiting cases where the ground state of the theory is known, the variational ansatz can capture this behavior. The pure gauge part of the ansatz is benchmarked against the variational method based on complex periodic Gaussian states presented in chapter 4 by comparing the variational ground state energies, showing agreement over the whole coupling region. Moreover, for the full compact QED theory with dynamical fermions the whole ansatz, including the fermionic part, is benchmarked for two fermion flavors at zero chemcial potential against a Euclidean Monte Carlo study [111] since the sign-problem is absent in that case. To demosntrate the capabilities of the variational method also

in sign-problem affected regimes, density-induced phase transition for two fermion flavors at non-zero chemcial potential are studied.

The content of this chapter is based on Ref. [3]

5.2 Executive summary

The conventional approach of studying lattice gauge theories in the action-based formulations using Euclidean Monte Carlo simulations is hindered by the sign-problem in certain regimes, e.g. at finite chemical potential. To study these regimes with variational methods in a Hamiltonian framework one faces the challenge of an infinite-dimensional gauge field Hilbert space and the need to find a suitable gauge-invariant ansatz that couples dynamical fermions to gauge fields.

In the following sections a variational Monte Carlo algorithm for continuous gauge groups is presented, i.e. the infinite-dimensional Hilbert space of the $U(1)$ gauge field can be captured without the need to truncate. The method is demonstrated for $(2+1)$-dimensional compact QED with dynamical fermions at finite density, a regime plagued by the sign-problem. The $U(1)$ gauge field on every link can be characterized either by a compact angular variable $\theta \in [0, 2\pi)$ or an integer-valued electric field variable. The construction of the variational ansatz is performed in terms of the compact angular variables.

The ansatz comprises of two components. The first component is a Jastrow-type ansatz state that is constructed out of gauge-invariant plaquette variables. It describes the pure gauge dynamics of compact QED and is related to the variational method presented in chapter 4 that successfully approximated ground states and real-time dynamics in pure gauge compact QED.

The second component describes the interactions of the gauge field with the dynamical fermions. Formulated in terms of compact $U(1)$ variables, one needs to specify a fermionic state for every gauge field configuration in such a way that the overall integral over all gauge field configurations is gauge-invariant. This is achieved by using gauge-field dependent fermionic Gaussian states based on the eigendecomposition of the gauge-matter Hamiltonian. The gauge-matter Hamiltonian describes the interactions between dynamical fermions and gauge fields and is by construction gauge-invariant. Its eigenstates are gauge-field dependent fermionic Gaussian states and gauge-invariant. If one fixes a gauge-field configuration in the gauge-matter Hamiltonian one obtains a quadratic operator that can be efficiently diagonalized. This allows to construct a gauge-invariant ansatz that can capture gauge-matter interactions. Crucially, the parametrization of these states is done in a way to guarantee that the number of parameters increases only at a polynomial rate as the size of the system grows.

Since the gauge-field dependent fermionic Gaussian states retain some of their fermionic Gaussian state properties, part of the variational ansatz can be evaluated analytically. In particular, since fermionic Gaussian states are normalized, the fermion-gauge part of the ansatz does not show up in the norm. This is advantageous as expectation values are evaluated with Monte Carlo techniques and since only the pure gauge part appears in the norm of the state and thus contributes to the probability distribution that needs to be sampled, updates in the resulting Monte Carlo algorithm are not demanding numerically. The exact diagonalization of the gauge-matter Hamiltonian is required at every measurement step in the Monte Carlo scheme and can be performed efficiently as it scales cubically with system size.

To verify the capabilities of the variational Monte Carlo method, several benchmarks are conducted. First, it is demonstrated also numerically that gauge invariance is indeed preserved. Secondly, the ansatz is tested in limiting cases, such as the weak-coupling ($g^2 \to 0$) and strong-coupling ($g^2 \to \infty$) limits, where it is shown to be exact.

The performance of the ansatz is also compared to other methods. For example, the ground state energy for the pure gauge theory is compared to the variational method presented in chapter 4 and a recent neural-network based study [100], demonstrating agreement over the entire coupling region. Additionally, for compact QED with dynamical fermions, the flux energy per plaquette is computed and compared to a Euclidean Monte Carlo study at zero chemical potential [111], which also agrees over the whole coupling region. The degree of antiferromagnetic order in the ground state is also examined, with the extrapolated value for a confinement-deconfinement transition found to be in qualitative agreement with the Monte Carlo study, although slightly lower. To demonstrate the method's effectiveness in sign-problem affected regimes, a density-induced phase transition for two fermion flavors at non-zero chemical potential is studied, with qualitatively similar phenomena observed as in a previous tensor network study in one dimension [75].

The following sections are structured as follows. Section 5.3 briefly reviews the compact QED model with dynamical fermions. Then the variational Monte Carlo method is presented, including the gauge-invariant construction of the variational state, the numerical evaluation with Monte Carlo techniques, and the adaptation of variational parameters. In section 5.4, we evaluate the performance of our ansatz by benchmarking against limiting cases of the model with known ground states and other numerical methods. Section 5.5 investigates a sign-problem affected regime by studying the density-induced phase transition for two fermion flavors at non-zero chemical potential.

5.3 The variational Monte Carlo method

5.3.1 Short review of $(2+1)$-dimensional compact QED with dynamical fermions

We study $(2+1)$-dimensional compact quantum electrodynamics (cQED_3) coupled to dynamical fermions. The model is defined on an $L \times L$ square lattice with periodic boundary conditions. We work with staggered fermions [8] which are suitable for studying chiral symmetry breaking. The fermions can appear in several species α which can be subject to different chemical potentials μ_α (in some scenarios they are also given a mass m). The Hamiltonian reads

$$\begin{aligned} H =& \frac{g^2}{2} \sum_{\mathbf{x},i} \hat{E}^2_{\mathbf{x},i} + g_{\text{mag}} \sum_{\mathbf{p}} \left(1 - \cos\left(\hat{\theta}_{\mathbf{p}}\right)\right) \\ & - t \sum_{\mathbf{x},i,\alpha} \psi^\dagger_{\mathbf{x},\alpha} e^{i\hat{\theta}_{\mathbf{x},i}} \psi_{\mathbf{x}+\mathbf{e}_i,\alpha} + h.c. \\ & + \sum_{\mathbf{x},\alpha} \left(m(-1)^{\mathbf{x}} + \mu_\alpha\right) \psi^\dagger_{\mathbf{x},\alpha} \psi_{\mathbf{x},\alpha} \\ \equiv & H_E + H_B + H_{GM} + H_M \end{aligned} \tag{5.1}$$

where $\psi_{\mathbf{x},\alpha}$ denotes the fermionic annihilation operator for site $\mathbf{x}$ and species α. The gauge field operator $\hat{\theta}_{\mathbf{x},i}$ and the electric field operator $\hat{E}_{\mathbf{x},i}$ fulfill the canonical commutation relations, $[\hat{\theta}_{\mathbf{x},i}, \hat{E}_{\mathbf{y},j}] = i\delta_{ij}\delta_{\mathbf{x},\mathbf{y}}$. Accordingly, the gauge field on a link can be represented either by an integer-valued electric field variable, $\hat{E}_{\mathbf{x},i} \left|E_{\mathbf{x},i}\right\rangle = E_{\mathbf{x},i} \left|E_{\mathbf{x},i}\right\rangle$ ($E_{\mathbf{x},i} \in \mathbb{Z}$), or by an element of the $U(1)$ gauge group, $\hat{\theta}_{\mathbf{x},i} \left|\theta_{\mathbf{x},i}\right\rangle = \theta_{\mathbf{x},i} \left|\theta_{\mathbf{x},i}\right\rangle$ ($\theta_{\mathbf{x},i} \in [0, 2\pi)$). We will mostly use the group element representation throughout the manuscript. In this representation, the electric field operator has the form $\hat{E}_{\mathbf{x},i} = -i\partial/\partial\theta_{\mathbf{x},i}$. The plaquette operator $\hat{\theta}_{\mathbf{p}} = \hat{\theta}_{\mathbf{x},1} + \hat{\theta}_{\mathbf{x}+\mathbf{e}_1,2} - \hat{\theta}_{\mathbf{x}+\mathbf{e}_2,1} - \hat{\theta}_{\mathbf{x},2}$ is the clockwise summation of link operators around plaquette $\mathbf{p}$ where $\mathbf{x}$ is the site at the bottom left corner. The labelling conventions are illustrated in Fig. 5.3.1. The magnetic coupling g_{mag} is usually chosen to be $\frac{1}{g^2}$ but we keep it general for the moment.

The local symmetry of the model is generated by the Gauss law operators

$$\hat{G}_{\mathbf{x}} = \sum_{i=1}^{2} \left(\hat{E}_{\mathbf{x},i} - \hat{E}_{\mathbf{x}-\mathbf{e}_i,i}\right) - \hat{Q}_{\text{stag}} \tag{5.2}$$

where the staggered charge operator $\hat{Q}_{\text{stag},\mathbf{x}}$ is defined as

$$\hat{Q}_{\text{stag},\mathbf{x}} = \sum_{\alpha=1}^{N_f} \left(\psi^\dagger_{\mathbf{x},\alpha}\psi_{\mathbf{x},\alpha} - \frac{1}{2}(1 + (-1)^{\mathbf{x}})\right). \tag{5.3}$$

Physical states $|\text{phys}\rangle$ must be eigenstates of all Gauss law operators

$$\hat{G}_{\mathbf{x}} |\text{phys}\rangle = q_{\mathbf{x}} |\text{phys}\rangle \quad \forall \mathbf{x} \tag{5.4}$$

where eigenvalues $q_{\mathbf{x}}$ correspond to different static charge configurations.

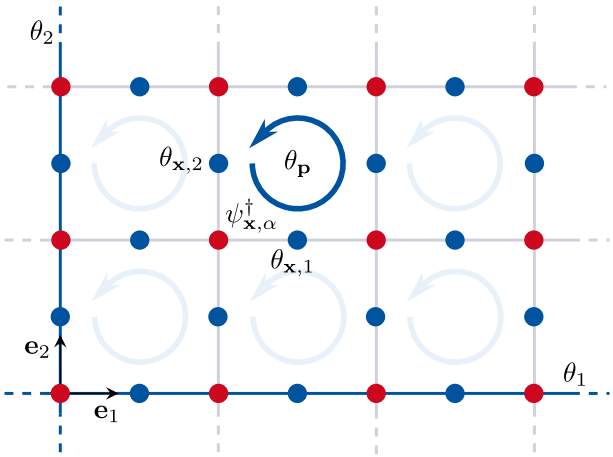

Figure 5.3.1: Naming conventions on the periodic lattice: the gauge field degrees of freedom $\theta_{\mathbf{x},i}, E_{\mathbf{x},i}$ (blue) reside on the links $\mathbf{x}, i$ while the fermionic degrees of freedom $\psi^\dagger_{\mathbf{x},\alpha}$ (red), which can come in several species α, are located on the sites $\mathbf{x}$. The circular arrows on the plaquettes denote the plaquette variables $\theta_{\mathbf{p}}$. The global loops θ_i wind around the axis given by $\mathbf{e}_i$ and are illustrated by blue lines.

5.3.2 State construction

Since our method is based on variational Monte Carlo, we will explain it in several steps (sketched in Fig. 5.3.2): we first discuss the state construction and motivate the choice of our ansatz. In the second step, we explain the evaluation procedure of our ansatz based on Monte Carlo sampling. In the third and final step, we discuss the adaptation of variational parameters based on stochastic reconfiguration. We construct our ansatz state in the gauge field basis where states are characterized by all $U(1)$ gauge link variables $\theta_{\mathbf{x},i}$, $\left|\{\theta_{\mathbf{x},i}\}\right\rangle \equiv \otimes_{\mathbf{x},i} \left|\theta_{\mathbf{x},i}\right\rangle$. A general *gauge field* state can then be defined by

$$\left|\Psi_G\right\rangle = \prod_{\mathbf{x},i} \int_0^{2\pi} d\theta_{\mathbf{x},i}\, \Psi_G(\{\theta_{\mathbf{x},i}\}) \left|\{\theta_{\mathbf{x},i}\}\right\rangle \tag{5.5}$$

where $\Psi_G(\{\theta_{\mathbf{x},i}\})$ is a function over all gauge link variables $\theta_{\mathbf{x},i}$.

To extend the above to an arbitrary state $\left|\Psi\right\rangle$ of the cQED$_3$ model introduced in section 5.3.1 (i.e. including fermions) we need to specify a fermionic Fock state $\left|\Psi_F(\{\theta_{\mathbf{x},i}\})\right\rangle$ for every gauge field configuration $\{\theta_{\mathbf{x},i}\}$:

$$\begin{aligned} \left|\Psi\right\rangle &= \prod_{\mathbf{x},i} \int_0^{2\pi} d\theta_{\mathbf{x},i}\, \Psi_G(\{\theta_{\mathbf{x},i}\}) \left|\Psi_F(\{\theta_{\mathbf{x},i}\})\right\rangle \left|\{\theta_{\mathbf{x},i}\}\right\rangle \\ &\equiv \int D\theta\, \Psi_G(\theta) \left|\Psi_F(\theta)\right\rangle \left|\theta\right\rangle \end{aligned} \tag{5.6}$$

where we abbreviated for ease of notation the gauge field configurations $\{\theta_{\mathbf{x},i}\}$ as θ and the measure as $\int D\theta = \prod_{\mathbf{x},i} \int_0^{2\pi} d\theta_{\mathbf{x},i}$. This notation will be used throughout the chapter.

One should note that an arbitrary state $\left|\Psi\right\rangle$ as given above is a priori not gauge-invariant. Thus, the gauge invariance condition for physical states in eq. (5.4) severely restricts the possible choices for $\Psi_G(\theta)$ and $\left|\Psi_F(\theta)\right\rangle$.

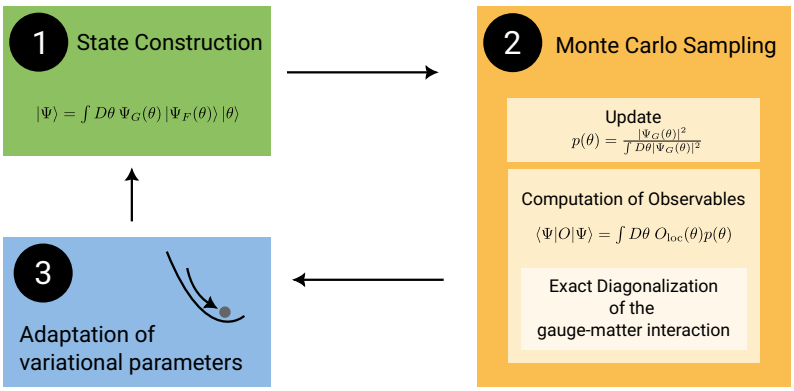

Figure 5.3.2: Scheme of variational Monte Carlo procedure: the ansatz is formulated in the full gauge field basis denoted by $|\theta\rangle$, in our case the $U(1)$ gauge group, consisting of a pure gauge part $\Psi_G(\theta)$ and gauge-field dependent fermionic Gaussian states $|\Psi_F(\theta)\rangle$. Expectation values of observables O can be carried out analytically w.r.t. the fermionic part (which involves the eigendecomposition of the gauge-matter interactions for fixed θ). The resulting expressions $O_{\rm loc}(\theta)$ are diagonal in θ and sampled with Monte Carlo techniques according to a probability distribution $p(\theta)$ in which only $\Psi_G(\theta)$ appears since the gauge-field dependent fermionic Gaussian states are normalized. The variational parameters are adapted according to stochastic reconfiguration.

The state $|\Psi\rangle$ defined above is completely general. From now on we will use the form of $|\Psi\rangle$ as the basis to construct our variational ansatz state which will be defined by specifying the pure gauge part $\Psi_G(\theta)$ and the fermionic ansatz $|\Psi_F(\theta)\rangle$.

Intuitively, the role of $\Psi_G(\theta)$ and $|\Psi_F(\theta)\rangle$ in our construction can be motivated as follows: $\Psi_G(\theta)$ is designed to approximate the ground state of the pure gauge model $H_{\rm KS} \equiv H_B + H_E$ (the Kogut-Susskind Hamiltonian [8]) whereas $|\Psi_F(\theta)\rangle$ is designed to approximate the low-energy physics of the fermionic Hamiltonian $H_{\rm fer} \equiv H_E + H_{GM} + H_M$ which neglects the self-interactions of the gauge field.

The pure gauge part of the ansatz

In this section we motivate and describe the pure gauge part $\Psi_G(\theta)$ of our variational state. In chapter 4, based on ref. [2], it was shown that

$$\phi_G(\theta) = \sum_{N_{\mathbf{p}}=-\infty}^{+\infty} e^{-\frac{1}{2}(\theta_{\mathbf{p}}-2\pi N_{\mathbf{p}})\alpha_{\mathbf{p}\mathbf{p}'}(\theta_{\mathbf{p}'}-2\pi N_{\mathbf{p}'})} \tag{5.7}$$

is a good ansatz for the ground state of compact QED with static charges. It is a Gaussian in the plaquette variables $\theta_{\mathbf{p}}$ that is made periodic by an infinite sum over the integer-valued variables $N_{\mathbf{p}}$ ($\alpha_{\mathbf{p}\mathbf{p}'}$ are variational parameters). The periodicity is important to account for the compactness of the $U(1)$ gauge field.

Here, we would like to find an ansatz which has a similar expressive power as the states above but at the same time is suitable for a variational Monte Carlo simulation directly in θ (without resorting to the sums above). A useful hint is given by the Villain approximation [99] which states

$$e^{\gamma(1-\cos(\theta))} \to \sum_N e^{-\frac{1}{2}\gamma(\theta-2\pi N)^2} \tag{5.8}$$

for $\gamma \to \infty$. Therefore, a suitable ansatz state could be

$$e^{-\sum_{\mathbf{p}\mathbf{p}'} \cos(\theta_{\mathbf{p}})\alpha_{\mathbf{p},\mathbf{p}'} \cos(\theta_{\mathbf{p}'})+\sum_{\mathbf{p}} \beta_{\mathbf{p}} \cos(\theta_{\mathbf{p}})} \tag{5.9}$$

with the matrix α and the vector β being variational parameters. We will choose α and β to be real since we are interested here in low-energy properties. For the study of real-time dynamics (which will be investigated in a future work) we would choose the variational parameters to be complex. Apart from the cosine terms we can add sine terms, combine them in a vector $b(\theta) = (\cos(\theta_{\mathbf{p}_1}), .., \cos(\theta_{\mathbf{p}_N}), \sin(\theta_{\mathbf{p}_1}), .., \sin(\theta_{\mathbf{p}_N}))$ and generalize the above state to

$$\Psi_G(\theta) = e^{-\frac{1}{2} b(\theta)^T \alpha b(\theta) - \beta^T b(\theta)} \tag{5.10}$$

which will be the variational ansatz for the pure gauge field dynamics entering the full ansatz as in eq. (5.6).

In the case of periodic boundary conditions there are two inequivalent global non-contractible loops (inequivalent in the sense that they can not be transformed into each other by plaquette operations). We choose them to be θ_1 (winding around the lattice along the x_1-axis), and θ_2 (along the x_2-axis), respectively (see Fig. 5.3.1). We incorporate them in our ansatz by expanding the vector $b(\theta)$ by the entries $\cos(\theta_1), \cos(\theta_2), \sin(\theta_1)$ and $\sin(\theta_2)$. This is necessary because upon the coupling of compact QED to *dynamical* fermions, θ_1 and θ_2 become dynamical variables due to the appearance of gauge-matter interactions where the phase $e^{i\theta_{\mathbf{x},i}}$ appears. If expressed in terms of gauge-invariant variables, it contains contributions from both plaquette variables $\theta_{\mathbf{p}}$ and the global loops θ_1 and θ_2, as described in chapter 3. For static charges, the magnetic Hamiltonian is the only term depending on the gauge field variables $\theta_{\mathbf{x},i}$ which can be expressed entirely in terms of plaquette variables $\theta_{\mathbf{p}}$ such that the global loop variables only set different topological sectors (similar to the toric code).

For all our purposes it turned out that all variational parameters in α corresponding to the global loop variables were not relevant and that it was sufficient to only keep the global loop parameters in β variational. After imposing translational invariance we thus remained with $2N + 4$ variational parameters for α and 6 variational parameters for β (with $N = L^2$ the number of lattice sites).

Since $b(\theta)$ contains only closed loops the gauge field part $\Psi_G(\theta)$ as a function of $b(\theta)$ automatically preserves gauge invariance.

The fermionic part of the ansatz: gauge-invariant fermionic Gaussian states

The fermionic part of our variational ansatz $|\Psi_F(\theta)\rangle$ is a generalization of fermionic Gaussian states that can incorporate interactions between fermions and gauge fields while preserving gauge invariance. The overall state $\int D\theta\, |\Psi_F(\theta)\rangle\, |\theta\rangle$ is an integral over all gauge field configurations where for every gauge field configuration θ we define a fermionic Gaussian state $|\Psi_F(\theta)\rangle$. The motivation for this construction is that the resulting state, an infinite superposition of Gaussian states, is a powerful ansatz state as it is clearly not Gaussian anymore and can capture correlations beyond the Gaussian realm. At the same time, we retain for every $|\Psi_F(\theta)\rangle$ the properties of fermionic Gaussian states which allows us to compute part of the expectation values analytically. The number of variational parameters is shown to scale only polynomially in the system size and not exponentially as the number of gauge field configurations.

Recalling that every pure fermionic Gaussian state can be represented by a unitary operator U_{GS} acting on some reference state $|\Psi_0\rangle$ [114], we carry out an analogous procedure for every gauge field configuration θ to construct gauge-field dependent fermionic Gaussian states as

$$|\Psi_F(\theta)\rangle = U_{GS}(\theta)\,|\Psi_0\rangle \tag{5.11}$$

In our method, the reference state $|\Psi_0\rangle$ will be chosen as the ground state of $H_{\text{fer}} = H_E + H_{GM} + H_M$ in the strong-coupling limit ($g^2 \to \infty$), i.e. the regime where the electric term dominates so that electric field excitations are strongly suppressed. In the following we will refer to strong- and weak-coupling always w.r.t. the relative strength of the electric Hamiltonian H_E (quantified by its coupling constant g^2). If we only consider H_E in the strong-coupling limit, $|\Psi_0\rangle$ will be a Fock state where all fermions are fixed to certain sites (the exact form of the state will depend on the number of fermion flavors and the configuration of background charges). However, $|\Psi_0\rangle$ does not need to be Gaussian but one can also include perturbations induced by gauge-matter interactions H_{GM}, e.g. it is known that for two fermion flavors at half-filling the strong-coupling ground state in second-order perturbation theory is the ground state of the Heisenberg model. It can be shown that its properties can be incorporated in the reference state $|\Psi_0\rangle$ which can even be kept variational (for details see Appendix 5.C).

For simplicity of the discussion, we will assume in the following a Gaussian reference state and only one flavor of staggered fermions (how the ansatz can be readily extended to multiple flavors is described in Appendix 5.B). In the sector without background charges the reference state is chosen to be the Dirac state $|D\rangle$

$$|\Psi_0\rangle = \prod_{\mathbf{x}\in\mathcal{O}} \psi^\dagger_{\mathbf{x}}\,|0\rangle \equiv |D\rangle \tag{5.12}$$

i.e. with all odd sites $\mathcal{O}$ occupied. This corresponds to the zero charge sector with no electric field present.

The Gaussian operator $U_{GS}(\theta)$ acting on $|\Psi_0\rangle$ is defined as

$$U_{GS}(\theta) = \exp\left(\frac{i}{2}\sum_{\mathbf{x},\mathbf{y}} \psi^\dagger_{\mathbf{x}}\xi(\theta)_{\mathbf{xy}}\psi_{\mathbf{y}}\right) \tag{5.13}$$

where $\xi(\theta)$ is dependent on the gauge field and on the variational parameters. The gauge-field dependence has to be chosen in a way that respects gauge invariance. This can be achieved by defining $\xi(\theta)$ via the eigendecomposition of the gauge-matter Hamiltonian which can be written as

$$H_{GM} = \int D\theta\; |\theta\rangle\langle\theta|\,\vec{\psi}^\dagger_{\mathbf{x}} h_{GM}(\theta)_{\mathbf{xy}}\vec{\psi}_{\mathbf{y}} \tag{5.14}$$

with $\vec{\psi}_{\mathbf{x}} \equiv (\psi_{\mathbf{x}_1}, ..., \psi_{\mathbf{x}_N})^T$ a vector of all fermionic annihilation operators. The matrix $h_{GM}(\theta)$ is hermitian and can be diagonalized for a specific gauge field configuration θ as $h_{GM}(\theta) = V(\theta)\Lambda(\theta)V(\theta)^\dagger$. We use $V(\theta)$ to rewrite $\xi(\theta)$ as

$$\xi(\theta)_{\mathbf{xy}} = V(\theta)_{\mathbf{x}i}\tilde{\xi}_{ij}V(\theta)^\dagger_{j\mathbf{y}} \tag{5.15}$$

with $\tilde{\xi}$ containing the variational parameters. Note that $\tilde{\xi}$ does not depend on the gauge field configuration and thus the number variational parameters scales quadratically

with the system size (linearly for our choice of parametrization, see Appendix 5.B). Putting everything together, the fermionic part of the ansatz for one fermion flavor takes the form

$$|\Psi_F(\theta)\rangle = \exp\left(\frac{i}{2}\sum_{\mathbf{x},\mathbf{y}} \psi^\dagger_{\mathbf{x}} V(\theta)_{\mathbf{x}i} \tilde{\xi}_{ij} V(\theta)^\dagger_{j\mathbf{y}} \psi_{\mathbf{y}}\right)|D\rangle \tag{5.16}$$

and the whole variational ansatz state $|\Psi\rangle$ is thus fully defined according to eq. (5.6).

Gauge invariance of $|\Psi\rangle$ follows from the fact that H_{GM} and its eigenstates are gauge-invariant since the construction of $|\Psi_F(\theta)\rangle$ given in eq. (5.16) is formulated in terms of these eigenstates.

Since the gauge invariance condition in eq. (5.4) is local in θ, every realization of the state in a Monte Carlo simulation will be gauge-invariant, i.e. even with an imperfect sampling algorithm the unphysical part of the Hilbert space is never accessed.

The motivation for the choice of ansatz above is on the one hand that it ensures gauge invariance but more importantly, by choosing the matrix $\tilde{\xi}$ appropriately, the occupation of the eigenstates of H_{GM} can be tuned which allows to obtain good ground state approximations even in regimes where strong gauge field fluctuations are present. This has to be seen in contrast to mean-field descriptions where a certain gauge field pattern is fixed and the resulting fermionic theory is studied. The latter has the problem, which is particularly relevant in the study of quantum spin liquid states (where the lattice gauge theory emerges as an effective low-energy description), that it often remains unclear whether the spin liquid state is stable against gauge field fluctuations [9].

The cost of working with the ansatz is that the eigendecomposition of $h_{GM}(\theta)$ needs to be carried out at every measurement step of the Monte Carlo algorithm. However, $h_{GM}(\theta)$ is a hermitian $N \times N$ matrix where N is the number of lattice sites such that the cost is $\mathcal{O}(N^3)$ which can be done efficiently. Note that the number of fermion flavors does not enter as the gauge-matter interaction is the same for all flavors.

The fermionic ansatz state in eq. (5.16) is normalized since the Gaussian operator acting on the Dirac vacuum is unitary. This is beneficial for the variational Monte Carlo simulation since it will not contribute to the probability distribution that needs to be sampled. Thus, no sampling problems related to fermion determinants can occur in this method as opposed to action-based Monte Carlo algorithms.

So far we have not specified the matrix $\tilde{\xi}$ in eq. (5.16) containing the fermionic variational parameters. For that we consider the eigendecomposition of $h_{GM}(\theta)$, denoted as $h_{GM}(\theta)\,|w_i(\theta)\rangle = \lambda_i(\theta)\,|w_i(\theta)\rangle$, $i \in \{1,..,N\}$. Assuming an $L \times L$ lattice with L even, the spectrum of $h_{GM}(\theta)$ is symmetric around zero, i.e. we have $N/2$ pairs of eigenvectors $|w_{k+}(\theta)\rangle$ and $|w_{k-}(\theta)\rangle$ ($k \in \{1,..,N/2\}$) such that $|w_{k+}(\theta)\rangle$ corresponds to the eigenvalue $+\lambda_k(\theta)$ and $|w_{k-}(\theta)\rangle$ to the eigenvalue $-\lambda_k(\theta)$. A useful feature of these pairs is their structure in the position basis as they can be written as two vectors $|w_{ke}(\theta)\rangle$, $|w_{ko}(\theta)\rangle$ which are residing exclusively on even (respectively odd) lattice sites:

$$|w_{k+}(\theta)\rangle = \frac{1}{\sqrt{2}}\left(|w_{ke}(\theta)\rangle + |w_{ko}(\theta)\rangle\right) \tag{5.17}$$

$$|w_{k-}(\theta)\rangle = \frac{1}{\sqrt{2}}\left(|w_{ke}(\theta)\rangle - |w_{ko}(\theta)\rangle\right) \tag{5.18}$$

This allows us to write the strong-coupling state in eq. (5.12), where the fermions occupy all odd sites, as a product over all pairs k where in each pair the odd superpositon

is occupied, $|w_{k-}(\theta)\rangle = \frac{1}{\sqrt{2}}\left(|w_{ke}(\theta)\rangle - |w_{ko}(\theta)\rangle\right)$. The purpose of $\tilde{\xi}$ in eq. (5.16) is then to smoothly transform this equal superposition of $|w_{k+}(\theta)\rangle$ and $|w_{k-}(\theta)\rangle$ into a state where all $|w_{k-}(\theta)\rangle$ are occupied, corresponding to the ground state of H_{GM}. Thus, $\tilde{\xi}$ allows us to transform smoothly from the strong-coupling ground state to the weak-coupling ground state. For more details on $\tilde{\xi}$ and the specific choice of parametrization see Appendix 5.B.

5.3.3 Evaluating expectation values

In this section we describe how Monte Carlo techniques can be used to compute various expectation values for the variational ansatz presented in the previous section. Throughout the following discussion the variational parameters are kept fixed, their adaptation will be discussed in the next section.

For the computation of an observable O with the full ansatz $|\Psi\rangle$ from eq. (5.6) we obtain

$$\begin{aligned}\frac{\langle\Psi|O|\Psi\rangle}{\langle\Psi|\Psi\rangle} &= \frac{\int D\theta\, \langle\Psi_F(\theta)|\,\overline{\Psi_G}(\theta)\, O\,\Psi_G(\theta)\,|\Psi_F(\theta)\rangle}{\int D\theta\,|\Psi_G(\theta)|^2\,\underbrace{\langle\Psi_F(\theta)|\Psi_F(\theta)\rangle}_{=1}} \\ &= \frac{\int D\theta\, O_{\text{loc}}(\theta)|\Psi_G(\theta)|^2}{\int D\theta\,|\Psi_G(\theta)|^2} = \int D\theta\, O_{\text{loc}}(\theta) p(\theta)\end{aligned} \tag{5.19}$$

where $|\Psi_F(\theta)\rangle$ is absent in the norm since it is already normalized by construction (see eq. (5.16)) so that the probability distribution $p(\theta)$ depends only on $\Psi_G(\theta)$. The fermionic part of the ansatz thus only appears in the numerator for the evaluation of O which is carried out analytically and only the remaining expression $O_{\text{loc}}(\theta)$ is sampled in a Monte Carlo simulation.

We split the calculation of $O_{\text{loc}}(\theta)$ in two parts: since O is a priori not diagonal in θ (e.g. all electric observables involve derivatives w.r.t. θ) we first compute the action of O on our ansatz $|\Psi\rangle$ which gives rise to an expression $O_{\text{fer}}(\theta)$ that is diagonal in θ but might still contain fermionic operators (e.g. due to derivatives of the fermionic ansatz $|\Psi_F(\theta)\rangle$):

$$O\int D\theta\,\Psi_G(\theta)\,|\Psi_F(\theta)\rangle\,|\theta\rangle = \int D\theta\, O_{\text{fer}}(\theta)\Psi_G(\theta)\,|\Psi_F(\theta)\rangle\,|\theta\rangle \tag{5.20}$$

$O_{\text{loc}}(\theta)$ is then derived by evaluating $O_{\text{fer}}(\theta)$ w.r.t. the fermionic ansatz

$$O_{\text{loc}}(\theta) = \langle\Psi_F(\theta)|\,O_{\text{fer}}(\theta)\,|\Psi_F(\theta)\rangle = \frac{\langle\Psi_F(\theta)|\,O\Psi_G(\theta)\,|\Psi_F(\theta)\rangle}{\Psi_G(\theta)} \tag{5.21}$$

which is now a real-valued function that can be readily sampled in a Monte Carlo simulation.

The probability distribution $p(\theta)$ according to which we need to sample is only dependent on the gauge part $\Psi_G(\theta)$ defined in eq. (5.10):

$$p(\theta) = \frac{|\Psi_G(\theta)|^2}{\int D\theta\,|\Psi_G(\theta)|^2} = \frac{e^{-b^T(\theta)\alpha b(\theta) - 2\beta^T b(\theta)}}{\int D\theta\, e^{-b^T(\theta)\alpha b - 2\beta^T b(\theta)}} \equiv \frac{e^{-S(\theta)}}{\int D\theta\, e^{-S(\theta)}} \tag{5.22}$$

The method described above has to be contrasted with usual variational Monte Carlo methods [115] where the whole trial wavefunction contributes to the probability distribution and the local quantities $O_{\text{loc}}(\theta)$ do not involve taking expectation values w.r.t. some part of the ansatz.

Having discussed the general procedure, the computation of observables can be divided into three groups by level of difficulty: the first group consists of observables that are not diagonal in θ (all electric quantities such as H_E) and thus first need to be brought into a diagonal form $O_{\text{fer}}(\theta)$. These observables are the most involved. The second group of observables are already of that form but since $O_{\text{fer}}(\theta)$ is still a fermionic operator it needs to be evaluated w.r.t. $|\Psi_F(\theta)\rangle$ to obtain $O_{\text{loc}}(\theta)$ (e.g. H_{GM} or H_M). The third group of observables is already of the form $O_{\text{loc}}(\theta)$ and can be readily sampled in a Monte Carlo simulation (e.g. H_B).

Two things need to be shown to demonstrate that our variational ansatz can be used efficiently: first, the efficient computation of $O_{\text{loc}}(\theta)$ and secondly, efficient sampling of the probability distribution $p(\theta)$. Thus, in the following, we first show exemplary for the Hamiltonian how $O_{\text{loc}}(\theta)$ is derived, i.e. we compute the local energy $H_{\text{loc}}(\theta)$. In a second step, we explain the Monte Carlo simulation, in particular how samples from $p(\theta)$ are generated using Metropolis algorithm.

Computation of the local energy $H_{\text{loc}}(\theta)$

The electric Hamiltonian H_E is the only term of the Hamiltonian defined in eq. (5.1) that is not diagonal in θ (the most difficult type of observable to compute, as discussed above). We thus focus on H_E and discuss other terms briefly at the end of this section.

The electric Hamiltonian corresponds to second order derivatives in the gauge field variables $\theta_{\mathbf{x},i}$. Since our ansatz consists of a fermionic part $|\Psi_F(\theta)\rangle$ and a pure gauge part $\Psi_G(\theta)$, the electric energy has a solely fermionic contribution, a pure gauge contribution and a crossterm between the two, denoted as:

$$\langle H_E\rangle = \langle H_E\rangle_{ff} + \langle H_E\rangle_{gg} + \langle H_E\rangle_{fg} \tag{5.23}$$

We start by considering $\langle H_E\rangle_{gg}$, the part originating from taking twice the derivative of $\Psi_G(\theta)$ whose construction is based on the vector $b(\theta)$ (see eq. (5.10)). Hence, we need to compute the derivative of $b(\theta)$ with respect to $\theta_{\mathbf{x},i}$ which gives rise to the vector

$$\begin{aligned} b_{\mathbf{x},i}(\theta) = \delta_{\mathbf{p},(\mathbf{x},i)}(&-\sin\left(\theta_{\mathbf{p}_1}\right), .., -\sin\left(\theta_{\mathbf{p}_N}\right), \\ &\cos\left(\theta_{\mathbf{p}_1}\right), .., \cos\left(\theta_{\mathbf{p}_N}\right)) \end{aligned} \tag{5.24}$$

with

$$\delta_{\mathbf{p},(\mathbf{x},i)} = \begin{cases} 1 & \text{if} \quad (\mathbf{x},i) \in \mathbf{p} \quad \text{clockwise} \\ -1 & \text{if} \quad (\mathbf{x},i) \in \mathbf{p} \quad \text{anti-clockwise} \\ 0 & \text{else} \end{cases} \tag{5.25}$$

where $(\mathbf{x},i) \in \mathbf{p}$ clockwise (anti-clockwise) means that the link $(\mathbf{x},i)$ is contained in the plaquette $\mathbf{p}$ and the orientation of the link is parallel (anti-parallel) to the orientation of the plaquette. For periodic boundary conditions we have the additional entries $\cos(\theta_j)$ and $\sin(\theta_j)$ in $b(\theta)$ corresponding to the global loops θ_1 and θ_2. They give rise to the derivatives $-\sin(\theta_j)$ and $\cos(\theta_j)$ if $(\mathbf{x},i)$ lies on the x_j-axis and otherwise zero.

The electric energy of the pure gauge part and the corresponding local quantity

$H_{E,gg,\text{loc}}(\theta)$ is then derived as

$$\langle H_E \rangle_{gg} = \frac{\int D\theta \frac{g^2}{2} \sum_{\mathbf{x},i} \left(b^T(\theta)\alpha b_{\mathbf{x},i}(\theta) + \beta^T b_{\mathbf{x},i}(\theta) \right)^2 e^{-S(\theta)}}{\int D\theta\, e^{-S(\theta)}} \equiv \int D\theta H_{E,gg,\text{loc}}(\theta) p(\theta) \tag{5.26}$$

with the probability distribution $p(\theta)$ and $S(\theta) = b^T(\theta)\alpha b(\theta) + 2\beta^T b(\theta)$, both defined in eq. (5.22). The part of the electric Hamiltonian acting only on $\Psi_G(\theta)$ can therefore be written in a simple diagonal form in the gauge field basis.

It is more difficult to compute $H_{E,ff,\text{loc}}(\theta)$, i.e. the local quantity corresponding to derivatives of the fermionic ansatz $|\Psi_F(\theta)\rangle$. As discussed earlier, we first derive an expression $H_{E,ff,\text{fer}}(\theta)$ that will be diagonal in θ but still contains fermionic operators (see Appendix 5.A for details):

$$\begin{aligned} \langle H_E \rangle_{ff} =& \frac{g^2}{2} \int D\theta\, p(\theta) \langle \Psi_F(\theta) | \sum_{\mathbf{x},i} -\frac{\partial^2}{\partial \theta_{\mathbf{x},i}^2} | \Psi_F(\theta) \rangle \\ =& \frac{g^2}{2} \int D\theta\, p(\theta) \sum_{\mathbf{x},i} \langle \Psi_F(\theta) | \vec{\psi}^\dagger f_{\mathbf{x},i}(\theta) \vec{\psi} \vec{\psi}^\dagger f_{\mathbf{x},i}(\theta) \vec{\psi} | \Psi_F(\theta) \rangle \\ \equiv& \int D\theta\, p(\theta) \langle \Psi_F(\theta) | H_{E,ff,\text{fer}}(\theta) | \Psi_F(\theta) \rangle \end{aligned} \tag{5.27}$$

with

$$f_{\mathbf{x},i}(\theta) = \frac{1}{i} \left(\partial_{\theta_{\mathbf{x},i}} e^{i\xi(\theta)} \right) e^{-i\xi(\theta)}. \tag{5.28}$$

The form of $f_{\mathbf{x},i}(\theta)$ above is for a general gauge-field dependent fermionic Gaussian state characterized by some $\xi(\theta)$. To get an expression explicitly diagonal in θ we insert our ansatz $\xi(\theta) = V(\theta)\tilde{\xi}V^\dagger(\theta)$ defined in eq. (5.15) which is based on the eigendecomposition of the gauge-matter Hamiltonian, $h_{GM}(\theta) = V(\theta)\Lambda(\theta)V^\dagger(\theta)$. We obtain (see Appendix 5.A for the derivation):

$$f_{\mathbf{x},i}(\theta) = \vec{\psi}^\dagger V(\theta) \left(\alpha^{\mathbf{x},i}(\theta) - e^{i\tilde{\xi}} \alpha^{\mathbf{x},i}(\theta) e^{-i\tilde{\xi}} \right) V^\dagger(\theta) \vec{\psi} \tag{5.29}$$

with $\alpha^{\mathbf{x},i}(\theta) = -iV^\dagger(\theta)\partial_{\theta_{\mathbf{x},i}} V(\theta)$. We can find an explicit expression for $\alpha^{\mathbf{x},i}(\theta)$ which amounts to finding the derivatives of the eigenvectors of $h_{GM}(\theta)$:

$$\alpha_{kl}^{\mathbf{x},i}(\theta) = \frac{V_{k\mathbf{x}}^\dagger(\theta) e^{i\theta_{\mathbf{x},i}} V(\theta)_{\mathbf{x}+\mathbf{e}_i l} - h.c.}{\lambda_l(\theta) - \lambda_k(\theta)} \tag{5.30}$$

where $\lambda_i(\theta)$ are the eigenvalues of $h_{GM}(\theta)$. The final expression for $H_{E,ff,\text{fer}}(\theta)$ is thus diagonal in θ but still a quartic fermionic operator. This form of the electric Hamiltonian intuitively illustrates that the gauge field mediates interactions between the fermions.

In the following we want to evaluate these fermionic interactions w.r.t. the fermionic state $|\Psi_F(\theta)\rangle$ as shown in the last row in eq. (5.27) to compute the local electric energy $H_{E,ff,\text{loc}}(\theta)$ that can then be measured in our Monte Carlo simulation.

As a side note we want to mention that $|\Psi_F(\theta)\rangle$ in its general form defined in eq. (5.11) does not need to be Gaussian as one can also choose a Non-Guassian reference state $|\Psi_0\rangle$. This might be useful if one is particularly interested in the strong-coupling regime (from the high-energy physics perspective one is usually interested in

the weak-coupling region where the continuum limit is located). In the strong-coupling regime the electric field is strongly suppressed and the Hilbert space effectively reduces to a fermionic Fock space. Such models can be tackled by other many-body methods (e.g. tensor networks) which are not suitable for lattice gauge theories with infinte-dimensional local Hilbert spaces. One could combine our ansatz with such methods by carrying out the unitary transformation given by the fermionic Gaussian operator $U_{GS}(\theta)$ (acting on top of $|\Psi_0\rangle$) so that the remaining expression can be evaluated w.r.t. the reference state $|\Psi_0\rangle$ whose fermionic correlation functions could be computed with another method (in Appendix 5.C we demonstrate this for two fermion flavors at half-filling where the effective model is the Heisenberg model).

If we focus, however, on the case of one fermion flavor and the Gaussian reference state $|D\rangle$ as defined in eq. (5.16), we need to evaluate a fermionic Gaussian state for every gauge field configuration θ. The fermionic expectation values in eq. (5.27) can then be computed as

$$\begin{aligned}\langle\Psi_F(\theta)|\vec{\psi}^\dagger f_{\mathbf{x},i}(\theta)\vec{\psi}\vec{\psi}^\dagger f_{\mathbf{x},i}(\theta)\vec{\psi}|\Psi_F(\theta)\rangle = &\,\mathrm{Tr}\left(\left(\mathbb{1}-\Gamma_{\psi\psi^\dagger}(\theta)\right)f_{\mathbf{x},i}(\theta)\right)^2 \\ &+\mathrm{Tr}\left(\left(\mathbb{1}-\Gamma_{\psi\psi^\dagger}(\theta)\right)f_{\mathbf{x},i}(\theta)\Gamma_{\psi\psi^\dagger}(\theta)f_{\mathbf{x},i}(\theta)\right)\end{aligned} \tag{5.31}$$

where $\Gamma_{\psi\psi^\dagger}(\theta) = V(\theta)\tilde{\Gamma}V(\theta)^\dagger$ is the covariance matrix of the Gaussian state $|\Psi_F(\theta)\rangle$ and $\tilde{\Gamma} = e^{i\tilde{\xi}}V(\theta)^\dagger\Gamma_0 V(\theta)e^{-i\tilde{\xi}}$ with Γ_0 the covariance matrix of the reference state $|D\rangle$ and $\tilde{\xi}$ containing the variational parameters (see eq. (5.15)). Inserting the expectation values above in eq. (5.27) gives $H_{E,ff,\mathrm{loc}}(\theta)$.

The last remaining part of the electric Hamiltonian, the crossterm $\langle H_E\rangle_{fg}$, involves a quadratic expression in the fermions coming from $|\Psi_F(\theta)\rangle$ and a derivative in $b(\theta)$ coming from $\Psi_G(\theta)$ and is thus easier to compute than the quartic expressions in the pure fermionic contribution (for the explicit form see Appendix 5.A).

Other parts of the Hamiltonian are easier to evaluate since they are already diagonal in the gauge field basis. For the sake of completeness we will provide them here briefly. First, the magnetic part which is directly suitable for Monte Carlo sampling:

$$\langle H_B\rangle = g_{\mathrm{mag}}\int D\theta\sum_{\mathbf{p}}\left(1-\cos(\theta_{\mathbf{p}})\right)p(\theta) \equiv \int D\theta H_{B,\mathrm{loc}}(\theta)p(\theta) \tag{5.32}$$

The gauge-matter interactions are already diagonal and only quadratic in the fermions:

$$\begin{aligned}\langle H_{GM}\rangle &= -t\int D\theta\vec{\psi}^\dagger h_{GM}(\theta)\vec{\psi}p(\theta) \\ &= -t\int D\theta\,\mathrm{Tr}\left(\left(\mathbb{1}-\Gamma_{\psi\psi^\dagger}(\theta)\right)h_{GM}(\theta)\right)p(\theta) \\ &\equiv \int D\theta H_{GM,\mathrm{loc}}(\theta)p(\theta)\end{aligned} \tag{5.33}$$

where the quadratic expressions in the fermions are evaluated in analogy to the electric part of the Hamiltonian. In the same fashion are other purely fermionic parts evaluated such as the mass term H_M.

In terms of computational cost the local electric energy $H_{E,\mathrm{loc}}(\theta)$ is the most difficult part to evaluate. Naively, one expects the required number of operations for evaluating it to be $\mathcal{O}(N^4)$ (N the number of lattice sites) but with the chosen parametrization of $\tilde{\xi}$ it can be shown to be $\mathcal{O}(N^3)$ (see Appendix 5.B).

Monte Carlo algorithm

In the following we show how to efficiently evaluate an observable O with our ansatz $|\Psi\rangle$ in a Monte Carlo simulation given an expression for $O_{\text{loc}}(\theta)$. The expectation value of O is computed as an average over N samples θ_i drawn from the probability distribution $p(\theta)$:

$$\frac{\langle\Psi|O|\Psi\rangle}{\langle\Psi|\Psi\rangle} = \int D\theta\, O_{\text{loc}}(\theta)p(\theta) \approx \frac{1}{N}\sum_{i=1}^{N} O_{\text{loc}}(\theta_i) \tag{5.34}$$

The samples θ_i are generated by a Markov chain $\theta_1 \to \ldots \to \theta_i \to \ldots \to \theta_N$ using Metropolis algorithm [23].

One iteration in this procedure, i.e. $\theta_i \to \theta_{i+1}$, is described as follows: starting from θ_i a new configuration θ' is proposed according to some update scheme. In our case this involves sweeping through every link of the lattice and performing local updates on the gauge variables $\theta_{\mathbf{x},i}$. At the same time, we also perform global updates to switch between different monopole-like configurations which is hard to achieve with local updates (for details on the update scheme see Appendix 5.D). Recalling from eq. (5.22) the form $p(\theta) \sim e^{-S(\theta)}$ of our probability distribution, we compute the transition probability $p(\theta \to \theta') = e^{-S(\theta')}/e^{-S(\theta_i)} = e^{-\Delta S}$. In the acceptance step, a random number u between zero and one is generated and the new configuration is accepted if $e^{-\Delta S} \geq u$, i.e. $\theta_{i+1} = \theta'$. Otherwise, the configuration θ' is rejected and $\theta_{i+1} = \theta_i$. In the first phase of the Monte Carlo simulation (the warm-up phase) these iterations are performed to equilibrate the system (i.e. reach configurations with sufficiently low weight $S(\theta)$) and only after that the configurations θ_i are used to compute the expectation value in eq. (5.34).

The numerical cost of performing Metropolis algorithm depends on computing the transition probability between the old configuration θ and the proposed configuration θ'. For local updates they differ only in a single link variable $\theta_{\mathbf{x},i}$, respectively two plaquette variables $\theta_{\mathbf{p}}$. The vector $b(\theta)$, constructed out of $\sin(\theta_{\mathbf{p}})$ and $\cos(\theta_{\mathbf{p}})$, is thus changed in four places. Since $S(\theta)$ is bilinear in $b(\theta)$, the cost of computing ΔS is of order $\mathcal{O}(N)$ where N is the number of lattice sites. Sweeping through the lattice with this procedure is thus of order $\mathcal{O}(N^2)$. For the global updates the transition probability requires $\mathcal{O}(N^2)$ operations but is only performed $\mathcal{O}(1)$ times so that the cost of a full update is $\mathcal{O}(N^2)$.

Having such a low cost for updates has several advantages: we can perform multiple local and global updates to further decorrelate expensive measurements. The acceptance probability in our simulations stays on a high level throughout the whole coupling region (see Appendix 5.D). Moreover, if we parallelize the Monte Carlo simulation with multiple runners there is practically no overhead due to the warm-up phase.

5.3.4 Adaption of variational parameters

In the last section we described the evaluation with our Monte Carlo scheme for a fixed set of variational parameters. To study ground states and dynamical phenomena we need to adjust the variational parameters accordingly. Here, we focus on the study of ground state properties but the discussion can be readily extended to time-evolution phenomena as we use an imaginary time-evoultion procedure (called stochastic reconfiguration in the variational Monte Carlo language [113]) to find the optimal set of

parameters. We project the equations of motion onto the tangent plane of our variational manifold. For every variational parameter γ_i, either fermionic (in $\tilde{\xi}$) or pure gauge (in α and β) we define a corresponding tangent vector $|\Psi_i\rangle \equiv \mathbb{P}_\Psi \left(\partial_{\gamma_i} |\Psi\rangle\right)$ where $\mathbb{P}_\Psi$ ensures orthogonality to $|\Psi\rangle$:

$$\mathbb{P}_\Psi(|\psi\rangle) \equiv |\psi\rangle - \langle\Psi|\psi\rangle\,|\Psi\rangle \tag{5.35}$$

All tangent vectors in our ansatz are linearly independent which allows to invert the Gram matrix $G_{ij} \equiv \langle\Psi_i|\Psi_j\rangle$. This can be intuitively explained by considering the different types of tangent vectors: the ones corresponding to the fermionic parameters are related to the single-particle eigenstates of the gauge-matter Hamiltonian and are therefore orthogonal. The tangent vectors corresponding to the pure gauge part are quadratic (for α) or linear (for β) in the entries of the vector $b(\theta)$ which are related to the different plaquette variables $\theta_{\mathbf{p}}$, thus leading to linearly independent tangent vectors. The imaginary time evolution of the variational parameters can then be expressed in the following way:

$$-\dot{\gamma}_i = \frac{1}{2}\sum_j (G^{-1})_{ij}\frac{\partial E}{\partial \gamma_j} \tag{5.36}$$

with $E \equiv \frac{\langle\Psi|H|\Psi\rangle}{\langle\Psi|\Psi\rangle}$ the variational energy (whose evaluation was described in the previous section) and $\dot{\gamma} \equiv \frac{\partial\gamma}{\partial\tau}$.

The gradient of the variational energy and the Gram matrix need to be measured in a Monte Carlo simulation. The cost of both can be shown to scale in the same way as the cost of computing the variational energy (see Appendix 5.E). Summarizing, the computational complexity of our variational Monte Carlo algorithm is $\mathcal{O}(N^2)$ for the update procedure and $\mathcal{O}(N^3)$ for the measurement procedure, thus allowing for an efficient implementation.

5.4 Benchmarking of the variational method

Now, we have all the ingredients to apply our variational method: We constructed a gauge-invariant state and showed how it can be efficiently evaluated for a fixed set of parameters using Monte Carlo sampling. Additionally, we have a scheme to adapt the parameters using stochastic reconfiguration.

In the following section, we investigate the validity of the variational method. It will be threefold: first, to confirm the analytical arguments about gauge invariance of the ansatz given in the previous section we will show numerically that our state is gauge-invariant up to machine precision. Secondly, we investigate different limiting cases of cQED$_3$ where the ground states are known. In the last part, we benchmark our results for the $N_f = 2$ case at half-filling (in the sector of exactly one fermion per lattice site) with a recent Monte Carlo simulation [111].

5.4.1 Gauge invariance

To also show numerically that gauge invariance is manifest in our ansatz we compute the expectation value of the Gauss law operator $\langle G_{\mathbf{x}}\rangle$ (as defined in eq. (5.2)) for every site $\mathbf{x}$ and plot $\langle G_{\mathbf{x}}\rangle - q_{\mathbf{x}}$ for the whole lattice since this quantity needs to be zero

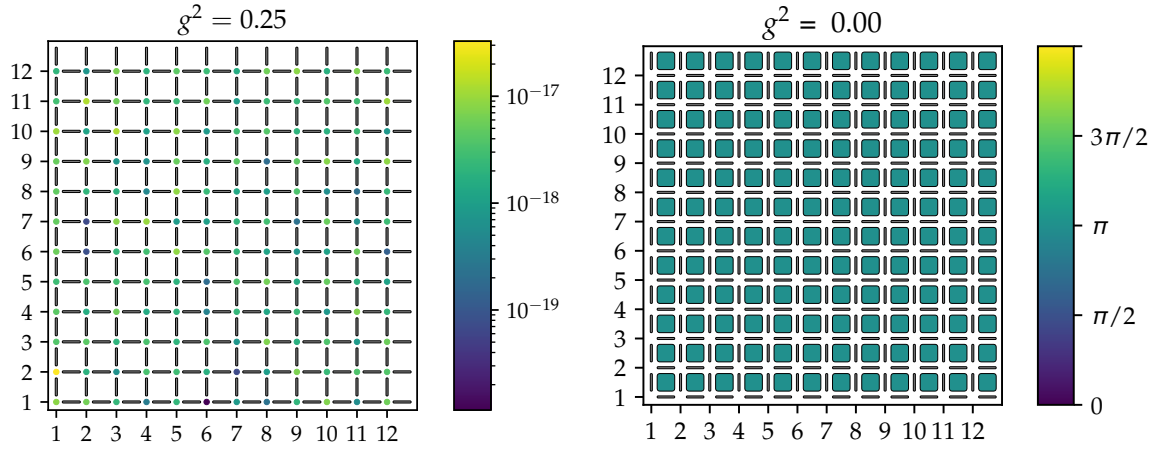

Figure 5.4.1: (Left): Gauss law violation $\langle G_{\mathbf{x}} \rangle - q_{\mathbf{x}}$ for a 12×12 lattice at $g^2 = 0.25$, $t = 1$ and $g_{\text{mag}} = -1$ with a random choice of variational parameters and a sampling size of $N = 10$. The Gauss law violation is of the order of machine precision even for a small sampling size, demonstrating that the ansatz is inherently gauge-invariant. (Right): the flux $\theta_{\mathbf{p}}$ per plaquette is shown for the variational ground state at $g^2 = 0.0$, $t = 1$ and $g_{\text{mag}} = -1$ for a 12×12 lattice. The average deviation of $\theta_{\mathbf{p}}$ from π is on the order of 10^{-4}. The global loops θ_1 and θ_2 (winding around the axes of the lattice) also acquire a π-flux with a similar deviation as the plaquette fluxes.

for a physical, gauge-invariant state, see eq. (5.4). We choose different variational parameters, different lattice sizes and different sampling sizes but the violation of the Gauss law is always found to be of the order of machine precision, i.e. $\langle G_{\mathbf{x}} \rangle - q_{\mathbf{x}} \lesssim 10^{-16}$. One such configuration for a very small sampling size of $N = 10$ and a system size $L = 12$ is illustrated in Fig. 5.4.1.

5.4.2 Limiting cases

It is useful to consider the limiting cases of compact QED with fermionic matter and convince ourselves that the ground state properties can be captured accurately by our method. In the following, we consider massless fermions without chemical potentials.

We first study the limit $g^2 \to 0$ while keeping t and g_{mag} fixed: it is well known that in this limit the gauge field forms a π-flux pattern and the fermions fill up the lower band at half-filling [116]. A typical problem in mean-field theory is to investigate the stability of the π-flux pattern against gauge field fluctuations. This can be studied naturally in our ansatz by watching the parameter flow upon increasing the electric coupling constant g^2. The π-flux state itself is naturally incorporated in our ansatz since we can fix the gauge field to a certain configuration by tuning the β-parameters to a very high value such that the constraint $\cos \theta_{\mathbf{p}} = -1$ is enforced for all plaquettes. In addition, since we have periodic boundary conditions, we also need to choose the optimal flux configuration for the global non-contractible loops which depends on the size of the lattice. To accomplish that it is important to have a global update in our update scheme since these global changes in the configuration can not be captured by only updating plaquettes locally. Finding the π-flux state is in general a useful test for our update scheme since the probability distribution needs to approximate a delta distribution for which a good update scheme is required. The fermionic part is

obtained by tuning the variational parameters of the fermions in such a way that for all flux configurations the lower half of the band is occupied (which corresponds to choosing all fermionic parameters $\xi_i = 1$ as described in Appendix 5.B). The result of our variational optimization is an accurate representation of the π-flux state with an average deviation on the order of 10^{-8} from $\cos\theta_{\mathbf{p}} = -1$, respectively an average deviation on the order of 10^{-4} from $\theta_{\mathbf{p}} = \pi$ (depicted in Fig. 5.4.1).

Next we consider the opposite limit to the π-flux state, the strong-coupling limit with large g^2. In this limit, the electric energy dominates and some fluctuations are introduced in second-order perturbation theory by the gauge-matter Hamiltonian. For one fermion flavor this perturbation does not have a large effect and the ground state is described by a Gaussian state. For two fermion flavors, however, one can have correlated hopping processes which at half-filling give rise to the Heisenberg Hamiltonian. Both cases can be captured by construction in our ansatz since we design the fermionic part of the ansatz in such a way that our gauge-field dependent Gaussian operator acts on a strong-coupling reference state $|\Psi_0\rangle$ (see eq. (5.11)) and we can choose that reference state according to our needs. We can either choose a Gaussian state for $|\Psi_0\rangle$ or include more advanced methods, e.g. to approximate the Heisenberg ground state we can include spin wave theory in $|\Psi_0\rangle$ (see Appendix 5.C).

We also benchmark for the limiting case that the gauge-matter interactions vanish ($t = 0$) so that fermions and gauge-field decouple and we obtain the standard pure gauge compact QED described by the Kogut-Susskind Hamiltonian $H_{KS} = H_E + H_B$ with $g_{\text{mag}} = \frac{1}{g^2}$ [8]. We therefore only consider the pure gauge part of our ansatz (setting our fermionic variational parameters to zero, $\tilde{\xi} = 0$). We benchmark our ansatz against the variational method presented in chapter 4 which has given good ground state and real-time dynamics of compact QED (the results were recently confirmed by another variational study [100]). We compare the ground state energy of both methods for an $L = 8 \times 8$ for the whole coupling region of g^2 (since g^2 is the only coupling constant in pure gauge compact QED). We find that our results agree very well for the whole coupling region (with a maximal difference of half a percent) while our method performs a tiny bit better at large couplings where the method in chapter 4 gives minimally better results for small g^2. The benchmark is illustrated in Fig. 5.4.2.

5.4.3 Benchmark against Euclidean Monte Carlo

Benchmarking for cQED$_3$ including dynamical fermions is in general difficult since in most scenarios a sign-problem occurs so that no Euclidean Monte Carlo studies exist. However, it was shown to be absent for an even fermion number at zero chemical potential [111]. This was exploited in order to perform determinantal Monte Carlo simulations. Thus, it is natural to compare our ansatz with the Monte Carlo simulations for the case of $N_f = 2$ fermionic species at half-filling. The analysis in ref. [111] revolves around the question of whether a confinement-deconfinement transition takes place and what the nature of this phase transitions is.

We fix the magnetic coupling and the gauge-matter coupling to $g_{\text{mag}} = -1$ and $t = 1$ and will mostly vary the electric coupling g^2. The first observable that is compared is the flux energy per plaquette $\cos(\theta_{\mathbf{p}})$ averaged over the whole lattice. Our results are shown in Fig. 5.4.2. We see agreement over the whole coupling region of g^2 with Fig. 13 in ref. [111]. Note that in ref. [111] a different convention for the electric coupling is used differing by a factor 4. Thus, the upper end of the coupling ranges is

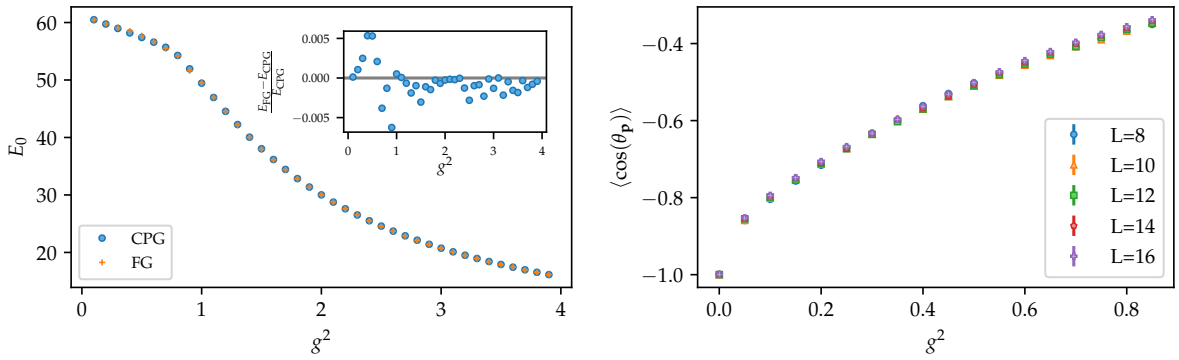

Figure 5.4.2: (Left): Benchmark for pure gauge compact QED_3 of our ansatz (denoted by FG) against the variational method in chapter 4 based on complex periodic Gaussian states (denoted by CPG): we compare the ground state energy E_0 for an 8×8 lattice over the whole coupling region and compute the relative error (see inset). (Right): Benchmark for compact QED_3 coupled to $N_f = 2$ species of dynamical fermions at half-filling: the shown averaged flux energy per plaquette $\cos(\theta_{\mathbf{p}})$ in the variational ground state is to be compared with results obtained in an Euclidean Monte Carlo study shown in Fig. 13 in ref. [111]. The data agrees over the whole coupling region, showing no evidence of a discontinuous phase transition.

the same while our lower end goes further down to $g^2 = 0$. Since we also do not observe finite-size effects it supports the claim in ref. [111] that there is no discontinuous phase transition taking place.

In the second part we study fermionic observables, related to the fermionic correlations of the ground state. These are used in ref. [111] to probe a phase transition between a deconfined U(1) spin-liquid and a confined phase exhibiting antiferromagnetic order (AFM). The observable that is computed is the spin structure factor $\chi_S(\mathbf{k})$:

$$\chi_S(\mathbf{k}) = \frac{1}{L^4} \sum_{\mathbf{x},\mathbf{y}} \sum_{\alpha,\beta=1,2} \left\langle S^{\alpha}_{\beta}(\mathbf{x}) S^{\beta}_{\alpha}(\mathbf{y}) \right\rangle e^{i\mathbf{k}(\mathbf{x}-\mathbf{y})} \tag{5.37}$$

with $S^{\alpha}_{\beta}(\mathbf{x}) = \psi^{\dagger}_{\mathbf{x},\alpha}\psi_{\mathbf{x},\beta} - 1/2\delta_{\alpha\beta}\sum_{\gamma}\psi^{\dagger}_{\mathbf{x},\gamma}\psi_{\mathbf{x},\gamma}$. From the spin structure factor one can compute the AFM correlation ratio defined as

$$r_{\text{AFM}} = 1 - \frac{\chi_S((\pi,\pi) + \delta\mathbf{k})}{\chi_S((\pi,\pi))} \tag{5.38}$$

which quantifies the strength of AFM order ($\delta\mathbf{k} = (2\pi/L, 0)$ denotes the smallest momentum vector). The question addressed in ref. [111] is whether in the thermodynamic limit AFM order persists down to $g^2 = 0$, in other words whether the π-flux state is stable against gauge-field fluctuations. The AFM correlation ratio is computed up to lattice sizes of 16×16 and the crossing points between neighboring lattice sizes are extracted. The crossing points are extrapolated to the thermodynamic limit, resulting in $g^2_{c,\infty} = 0.15(2)$. The procedure is shown in Fig. 5.4.3 which is to be compared with the Euclidean Monte Carlo study in ref. [111] where the extrapoled value is $g^2_{c,\infty,\text{EMC}} = 0.40(5)$. We thus obtain qualitatively similar results in the sense that both extrapolated values are significantly larger than zero and indicate a possible phase transition but the value in our method is lower compared to ref. [111].

Another interesting quantity are the spin-spin correlations as defined in eq. (5.37). We compute the decay of spin correlations on a 16×16 lattice both in the weak-coupling

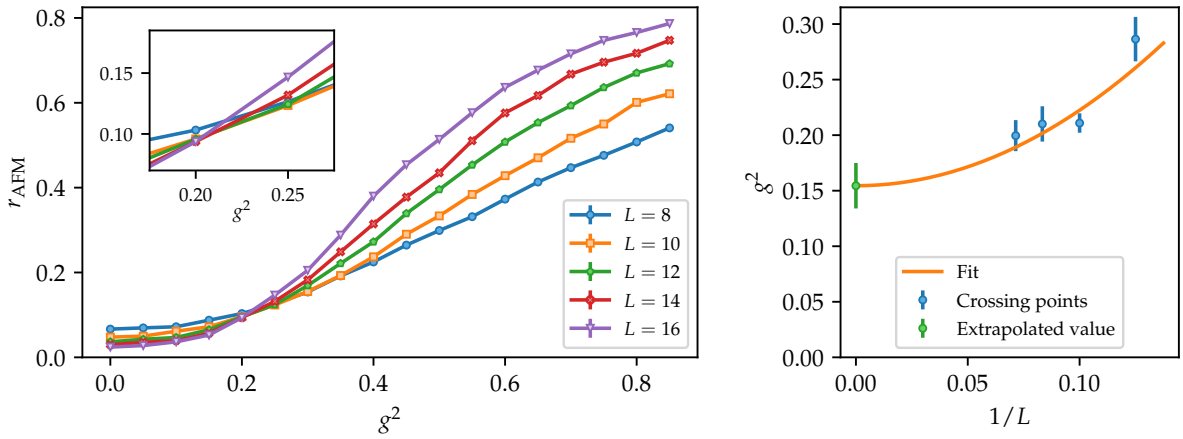

Figure 5.4.3: Benchmark for compact QED$_3$ coupled to $N_f = 2$ species of dynamical fermions at half-filling: we compute the AFM correlation ratio r_{AFM} in the variational ground state for lattice size up to 16×16 (left). The AFM correlation ratio is computed from the spin correlations and quantifies the strength of antiferromagnetic order. The crossing points are extracted and extrapolated to the thermodynamic limit, resulting in $g^2_{c,\infty} = 0.15(2)$ (right). This is to be compared with the Euclidean Monte Carlo study in ref. [111] where also a non-zero coupling was extrapolated but at a higher value of $g^2_{c,\infty,\mathrm{EMC}} = 0.40(5)$.

region ($g^2 = 0.1$) and in a more strongly-coupled region ($g^2 = 0.85$). The result for both the full correlation function and only the connected part is shown in Fig. 5.4.4. At stronger coupling the correlation function decays to a constant value which is lower than predicted by the Heisenberg model (as to be expected since $g^2 = 0.85$ is still too small for a Heisenberg description). The connected correlation function decays exponentially as expected. At weak coupling the connected correlation function rather decays algebraically, as expected for a gapless spin liquid. The form of the decay is very similar to one in the Euclidean Monte Carlo study (see Fig. 4 in ref. [111]).

We can thus, at least qualitatively, support the claim in ref. [111] that there is indeed a deconfined phase which, however, only persists up to a smaller coupling of $g^2_{c,\infty} = 0.15(2)$ in our case. One should note though that for the extrapolation of the AFM correlation ratio and also the computation of the spin structure factor is very sensitive to errors (as also mentioned in ref. [111]) so that a quantitative difference can be expected.

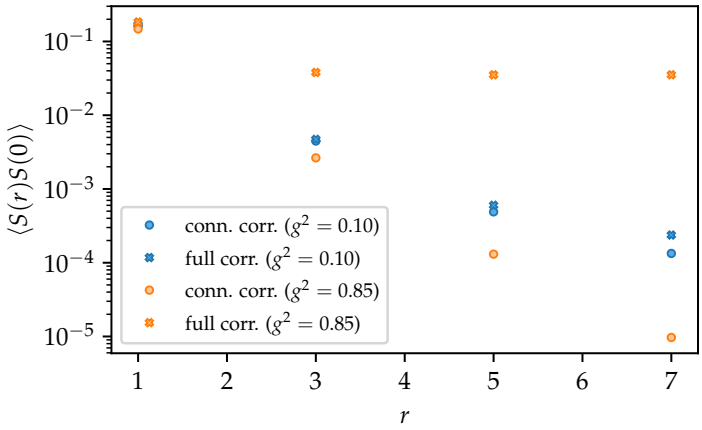

Figure 5.4.4: Benchmark for compact QED$_3$ coupled to $N_f = 2$ species of dynamical fermions at half-filling: we compute the decay of spin correlations (both for the full correlation function and the connected correlation function) in the variatonal ground state for a 16×16 lattice at weak coupling ($g^2 = 0.1$) and at stronger coupling ($g^2 = 0.85$). Note that we only use odd distances in r to avoid oscillations. At strong coupling (where one expects behaviour similar to the Heisenberg model) the full correlations decay to a constant while the connected part decays exponentially. At weak coupling the decay is rather algebraically, similar to the decay shown in the Euclidean Monte Carlo study in Fig. 4 in ref. [111].

5.5 Sign-problem affected regimes

In this section, we access regimes where the sign-problem is present in order to demonstrate that our method does not suffer from the sign-poblem. Having benchmarked our ansatz for the scenario of two flavors of fermions at half-filling, i.e. zero chemical potential, it is natural to study this configuration at finite chemical potential.

We specifically want to look at a scenario that has been used in one dimension with tensor networks [75] to demonstrate overcoming the sign-problem and extend it to two dimensions. In the referenced work the authors study density-induced phase transitions due to varying flavor-dependent chemical potentials. Analogously to ref. [75], we look at the case of massless and massive fermions.

We fix the parameters in the Hamiltonian given in eq. (5.1) to the values $t = 1$, $g_{\text{mag}} = -1$ and $g^2 = 0.2$, similar to the benchmarked case in the previous section. Only the staggered mass m and the chemical potentials μ_1 and μ_2 will be changed. To make this explicit we rewrite the Hamiltonian as

$$\begin{aligned} H =& H_E + H_B + H_{GM} + H_M(m) \\ =& H_0(m) + \mu_1 N_1 + \mu_2 N_2 \\ =& H_0(m) + \frac{\mu_+}{2} N - \frac{\mu_-}{2} \Delta N \end{aligned} \tag{5.39}$$

with the conserved quantities $N_1 = \sum_{\mathbf{x}} \psi^\dagger_{\mathbf{x},1} \psi_{\mathbf{x},1}$ and $N_2 = \sum_{\mathbf{x}} \psi^\dagger_{\mathbf{x},2} \psi_{\mathbf{x},2}$. Alternatively, one can also use the total number of fermions $N = N_1 + N_2$ and their imbalance (sometimes called isopsin number) $\Delta N = N_1 - N_2$ as conserved quantities. Respectively, one defines the chemical potentials $\mu_+ = (\mu_1 + \mu_2)$ and $\mu_- = (\mu_1 - \mu_2)$. The rest of the Hamiltonian is contained in $H_0(m)$ which only depends on m.

The Hamiltonian is block-diagonal and different sectors are labelled with N and ΔN. In analogy to ref. [75], we fix the total number of fermions N to the number of lattice

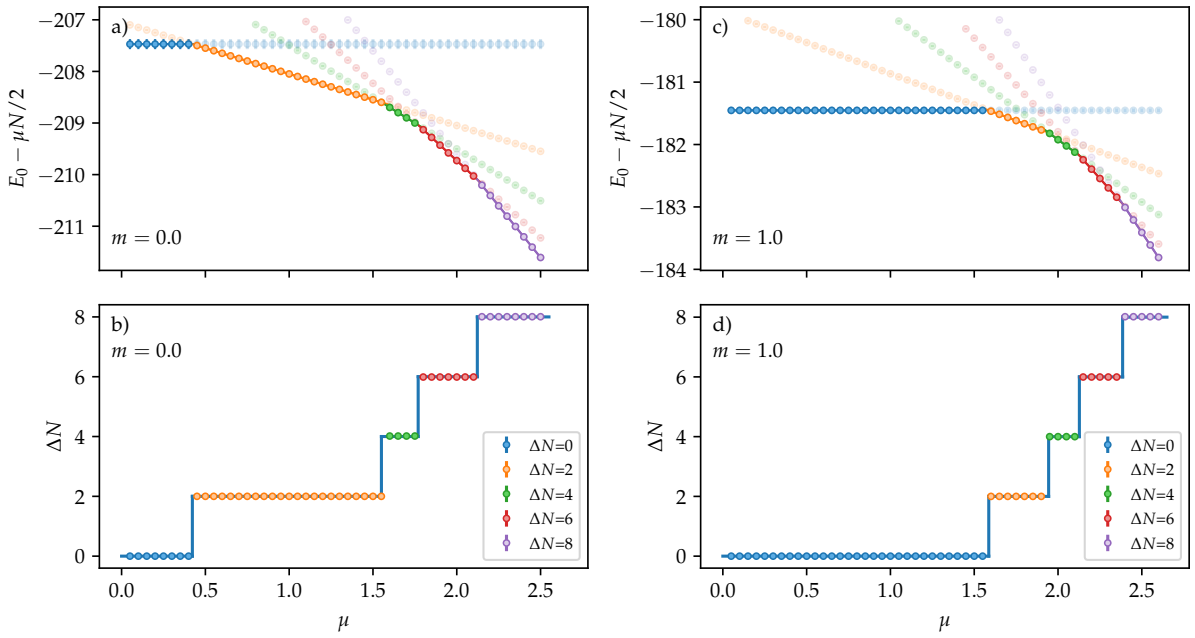

Figure 5.5.1: Finite chemical potential study for compact QED$_3$ coupled to $N_f = 2$ species of dynamical fermions: we compute the variational ground state energies (corrected by an overall constant $\mu N/2$) on an 8×8 lattice for different isospin numbers ΔN depending on the chemical potential difference μ between the two species. We study both the case of massless and massive fermions (see top row, (a,c)). By computing the crossing points between the ground state energies we can extract the phase transitions between neighboring ΔN phases (see bottom row, (b,d)).

sites and study the nature of the ground state (characterized by ΔN) depending on μ_-, the isospin chemical potential. Since the energy (up to a constant) only depends on μ_-, we set $\mu_2 = 0$ so that $\mu_+ = \mu_- = \mu_1 \equiv \mu$. The ground state energy for each sector can then be written as

$$E_{\Delta N,N}(\mu, m) = N\frac{\mu}{2} - \Delta N\frac{\mu}{2} + E_{0,\Delta N,N}(m) \tag{5.40}$$

where $E_{0,\Delta N,N}(m)$ is the ground state w.r.t. $H_0(m)$ for fixed N and ΔN.

We ran our simulations on an 8×8 lattice where we saw that finite-size effects were negligible for our purposes. To detect the phase transitions between different ΔN phases we compute the variational ground state energy for a given ΔN to determine $E_{0,\Delta N,N}(m)$. We plot the ground state energy of every ΔN-sector subtracted by the constant given by the total number of fermions, i.e. $E_{\Delta N,N}(\mu, m) - N\frac{\mu}{2}$. The crossing points between different ΔN energies give us the location of the phase transitions.

The result of that procedure for the massless case is shown in Fig. 5.5.1(a) which then allows us to plot the ΔN phase transitions, illustrated in Fig. 5.5.1(b). For the massive case we choose a staggered mass of $m = 1.0$ and repeat the same procedure as in the massless case. The result for the ground state energy is shown in Fig. 5.5.1(c) whereas the phase transitions are shown in Fig. 5.5.1(d).

When comparing the massless and massive case it becomes clear that the phase transitions are all shifted to higher values of μ. However, the extent of this shift depends strongly on the isospin number. While phase transitions between small ΔN are severely affected by the staggered mass term (in particular the transition between $\Delta N = 0$ and

$\Delta N = 2$ which shifted from $\mu = 0.5$ to $\mu = 1.5$), phase transitions for larger ΔN are relatively unaffected (e.g. the phase transition between $\Delta N = 6$ and $\Delta N = 8$ shifts only slightly from $\mu = 2.2$ to $\mu = 2.3$). This is in agreement with the results of the tensor-network study in one dimension [75].

The reason for this behaviour lies in the different changes in ground state energy $E_{0,\Delta N,N}(m)$ for different ΔN if we go from $H_0(m = 0)$ to $H_0(m = 1)$. Qualitatively, this can be explained with the fact that for larger isospin numbers ΔN the imbalance in occupation between even and odd sites (the lattice analogue of the chiral condensate) becomes smaller and thus gets more penalized by a staggered mass term. Hence, the phase transitions shift to higher values in chemical potential. Since this effect is stronger for smaller isospin number, it mostly affects transitions between such phases.

5.6 Conclusion

To investigate higher-dimensional lattice gauge theories with dynamical fermions without truncating the gauge field Hilbert space, we propose a variational, sign-problem-free Monte Carlo method and apply it to $(2+1)$-dimensional compact QED with dynamical fermions. We evaluate the performance of the ansatz by comparing it with the limiting cases of the model, other variational methods [2], and a Euclidean Monte Carlo study [111]. To explore sign-problem affected regimes, we study the model at finite chemical potential and detect density-induced phase transitions for both massless and massive staggered fermions, thus extending results from one dimension which were obtained using tensor networks [75].

The variational ansatz consists of a Jastrow-type ansatz state that describes the ground state of pure gauge compact QED (similar to the periodic Gaussian states presented in chapter 4) and a gauge-fermion part that is an infinite superposition of gauge-field dependent fermionic Gaussian states. The fermionic Gaussian state is defined such that its integral over all gauge field configurations is gauge-invariant and tractable. The gauge-field dependent variational parameters are obtained by the eigendecomposition of the gauge-matter Hamiltonian. We can reach large lattice sizes as exact diagonalization can be performed efficiently ($\mathcal{O}(N^3)$ in system size) at every measurement step in the sampling algorithm.

In the future, we plan to extend the method to other higher-dimensional lattice gauge theories, such as three-dimensional or non-Abelian lattice gauge theories. This only requires changes in the pure gauge part of the ansatz, while the fermionic part can remain the same. The presented method could also be helpful in controlling the errors caused by truncation in the gauge field Hilbert space when simulating lattice gauge theories on quantum devices.

APPENDIX

5.A DETAILS ON THE COMPUTATION OF THE LOCAL ELECTRIC ENERGY $H_{E,\mathrm{LOC}}(\theta)$

The most difficult observables to compute in our variational Monte Carlo scheme are electric quantites, with the electric energy being its most prominent representative. In section 5.3.3, we discussed the computation of $\langle H_E \rangle$ which according to eq. (5.23) consists of three parts: $\langle H_E \rangle = \langle H_E \rangle_{ff} + \langle H_E \rangle_{gg} + \langle H_E \rangle_{fg}$. To evaluate them one needs the local quantity $H_{E,\mathrm{loc}}(\theta)$ that can sampled in a Monte Carlo simulation (see eq. (5.21)). In the body of the manuscript we derived $H_{E,gg,\mathrm{loc}}(\theta)$ and gave the final result for $H_{E,ff,\mathrm{loc}}(\theta)$. In the following we present some details on the derivation of $H_{E,ff,\mathrm{loc}}(\theta)$ and give the final result for the crossterm $H_{E,fg,\mathrm{loc}}(\theta)$.

The computation of $H_{E,ff,\mathrm{loc}}(\theta)$ involves deriving the fermionic Gaussian operator $U_{GS}(\theta)$ defined in eq. (5.16) w.r.t. $\theta_{\mathbf{x},i}$ which results in the form of $f_{\mathbf{x},i}(\theta)$ given in eq. (5.28):

$$
\begin{aligned}
&\frac{1}{i}\left(\partial_{\theta_{\mathbf{x},i}} U_{GS}(\theta)\right) U_{GS}^{\dagger}(\theta) \\
&= \int_0^1 dt \exp\left(it \sum_{\mathbf{x},\mathbf{y}} \psi_{\mathbf{x}}^{\dagger} \xi(\theta)_{\mathbf{xy}} \psi_{\mathbf{y}} \right) \sum_{\mathbf{x},\mathbf{y}} \psi_{\mathbf{x}}^{\dagger} \frac{\partial \xi(\theta)_{\mathbf{xy}}}{\partial \theta_{\mathbf{x},i}} \psi_{\mathbf{y}} \exp\left(-it \sum_{\mathbf{x},\mathbf{y}} \psi_{\mathbf{x}}^{\dagger} \xi(\theta)_{\mathbf{xy}} \psi_{\mathbf{y}} \right) \\
&= \sum_{\mathbf{x},\mathbf{y},\mathbf{x}',\mathbf{y}'} \psi_{\mathbf{x}}^{\dagger} \int_0^1 dt \left[\exp\left(it\xi(\theta)\right)\right]_{\mathbf{x}\mathbf{x}'} \left[\frac{\partial \xi(\theta)}{\partial \theta_{\mathbf{x},i}}\right]_{\mathbf{x}'\mathbf{y}'} \left[\exp\left(-it\xi(\theta)\right)\right]_{\mathbf{y}'\mathbf{y}} \psi_{\mathbf{y}} \qquad (5.41) \\
&= \vec{\psi}^{\dagger} \int_0^1 dt \exp\left(it\xi(\theta)\right) \frac{\partial \xi(\theta)}{\partial \theta_{\mathbf{x},i}} \exp\left(-it\xi(\theta)\right) \vec{\psi} \\
&= \vec{\psi}^{\dagger} \frac{1}{i} \left(\partial_{\theta_{\mathbf{x},i}} e^{i\xi(\theta)}\right) e^{-i\xi(\theta)} \vec{\psi} \equiv \vec{\psi}^{\dagger} f_{\mathbf{x},i}(\theta) \vec{\psi}
\end{aligned}
$$

where $\vec{\psi}$ is a vector of the fermionic annihilation operators $\psi_{\mathbf{x}}$ and we used the identity:

$$
\partial_{\theta} e^{M(\theta)} = \int_0^1 dt e^{tM(\theta)} \left(\partial_{\theta} M(\theta)\right) e^{-tM(\theta)} e^{M(\theta)}. \qquad (5.42)
$$

If we carry out the second derivative $\partial_{\theta_{\mathbf{x},i}}$ we obtain an additional term corresponding to the derivative of $f_{\mathbf{x},i}(\theta)$ which vanishes. Thus, we remain with another contribution $\vec{\psi}^{\dagger} f_{\mathbf{x},i}(\theta) \vec{\psi}$ due to the derivative of $U_{GS}(\theta)$, resulting in the fermionic operator $H_{E,ff,\mathrm{fer}}(\theta)$ in eq. (5.27). Inserting $\xi(\theta) = V(\theta)\tilde{\xi}V^{\dagger}(\theta)$ defined in eq. (5.15) we derive

an explicit expression for $f_{\mathbf{x},i}(\theta)$:

$$\begin{aligned} f_{\mathbf{x},i}(\theta) =& -i\partial_{\theta_{\mathbf{x},i}} \left(e^{iV(\theta)\tilde{\xi}V^\dagger(\theta)}\right) e^{-iV(\theta)\tilde{\xi}V^\dagger(\theta)} \\ =& V(\theta) \left(\frac{1}{i} V^\dagger(\theta)\partial_{\theta_{\mathbf{x},i}} V(\theta) + e^{i\tilde{\xi}} \frac{1}{i} \underbrace{\partial_{\theta_{\mathbf{x},i}} V^\dagger(\theta) V(\theta)}_{=-V^\dagger(\theta)\partial_{\theta_{\mathbf{x},i}} V(\theta)} e^{-i\tilde{\xi}} \right) V^\dagger(\theta) \\ =& V(\theta) \left(\alpha^{\mathbf{x},i}(\theta) - e^{i\tilde{\xi}} \alpha^{\mathbf{x},i}(\theta) e^{-i\tilde{\xi}} \right) V^\dagger(\theta) \end{aligned} \tag{5.43}$$

with $V(\theta)$ defined by the eigendecomposition of $h_{GM}(\theta) = V(\theta)\Lambda(\theta)V^\dagger(\theta)$ and $\alpha^{\mathbf{x},i}(\theta) = -iV^\dagger(\theta)\partial_{\theta_{\mathbf{x},i}} V(\theta)$ containing the derivatives of the eigenvectors of $h_{GM}(\theta)$. An explicit expression for $\alpha^{\mathbf{x},i}(\theta)$ can be derived by using a connection with the derivative of $h_{GM}(\theta)$:

$$\begin{aligned} \alpha^{\mathbf{x},i}_{kl}(\theta) &= -i \frac{V^\dagger_{k\mathbf{x}'}(\theta) \frac{\partial h_{GM}(\theta)_{\mathbf{x}'\mathbf{x}''}}{\partial \theta_{\mathbf{x},i}} V(\theta)_{\mathbf{x}''l}}{\lambda_l(\theta) - \lambda_k(\theta)} \\ &= \frac{V^\dagger_{k\mathbf{x}}(\theta) e^{i\theta_{\mathbf{x},i}} V(\theta)_{\mathbf{x}+\mathbf{e}_i l} - h.c.}{\lambda_l(\theta) - \lambda_k(\theta)}. \end{aligned} \tag{5.44}$$

Since the derivative of $h_{GM}(\theta)$ is non-zero only for sites adjacent to the link $\mathbf{x}, i$ the expression for $\alpha^{\mathbf{x},i}(\theta)$ simplifies significantly. With the diagonal expressions for $f_{\mathbf{x},i}(\theta)$ as given above, $H_{E,ff,\mathrm{loc}}(\theta)$ is straightforwardly computed as explained in the body of the manuscript.

The derivation of $H_{E,fg,\mathrm{loc}}(\theta)$ involves a derivative of $\Psi_G(\theta)$ which is expressed via the vector $b_{\mathbf{x},i}(\theta)$ defined in eq. (5.24) and a derivative of $|\Psi_F(\theta)\rangle$ resulting in a quadratic fermionic operator as discussed above:

$$\begin{aligned} \langle H_E \rangle_{fg} =& \frac{g^2}{2} \sum_{\mathbf{x},i} \int D\theta\, p(\theta) 2 \langle \Psi_F(\theta) | \vec{\psi}^\dagger f_{\mathbf{x},i}(\theta) \vec{\psi} | \Psi_F(\theta) \rangle \left(ib^T(\theta)\alpha b_{\mathbf{x},i}(\theta) + i\beta^T b_{\mathbf{x},i}(\theta) \right) \\ =& \frac{g^2}{2} \sum_{\mathbf{x},i} \int D\theta\, p(\theta) 2 \,\mathrm{Tr}\left(\left(\mathbb{1} - \Gamma_{\psi\psi^\dagger}(\theta) \right) f_{\mathbf{x},i}(\theta) \right) \left(ib^T(\theta)\alpha b_{\mathbf{x},i}(\theta) + i\beta^T b_{\mathbf{x},i}(\theta) \right) \\ \equiv& \int D\theta\, p(\theta) H_{E,fg,\mathrm{loc}}(\theta) \end{aligned} \tag{5.45}$$

where we used the covariance matrix of the fermionic Gaussian state $\Gamma_{\psi\psi^\dagger}(\theta)$ as defined in eq. (5.31). For ground state studies as considered in this manuscript the variational parameters α and β are chosen real such that the electric energy of the cross term vanishes.

5.B Details on the structure of $\tilde{\xi}$

In the following we provide details on the parametrization of the matrix $\tilde{\xi}_{ij}$ containing the fermionic variational parameters. Recall that $\tilde{\xi}$ is formulated in the eigenbasis of the gauge-matter Hamiltonian, $h_{GM}(\theta)_{\mathbf{xy}} = V(\theta)_{\mathbf{x}i}\Lambda(\theta)_i V(\theta)^\dagger_{i\mathbf{y}}$. It allows to control the fermionic state in terms of eigenstates of the gauge-matter Hamiltonian.

In principle one can keep all parameters variational, however, one can simplify the structure of $\tilde{\xi}$ by considering the structure of the eigenstates as already discussed in section 5.3.2. This can be emphasized by considering the two limits of the fermionic Hamiltonian $H_{\text{fer}} = H_E + H_{GM}$, i.e. the strong-coupling limit ($g^2 \to \infty$, H_E dominates) and the weak-coupling limit ($g^2 \to 0$, H_{GM} dominates) and how this fermionic state looks in terms of the eigenbasis of the gauge-matter Hamiltonian.

In the strong-coupling limit the ground state is in a positional eigenstate, e.g. for one flavor all odd sites are occupied, $|D\rangle = \prod_{\mathbf{x}\in\mathcal{O}} \psi_{\mathbf{x}} |0\rangle$. This is already incorporated in the ansatz by setting the whole matrix $\tilde{\xi}$ to zero so that only the strong coupling reference state $|D\rangle$ remains but it is instructive to think of this state in terms of eigenstates of the gauge-matter Hamiltonian. Following the discussion in section 5.3.2 we can rewrite the state as

$$|D\rangle = \int D\theta \prod_i \frac{1}{\sqrt{2}} \left(\psi^\dagger_{i+}(\theta) - \psi^\dagger_{i-}(\theta)\right) |0\rangle \tag{5.46}$$

where we used the labeling of the eigenstates as in section 5.3.2 where $\psi^\dagger_{i+}(\theta)|0\rangle$ denotes the single-particle eigenstate of H_{GM} with eigenvalue $\lambda_i(\theta)$ and, respectively, $-\lambda_i(\theta)$ for $\psi^\dagger_{i-}(\theta)|0\rangle$. On the other hand, in the weak-coupling limit the ground state is described by the occupation of all eigenstates with negative eigenvalue, i.e. the lower band,

$$|\Psi_{0,GM}\rangle = \int D\theta \prod_i \psi^\dagger_{i-}(\theta) |0\rangle \tag{5.47}$$

Thus, one can smoothly transform from the strong coupling ground state to the weak coupling ground state by performing for every pair i of single-particle eigenstates ($\psi^\dagger_{i+}(\theta)|0\rangle$ and $\psi^\dagger_{i-}(\theta)|0\rangle$) the transformation

$$\frac{1}{\sqrt{2}} \left(\psi^\dagger_{i+}(\theta) - \psi^\dagger_{i-}(\theta)\right) |0\rangle \to \psi^\dagger_{i-}(\theta)|0\rangle . \tag{5.48}$$

Viewed in terms of the covariance matrix for the single-particle eigenstates $\psi^\dagger_{i+}(\theta)|0\rangle$ and $\psi^\dagger_{i-}(\theta)|0\rangle$, this amounts to $\frac{1}{2}(\mathbb{1} - \sigma_x) \to \frac{1}{2}(\mathbb{1} + \sigma_z)$. This can be incorporated into $\tilde{\xi}$ by choosing the submatrix of $\tilde{\xi}$ related to the $\psi^\dagger_{i+}(\theta)|0\rangle$ and $\psi^\dagger_{i-}(\theta)|0\rangle$ eigenstates (a 2×2-matrix) as $\tilde{\xi}|_i = -\frac{\pi}{4}\sigma_y \xi_i$ (where ξ_i is a variational parameter) so that changing ξ_i from zero to one smoothly transforms from the weak-coupling to the strong-coupling ground state. We thus end up with $N/2$ fermionic variational parameters ($N = L^2$ the number of lattice sites) and a block-diagonal form of $\tilde{\xi}$:

$$\tilde{\xi} = \begin{pmatrix} \tilde{\xi}|_1 & 0 & \dots & 0 \\ 0 & \tilde{\xi}|_2 & \ddots & \vdots \\ \vdots & \ddots & \ddots & 0 \\ 0 & \dots & 0 & \tilde{\xi}|_{N/2} \end{pmatrix} \tag{5.49}$$

For the case of $N_f = 2$ fermion flavors (and potentially even more flavors) one can choose a similar block-diagonal structure where one now blocks the single-particle eigenstates of both flavors together, i.e. $\psi^\dagger_{1,i+}(\theta)|0\rangle, \psi^\dagger_{1,i-}(\theta)|0\rangle, \psi^\dagger_{2,i+}(\theta)|0\rangle, \psi^\dagger_{2,i-}(\theta)|0\rangle$. The individual blocks $\tilde{\xi}|_i$ are then 4×4-matrices (or more generally $2N_f \times 2N_f$-matrices). The variational parametrization of these blocks is kept general as this allows to control certain properties between the two species, e.g. the imbalance ΔN between the two

species as was used for the study of sign-problem affected regimes in section 5.5. The block-diagonal structure allows even for multiple fermion flavors to compute the local energy $H_{\text{loc}}(\theta)$, in particular $H_{E,\text{loc}}(\theta)$, (see section 5.3.3) with a computational cost of only $\mathcal{O}(N^3)$.

5.C Choosing a non-Gaussian reference state for the strong-coupling limit

Our fermionic state construction is based on a gauge-field dependent fermionic Gaussian operator $U_{GS}(\theta)$ acting on a strong-coupling reference state $|\Psi_0\rangle$ (see eq. (5.11)). In this section we show that this reference state can also be chosen non-Gaussian, using the example of $N_f = 2$ fermionic species at half-filling as discussed in the body of the manuscript. In the strong-coupling limit ($g^2 >> 1$) the lattice gauge theory reduces to an effective fermionic theory where the electric field vanishes to zeroth order. In second-order perturbation theory one can have virtual hopping processes between the two fermion species in opposite directions. This gives effectively rise to fermionic interactions as can be seen in our ansatz by the appearance of quartic expressions in the fermions (see eq. (5.27)). In the considered sector of one fermion per site this allows a mapping to a spin Hamiltonian, the Heisenberg model [117]. This can be incorporated in the ansatz by using a good approximation of the ground state of the effective fermionic theory (the Heisenberg model in our case) as reference state $|\Psi_0\rangle$. This ground state approximation can be obtained using any method of choice, e.g. tensor networks or spin wave theory (as was chosen in our case).

The most difficult terms to evaluate in this scenario involve again quartic fermionic operators of the form

$$\langle\Psi_0|\vec{\psi}^\dagger f_{\mathbf{x},i,N_f=2}(\theta)\vec{\psi}\vec{\psi}^\dagger f_{\mathbf{x},i,N_f=2}(\theta)\vec{\psi}|\Psi_0\rangle \tag{5.50}$$

with $\vec{\psi} = (\vec{\psi}_1, \vec{\psi}_2)^T$ now containing annihilation operators of both fermionic species. In the expression above we already performed the unitary transformation defined by $U_{GS}(\theta)$ resulting in a slightly different form of $f_{\mathbf{x},i}(\theta)$ compared to eq. (5.28):

$$\begin{aligned} &f_{\mathbf{x},i,N_f=2}(\theta) \\ &= \begin{pmatrix} V(\theta) & 0 \\ 0 & V(\theta) \end{pmatrix} \left[e^{-i\tilde{\xi}} \begin{pmatrix} \alpha^{\mathbf{x},i}(\theta) & 0 \\ 0 & \alpha^{\mathbf{x},i}(\theta) \end{pmatrix} e^{i\tilde{\xi}} - \begin{pmatrix} \alpha^{\mathbf{x},i}(\theta) & 0 \\ 0 & \alpha^{\mathbf{x},i}(\theta) \end{pmatrix} \right] \begin{pmatrix} V^\dagger(\theta) & 0 \\ 0 & V(\theta)^\dagger \end{pmatrix} \\ &\equiv \begin{pmatrix} f(\theta)_{11} & f(\theta)_{12} \\ f(\theta)_{12}^\dagger & f(\theta)_{22} \end{pmatrix} \end{aligned} \tag{5.51}$$

For ease of notation we dropped the subscripts for the submatrices of $f(\theta)$ in the last row. The fermionic operator $\vec{\psi}^\dagger f_{\mathbf{x},i,N_f=2}(\theta)\vec{\psi}$ can be written in the individual components of the fermionic species as

$$\vec{\psi}^\dagger f_{\mathbf{x},i,N_f=2}(\theta)\vec{\psi} = \vec{\psi}_1^\dagger f(\theta)_{11}\vec{\psi}_1 + \vec{\psi}_2^\dagger f(\theta)_{22}\vec{\psi}_2 + \vec{\psi}_1^\dagger f(\theta)_{12}\vec{\psi}_2 + \vec{\psi}_2^\dagger f(\theta)_{12}^\dagger\vec{\psi}_1. \tag{5.52}$$

The fermionic expressions appearing in eq. (5.50) then take the general form (explicitly writing out the site dependence): $\vec{\psi}^\dagger_{\alpha\mathbf{x}} f(\theta)_{\alpha\alpha',\mathbf{x}\mathbf{x}'}\vec{\psi}_{\alpha'\mathbf{x}'}\vec{\psi}^\dagger_{\beta\mathbf{y}} f(\theta)_{\beta\beta',\mathbf{y}\mathbf{y}'}\vec{\psi}_{\beta'\mathbf{y}'}$. Since the expression in eq. (5.50) is evaluated w.r.t. the strong coupling vacuum $|\Psi_0\rangle$ we can

project this expression onto the spin subspace with $\sum_{\alpha=1,2} \psi^\dagger_{\alpha\mathbf{x}}\psi_{\alpha\mathbf{x}} = 1$ for all $\mathbf{x}$. This simplifies the expression since only combinations of fermionic operators remain that respect the single occupancy constraint, i.e. either $\mathbf{x} = \mathbf{x}'$ and $\mathbf{y} = \mathbf{y}'$ or $\mathbf{x} = \mathbf{y}'$ and $\mathbf{x}' = \mathbf{y}$. If we further keep only contributions that are known to be non-zero for the Heisenberg ground state, we can express the expectation value in eq. (5.50) in terms of the spin correlations:

$$\begin{aligned}
&\langle\Psi_0|\vec{\psi}^\dagger f_{\mathbf{x},i,N_f=2}(\theta)\vec{\psi}\vec{\psi}^\dagger f_{\mathbf{x},i,N_f=2}(\theta)\vec{\psi}|\Psi_0\rangle \\
=&\sum_{\mathbf{x},\mathbf{y}} \frac{1}{4}\left(|f(\theta)_{11,\mathbf{xy}}|^2 + |f(\theta)_{22,\mathbf{xy}}|^2 + 2|f(\theta)_{12,\mathbf{xy}}|^2 + f(\theta)_{11,\mathbf{xx}}f(\theta)_{11,\mathbf{yy}}\right. \\
&\qquad \left. + f(\theta)_{22,\mathbf{xx}}f(\theta)_{22,\mathbf{yy}} + 2f(\theta)_{11,\mathbf{xx}}f(\theta)_{22,\mathbf{yy}}\right) \\
+&\sum_{\mathbf{x},\mathbf{y}} \langle S^z_\mathbf{x}\rangle \left(f(\theta)_{11,\mathbf{xx}}f(\theta)_{11,\mathbf{yy}} - f(\theta)_{22,\mathbf{xx}}f(\theta)_{22,\mathbf{yy}} + f(\theta)_{11,\mathbf{xx}}f(\theta)_{22,\mathbf{yy}}\right. \\
&\qquad \left. - f(\theta)_{22,\mathbf{xx}}f(\theta)_{11,\mathbf{yy}}\right) \\
+&\sum_{\mathbf{x},\mathbf{y}} \langle S^z_\mathbf{x}S^z_\mathbf{y}\rangle \left(2|f(\theta)_{12,\mathbf{xy}}|^2 - |f(\theta)_{11,\mathbf{xy}}|^2 - |f(\theta)_{22,\mathbf{xy}}|^2 + f(\theta)_{11,\mathbf{xx}}f(\theta)_{11,\mathbf{yy}}\right. \\
&\qquad \left. + f(\theta)_{22,\mathbf{xx}}f(\theta)_{22,\mathbf{yy}} - 2f(\theta)_{11,\mathbf{xx}}f(\theta)_{22,\mathbf{yy}}\right) \\
+&\sum_{\mathbf{x},\mathbf{y}} 2\langle S^+_\mathbf{x}S^-_\mathbf{y}\rangle \left(f(\theta)_{12,\mathbf{xx}}\overline{f(\theta)}_{12,\mathbf{yy}} - f(\theta)_{11,\mathbf{xy}}f(\theta)_{22,\mathbf{yx}}\right)
\end{aligned} \tag{5.53}$$

where all spin correlations are evaluated w.r.t. $|\Psi_0\rangle$. We chose spin wave theory to approximate the ground state of the Heisenberg model [118]. One can even make the parameters of the spin waves variational and thus interpolate between a Gaussian state (the Neel state) and spin wave theory.

5.D Update scheme of the Monte Carlo algorithm

In this section we provide some more details on the update scheme in our Monte Carlo algorithm. As the cost of updates is quite low, we are free to perform various types of updates.

For local updates we perform the update of a link $\theta_{\mathbf{x},i}$ which changes the two plaquette variables that contain the link, for one of them the value of $\theta_\mathbf{p}$ is raised, for the other, respectively, lowered. One can extend this update scheme if one changes a second link variable in on one of the two plaquettes in such a way that it compensates the change due to $\theta_{\mathbf{x},i}$ and $\theta_\mathbf{p}$ is unchanged. Thus, only one of the two plaquettes containing the link variable $\theta_{\mathbf{x},i}$ will be updated and another plaquette that is next-nearest neighbor to it. Performing this procedure for all possible pairs, we update six pairs of next-nearest neighbor plaquettes.

The global updates are related to changes in the gauge field configuration that are hard to obtain by iteratively applying local updates. It turned out that one such configuration is a change in all plaquettes $\theta_\mathbf{p}$ by $2\pi/N$ and a change in a specific plaquette

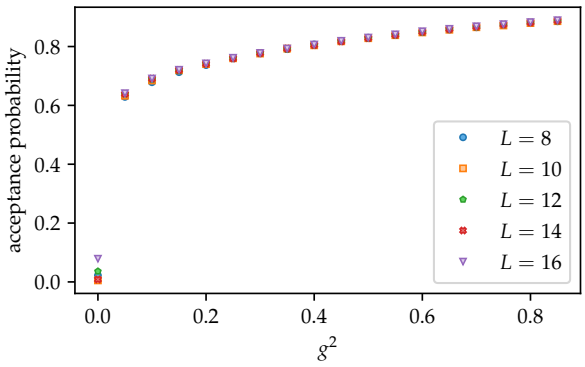

Figure 5.D.1: The acceptance probability in the variational ground states of the $N_f = 2$ model. The acceptance probability is on a high level down to the lowest non-zero coupling and only for $g^2 = 0.0$ it sharply drops. This is expected since the ground state there is diagonal in θ with all plaquettes $\theta_{\mathbf{p}}$ having π flux so that our variational probability, while approaching the delta distribution, gets lower and lower in acceptance probability.

$\theta_{\mathbf{p}'}$ by $-2\pi(1-1/N)$ with N the number of plaquettes. The corresponding link configuration $\theta_{\mathbf{x},i}$ to create such a change in $\theta_{\mathbf{p}}$ can be computed via the lattice Green's function:

$$\begin{aligned} \phi^{\text{glob}}_{\mathbf{p}} &= \frac{1}{\sqrt{N}} \sum_{\mathbf{k}} e^{i\mathbf{k}\mathbf{p}} \frac{\tilde{Q}(\mathbf{k})}{4 - 2\cos(k_x) - 2\cos(k_x)} \\ \theta^{\text{glob}}_{\mathbf{x},i} &= \epsilon_{ij} \Delta^{(-)}_j \phi^{\text{glob}}_{\mathbf{p}} = \epsilon_{ij} \left(\phi^{\text{glob}}_{\mathbf{p}} - \phi^{\text{glob}}_{\mathbf{p}-\mathbf{e}_j} \right) \end{aligned} \tag{5.54}$$

where $\tilde{Q}(\mathbf{k})$ is the Fourier transform of $Q(\mathbf{p})$ which contains the desired changes in plaquette variables $\theta_{\mathbf{p}}$ that we want to create. In a first step a scalar field $\phi^{\text{glob}}_{\mathbf{p}}$ on the plaquettes is generated from $Q(\mathbf{p})$, from which one can derive the link variables $\theta^{\text{glob}}_{\mathbf{x},i}$ by applying the lattice curl to ϕ^{glob} which involves the plaquettes $\mathbf{p}$ and $\mathbf{p} - \mathbf{e}_j$ that contain the link $\mathbf{x}, i$. With the procedure above various kinds of global updates can be performed by choosing $Q(\mathbf{p})$ appropriately.

As supporting evidence that our update scheme gives reasonable results we provide in Fig. 5.D.1 the acceptance probability in the variational ground states of the $N_f = 2$ model where we compared our results with Euclidean Monte Carlo results (see 5.4.3). Throughout the whole coupling region the acceptance probability is on a high level, except for $g^2 = 0.0$ where it is expected since the ground state is the π-flux state and our probability distribution approximates a delta distribution.

The Monte Carlo simulation for all data is performed with at least 100 full warm-up updates where each update is performed as described above. More warm-up updates are possible in principle, but have not improved the results. After the warm-up at least 10,000 measurement steps are performed. The errors of the Monte Carlo results are estimated by a re-binning analysis.

5.E Details on gradient and Gram matrix

In this section we sketch the computation of the gradient of the variational energy and the Gram matrix using Monte Carlo simulation as required for the adaptation of the parameters with stochastic reconfiguration. Starting with the gradient, we first recall

the form of the variational energy in terms of the local energy $H_{\text{loc}}(\theta)$:

$$\frac{\langle\Psi|H|\Psi\rangle}{\langle\Psi|\Psi\rangle} = \frac{\int D\theta\, H_{\text{loc}}(\theta)|\Psi_G(\theta)|^2}{\int D\theta\, |\Psi_G(\theta)|^2} = \frac{\int D\theta\, H_{\text{loc}}(\theta) e^{-b^T(\theta)\alpha b(\theta) - 2\beta^T b(\theta)}}{\int D\theta\, e^{-b^T(\theta)\alpha b - 2\beta^T b(\theta)}} = \int D\theta\, H_{\text{loc}}(\theta) p(\theta) \tag{5.55}$$

The gradient will involve derivatives of $H_{\text{loc}}(\theta)$ w.r.t. all variational parameters and derivatives of $p(\theta)$ but these only w.r.t. the pure gauge parameters α and β. We provide the latter (denoted by the subscript $p(\theta)$) exemplary for the matrix element $\alpha_{\mathbf{p}\mathbf{p}'}$ (the expressions for β are analogous but easier since the corresponding term in the exponential is only linear in $b(\theta)$):

$$\begin{aligned}\frac{\partial \langle E\rangle_{p(\theta)}}{\partial \alpha_{\mathbf{p}\mathbf{p}'}} =& \frac{\int D\theta\, H_{\text{loc}}(\theta)\left(-b(\theta)_{\mathbf{p}} b(\theta)_{\mathbf{p}'}\right) e^{-b^T(\theta)\alpha b(\theta) - 2\beta^T b(\theta)}}{\int D\theta\, e^{-b^T(\theta)\alpha b - 2\beta^T b(\theta)}} \\ &- \frac{\langle\Psi|H|\Psi\rangle}{\langle\Psi|\Psi\rangle} \frac{\int D\theta\, \left(-b(\theta)_{\mathbf{p}} b(\theta)_{\mathbf{p}'}\right) e^{-b^T(\theta)\alpha b(\theta) - 2\beta^T b(\theta)}}{\int D\theta\, e^{-b^T(\theta)\alpha b - 2\beta^T b(\theta)}}\end{aligned} \tag{5.56}$$

where the first term is from the derivative of $|\Psi_G(\theta)|^2$ in the numerator and the second term from the denominatior. Both can be efficiently evaluated. Regarding derivatives of $H_{\text{loc}}(\theta)$, only $H_{E,\text{loc}}(\theta)$ depends on the variational parameters α and β through the expression $b^T(\theta)\alpha b_{\mathbf{x},i}(\theta) + \beta^T b_{\mathbf{x},i}(\theta)$. Therefore derivatives are easily calculated, e.g. $b(\theta)_{\mathbf{p}} b_{\mathbf{x},i}(\theta)_{\mathbf{p}'}$ for the matrix element $\alpha_{\mathbf{p}\mathbf{p}'}$. The derivatives of $H_{\text{loc}}(\theta)$ w.r.t. the fermionic parameters ξ_i are non-zero for H_E, H_{GM} and H_M and can be shown to take the schematic form

$$\frac{\partial}{\partial \xi_i} \text{Tr}\left(\tilde{\Gamma}\left(\tilde{\xi}\right) \sum_{\mathbf{x},i} A_{\mathbf{x},i}(\theta)\right) = i \sum_{kl} \left(\frac{\tilde{\xi}}{\partial \xi_i}\right)_{kl} \left(\tilde{\Gamma}\left(\tilde{\xi}\right) \sum_{\mathbf{x},i} A_{\mathbf{x},i}(\theta) - \sum_{\mathbf{x},i} A_{\mathbf{x},i}(\theta) \tilde{\Gamma}\left(\tilde{\xi}\right)\right)^T_{kl} \tag{5.57}$$

where $\tilde{\Gamma}\left(\tilde{\xi}\right)$ is defined in eq. (5.31) and $A_{\mathbf{x},i}(\theta)$ is some gauge-field dependent matrix containing a link dependence. Since only the right term (that is transposed) needs to be computed in a Monte Carlo simulation and the whole derivative can be post-processed, the computational cost of the derivatives scales the same as the computation of the variational energy.

For the computation of the Gram matrix $G_{ij} \equiv \langle\Psi_i|\Psi_j\rangle$ it is useful to look at the tangent vectors first. The tangent vectors corresponding to the fermionic parameters ξ_i are related to the single-particle eigenstates of the gauge-matter Hamiltonian and can therefore be shown to be orthogonal. The tangent vectors corresponding to α and β are quadratic, respectively linear, in the vector $b(\theta)$ (defined for eq. (5.10)):

$$\begin{aligned}\left|\Psi_{\alpha_{\mathbf{p},\mathbf{p}'}}\right\rangle &= \int D\theta\, b(\theta)_{\mathbf{p}} b(\theta)_{\mathbf{p}'} e^{-\frac{1}{2}b(\theta)^T\alpha b(\theta) - \beta^T b(\theta)} |\Psi_F(\theta)\rangle |\theta\rangle \\ \left|\Psi_{\beta_{\mathbf{p}}}\right\rangle &= \int D\theta\, b(\theta)_{\mathbf{p}} e^{-\frac{1}{2}b(\theta)^T\alpha b(\theta) - \beta^T b(\theta)} |\Psi_F(\theta)\rangle |\theta\rangle\end{aligned} \tag{5.58}$$

The local quantity $O_{\text{loc}}(\theta)$ that needs to be sampled in a Monte Carlo simulation thus takes a simple form that is very similar to the gradient of the norm $\langle\Psi|\Psi\rangle$ that needs to be computed for the gradient of the variational energy (see eq. (5.56)). Since we use translational invariance to parametrize α, the tangent vectors will be related to the Fourier components $\tilde{b}(\theta)_{\mathbf{k}}$ and not $b(\theta)_{\mathbf{p}} b(\theta)_{\mathbf{p}'}$. The part of Gram matrix related to the overlaps between α-tangent vectors will thus involve sampling $\tilde{b}(\theta)_{\mathbf{k}} \tilde{b}(\theta)_{\mathbf{k}'}$, thus being of size $\mathcal{O}(N^2)$ and efficiently tractable.

Acknowledgements

I am extremely grateful to many people who have been part of my journey throughout the last years, which would not have been possible without their help and support.

First of all, I am deeply indebted to my supervisor Ignacio Cirac for his guidance during my PhD, and for giving me the freedom to pursue any research direction I wanted. His vast knowledge over many different areas of physics, his physical intuition and desire to do original research has influenced me a lot as a scientist. I am also grateful for his kindness, leadership and guidance as a mentor.

I would also like to thank Erez Zohar for being a co-supervisor during the start of my phd, for being a great collaborator and a great host during my stay in Israel despite the pandemic. I hope to visit you soon again in Israel under better circumstances.

Another big factor that my stay in Israel was still fun even though being in lockdown was Patrick Emonts. You were a great flatmate and we really made the most of our time there. Also thank you for all our collaborations and teaching me various skills that are too numerous to list here, ranging from writing good code to bouldering.

I would also like to thank all the people at MPQ who created a unique environmemt, both scientifically and socially. To only name a few, I want to thank Giacomo Giudice, Caroline de Groot, Cosimo Rusconi, Flavio Baccari, Sirui Lu, Tommaso Guaita, Miguel Bello Gamboa, Aslı Çakan, Albert Gasull Celades, Georgios Styliaris, Jiří Guth Jarkovský, Marti Perarnau Llobet, Ivan Kukuljan, Irene Papaefstathiou, Adrian Franco-Rubio, David Stephen and Dominik Wild. Special thanks go to Andrea Kluth, who helped in so many administrative matters and is one of the backbones of this group.

Also, I would like to thank Johannes Knörzer and Eduardo Sanchez-Burillo for starting the tradition of having a chess lunch, which I enjoyed a lot. Special thanks also go to Anna Hackenbroich and Bennet Windt for being great office mates, I will miss our coffee breaks.

I would also like to thank my friends from school and university, who after all these years I can always rely on.

Also, I would like to thank my family. Words cannot express my gratitude for your unwaivering support. Without you, this endeavor would not have been possible.

Finally, to Muriel, for walking this path with me and being a constant source of support.

BIBLIOGRPAHY

[1] Julian Bender and Erez Zohar. „Gauge Redundancy-Free Formulation of Compact QED with Dynamical Matter for Quantum and Classical Computations“. In: *Physical Review D* 102.11 (Dec. 2020), p. 114517. DOI: 10.1103/PhysRevD.102.114517.

[2] Julian Bender et al. „Real-Time Dynamics in 2+1D Compact QED Using Complex Periodic Gaussian States“. In: *Physical Review Research* 2.4 (Oct. 2020), p. 043145. DOI: 10.1103/PhysRevResearch.2.043145.

[3] Julian Bender, Patrick Emonts, and J. Ignacio Cirac. *A Variational Monte Carlo Algorithm for Lattice Gauge Theories with Continuous Gauge Groups: A Study of (2+1)-Dimensional Compact QED with Dynamical Fermions at Finite Density*. Apr. 12, 2023. arXiv: 2304.05916 [hep-lat, quant-ph]. URL: http://arxiv.org/abs/2304.05916. preprint.

[4] J. Bender et al. „Digital Quantum Simulation of Lattice Gauge Theories in Three Spatial Dimensions“. In: *New Journal of Physics* 20.9 (Sept. 2018), p. 093001. DOI: 10.1088/1367-2630/aadb71.

[5] M.E. Peskin and D.V. Schroeder. *An Introduction to Quantum Field Theory*. Reading, Mass: Addison-Wesley Pub. Co, 1995.

[6] S Carlip. „Quantum Gravity: A Progress Report“. In: *Reports on Progress in Physics* 64.8 (Aug. 1, 2001), pp. 885–942. DOI: 10.1088/0034-4885/64/8/301.

[7] K.G. Wilson. „Confinement of Quarks“. In: *Physical Review D* 10.8 (Oct. 1974), pp. 2445–2459. DOI: 10.1103/PhysRevD.10.2445.

[8] J. Kogut and L. Susskind. „Hamiltonian Formulation of Wilson's Lattice Gauge Theories“. In: *Physical Review D* 11.2 (Jan. 1975), pp. 395–408. DOI: 10.1103/PhysRevD.11.395.

[9] Ian Affleck and J. Brad Marston. „Large-n Limit of the Heisenberg-Hubbard Model: Implications for High- Tc Superconductors“. In: *Physical Review B* 37.7 (Mar. 1988), pp. 3774–3777. DOI: 10.1103/PhysRevB.37.3774.

[10] Walter Rantner and Xiao-Gang Wen. „Electron Spectral Function and Algebraic Spin Liquid for the Normal State of Underdoped High Tc Superconductors“. In: *Physical Review Letters* 86.17 (Apr. 2001), pp. 3871–3874. DOI: 10.1103/PhysRevLett.86.3871.

[11] S Aoki et al. „FLAG Review 2019“. In: *The European Physical Journal C* 80.2 (2020), pp. 1–268.

[12] M. Troyer and U.-J. Wiese. „Computational Complexity and Fundamental Limitations to Fermionic Quantum Monte Carlo Simulations“. In: *Physical Review Letters* 94.17 (May 2005). DOI: 10.1103/PhysRevLett.94.170201.

[13] Jonathan P. Dowling and Gerard J. Milburn. „Quantum Technology: The Second Quantum Revolution“. In: *Philosophical Transactions of the Royal Society of London. Series A: Mathematical, Physical and Engineering Sciences* 361.1809 (Aug. 15, 2003). Ed. by A. G. J. MacFarlane, pp. 1655–1674. DOI: 10.1098/rsta.2003.1227.

[14] R. Feynman. „Simulating Physics with Computers“. In: *International Journal of Theoretical Physics* 21.6 (June 1982), pp. 467–488.

[15] Mari Carmen Bañuls et al. „Simulating Lattice Gauge Theories within Quantum Technologies“. In: *The European Physical Journal D* 74.8 (Aug. 2020), p. 165. DOI: 10.1140/epjd/e2020-100571-8.

[16] C. J. Hamer, Zheng Weihong, and J. Oitmaa. „Series Expansions for the Massive Schwinger Model in Hamiltonian Lattice Theory“. In: *Physical Review D* 56.1 (July 1997), pp. 55–67. DOI: 10.1103/PhysRevD.56.55.

[17] Mari Carmen Bañuls et al. „Efficient Basis Formulation for $(1+1)$-Dimensional SU(2) Lattice Gauge Theory: Spectral Calculations with Matrix Product States“. In: *Physical Review X* 7.4 (Nov. 2017). DOI: 10.1103/PhysRevX.7.041046.

[18] A. M. Polyakov. „Quark Confinement and Topology of Gauge Theories“. In: *Nuclear Physics B* 120.3 (1977), pp. 429–458. DOI: 10.1016/0550-3213(77)90086-4.

[19] K Wilson. „The Renormalization Group and the ε Expansion“. In: *Physics Reports* 12.2 (Aug. 1974), pp. 75–199. DOI: 10.1016/0370-1573(74)90023-4.

[20] M. Tanabashi et al. „Review of Particle Physics“. In: *Physical Review D* 98.3 (Aug. 17, 2018), p. 030001. DOI: 10.1103/PhysRevD.98.030001.

[21] Matthias Neubert. *Les Houches Lectures on Renormalization Theory and Effective Field Theories*. Feb. 17, 2020. arXiv: 1901.06573 [hep-ph]. URL: http://arxiv.org/abs/1901.06573. preprint.

[22] J. Smit. *Introduction to Quantum Fields on a Lattice*. Cambridge Lecture Notes in Physics. Cambridge University Press, 2002.

[23] Nicholas Metropolis et al. „Equation of State Calculations by Fast Computing Machines“. In: *The Journal of Chemical Physics* 21.6 (June 1953), pp. 1087–1092. DOI: 10.1063/1.1699114.

[24] Simon Duane et al. „Hybrid Monte Carlo“. In: *Physics Letters B* 195.2 (Sept. 1987), pp. 216–222. DOI: 10.1016/0370-2693(87)91197-X.

[25] H.B. Nielsen and M. Ninomiya. „A No-Go Theorem for Regularizing Chiral Fermions“. In: *Physics Letters B* 105.23 (1981), pp. 219–223. DOI: 10.1016/0370-2693(81)91026-1.

[26] P. H. Ginsparg and K. G. Wilson. „A Remnant of Chiral Symmetry on the Lattice“. In: *Physical Review D: Particles and Fields* 25.10 (May 1982), pp. 2649–2657. DOI: 10.1103/PhysRevD.25.2649.

[27] D.B. Kaplan. „A Method for Simulating Chiral Fermions on the Lattice“. In: *Physics Letters B* 288.34 (1992), pp. 342–347. DOI: 10.1016/0370-2693(92)91112-M.

[28] Michael Creutz. „Gauge Fixing, the Transfer Matrix, and Confinement on a Lattice“. In: *Physical Review D* 15.4 (Feb. 15, 1977), pp. 1128–1136. DOI: 10.1103/PhysRevD.15.1128.

[29] J. Ignacio Cirac and Peter Zoller. „Goals and Opportunities in Quantum Simulation“. In: *Nature Physics* 8 (Apr. 2012), p. 264. DOI: 10.1038/nphys2275.

[30] H. F. Trotter. „On the Product of Semi-Groups of Operators“. In: *Proceedings of the American Mathematical Society* 10.4 (1959), pp. 545–551. DOI: 10.2307/2033649.

[31] S. Lloyd. „Universal Quantum Simulators“. In: *Science* 273.5278 (1996), pp. 1073–1078. DOI: 10.1126/science.273.5278.1073.

[32] Joschka Roffe. „Quantum Error Correction: An Introductory Guide“. In: *Contemporary Physics* 60.3 (July 3, 2019), pp. 226–245. DOI: 10.1080/00107514.2019.1667078.

[33] J. Preskill. „Quantum Computing in the NISQ Era and Beyond“. In: *Quantum* 2 (Aug. 2018), p. 79. DOI: 10.22331/q-2018-08-06-79.

[34] E. A. Martinez et al. „Real-Time Dynamics of Lattice Gauge Theories with a Few-Qubit Quantum Computer“. In: *Nature* 534 (2016), pp. 516–519. DOI: 10.1038/nature18318.

[35] Frederik Görg et al. „Realization of Density-Dependent Peierls Phases to Engineer Quantized Gauge Fields Coupled to Ultracold Matter“. In: *Nature Physics* 15.11 (Nov. 2019), pp. 1161–1167. DOI: 10.1038/s41567-019-0615-4.

[36] Christian Schweizer et al. „Floquet Approach to Z2 Lattice Gauge Theories with Ultracold Atoms in Optical Lattices“. In: *Nature Physics* 15.11 (Nov. 2019), pp. 1168–1173. DOI: 10.1038/s41567-019-0649-7.

[37] Bing Yang et al. „Observation of Gauge Invariance in a 71-Site Bose-Hubbard Quantum Simulator“. In: *Nature* 587.7834 (Nov. 2020), pp. 392–396. DOI: 10.1038/s41586-020-2910-8.

[38] Alexander Mil et al. „A Scalable Realization of Local U(1) Gauge Invariance in Cold Atomic Mixtures“. In: *Science* 367.6482 (Mar. 2020), pp. 1128–1130. DOI: 10.1126/science.aaz5312.

[39] E. Zohar, J. I. Cirac, and B. Reznik. „Simulating (2 + 1)-Dimensional Lattice QED with Dynamical Matter Using Ultracold Atoms“. In: *Physical Review Letters* 110.5 (Jan. 2013). DOI: 10.1103/PhysRevLett.110.055302.

[40] Robert Ott et al. „Scalable Cold-Atom Quantum Simulator for Two-Dimensional QED“. In: *Physical Review Letters* 127.13 (Sept. 2021), p. 130504. DOI: 10.1103/PhysRevLett.127.130504.

[41] E. Zohar et al. „Digital Quantum Simulation of Z 2 Lattice Gauge Theories with Dynamical Fermionic Matter“. In: *Physical Review Letters* 118.7 (Feb. 2017). DOI: 10.1103/PhysRevLett.118.070501.

[42] Anthony Ciavarella, Natalie Klco, and Martin J. Savage. „Trailhead for Quantum Simulation of SU(3) Yang-Mills Lattice Gauge Theory in the Local Multiplet Basis“. In: *Physical Review D* 103.9 (May 2021), p. 094501. DOI: 10.1103/PhysRevD.103.094501.

[43] D. Horn. „Finite Matrix Models with Continuous Local Gauge Invariance“. In: *Physics Letters B* 100.2 (1981), pp. 149–151. DOI: 10.1016/0370-2693(81)90763-2.

[44] P. Orland and D. Rohrlich. „Lattice Gauge Magnets: Local Isospin from Spin“. In: *Nuclear Physics B* 338.3 (1990), pp. 647–672. DOI: 10.1016/0550-3213(90)90646-U.

[45] S Chandrasekharan and U.-J Wiese. „Quantum Link Models: A Discrete Approach to Gauge Theories“. In: *Nuclear Physics B* 492.1-2 (May 1997), pp. 455–471. DOI: 10.1016/S0550-3213(97)80041-7.

[46] R. Brower, S. Chandrasekharan, and U.-J. Wiese. „QCD as a Quantum Link Model“. In: *Physical Review D* 60.9 (Sept. 1999). DOI: 10.1103/PhysRevD.60.094502.

[47] Ulrich Schollwöck. „The Density-Matrix Renormalization Group in the Age of Matrix Product States“. In: *Annals of Physics* 326.1 (Jan. 2011), pp. 96–192. DOI: 10.1016/j.aop.2010.09.012.

[48] P. Langacker. *The Standard Model and Beyond*. Series in High Energy Physics, Cosmology and Gravitation. Taylor & Francis, 2011.

[49] L. McLerran. „The Physics of the Quark-Gluon Plasma“. In: *Reviews of Modern Physics* 58.4 (Oct. 1986), pp. 1021–1064. DOI: 10.1103/RevModPhys.58.1021.

[50] K. Fukushima and T. Hatsuda. „The Phase Diagram of Dense QCD“. In: *Reports on Progress in Physics* 74.1 (Jan. 2011), p. 014001. DOI: 10.1088/0034-4885/74/1/014001.

[51] U.-J. Wiese. „Ultracold Quantum Gases and Lattice Systems: Quantum Simulation of Lattice Gauge Theories“. In: *Annalen der Physik* 525.10-11 (Nov. 2013), pp. 777–796. DOI: 10.1002/andp.201300104.

[52] E. Zohar, J.I. Cirac, and B. Reznik. „Quantum Simulations of Lattice Gauge Theories Using Ultracold Atoms in Optical Lattices“. In: *Reports on Progress in Physics* 79.1 (Jan. 2016), p. 014401. DOI: 10.1088/0034-4885/79/1/014401.

[53] M. Dalmonte and S. Montangero. „Lattice Gauge Theory Simulations in the Quantum Information Era“. In: *Contemporary Physics* 57.3 (July 2016), pp. 388–412. DOI: 10.1080/00107514.2016.1151199.

[54] M.C. Banuls and K. Cichy. „Review on Novel Methods for Lattice Gauge Theories“. 2019. arXiv: 1910.00257 [hep-lat].

[55] Jad C. Halimeh et al. „Robustness of Gauge-Invariant Dynamics against Defects in Ultracold-Atom Gauge Theories“. In: *Physical Review Research* 2.3 (Sept. 3, 2020), p. 033361. DOI: 10.1103/PhysRevResearch.2.033361.

[56] Jad C. Halimeh et al. „Gauge-Symmetry Protection Using Single-Body Terms“. In: *PRX Quantum* 2.4 (Oct. 18, 2021), p. 040311. DOI: 10.1103/PRXQuantum.2.040311.

[57] S. D. Drell et al. „Quantum Electrodynamics on a Lattice: A Hamiltonian Variational Approach to the Physics of the Weak-Coupling Region“. In: *Physical Review D: Particles and Fields* 19.2 (Jan. 1979), pp. 619–638. DOI: 10.1103/PhysRevD.19.619.

[58] Emilio Cobanera, Gerardo Ortiz, and Zohar Nussinov. „The Bond-Algebraic Approach to Dualities“. In: *Advances in Physics* 60.5 (Oct. 2011), pp. 679–798. DOI: 10.1080/00018732.2011.619814.

[59] David B. Kaplan and Jesse R. Stryker. „Gauss's Law, Duality, and the Hamiltonian Formulation of U(1) Lattice Gauge Theory“. In: *Physical Review D* 102.9 (Nov. 20, 2020), p. 094515. DOI: 10.1103/PhysRevD.102.094515.

[60] Judah F. Unmuth-Yockey. „A Gauge-Invariant, Rotor Hamiltonian from Dual Variables of 3D U(1) Gauge Theory“. In: *Physical Review D* 99.7 (Apr. 2019), p. 074502. DOI: 10.1103/PhysRevD.99.074502.

[61] Jan F. Haase et al. „A Resource Efficient Approach for Quantum and Classical Simulations of Gauge Theories in Particle Physics“. In: *Quantum* 5 (Feb. 4, 2021), p. 393. DOI: 10.22331/q-2021-02-04-393.

[62] Yannick Meurice. „Discrete Aspects of Continuous Symmetries in the Tensorial Formulation of Abelian Gauge Theories“. In: *Physical Review D: Particles and Fields* 102.1 (July 2020), p. 014506. DOI: 10.1103/PhysRevD.102.014506.

[63] Eduardo Fradkin and Stephen H. Shenker. „Phase Diagrams of Lattice Gauge Theories with Higgs Fields“. In: *Physical Review D: Particles and Fields* 19.12 (June 1979), pp. 3682–3697. DOI: 10.1103/PhysRevD.19.3682.

[64] Erez Zohar and J. Ignacio Cirac. „Eliminating Fermionic Matter Fields in Lattice Gauge Theories“. In: *Physical Review B* 98.7 (Aug. 2018), p. 075119. DOI: 10.1103/PhysRevB.98.075119.

[65] Erez Zohar and J. Ignacio Cirac. „Removing Staggered Fermionic Matter in U(N) and SU(N) Lattice Gauge Theories“. In: *Physical Review D: Particles and Fields* 99.11 (June 2019), p. 114511. DOI: 10.1103/PhysRevD.99.114511.

[66] L. Susskind. „Lattice Fermions“. In: *Physical Review D* 16.10 (Nov. 1977), pp. 3031–3039. DOI: 10.1103/PhysRevD.16.3031.

[67] Antonino Zichichi, ed. *New Phenomena in Subnuclear Physics*. Boston, MA: Springer US, 1977. DOI: 10.1007/978-1-4613-4208-3.

[68] J.B. Kogut. „An Introduction to Lattice Gauge Theory and Spin Systems“. In: *Reviews of Modern Physics* 51.4 (Oct. 1979), pp. 659–713. DOI: 10.1103/RevModPhys.51.659.

[69] L Tagliacozzo et al. „Optical Abelian Lattice Gauge Theories“. In: *Annals of Physics* 330 (2013), pp. 160–191. DOI: 10.1016/j.aop.2012.11.009.

[70] Javier Argüello-Luengo et al. „Analogue Quantum Chemistry Simulation“. In: *Nature* 574.7777 (2019), pp. 215–218. DOI: 10.1038/s41586-019-1614-4.

[71] N.E. Ligterink, N.R. Walet, and R.F. Bishop. „Toward a Many-Body Treatment of Hamiltonian Lattice SU(N) Gauge Theory“. In: *Annals of Physics* 284.2 (Sept. 2000), pp. 215–262. DOI: 10.1006/aphy.2000.6070.

[72] David J. Gross and Frank Wilczek. „Asymptotically Free Gauge Theories. I“. In: *Physical Review D* 8.10 (Nov. 1973), pp. 3633–3652. DOI: 10.1103/PhysRevD.8.3633.

[73] FLAG Working Group et al. „Review of Lattice Results Concerning Low-Energy Particle Physics“. In: *The European Physical Journal C* 74.9 (Sept. 2014). DOI: 10.1140/epjc/s10052-014-2890-7.

[74] Manu Mathur. „Harmonic Oscillator Pre-Potentials in *SU* (2) Lattice Gauge Theory“. In: *Journal of Physics A: Mathematical and General* 38.46 (Nov. 18, 2005), pp. 10015–10025. DOI: 10.1088/0305-4470/38/46/008.

[75] M.C. Bañuls et al. „Density Induced Phase Transitions in the Schwinger Model: A Study with Matrix Product States“. In: *Physical Review Letters* 118.7 (Feb. 2017), p. 071601. DOI: 10.1103/PhysRevLett.118.071601.

[76] B. Buyens et al. „Matrix Product States for Gauge Field Theories“. In: *Physical Review Letters* 113.9 (Aug. 2014). DOI: 10.1103/PhysRevLett.113.091601.

[77] B. Buyens, F. Verstraete, and K. Van Acoleyen. „Hamiltonian Simulation of the Schwinger Model at Finite Temperature“. In: *Physical Review D* 94.8 (Oct. 2016). DOI: 10.1103/PhysRevD.94.085018.

[78] B. Buyens et al. „Real-Time Simulation of the Schwinger Effect with Matrix Product States“. In: *Physical Review D* 96.11 (Dec. 2017). DOI: 10.1103/PhysRevD.96.114501.

[79] S. Kühn et al. „Non-Abelian String Breaking Phenomena with Matrix Product States“. In: *Journal of High Energy Physics* 2015.7 (2015), pp. 1–26. DOI: 10.1007/JHEP07(2015)130.

[80] T. Pichler et al. „Real-Time Dynamics in U(1) Lattice Gauge Theories with Tensor Networks“. In: *Physical Review X* 6.1 (Mar. 2016), p. 011023. DOI: 10.1103/PhysRevX.6.011023.

[81] P. Silvi et al. „Finite-Density Phase Diagram of a (1 + 1) - d Non-Abelian Lattice Gauge Theory with Tensor Networks“. In: *Quantum* 1 (Apr. 2017), p. 9. DOI: 10.22331/q-2017-04-25-9.

[82] Pietro Silvi et al. „The Tensor Networks Anthology: Simulation Techniques for Many-Body Quantum Lattice Systems“. In: *SciPost Physics Lecture Notes* (Mar. 2019). DOI: 10.21468/SciPostPhysLectNotes.8.

[83] Daniel Robaina, Mari Carmen Bañuls, and J. Ignacio Cirac. „Simulating 2 + 1 D Z3 Lattice Gauge Theory with an Infinite Projected Entangled-Pair State“. In: *Physical Review Letters* 126.5 (Feb. 2021), p. 050401. DOI: 10.1103/PhysRevLett.126.050401.

[84] Ferdinand Tschirsich, Simone Montangero, and Marcello Dalmonte. „Phase Diagram and Conformal String Excitations of Square Ice Using Gauge Invariant Matrix Product States“. In: *SciPost Physics* 6.3 (Mar. 2019). DOI: 10.21468/SciPostPhys.6.3.028.

[85] Timo Felser et al. „Two-Dimensional Quantum-Link Lattice Quantum Electrodynamics at Finite Density“. In: *Physical Review X* 10.4 (Nov. 25, 2020), p. 041040. DOI: 10.1103/PhysRevX.10.041040.

[86] Barak Bringoltz. „Volume Dependence of Two-Dimensional Large- N QCD with a Nonzero Density of Baryons“. In: *Physical Review D* 79.10 (May 2009), p. 105021. DOI: 10.1103/PhysRevD.79.105021.

[87] N. Parga. „Finite Temperature Behavior of Topological Excitations in Lattice Compact QED“. In: *Physics Letters B* 107.6 (Dec. 1981), pp. 442–445. DOI: 10.1016/0370-2693(81)91225-9.

[88] S. Ben-Menahem. „Confinement in Compact QED for Low Couplings“. In: *Physical Review D: Particles and Fields* 20.8 (Oct. 1979), pp. 1923–1933. DOI: 10.1103/PhysRevD.20.1923.

[89] Bernard Deconinck et al. „Computing Riemann Theta Functions“. In: *Mathematics of Computation* 73.247 (Dec. 2003), pp. 1417–1443. DOI: 10.1090/S0025-5718-03-01609-0.

[90] B. Svetitsky and L. G. Yaffe. „Critical Behavior at Finite-Temperature Confinement Transitions“. In: *Nuclear Physics B* 210.4 (1982), pp. 423–447. DOI: DOI:10.1016/0550-3213(82)90172-9.

[91] Michael Creutz. „Asymptotic-Freedom Scales“. In: *Physical Review Letters* 45.5 (Aug. 1980), pp. 313–316. DOI: 10.1103/PhysRevLett.45.313.

[92] Jan Ambjørn, Anthony J.G. Hey, and Steve Otto. „String Tensions for Lattice Gauge Theories in 2 + 1 Dimensions“. In: *Nuclear Physics B* 210.3 (Oct. 1982), pp. 347–368. DOI: 10.1016/0550-3213(82)90125-0.

[93] Mushtaq Loan et al. „Path Integral Monte Carlo Approach to the U(1) Lattice Gauge Theory in 2+1 Dimensions“. In: *Physical Review D* 68.3 (Aug. 2003), p. 034504. DOI: 10.1103/PhysRevD.68.034504.

[94] D. Horn, M. Weinstein, and S. Yankielowicz. „Hamiltonian Approach to Z (N) Lattice Gauge Theories“. In: *Physical Review D* 19.12 (June 1979), pp. 3715–3731. DOI: 10.1103/PhysRevD.19.3715.

[95] Lucas Hackl et al. „Geometry of Variational Methods: Dynamics of Closed Quantum Systems“. In: *SciPost Physics* 9.4 (Oct. 8, 2020), p. 048. DOI: 10.21468/SciPostPhys.9.4.048.

[96] Paul D. Coddington et al. „The Deconfining Transition for Finite-Temperature U(1) Lattice Gauge Theory in (2+1) Dimensions“. In: *Physics Letters B* 175.1 (July 1986), pp. 64–68. DOI: 10.1016/0370-2693(86)90332-1.

[97] M. N. Chernodub, E.-M. Ilgenfritz, and A. Schiller. „Lattice Study of 3 D Compact QED at Finite Temperature“. In: *Physical Review D* 64.5 (Aug. 2001), p. 054507. DOI: 10.1103/PhysRevD.64.054507.

[98] B. Svetitsky. „Symmetry Aspects of Finite-Temperature Confinement Transitions“. In: *Physics Reports* 132.1 (1986), pp. 1–53. DOI: DOI:10.1016/0370-1573(86)90014-1.

[99] J. Villain. „Theory of One- and Two-Dimensional Magnets with an Easy Magnetization Plane. II. The Planar, Classical, Two-Dimensional Magnet“. In: *Journal de Physique* 36.6 (1975), pp. 581–590. DOI: 10.1051/jphys:01975003606058100.

[100] Di Luo et al. *Gauge Equivariant Neural Networks for 2+1D U(1) Gauge Theory Simulations in Hamiltonian Formulation*. Nov. 6, 2022. arXiv: 2211.03198 [hep-lat]. URL: http://arxiv.org/abs/2211.03198. preprint.

[101] Aaron Williams. „Loopless Generation of Multiset Permutations Using a Constant Number of Variables by Prefix Shifts“. In: *Proceedings of the Twentieth Annual ACM-SIAM Symposium on Discrete Algorithms*. Society for Industrial and Applied Mathematics, Jan. 2009, pp. 987–996. DOI: 10.1137/1.9781611973068.107.

[102] L. Tagliacozzo et al. „Simulation of Non-Abelian Gauge Theories with Optical Lattices“. In: *Nature Communications* 4 (Oct. 2013), p. 2615. DOI: 10.1038/ncomms3615.

[103] Erik J. Gustafson. „Prospects for Simulating a Qudit-Based Model of (1+1) D Scalar QED“. In: *Physical Review D* 103.11 (June 2021), p. 114505. DOI: 10.1103/PhysRevD.103.114505.

[104] Tanmoy Bhattacharya et al. „Qubit Regularization of Asymptotic Freedom“. In: *Physical Review Letters* 126.17 (Apr. 2021), p. 172001. DOI: 10.1103/PhysRevLett.126.172001.

[105] Indrakshi Raychowdhury and Jesse R. Stryker. „Loop, String, and Hadron Dynamics in SU(2) Hamiltonian Lattice Gauge Theories“. In: *Physical Review D* 101.11 (June 2020), p. 114502. DOI: 10.1103/PhysRevD.101.114502.

[106] M.C. Bañuls et al. „The Mass Spectrum of the Schwinger Model with Matrix Product States“. In: *Journal of High Energy Physics* 2013.11 (Nov. 2013). DOI: 10.1007/JHEP11(2013)158.

[107] Falk Bruckmann, Karl Jansen, and Stefan Kühn. „O(3) Nonlinear Sigma Model in 1+1 Dimensions with Matrix Product States“. In: *Physical Review D* 99.7 (Apr. 2019), p. 074501. DOI: 10.1103/PhysRevD.99.074501.

[108] E. Rico et al. „Tensor Networks for Lattice Gauge Theories and Atomic Quantum Simulation“. In: *Physical Review Letters* 112.20 (May 2014). DOI: 10.1103/PhysRevLett.112.201601.

[109] Zhuo Chen et al. *Simulating 2+1D Lattice Quantum Electrodynamics at Finite Density with Neural Flow Wavefunctions*. Dec. 14, 2022. arXiv: 2212.06835 [hep-lat]. URL: http://arxiv.org/abs/2212.06835. preprint.

[110] S. Gazit, M. Randeria, and A. Vishwanath. „Emergent Dirac Fermions and Broken Symmetries in Confined and Deconfined Phases of Z2 Gauge Theories“. In: *Nature Physics* 13 (Feb. 2017), p. 484. DOI: 10.1038/nphys4028.

[111] Xiao Yan Xu et al. „Monte Carlo Study of Lattice Compact Quantum Electrodynamics with Fermionic Matter: The Parent State of Quantum Phases“. In: *Physical Review X* 9.2 (May 2019), p. 021022. DOI: 10.1103/PhysRevX.9.021022.

[112] Ivan Glasser et al. „Neural-Network Quantum States, String-Bond States, and Chiral Topological States“. In: *Physical Review X* 8.1 (Jan. 2018). DOI: 10.1103/PhysRevX.8.011006.

[113] Sandro Sorella. „Wave Function Optimization in the Variational Monte Carlo Method“. In: *Physical Review B* 71.24 (June 2005). DOI: 10.1103/PhysRevB.71.241103.

[114] Tao Shi, Eugene Demler, and J Ignacio Cirac. „Variational Study of Fermionic and Bosonic Systems with Non-Gaussian States: Theory and Applications“. In: *Annals of Physics* 390 (2018), pp. 245–302. DOI: 10.1016/j.aop.2017.11.014.

[115] Sandro Sorella. „Generalized Lanczos Algorithm for Variational Quantum Monte Carlo“. In: *Physical Review B* 64.2 (June 2001). DOI: 10.1103/PhysRevB.64.024512.

[116] Elliott H. Lieb. „Flux Phase of the Half-Filled Band“. In: *Physical Review Letters* 73.16 (Oct. 1994), pp. 2158–2161. DOI: 10.1103/PhysRevLett.73.2158.

[117] W. Heisenberg. „Zur Theorie des Ferromagnetismus“. In: *Zeitschrift fur Physik* 49.9-10 (Sept. 1928), pp. 619–636. DOI: 10.1007/BF01328601.

[118] T. Holstein and H. Primakoff. „Field Dependence of the Intrinsic Domain Magnetization of a Ferromagnet“. In: *Physical Review* 58.12 (Dec. 1940), pp. 1098–1113. DOI: 10.1103/PhysRev.58.1098.